



DISSERTATION

# Ice Nucleation Activity of Boreal Plants with Focus on Birch Trees

ausgeführt zum Zwecke der Erlangung des akademischen Grades einer  
Doktorin der Naturwissenschaften unter der Leitung von

Ao.Univ.Prof. Dr. Hinrich Grothe

Institut für Materialchemie, E165

eingereicht an der Technischen Universität Wien

Institut für technische Chemie

von

Laura Felgitsch

00630520

Wien, am

Unterschrift

## **Zusammenfassung (Deutsch)**

Zwei Drittel der Erde sind mit Wolken bedeckt. Die Erde ist daher eher ein weißer Planet als ein Blauer. Wolken haben großen Einfluss auf die Albedo<sup>1</sup> der Erde. Allerdings verhalten sich Wolken sehr unterschiedlich. Der Aggregatzustand des enthaltenen Wassers beeinflusst das Abregnen und die Wechselwirkung mit der ein- und ausfallenden Strahlung. Reines Wasser gefriert nicht bei 0 °C (dem thermodynamischen Gefrierpunkt von Wasser) da dieser Prozess kinetisch behindert wird. Tropfen im Mikrometermaßstab (wie sie in Wolken präsent sind) gefrieren typischerweise bei Temperaturen unter -36 °C. Verunreinigungen können diesen Prozess beeinflussen und die Gefriertemperatur zu höheren Temperaturen verschieben. Diese Verunreinigungen bezeichnet man als Eiskeime. Den Prozess selbst nennt man heterogene Nukleation. Bisher wurden solche Eiskeime in allen biologischen Bereichen gefunden. Sie spielen eine wichtige Rolle in der Existenz vieler Mikroorganismen mit einer großen Bandbreite an Aufgaben.

Diese Arbeit befasst sich mit dem Eisnukleationsverhalten von Pflanzen, deren natürlicher Lebensraum sich in die borealen Gebiete erstreckt. In diesen Gebieten herrscht Nachtfrost auch im Sommer und im Winter können die Temperaturen auf -40 °C fallen. Trotzdem hat das Leben auch unter diesen harschen Bedingungen Wege gefunden, um zu bestehen. Einige Pflanzen haben Mechanismen entwickelt, welche ihnen erlauben das Gefrieren von Wasser in ihrem Gewebe zu kontrollieren. Spezielle Moleküle regulieren dabei nicht nur Gefriertemperatur, sondern auch Kristallgröße und Zellstabilität. Diese Eigenschaft macht solche Pflanzen zu spannenden Kandidaten für Eisnukleationsexperimente.

Bisher ist nur wenig über die Eisnukleationsaktivität von Pflanzen bekannt. In 2001 konnten Diehl und Kollegen zeigen, dass Birkenpollen effiziente

---

<sup>1</sup> Vom lateinischen albedo „Weiße“

Eiskeime sind. Über zehn Jahre später zeigten Pummer et al. (2012), dass die Größe der enthaltenen Eiskeime im Submikrometerbereich liegt und dass sie leicht vom Pollen abgewaschen werden können. Durch die geringe Größe und ihre Stabilität gegenüber reaktiven sauerstoffhaltigen Spezies könnten diese Eiskeime eine extrem lange Lebensdauer in der Atmosphäre aufweisen.

Über die Chemie der Eiskeime von Birkenpollen ist weniger bekannt. Ein Ziel dieser Arbeit war es, diese näher zu bestimmen. Verwendete Methoden waren verschiedene biochemische Trennmethode (z.B. solid phase extraction) sowie Schwingungsspektroskopie. Weiters wurden chaotrope Reagenzien und Enzyme verwendet, um die Rolle von Proteinen im Prozess der heterogenen Eisnukleation besser zu verstehen.

Es wurde Material analysiert, welches von zehn verschiedenen Birken stammte. Alle untersuchten Proben (Primärholz, Sekundärholz, Blätter, Rinde und Bohrkerne von Stämmen) waren eisnukleationsaktiv. Die enthaltenen Eiskeime zeigten starke Ähnlichkeiten mit jenen aus Birkenpollen. Verschiedene Probenpräparationen und Extraktionsmethoden erlaubten es, nicht nur die Konzentration der enthaltenen Keime zu bestimmen, sondern auch die Konzentration der Keime, welche leicht in die Umwelt gelangen können.

Neben Birken wurden auch Beeren von verschiedenen mehrjährigen Pflanzen (schwarze Johannisbeere, Blaubeere, Moosbeere, Aronia, Preiselbeere, Holunder, Sanddorn, Himbeere und Vogelbeere) untersucht. Des Weiteren wurden Blätter von Blaubeere, Wacholder, Himbeere und Sanddorn analysiert. Alle Proben waren eisnukleationsaktiv. Das wird als Hinweis gewertet für die weite Verbreitung dieser Eigenschaft in borealen Pflanzen.

## **Summary (English)**

Two thirds of the Earth are covered by clouds, rendering our planet a white planet rather than a blue one. Hence, clouds have a huge impact on the albedo<sup>2</sup> of the Earth; however, not every cloud acts in the same manner. The microphysical state of the water present in clouds affects precipitation and lifespan of a cloud, as well as their radiative properties. Pure water does not freeze at 0°C (the thermodynamic freezing point of water), since freezing is a kinetically hindered process, but rather at far lower temperatures. Pure water droplets in the micrometre size range, such as cloud droplets, freeze only at temperatures around -36 °C. Impurities can influence the freezing process by shifting the freezing event to higher temperatures. These are called ice nucleating particles and the process is referred to as heterogeneous nucleation. So far, ice nucleating particles have been found in almost all kingdoms of life, playing a part in the life of many different organisms for a wide range of functions.

This work focusses on the ice nucleation activity of plants native to the boreal region. Boreal regions exhibit night frosts even during the warm seasons and winter temperatures that can be as cold as -40 °C. However, even under these conditions, life has prevailed and found various mechanisms to cope with the cold. Several plants have developed mechanisms, allowing them to control freezing within their tissue. They exhibit many different molecules regulating not just temperature but also crystal size and cell stability. These properties make plants native to the boreal regions very interesting candidates for ice nucleation research.

So far, very little is known about the ice nucleation activity of plants. In 2001, Diehl and colleagues showed that single birch pollen can act as efficient ice nucleating particles. More than ten years later, Pummer and colleagues (2012) published data showing that the size of the ice

---

<sup>2</sup> From the Latin word albedo "whiteness"

nucleating component is in the submicron size and that it can be easily washed off the pollen-surface. Due to its small size and its stability towards reactive oxygen species, it has the potential for a long atmospheric lifespan

The chemical nature of the ice nuclei extractable from birch pollen is not fully understood. One goal of this work is to further elucidate their composition. Different biochemical separation techniques (e.g. solid phase extraction cartridges) as well as vibrational spectroscopy were applied. Further, chaotropic reagents and enzymes are used to analyse the role of proteins in the process of heterogeneous ice nucleation.

The examined plant material was collected from several parts of ten different birch trees. In this work it was shown that all analysed parts of birch trees (primary wood, secondary wood, leaves, bark, and drill cores of the stem) were ice nucleation active. The contained ice nucleating particles show strong similarities to those found in pollen. Different sample preparations and extractions allowed us to estimate not just the total contained concentration in the plant material, but also the amount of ice nuclei that is easily accessible for the surrounding environment of the tree.

Apart from birch trees, berries from several perennial plants (black currant, blueberry, cranberry, chokeberry, lingonberry, sambucus, sea buckthorn, raspberry, and rowanberry) were investigated. Further leaves of blueberry, juniper, raspberry, and sea buckthorn were analysed. All samples were ice nucleation active, showing how far spread this ability is in the Boreal plant kingdom.

## **ACKNOWLEDGEMENT**

I would like to thank my family and friends for all their support and understanding. Especially my aunt Theresia, who always looked out for me, and Thomas, who is always by my side when I need him.

For funding I would like to thank the the FWF (Austrian Science Fund, project no. P 26040) and the FFG (Austrian Research Promotion Agency, project no. 850689). Further I would like to thank the TU Wien for funding, scholarships to attend conferences, all the supplies, and the opportunity of working in science itself.

I would like to thank every single cooperation partner. Though they are to many, to all be listed here, there are some, I want to point out especially:

David G. Schmale III (Virginia Tech), Cindy Morris (INRA), David Sands (Montana State University), and Regina Hitzenberger (University of Vienna) for all their support and help with my research and with my personal development as a scientist.

Martina Marchetti-Deschmann, Victor Weiss, and Günter Allmaier (TU Wien, CTA) for their support with the topic of biochemical analytics.

All my colleagues and fellow students at the institute (especially Verena, Clara, Astrid, and Philipp)

The wonderful bachelor and master students I got to work with, who where a delight, lots of fun, and an immense help.

And last but not least, my supervisor Hinrich Grothe, without whom this work would never have been possible. For all the freedoms I had, for every time you pushed me to work harder, for every task you threw in my way. I learned and improved so many skills under your guidance, which go way further than 'just' science and I am truly grateful for that.

## Table of content

1.	Introduction and Theory.....	8
1.1.	The Atmosphere of the Earth .....	8
1.2.	An Introduction to Water and Freezing.....	13
1.3.	Clouds and Aerosols .....	33
1.4.	Freezing and Anti-Freezing in Nature .....	38
1.5.	Biological Ice Nuclei.....	43
2.	Instrumental and Samples .....	49
2.1.	VODCA .....	49
2.1.1.	Data Treatment .....	55
2.2.	FT-IR-Spectroscopy .....	57
2.3.	Samples, Sampling and Treatment .....	59
2.3.1.	Birch Pollen Washing Water.....	59
2.3.2.	Tyrolian and Viennese Birches .....	59
2.3.3.	Microscopic Analysis of the Leaves .....	68
2.3.4.	Berries and Leaves from Different Plants.....	70
3.	Investigations on the Birch Pollen INMs.....	73
3.1.	Solid Phase Extraction .....	73
3.1.1.	Ammonium Sulphate Precipitation.....	78
3.2.	Size Exclusion Chromatography .....	84
3.3.	Urea and Enzyme Treatment .....	86
3.4.	Ozone Treatment .....	93
3.5.	Discussion – Analysis of Birch Pollen INPs .....	96

- 4. Ice Nucleation Activity of Plant Materials ..... 98
  - 4.1. Ice Nucleation Activity of Birch Trees ..... 98
    - 4.1.1. INA of Milled Samples..... 98
    - 4.1.2. Surface Extracts ..... 123
  - 4.2. Ice Nucleation Activity of Different Berries..... 141
    - 4.2.1. INA of Filtered and Unfiltered Samples..... 141
    - 4.2.2. Comparison of Samples ..... 150
    - 4.2.3. Ozone Treatment of Black Currant Juice..... 157
    - 4.2.4. Discussion – INPs Distribution Throughout Various Plants Native to the Boreal Region..... 159
  - 4.3. Discussion – INPs from Plants and their INA ..... 162
- 5. Summary and Conclusion ..... 165
- References: ..... 167
- Personal Publication List ..... 187
- Curriculum Vitae ..... 194



# 1. Introduction and Theory

## 1.1. The Atmosphere of the Earth

Atmosphere derives from the Greek words *atmos*, which translates into vapour, and *spharia* meaning sphere. It stretches right from the Earth's surface 10,000 km into space and is scene of uncountable different physical and chemical processes, many of which are crucial to life as we know it.

The atmosphere can be divided in five zones, which are separated by boundary layers characterized by an inversion of the temperature gradient, the so-called pauses. The pauses hinder exchange between the different layers. A schematic depiction of the atmosphere is given in Figure 1, the vertical temperature profile is depicted in Figure 2.

The lowest layer is called troposphere and stretches directly from the ground up to an altitude of  $\sim 10$  km (varying depending on the location and weather). It often gets divided in planetary boundary layer (from the Earth's surface to approx. 1 km altitude) and free troposphere (ranging between 1 km altitude and the tropopause). The temperature declines with increasing altitude throughout the whole troposphere, reaching an average temperature of approx.  $-56^{\circ}\text{C}$  at maximum height. The lowest part of the troposphere gets heated directly by the surface of the Earth. Due to this primary heat source, the temperature decline with altitude is almost linear with distance to the surface of the Earth. This temperature profile promotes vertically mixing and turbulences, which motivated the naming of the troposphere, deriving from the Greek word *tropos*, meaning turn. The troposphere is the region were most of the atmospheric water vapour can be found and consequently the troposphere is the locality of nearly all of Earth's weather. The troposphere accounts only for a small fraction of the total height of the atmosphere, however, it contains 80% of

the total atmospheric mass. The limits of the troposphere are set by the tropopause, where the temperature gradient reverts. (Seinfeld & Pandis, 1998, pp. 6f.; Salby, 2012, pp. 14f.)

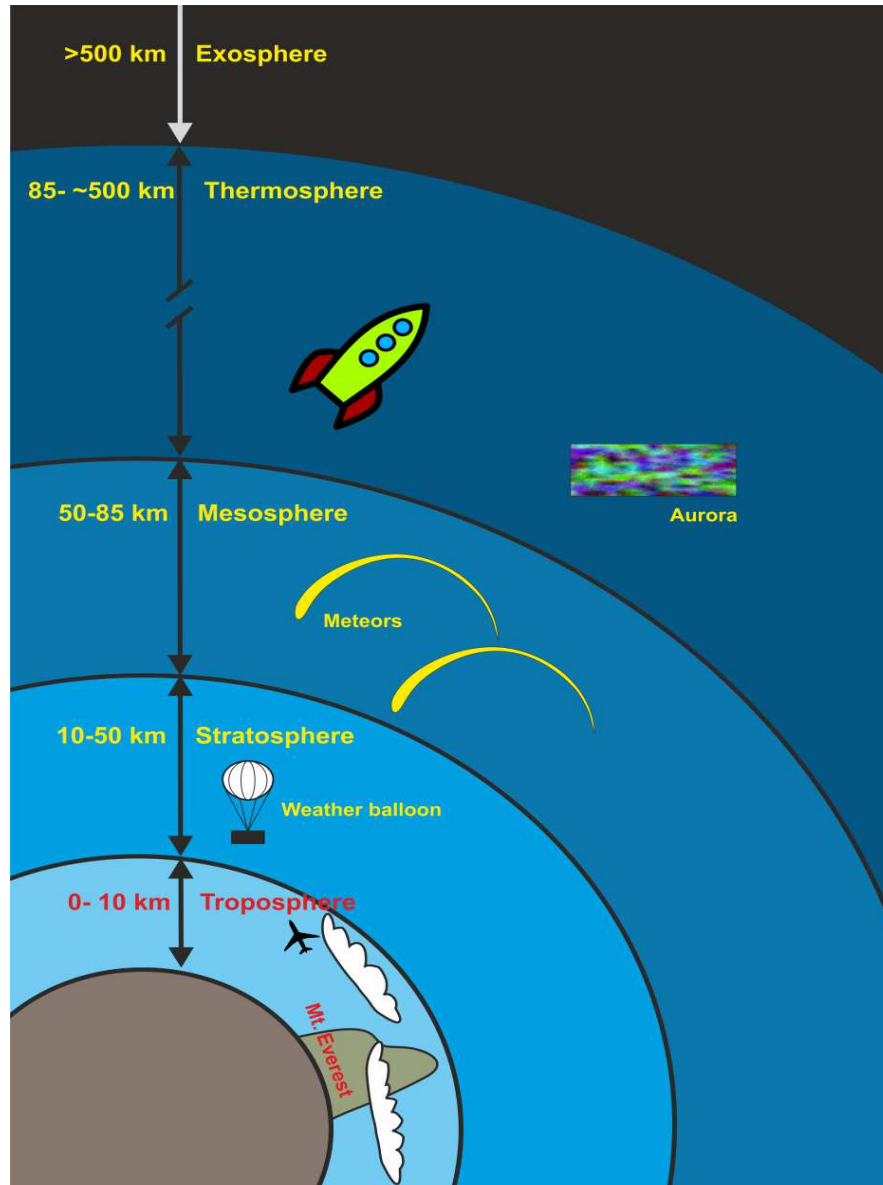


**Figure 1: Schematic depiction of the different regions of the atmosphere. Heights are approximations. (see e.g. <https://www.nasa.gov><sup>3</sup> or <https://www.britannica.com><sup>4</sup>)**

<sup>3</sup> [https://www.nasa.gov/mission\\_pages/sunearth/science/atmosphere-layers2.html](https://www.nasa.gov/mission_pages/sunearth/science/atmosphere-layers2.html) (25.07.2019)

<sup>4</sup> <https://www.britannica.com/science/atmosphere> (25.07.2019)

The second layer is called stratosphere and extends from the tropopause to ~50 km altitude. Within the stratosphere, temperatures increase with altitude reaching approx.  $-2^{\circ}\text{C}$  at its maximum at the tropopause. The increase in temperature is caused by the ozone layer, which absorbs ultraviolet radiation. Due to this temperature profile, vertical exchange processes within the stratosphere are very slow. (Seinfeld & Pandis, 1998, pp. 7f.; Salby, 2012, p. 15)

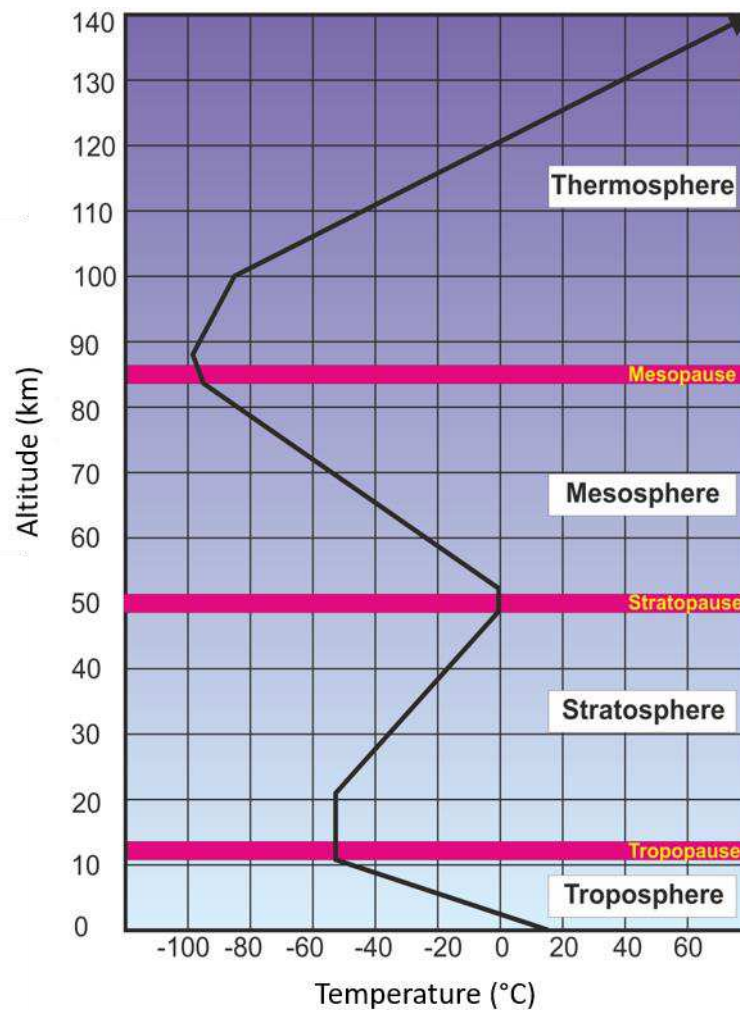


**Figure 2: Vertical temperature profile of the lower part of the atmosphere (surface of the Earth up to the lower thermosphere) (see e.g. Saha, 2008 p. 20) .**

The stratopause is followed by the mesosphere, which extends from ~50 km to ~85 km. Ozone heating diminishes in these altitudes, leading to a temperature drop throughout the mesosphere with increasing

altitude. This drop is so drastic that the mesopause is the coldest part of the atmosphere. This temperature profile leads to rapid vertical mixing. (Seinfeld & Pandis, 1998, p. 7; Salby, 2012 pp. 15f.)

The thermosphere occupies the region above the mesopause, starting at 85 km. The temperature of the thermosphere increases with increasing altitude due to the absorption of energetic solar radiation by N<sub>2</sub> and O<sub>2</sub> leading to a plasma of free electrons and ions. (Seinfeld & Pandis, 1998, p. 7; Salby, 2012, p. 5)

The outermost part of our atmosphere, the so-called exosphere, is situated above 500 km. This altitude is also known as the critical level. While at lower altitudes gas molecules collide frequently, a significant number of molecules that passes the exosphere do not experience a single collision. In most cases the gravitational field of the Earth is strong enough to pull the gas molecules back into denser parts of the atmosphere. However, molecules with sufficient velocities leave the atmosphere into space. (Salby, 2012, p. 12)

The major gaseous constituents of the atmosphere are nitrogen (78 %), oxygen (21 %), and argon (1 %). Though the atmosphere is constituted mainly of inert gases (at normal temperature), it is a potent oxidizing medium. This ability mainly derives from free radicals, which are present in very small concentrations. The most important in the troposphere is the hydroxyl radical (OH•), which reacts with nearly every molecular species present in the atmosphere. Further, several species that are less active than radicals, but still potent oxidizers are present in the atmosphere in trace amounts (e.g. ozone and nitrogen oxides). Major constituents with their concentration given as number fractions and average mixing ratios are given in Table 1. The average mixing ratios are given in ppm (parts per million), which is equivalent to μmol/mol. (Seinfeld & Pandis, 1998, pp. 19-23; Caballero, 2014, pp. 1-1)

**Table 1: Major constituents, their atmospheric number fractions in percent and average mixing ratio in ppm. Number fractions are given with respect to dry air (except for water vapour) (Seinfeld & Pandis, 1998, p. 22; Caballero, 2014, p. 1-1):**

<b>Constituent</b>	<b>Number Fraction (%)</b>	<b>Average Mixing ratio (ppm)</b>
Nitrogen (N <sub>2</sub> )	78	780,840
Oxygen (O <sub>2</sub> )	21	209,460
Argon (Ar)	1	9,340
Carbon dioxide (CO <sub>2</sub> )	0,04	355
Neon (Ne)	0,002	18
Helium (He)	0,0005	5.2
Methane (CH <sub>4</sub> )	0,0002	16
Krypton (Kr)	0,0001	1.1
Hydrogen (H <sub>2</sub> )	0,00006	0.6
Water vapour (H <sub>2</sub> O)	0-5	Variable
Ozone (O <sub>3</sub> )	0,00001	10 <sup>-2</sup> -10 <sup>-1</sup>

When looking at cloud formation, the most important molecular atmospheric constituent is water vapour. Number concentrations range from 0% to 5% depending on the location (higher values at the tropical Indian Ocean, lowest values at the surface of the big deserts). Its concentration also depends on altitude with highest concentrations near the surface of the Earth due to its major source being the oceans (with rivers, lakes, polar ice sheets and glaciers also playing a minor role). This atmospheric water can condense in liquid as well as in solid form in our atmosphere, which is a characteristic no other gaseous component achieves. Both, liquid water and ice crystals play a crucial role in clouds. (Wang, 2013, pp. 1f.)

## 1.2. An Introduction to Water and Freezing

Water is a triatomic, nonlinear molecule with an oxygen atom in its centre bonding to two hydrogen atoms. It has an angle of  $104.5^\circ$  and a bond length of the covalent bond between oxygen and hydrogen of  $0.957 \text{ \AA}$  (depicted in Figure 3). Oxygen and hydrogen differ strongly in their electronegativity. This leads to non-uniformity of the electron density and therefore to a dipole moment (1.85 Debye [D]). (Pruppbacher & Klett, 1997, pp. 74f.; Wang, 2013, pp. 68ff.)

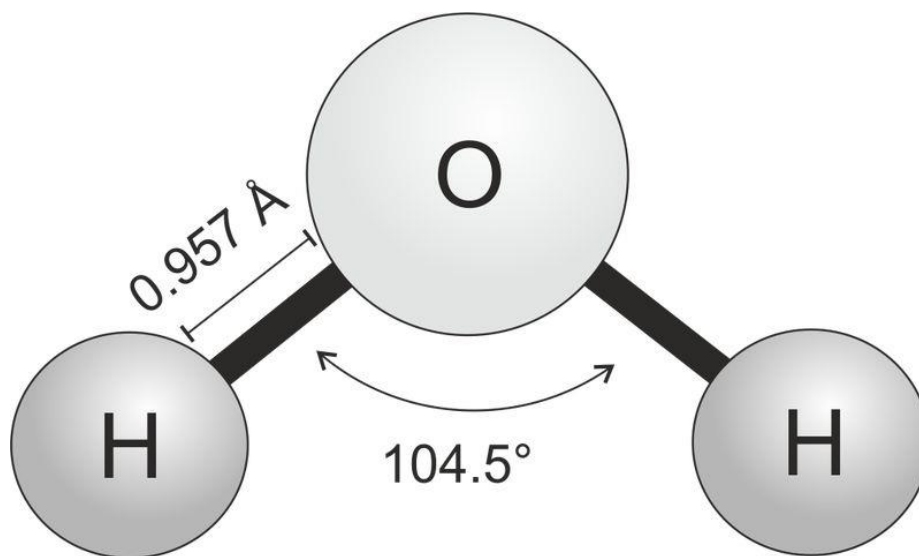


**Figure 3: Water molecule depicted with angle between the two hydrogen atoms and bond length. (Wang, 2013, p. 69)**

Water can be present in liquid, solid, and gaseous phase, which can transition into each other depending on the surrounding conditions. These phase properties are captured in the phase diagram (see Figure 4), which depicts the thermodynamically stable phases for given temperatures and pressures. These properties of water are a direct product of its molecular structure.

Regarding water in a phase, rather than a single molecule, it is easiest to start with water vapour, its gaseous state. A gas, if ideal, is defined by classical thermodynamics as a system with molecules not interacting with

each other, except during elastic collisions. Further movement and distribution follow a random fashion. However, since water exhibits a substantial dipole moment, it cannot be regarded as an ideal gas but as a real gas with attractive and repulsive interactions. The electrostatic dipole moment fosters interactions and leads to the formation of clusters (from dimers to higher ordered polymers, depending on the saturation) in the gas phase. (Pruppbacher & Klett, 1997 p. 77; Wang, 2013, p. 71)

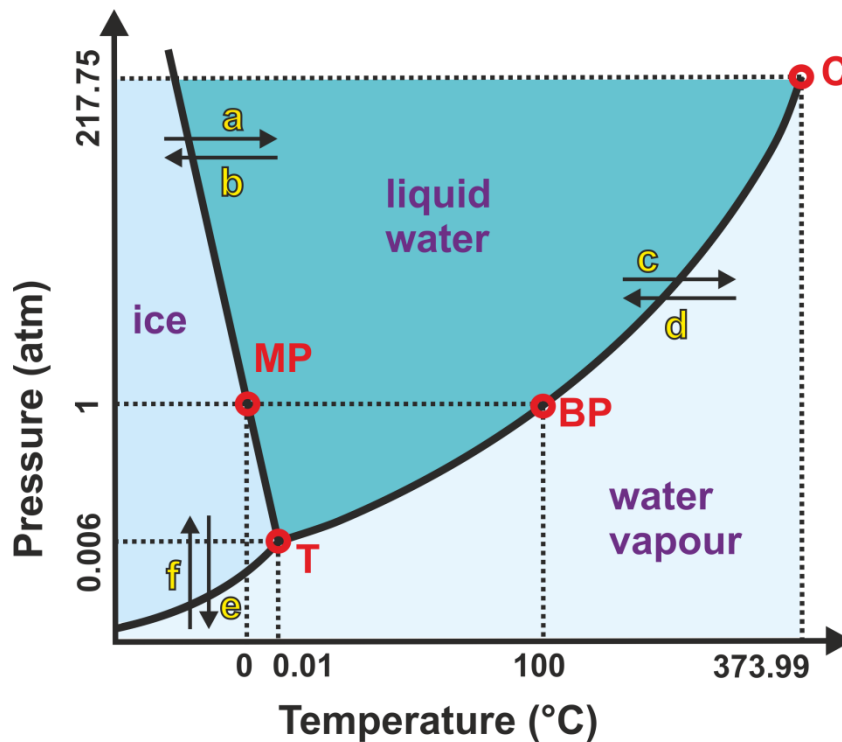


**Figure 4: Schematic of the phase diagram of water. The triplet point (T), the critical point (C), as well as boiling point (BP) and melting point (MP) at atmospheric pressure are marked in red. Phase transformations are indicated with arrows: (a) melting, (b) freezing, (c) evaporating, (d) condensation, (e) sublimation, and (f) deposition. #**

While the interaction in the gas phase are limited, with pressure determining the collision rate, liquid water is defined by interactions between molecules. Two main attracting forces exist between the molecules in a liquid phase. The first are dipole-dipole interactions. This force appears between polar molecules and is a result of electrostatic interactions between positive and negative charges. It depends highly on

the differences of the electronegativity of the atoms present in the involved molecule. The second force is the so-called van der Waals force, which is far weaker than the dipole-dipole interaction. As electrons are delocalized in orbital geometries, the charge of the electron cloud of a molecule shifts in space over time. This leads to the formation of short-lived, permanently changing dipole moments. These dipoles induce corresponding dipoles in neighbouring molecules which leads to an attracting force. The van der Waals force highly depends on the size of the molecules and the number of electrons (if size and number increase, the force increases). Van der Waals forces are the only attracting force between non-polar molecules, but are present between polar molecules as well. (Mortimer and Müller, 2003 pp. 165ff.)

Water molecules are quite small. They exhibit a density of about  $1 \text{ g cm}^{-3}$ . This density equals  $\sim 3 \cdot 10^{22}$  molecules per  $\text{cm}^3$ . The density is temperature dependent with its maximum at  $4^\circ\text{C}$  (as the water structure collapses at this temperature). Liquid water is dominated by fluctuating molecular interaction. Within the liquid phase, we find rather rapid movements. Water exhibits self-diffusion coefficients of  $D=2.3 \cdot 10^{-9} \text{ cm}^2 \text{ s}^{-1}$  for  $25^\circ\text{C}$ ,  $D=1.12 \cdot 10^{-9} \text{ cm}^2 \text{ s}^{-1}$  for  $2.65^\circ\text{C}$ , and  $D=0.158 \cdot 10^{-9} \text{ cm}^2 \text{ s}^{-1}$  for  $-35.35^\circ\text{C}$  (present as supercooled liquid) (Price, Ide and Arata, 1999). Further, water forms hydrogen bonds, a special form of dipole-dipole interactions. Hydrogen bonds are strong intermolecular electrostatic forces. This type of bond describes the interaction between hydrogen and (in case of water) the electronegative oxygen of a neighbouring molecule, which is weaker than a covalent bond, but stronger than the van der Waals force (Wang, 2013, pp. 70f.). Each water molecule can form four hydrogen bonds. These bonds play a minor role in the gas phase but are crucial in the liquid and solid phase. Water shows quite a wide range of anomalies in physical and chemical properties, i.e. behaviours that differ from most other fluids. Examples for



these anomalies are e.g. the high value for the critical vapour-liquid temperature or its expansion during crystallization. Many of these anomalies are directly linked to the formation of hydrogen bonds (Brovchenko and Oleinikova, 2008), showing just how crucial these bonds are for the properties of water as we know it. If water would be monitored on an extremely short time scale, one would observe a gel rather than a liquid, being held together by clusters of hydrogen bonds (Geru, 2014). However, individual hydrogen bonds have a quite short lifetime. Rotations and other thermal motions lead to the breakage and reformation of those bonds in the  $10^{-12}$ - $10^{-9}$  s time scale resulting in a constantly changing network of water molecules, with water clusters  $(\text{H}_2\text{O})_n$  differing in their stability (Geru, 2014).

Liquid phases will experience surface tension. The surface tension  $\sigma$  of a fluid is defined thermodynamically as energy per surface area:

$$\sigma = \frac{E_{sf}}{A} \quad (\text{Equation 1})$$

with  $E_{sf}$  as surface free energy, and  $A$  as total surface area. Since a system strives to achieve a state of minimum energy, it will try to minimize its surface area. The ideal shape for minimum surface area per volume is a sphere. Since the surface tension of water is rather small, it typically does not form perfect spheres (an example for a liquid forming perfect spheres is mercury). The surface tension of water is highly dependent on temperature and impurities. It decreases with temperature due to the increased thermal agitation of the water molecules. Impurities can have positive and negative effects depending on their chemical nature. There is a large variety of molecules, which act as so-called surfactants and reduce the surface tension. Inorganic salts on the other hand can have the opposite effect (e.g. sodium chloride). (Wang, 2013, p. 108f.)

Pruppbacher and Klett suggested the following formula for the relationship of temperature and surface tension between liquid water and water vapour ( $\sigma_{w,v}$ ):

$$\sigma_{w,v} = \sum_{n=0}^6 a_n T^n \quad (\text{Equation 2})$$

with the values:  $a_0=75.93$ ,  $a_1=0.115$ ,  $a_2=6.818 \cdot 10^{-2}$ ,  $a_3=6.511 \cdot 10^{-3}$ ,  $a_4=2.933 \cdot 10^{-4}$ ,  $a_5=6.283 \cdot 10^{-6}$ , and  $a_6=5.285 \cdot 10^{-8}$ ; with  $\sigma_{w,v}$  in  $\text{erg cm}^{-2}$  (erg is equivalent with  $10^{-7}$  J) and  $T$  (temperature in  $^{\circ}\text{C}$ ). This suggested extrapolation is applicable for temperatures above  $-40^{\circ}\text{C}$ .  $\sigma_{w,v} \approx \sigma$  (the surface tension between water and air) leading to values of  $\sigma \approx 75.93$   $\text{erg cm}^{-2}$  (for  $T=0^{\circ}\text{C}$ ) and  $\approx 88$   $\text{erg cm}^{-2}$  ( $T=-40^{\circ}\text{C}$ ). (Pruppbacher & Klett, 1997 p. 130; Khvorostyanov & Curry, 2014, p. 111)

When comparing bulk water with small water droplets, their thermal and chemical equilibrium are the same. However, the mechanical equilibrium of a small droplet differs from larger quantities of water, due to its curved surface. In the case of a water droplet being surrounded only by water vapour, the mechanical equilibrium of a water droplet can be expressed with the Young-Laplace equation:

$$\Delta p = \frac{2\sigma}{r} \quad (\text{Equation 3})$$

with  $\Delta p$  being the pressure jump across a spherical surface (or e.g. a meniscus in a capillary) with the radius  $r$ . (Pruppbacher & Klett, 1997, pp. 127f.; Wang, 2013, pp. 110f.)

To get a better idea about the equilibrium of two complex phases separated by a curved interface, one can use the generalized Clausius-Clapeyron equation:

$$-\frac{\Delta h}{T^2} dT + \frac{\Delta v}{T} dp' - \frac{v''}{T} d\left(\frac{2\sigma}{r}\right) + R d \ln\left(\frac{a'}{a''}\right) = 0 \quad (\text{Equation 4})$$

With  $h$  being the molar enthalpy,  $v$  the molar volume ( $v''$  being the molar volume of phase''),  $r$  the radius of the curvature,  $R$  the gas constant, and  $a$  the activity ( $a'$  the activity of phase' and  $a''$  the activity of phase''). The basic assumption for the here given equation is an aqueous solution droplet surrounded by a mixture of several gases with the condition that the system is in equilibrium and both phases form non-ideal solutions with several components (a non-ideal solution describes a system where the solvent and the solute interact). The first two terms arise from the conventional Clausius-Clapeyron equation, while the last two terms represent the curvature and solution effect. (Wang, 2013, pp. 116ff.; Khvorostyanov & Curry, 2014, p. 80)

When we consider the case of clouds, we have liquid water droplets surrounded by humid air. If we presume temperature and pressure to be constant while the equilibrium is achieved, and use the generalized Clausius-Clapeyron equation for the two phases, water (w) and vapour (v), we gain:

$$-\frac{v_w}{T} d\left(\frac{2\sigma}{r}\right) + R d \ln \left(\frac{a_w}{a_v}\right) \quad (\text{Equation 5})$$

If we consider the water phase pure,  $a_w=1$ . The gaseous phase is humid air and therefore has more than one component. Since the concentration of water vapour compared to dry air is quite small, we can assume an ideal system and neglect interactions. In this case the activity of vapour can be written as:

$$a_v \approx x_v = \frac{e_{sat,w}}{p} \quad (\text{Equation 6})$$

with  $x_v$  being the mole fraction of vapour,  $e_{sat,w}$  the saturation vapour pressure, and  $p$  the total pressure of the gas phase. Implementing this in the equation and integrating the equation from  $e_{sat,w} = e_{sat,\infty}$  (saturation

vapour pressure over a plane water surface) to  $e_{sat,w} = e_{sat,r}$  (saturation vapour pressure over a curved water surface) leads to:

$$e_{sat,r} = e_{sat,\infty} * e^{\frac{2v_w\sigma}{RT_r}} \quad (\text{Equation 7})$$

which is known as the Kelvin equation for saturation vapour pressure over curved liquid surfaces. (Wang, 2013, pp. 119f.)

For cloud droplets, the argument is always positive, so are the quantities of the exponential factor, which means, that the saturation vapour pressure over a droplet ( $e_{sat,r}$ ) is always greater than the saturation vapour pressure above a plane water surface ( $e_{sat,\infty}$ ). The relative humidity ( $RH$ ) is always given with respect to  $e_{sat,\infty}$ . Therefore, even environmental conditions of  $RH= 100\%$  are not enough to saturate a water droplet leading to the evaporation of the droplet. Yet it is observable that clouds can even survive relative humidities below 100%. This leads to the conclusion that a considerable amount of cloud droplets cannot consist of pure water alone. (Wang, 2013, p. 120)

If we want to understand the effect solutes have on the properties of a droplet, we can go back to Equation 7 and consider  $a_w \neq 1$ . Again we can substitute  $a_v$  with the molar fraction and integrate from  $e_{sat,w} = e_{sat,\infty}$  to  $e_{sat,w} = e_{sat,r}$  and from 1 to  $a_w$  leading to:

$$\frac{e_{sat,a}}{e_{sat,\infty}} = a_w e^{\frac{2v_w\sigma}{RT_r}} = a_w e^{\frac{2M_w\sigma}{RT\rho_w r}} \quad (\text{Equation 8})$$

which is a form of the Köhler equation, with  $M_w$  being the molar mass of water and  $\rho_w$  the molar bulk density. When we compare the consequences of the Köhler and the Kelvin equation, we can observe that in both cases, droplets grow indefinitely for very high relative humidities. However, for lower relative humidities, the Kelvin equation leads to the evaporation of the droplet, while the Köhler equation allows equilibria to be achieved,

depending on the solute and concentration, which can lead to the survival of the droplet. (Wang, 2013, p. 122f.; Khvorostyanov & Curry, 2014, p. 81f.)

Next to the influence on the saturation vapour pressure, solutes can have various other effects on the properties of water. An important one is freezing point depression:

$$\Delta T = E_G * b * i \quad (\text{Equation 9})$$

with  $E_G$  being the gyroscopic constant,  $b$  being the concentration of all solutes in mol kg<sup>-1</sup> and  $i$  being the van't Hoff-factor equalling the number of ions a molecule dissociates to (e.g. 2 for NaCl or 3 for K<sub>2</sub>SO<sub>4</sub>).  $E_G$  is a property of the solvent (in case of water it is -1.86°C kg mol<sup>-1</sup>), therefore this relation is based on the assumption that the freezing point depression is not dependent on the solvent itself, but only its concentration (a so-called colligative effect). This assumption works best for diluted samples. (Mortimer & Müller, 2003, pp. 214 ff.)

Water, of course, is also capable of interacting with solid phases. A water droplet in contact with a solid surface will spread depending on the wettability of the surface. This leads to a system with three phases (gas, liquid and solid). The angle between the surface and the water droplet is called contact angle (depicted in Figure 5) and can be determined by the equation:

$$\cos \theta = \frac{\sigma_{s,g} - \sigma_{l,s}}{\sigma_{l,g}} \quad (\text{Equation 10})$$

where  $\theta$  is the contact angle, and  $\sigma$  represents the interface energy between the different phases (s= solid, l= liquid, g= gaseous). (Wang, 2013, pp. 112f.)

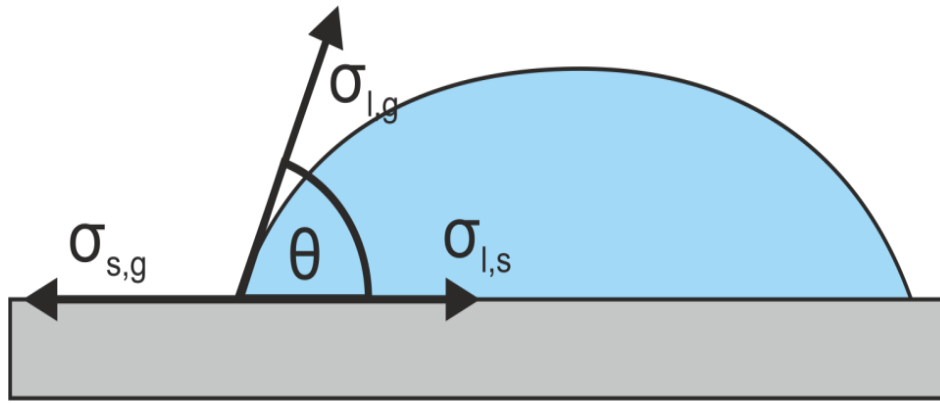


**Figure 5: Contact angle of a water droplet on a solid surface. The three  $\sigma$  represent the tension between the three different phases ( $s$ = solid,  $l$ = liquid,  $g$ = gaseous). The relation between the different tensions and the contact angle is given in equation 10. (Wang, 2013, pp. 113)**

When ice formation takes place, water undergoes a drastic change from the liquid phase, where water can move in many direction and ways, to the ice phase, consisting of a rather rigid crystalline structure. Ice is the thermodynamically stable aggregate state at temperatures of 0°C and below (at atmospheric pressure). Ice can be crystalline or amorphous. The most common ice structure is hexagonal ice, so called ice- $I_h$  (see Figure 6), which is stable from between 0°C and -80°C. Hexagonal ice is in Space group P63/mmc (194) with a  $D_{6h}$  symmetry and a six-fold screw axis<sup>5</sup>. Lattice constants of the unit sell are 4.5181 Å ( $a$ ) and 7.3560 Å ( $c$ ) (90°, 90°, 120°, 4 molecules, at 250 K)<sup>5</sup>.

At temperatures between -80°C and -100°C, the stable form of ice is cubic ice, so called ice- $I_c$ . Further, a stacking disordered ice is described in literature (ice- $I_{sd}$ ), consisting of both, hexagonal and cubic ice (Malkin *et al.*, 2012). In total, twelve types of crystalline ice structures are known (ice- $I_{sd}$  not included). However, most ice structures apart from cubic and hexagonal ice form under high-pressure conditions and therefore do not

<sup>5</sup> [http://www1.lsbu.ac.uk/water/hexagonal\\_ice.html](http://www1.lsbu.ac.uk/water/hexagonal_ice.html) (04.05.2019)

play a role in the atmosphere of the Earth. (Wang, 2013, pp. 73-81; Khvorostyanov & Curry, 2014, pp. 99ff.)

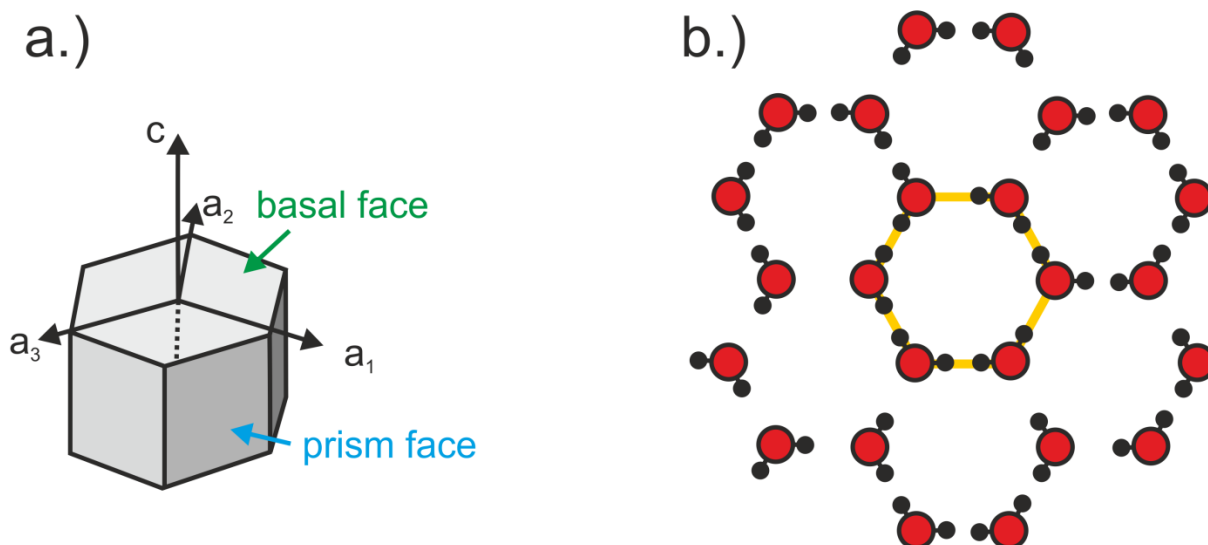


**Figure 6: Hexagonal ice ( $ice-I_h$ ): a.) crystallographic axes and faces. b.) view of the structure along the  $c$ -axis. The red spheres represent oxygen, hydrogen is marked black. The hexagonal structure is well visible along this axis and further marked with a yellow hexagon. (Wang, 2013, p. 74)**

Ice crystals usually exhibit steps on their surface due to dislocations in the crystal lattice. These steps vary in size with the smallest possible step being an elementary step which consists of only one layer of molecules. Further, ice crystals have a very specific surface feature called a quasi-liquid-layer (QLL). This property explains why two ice cubes will stick together, even at temperatures below  $0^\circ\text{C}$ . The thickness of the QLL decreases with decreasing temperature and increases with addition of salt. However, estimations of the actual thickness vary over two orders of magnitude. This could be due to a non-uniformity of the layer. It is the QLL that allows ice crystals in the atmosphere to interact with their environment as chemical properties differ from the solid ice lattice influencing interactions with e.g. trace gases. (Wang, 2013, pp. 127ff.)

If ice is formed by self-assembly of water molecules, without foreign substances interfering in the process, it is called homogeneous ice

nucleation. To achieve this, the water molecules must rearrange themselves into the crystalline ice structure. The water molecules in the liquid phase are already in contact, however, the formation of the new phase, not just requires the breakage of water-to-water-bonds but also the formation of water-to-ice bonds. Hereby a water molecule must transit from one equilibrium position, exhibiting a minimum potential energy, to a new equilibrium position. In order to do so it needs to overcome an energy barrier. One would expect water to freeze at 0°C, since hexagonal ice (the most common crystalline structure under atmospheric conditions) is the thermodynamically favoured aggregate state at this temperature. However, the energy barrier must be overcome and therefore the process is kinetically controlled. The result is a metastable state, which typically does not transition to stable states directly at equilibrium. In the case of water, the metastable phase between thermodynamically stable liquid water and ice is supercooled liquid water. (Pruppbacher & Klett, 1997, p.305f.; Khvorostyanov & Curry, 2014, p.289, p.300)

Due to fluctuations caused by thermal vibrations inside supercooled water, small clusters of ice (so called embryos) are formed. Below a critical size, these clusters will directly decay again due to their energetically unfavourable ratio of surface to bulk. However, as temperatures decrease, the ice phase is more and more favoured, leading to smaller ice embryos, needed to initiate stable ice growth. For example at -5°C, an embryo needs to consist of 45,000 molecules to grow stably, while at -40°C only 70 molecules are necessary (Zachariassen and Kristiansen, 2000). As soon as this size is reached, the phase transition can occur and the droplet freezes. In the atmosphere, droplets are known to supercool down to temperatures as low as -37°C (Murray *et al.*, 2010). (Wang, 2013, pp.158ff.; Khvorostyanov and Curry, 2014, pp. 290ff.)



Homogeneous freezing is a stochastic process; therefore, time plays a vital role. The crystallization of pure water starts in the subsurface of the water bulk (Vrbka and Jungwirth, 2006) and is strongly dependent on the used volume (Bigg, 1953) due to its stochastic nature. When observing small water clusters of a few thousand molecules, they will not crystallize into ice-I<sub>h</sub> but will rather form the kinetically favoured cubic structure ice-I<sub>c</sub> (Huang and Bartell, 1995). The same behaviour has also been observed for small droplets in the low micrometre size range (Murray, Knopf and Bertram, 2005; Murray and Bertram, 2006). This ice shows stacking disorders (with ice-I<sub>h</sub>). The stacking disorders increase in number as the droplet size increases (Murray and Bertram, 2006). Crystals in a size range <2µm will instantly lose any heat produced by crystallization. This is not true for bigger droplets. Their released heat allows the cubic ice to re-crystallize into the hexagonal structure (Murray *et al.*, 2010). However, measurements on droplets in a larger size range suggested that ice-I<sub>c</sub> is always the initial ice phase crystallizing homogeneously (Murray and Bertram, 2006, 2008).

To describe the freezing process, one can use the classical nucleation theory (CNT)(embryos are assumed spherical in this approach) (Ickes *et al.*, 2015):

$$\Delta G = 4\pi r^2 \sigma_{iw}(T) - \frac{4\pi r^3 k_B T \ln S_i}{3v_{ice}(T)} \quad (\text{Equation 11})$$

where  $r$  is the radius of the embryo,  $\sigma_{iw}$  the interfacial tension at the ice/water interface,  $k_B$  the Boltzmann constant,  $S_i$  the ratio between of the saturation vapour pressure over the two phases, and  $v_{ice}$  the volume of a water molecule in an embryo.

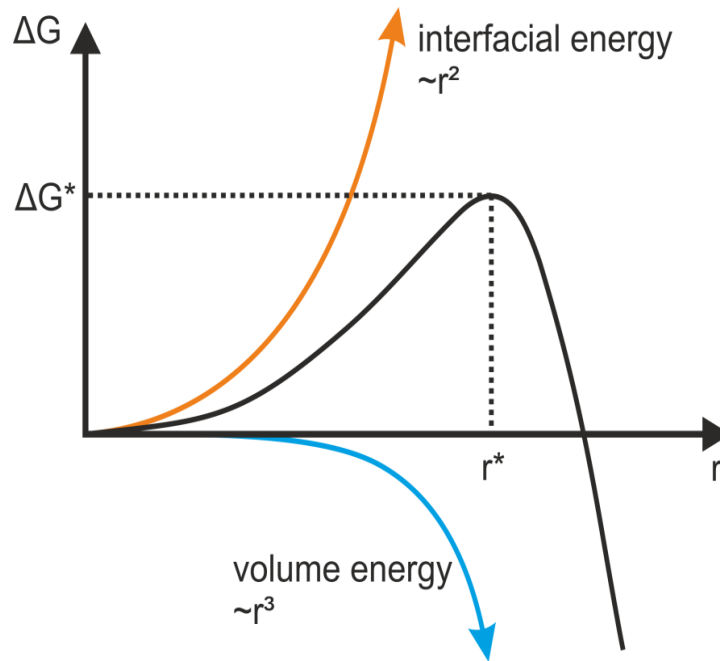


**Figure 7: The Gibbs free energy as function of radius, resulting from an interface and a volume term which is given by the classical nucleation theory.**

The formula can be divided in an interfacial (marked as orange) and a volume term (marked in blue). The resulting curve is depicted in black in Figure 7. For small radii the surface term dominates the resulting curve. Since work has to be done to create a new surface, the surface term is positive, leading to an increase in  $\Delta G$  with increasing radius (Ten Wolde and Frenkel, 1999). When the Gibbs free energy is increasing, embryos would need additional energy to grow. Therefore, growth does not happen in that regime of the curve. However, the curve has a maximum Gibbs free energy at a critical cluster radius ( $r^*$ ). From there on, there volume term, which is proportional to  $r^3$  outweighs the surface term, which grew slower, since it is proportional to  $r^2$ . Thus, after the maximum, the Gibbs free energy decreases again, and embryos can experience stable growth. Therefore, it is called critical Gibbs free energy ( $\Delta G^*$ ). Since the critical radius corresponds to the maximum  $\Delta G$ , it can be determined, resulting in (Ickes *et al.*, 2015):

$$r^* = \frac{2v_{ice}\sigma_{iw}}{k_B T \ln S_i} \quad (\text{Equation 12})$$

If the critical radius is included in the formula for the Gibbs free energy, it results in the critical Gibbs free energy ( $\Delta G^*$ ) (Ickes *et al.*, 2015):

$$\Delta G^* = \frac{16\pi v_{ice}^2 \sigma_{iw}^3}{3(k_B T \ln S_i)^2} \quad (\text{Equation 13})$$

An important tool to describe homogeneous nucleation is the nucleation rate coefficient  $J_{hom}$ . It depends on temperature and droplet size (Dorsch and Hacker, 1950; Levine, 1950; Bigg, 1953) as well as on time, i.e. the cooling rate (Bigg, 1953; Vali and Stansbury, 1966; Krämer *et al.*, 1999). Therefore stochastic freezing behaves as 1<sup>st</sup> order chemical kinetics with the nucleation rate as a function of temperature (Murray *et al.*, 2012). Using the Arrhenius form and our knowledge from CNT, one can define the nucleation rate coefficient  $J_{hom}$  (Murray *et al.*, 2012):

$$J_{hom} = A * e^{\left(\frac{-\Delta G^*}{kT}\right)} \quad (\text{Equation 14a})$$

$$\ln(J_{hom}) = \ln A - \frac{16\pi v_{ice}^2 \sigma_{iw}^3}{3k_B^3 3T^3 (\ln S_i)^2} \quad (J_{hom} = A * e^{\left(\frac{-\Delta G^*}{kT}\right)}) \quad (\text{Equation 14b})$$

Since  $J_{hom}$  is the number of nucleation events per unit volume and unit time, it is widely used to evaluate experimental data using the form (Huang and Bartell, 1995; Murray *et al.*, 2010):

$$J_{hom} = -\ln\left(\frac{1-f_{ice}}{V*t}\right) \quad (\text{Equation 15})$$

with  $V$  being the droplet volume,  $t$  the observation time, and  $f_{ice}$  being the frozen fraction:

$$f_{ice} = \frac{n_{frozen}}{n_{total}} \quad (\text{Equation 16})$$

Here,  $n_{total}$  is the total number of droplets and  $n_{frozen}$  is the number of homogeneously frozen droplets.

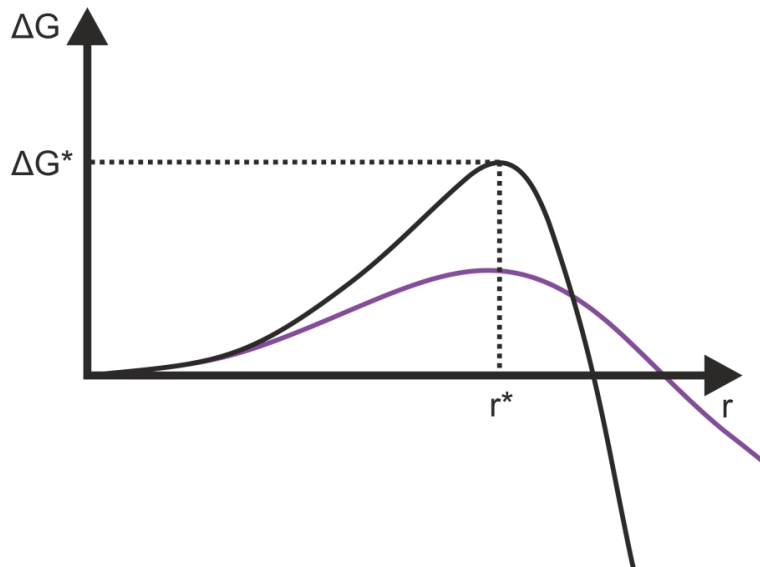


**Figure 8: Gibbs free energy as function of the embryo radius. The black curve corresponds to homogeneous freezing; the violet curve corresponds to heterogeneous freezing.**

Homogeneous freezing is a process of stochastic nature. This must be considered in the measurement method. In order to gain accurate results, the number of observed droplets must fulfil certain requirements.

As discussed before, cloud droplets, which are supercooled below  $-36\text{ }^\circ\text{C}$ , can freeze homogeneously in the atmosphere. Various substances are known that can trigger freezing at higher temperatures, so called ice nucleating particles (INPs). If freezing is initiated by a foreign substance, it is no longer homogeneous, but heterogeneous freezing. A graphic depiction of the influence of an INP on the Gibbs free energy is shown in Figure 8. The height of the maximum and therefore the critical Gibbs free energy is drastically reduced.

Four different theoretical modes of primary heterogeneous ice nucleation are defined (see Figure 9) (Wang, 2013, p. 174):

- Immersion and condensation freezing

The INP is immersed in the liquid droplet prior freezing. In the case of immersion mode, the nucleus does not act as a CCN (cloud condensation nuclei – particle that allows water to condensate on its surface) for the droplet it is immersed in. Condensation freezing on the other hand describes freezing triggered by INPs that act as CCN and initiated the cloud droplet.

- Contact freezing

The INP initiates freezing upon colliding with a supercooled droplet

- Deposition freezing

Water vapour deposits directly as ice on the INP and does not undergo a transition into the liquid phase.

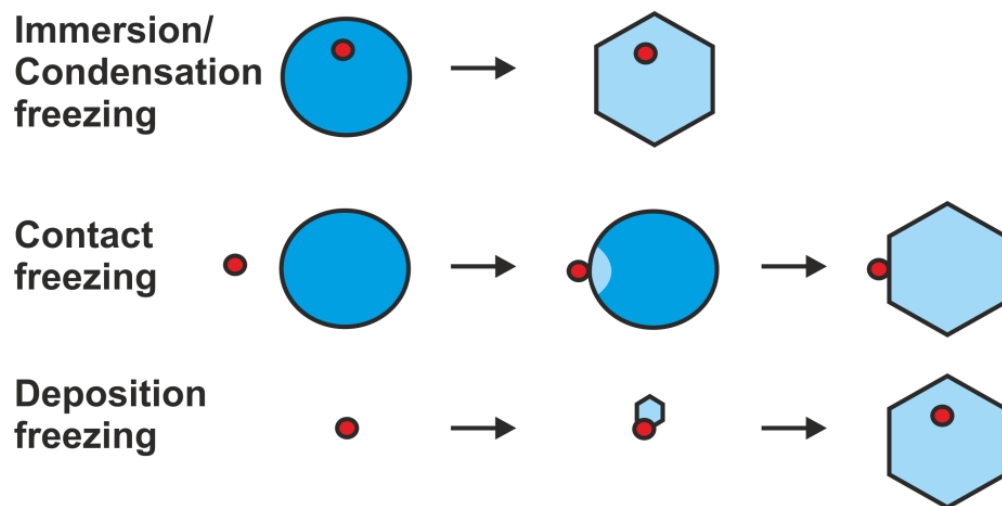


**Figure 9: Schematic depiction of immersion, contact, and deposition freezing.**

Further, two effects of secondary ice nucleation and growth (ice nucleation and growth due to other ice particles) are important in the atmosphere:

- Hallet-Mossop effect

Hallet and Mossop were able to show that ice crystals grow in the atmosphere by rimming (growth by collision of supercooled droplets with ice crystals) at approx.  $-5\text{ }^{\circ}\text{C}$  can throw off little ice splinters.

These splinters can act as INPs if colliding with surrounding supercooled droplets. (Hallett and Mossop, 1974)

- Bergeron–Findeisen process

Ice crystals grow on cost of neighbouring liquid droplets communicating over the gas phase, due to the reduced vapour pressure over ice particles compared to liquid droplets. (Findeisen, 1938)

Heterogeneous ice nucleation can be described singular or stochastic. The stochastic description uses the nucleation rate coefficient, which was introduced for homogeneous ice nucleation in equation 14a. Contrary to the homogeneous nucleation rate coefficient, the heterogeneous nucleation rate coefficient is independent of volume but depends on the contact area between water and the nucleus ( $\sigma_{i,w}$  [cm<sup>2</sup>]) and therefore the amount and surface area of the ice nucleation active substance in the droplet (Iannone *et al.*, 2011; Murray *et al.*, 2011). A small and a large droplet containing one nucleus each will freeze at the same temperature (Hartmann *et al.*, 2016). However, if the nuclei are evenly distributed in the liquid, a larger droplet will still contain more INPs than a smaller droplet containing the same concentration and therefore freeze statistically at higher temperatures. This leads to a pseudo-dependence of the heterogeneous nucleation rate coefficient on the droplet volume. For an even distribution of the INPs throughout the sample as in this case,  $\sigma_{i,w}$  can therefore be replaced by the droplet volume  $V$ . This leads to  $J_{hom}$  and the heterogeneous freezing homologue  $J_{het}$  having the same unit [cm<sup>-3</sup>s<sup>-1</sup>]. To describe stochastic freezing properties, classical nucleation theory (CNT) is often used to derive a contact angle for INPs from experimental data (e.g. Chen *et al.*, 2008; Wang & Knopf, 2011).

The second possible description for heterogeneous ice nuclei is the singular description. Each ice nucleation active substance triggers specific

freezing temperatures (Levine, 1950; Langham and Mason, 1958). In a mixture, the freezing temperature depends on the substance with the highest INA – Ice Nucleation Activity (Levine, 1950). One approach to describe these characteristics is the singular model, which neglects the time dependence and focusses on the specifics of nucleation sites (Vali, 1971, 1994; Murray *et al.*, 2012). A plot showing percentage of droplets frozen as a function of temperature can be interpreted as a cumulative nucleus spectrum, with the cumulative nucleus concentration  $K(T)$  [ $\text{cm}^{-3}$ ].  $K(T)$  indicates the number of all ice nucleation active particles or molecules active at temperatures above  $T$  and can be described as (Vali, 1971, 2019; Murray *et al.*, 2012):

$$K(T) = \frac{\ln(1-f_{ice})}{v} \quad (\text{Equation 17})$$

Stochastic and singular approach differ in their basic concept. The stochastic concept on one hand is based on time-dependency, while the singular model on the other hand, focusses on the active sites of INPs (Ervens and Feingold, 2012; Vali, 2014). Singular freezing experiments, which are often used in ice nucleation research (e.g. Connolly *et al.*, 2009; Crawford *et al.*, 2012; Wheeler & Bertram, 2012) only capture the initial freezing for each temperature of supersaturation. However, a number of experiments and models contradict the singular view (e.g. Kulkarni & Dobbie, 2010; Welti *et al.*, 2012; Wright & Petters, 2013; Alpert & Knopf, 2016). If freezing occurs rather rapid, time dependence might be negligible (Vali, 1971, 2008; Wright and Petters, 2013). One new approach to battle this problem is the soccer ball model (Niedermeier *et al.*, 2011). In this model, particles are assumed as being covered with different surface sites exhibiting different energy barriers, each following the stochastic rules of ice embryo formation (Niedermeier *et al.*, 2011).

As discussed in Section 1.3, glaciation of clouds can impact the terrestrial albedo and local climatic conditions. Therefore, knowledge about INPs and their presence in the atmosphere is important. INPs are found ubiquitously throughout different aerosol species. However, ice nucleation active material only represents a small part of total atmospheric aerosol. Typical total aerosol concentrations range between  $10^2 \text{ cm}^{-3}$  and  $10^3 \text{ cm}^{-3}$  for free troposphere and marine boundary layer concentrations and between  $10^2 \text{ cm}^{-3}$  and  $10^4 \text{ cm}^{-3}$  for continental boundary layer concentrations (Spracklen *et al.*, 2010). INP concentrations are much lower and range between  $10^{-1} \text{ cm}^{-3}$  and  $10^{-4} \text{ cm}^{-3}$  (Rogers *et al.*, 1998; DeMott *et al.*, 2010).

Many different substances, which differ widely in their size, origin, and chemical composition, have already been shown to act as INPs. Many of these substances are of biological origin, which will be discussed in Section 1.5. Also, several mineral dusts are ice nucleation active (e.g. Möhler *et al.*, 2006; Eastwood *et al.*, 2008; Zimmermann *et al.*, 2008), as e.g. *illite* (Hoffer, 1961), which is the most common mineral type in the atmosphere. The exact mechanism of ice nucleation activity of mineral dusts is unknown, however, surface irregularities and defects like steps, cracks, or cavities could play a crucial role in this process (Kulkarni and Dobbie, 2010; Zolles *et al.*, 2015; Kiselev *et al.*, 2017).

Soot can act as INP (e.g. DeMott, 1990; Gorbunov *et al.*, 2001; Popovicheva *et al.*, 2008). Since soot is not a uniform substance but covers a rather large range of different sizes, morphologies, and surface chemistry (functional groups and their arrangements), its ice nucleation activity also exhibits non-uniformity, depending on size, surface area and concentration of surface groups (Gorbunov *et al.*, 2001). Some studies suggest no effect of ozone oxidation (Dymarska *et al.*, 2006; Friedman *et al.*, 2011), however Brooks *et al.* (2014) observed the opposite effect.



Fresh soot is highly hydrophobic. Aging decreases this property. In theory, aging should increase the ice nucleation activity due to the better interaction with water; however, highly polar compounds on the surface could get dissolved in water, possibly leading to a decrease in the potential ice nucleation activity (Popovicheva *et al.*, 2008). Using graphene as proxy for soot, Häusler *et al.* (2018) found that the lattice order impacts the INA. Further, they were able to show that the number of functional sites and thus the surface hydrophilicity affects the influence on ice formation.

Another INP with possible atmospheric importance is volcanic ash. Durant *et al.* (2008) suggested, based on their review, typical initial freezing temperatures for fine particles (1-1000  $\mu\text{m}$  in diameter) of  $-13\text{ }^{\circ}\text{C}$  to  $-23\text{ }^{\circ}\text{C}$ . This matches more recent data for ash from the Eyjafjallajökull eruption in 2010 (Hoyle *et al.*, 2011). Smaller particles seem to induce lower freezing temperatures (Steinke *et al.*, 2011). The ash plume of the Eyjafjallajökull eruption impacted continental European aerosols, increasing the INP concentration over Germany even more drastically than intense Saharan dust events (Bingemer *et al.*, 2012). The active fraction and surface site density of the ash collected over Germany were higher than of the fresh aerosolized ash, collected at the eruption site, indicating that long range transport and atmospheric aging processes highly impact the ice nucleation activity of volcanic ash (Bingemer *et al.*, 2012).

### 1.3. Clouds and Aerosols

Clouds impact the Earth's climate. They are capable to scatter, diffract and reflect radiation. The global energy budget (depicted in Figure 10) describes the heat and radiation flows to and from the Earth. Clouds interfere in these processes in various ways. These interferences depend on several factors. One of the factors is the microphysical state of the cloud. Ice clouds tend to reflect a higher ratio of the incoming radiation back into the space compared to liquid clouds hence increasing the planetary albedo (Mishchenko et al., 1996) and therefore reducing the amount of radiation that can be converted into heat (see Figure 10 and Figure 11). However, cirrus clouds, which are typically high ice clouds, do not just reflect incoming solar radiation, but also trap outgoing longwave radiation, whereby the latter effect is expected to overweight in thin cirrus clouds (aircrafts produce thin cirrus clouds in the upper troposphere as contrails) (Forster et al., 2007).

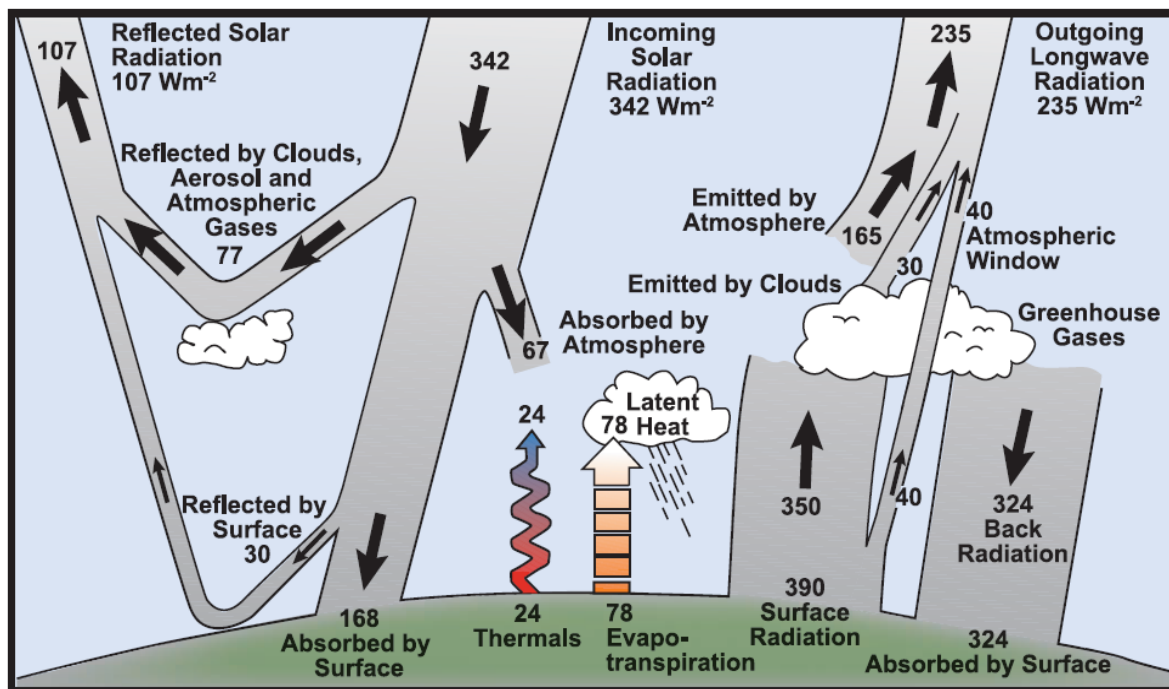
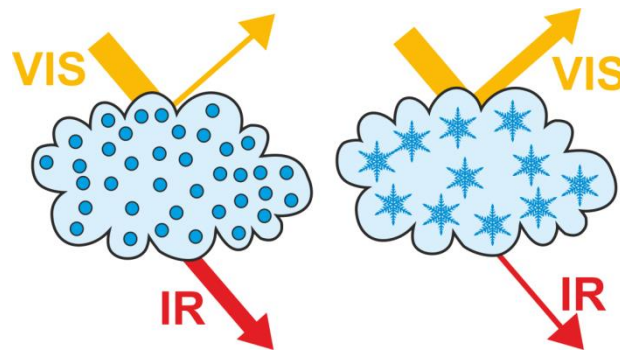


Figure 10: Annual global mean energy budget of the Earth (Units are  $\text{W m}^{-2}$ ) taken from the IPCC (Intergovernmental Panel on Climate Change) report 2007 (Le Treut et al., 2007 original source: Kiehl & Trenberth, 1997).

Aerosols describe small particles or droplets, which are suspended in air. Atmospheric aerosol plays an important role in cloud formation, as it can act as CCN or INP (depending on the particle itself). Only small particles can exhibit a larger atmospheric lifespan, since bigger particles will just sediment and deposit due to gravitation. Aerosol size is typically given as aerodynamic diameter, to compensate the wide array of different shapes and densities. The aerodynamic diameter is the diameter of a sphere with a density of  $1 \text{ g/cm}^3$  with the same floating behaviour as the regarded particle. Aerosols can be divided in nuclei mode ( $d < 0.1 \text{ }\mu\text{m}$ ), accumulation mode ( $0.1 \leq d \leq 2.5 \text{ }\mu\text{m}$ ) and coarse mode ( $d > 2.5 \text{ }\mu\text{m}$ ). Most aerosol particles are distinctively smaller than a cloud droplet and are easily manipulated by other particles and gaseous molecules leading to coagulation and aging. Aerosol concentrations vary widely with location. This is not just true for different sampling sites near the surface, but also when the concentrations are regarded depending on height, with a maximum typically close to the surface. (Wang, 2013, pp. 134-141)



**Figure 11: Different interactions with radiation (VIS= visible spectrum, IR= infrared radiation) of clouds consisting of liquid droplets (left) and ice crystals (right).**

In a very clean environment, the vapour pressure of water can exceed supersaturation (a state at which more water molecules are present in the gas phase as under normal conditions) without condensing into droplets. In order to do so, suitable particles (CCN) need to be present that provide a surface on which the vapour can condense. CCN can work in various

ways. One example for a CCN is sea salt. From the Köhler equation (Equation 8), we learn that pure water droplets will not survive in the atmosphere, even in an RH (relative humidity) of 100%. Further, ice crystals can form INPs are present (see Section 1.3).

Clouds consist of a large ensemble of small droplets or ice crystals suspended in air. They are formed by deposition or condensation of atmospheric water vapour. The formation of clouds depends on the relative humidity, which can be understood as a degree of water vapour saturation. It indicates the likeliness of condensation. Most cloud formation processes happen in the troposphere, which contains more than 99% of the atmospheric water vapour. Clouds can also form in the stratosphere, so called nacreous clouds. However, these clouds typically do not consist of pure water but rather of sulfuric or nitric acid aerosol particles. Since they are typically common in the stratosphere of the Polar Regions, they are often referred to as polar stratospheric clouds (PSCs). Further, so-called noctilucent clouds can form in the mesosphere. Noctiluent (night-glowing) refers to their bright appearance even during the night. This derives from the high altitude, where the sun is still shining after nightfall at the Earth's surface. (Wang, 2013, pp. 1ff.)

Clouds can be classified by altitude of their appearance into four groups, containing 10 different cloud families in total, which exhibit subtypes that will not be discussed here (Wang, 2013, pp. 5ff.; Khvorostyanov & Curry, 2014, pp. 10 ff.):

- High clouds:

High clouds form at a base height of 6 km or higher at temperatures which are typically below  $-40^{\circ}\text{C}$ . They generally consist of ice crystals of various forms. Since they are usually optically thin, they allow sun or moonlight to shine through them. Due to the ability of the contained ice crystals to refract light, high clouds can produce

halos. High clouds can be differentiated into three forms, cirrus (Ci), cirrocumulus (Cc), and cirrostratus clouds (Cs). Cirrus clouds show a hair-like filamentous structure, typically with curly edges. Cirrocumulus clouds exhibit a fish-scale-like structure with merged or separated elements in forms of grains or ripples. Their thickness is typically between 0.2 km and 0.4 km. Cirrostratus clouds consist of a layer that is transparent whitish in colour and can cover the sky partially or completely. Their thickness ranges between 0.1 km and 3 km.

Condensation contrails of planes typically act like cirrus clouds. They can influence the local climate in regions with heavy air traffic (Schumann, 1994).

- Middle clouds:

These clouds form at altitudes between 2 km and 6 km. They typically consist of water droplets or a mixture of water droplets and ice crystals, and can be divided into two groups, altostratus (As) and altocumulus clouds (Ac). altostratus clouds consist of a greyish to blueish sheet or layer of about 1 km thickness, while altocumulus clouds consist of white and grey patches, sheets, or layers.

- Low clouds:

Low clouds exhibit a base height below 2 km and mainly consist of liquid droplets, though they can contain ice crystals at cold conditions. They can be divided into three groups, stratus (St), stratocumulus (Sc), and nimbostratus clouds (Ns). Stratus and stratocumulus are typically associated with light rain fall or no rain at all, while nimbostratus (prefix *nimbo* meaning rain) is always associated with rain. Stratocumulus clouds have a chunky structure, while stratus and nimbostratus clouds are more continuous horizontally. Nimbostratus clouds exhibit a more diffuse appearance than stratus clouds.

- Clouds with vertical development:

This family contains the cumulus (Cu) and the cumulonimbus clouds (Cb). Both need relative strong updrafts to form. Cumulus clouds are typically white at their sunlit parts, with greyish, blueish bottoms. They are detached with sharp outlines. While cumulus clouds typically appear flattened, cumulonimbus clouds show a harsh vertical extend. Their top is usually flattened and tends to spread out. Cumulonimbus clouds produce heavy precipitation.

- Fog:

In general, fog is not considered a cloud. However, just as clouds, it consists of small water droplets or sometimes ice crystals, which are suspended in atmosphere. The vertical extend of fog typically ranges between a few and a couple of hundred meters.

## 1.4. Freezing and Anti-Freezing in Nature

Planet Earth is a rather cold place, with the vast majority of the water in our oceans exhibiting temperatures below 5°C. On the land, temperatures can get even colder. In the colder climatic zones, winter temperatures can easily drop as low as -30 to -70 °C. However, life prevails in all in all parts of our world, with organisms coping with the cold in different ways, some of which even in need of the cold to thrive. However, freezing still poses a challenge to life. Coping strategies to avoid freezing can be divided in four categories (Storey and Storey, 2004):

- Migration  
Migration distances are species dependant. While species like birds and butterflies travel long distances to reach warmer climatic regions, other species, e.g. frogs, migrate only short distances. Short distance migration is often used in order to achieve insulation.
- Insulation  
Insulation can depend on the environment. Some toads for example, burry themselves in the ground. Further, insulation can be an individual trait, manifesting itself by thicker fur, down feathers, or layers of body fat.
- Thermogenesis  
Endotherms are capable of maintaining their core body temperature via thermogenesis. Body fat plays a crucial role in this strategy.
- Development of cold hardiness  
Ectotherms are incapable of using thermogenesis as a strategy and therefore have to develop other coping mechanisms. These organisms developed several strategies to avoid or cope with freezing. Cold hardiness is often only developed in winter or coupled to a specific life stage of the organism (e.g. egg, spore, seed, etc.).

For most organisms, freezing is typically a lethal process causing several severe changes. Especially intracellular ice formation is fatal. Only a small number of organisms is known to survive this process, e.g. *Panagrolaimus davidi*, a nematode (Wharton and Ferns, 1995). However, intercellular ice formation is rarely the initial formation site for ice. In nature as well as laboratory studies, freezing typically starts in the extracellular spaces. To further protect cells from damage ice growth is generally propagated through this extracellular and extraorgan spaces. Ice will typically not propagate into cells, as long as the membrane is intact. However, extracellular ice can be just as dangerous for an organism as intercellular ice formation. It can lead to several severe injuries like rupture of capillaries. Further, extracellular ice changes the osmotic pressure in the cell and typically leads to a loss of most of the free water, which causes changes in e.g. pH value, ionic strength, or protein structure. Many of the initiated changes can have lethal consequences for the cells if severe enough. Further, cells, which were severely dehydrated, can rupture if the rehydration process upon thawing happens too quickly. However, if the solute concentration in a cell is high enough, the contained water will vitrify rather than crystallize in case of intracellular ice formation (Hirsh, Williams and Merymen, 1985), minimizing the physical damage done due to freezing. (Storey and Storey, 2004)

Freezing can be avoided or restricted by low molecular weight molecules (like polyhydric alcohols and saccharides) via colligative effects. The used substances vary widely between different organisms. Concentrations, which can exhibit a seasonal dependency, are often as high as 0.2-2 M or even higher. Further, for anhydrobiotic organisms, these substances can substitute hydration shells and therefore stabilize protein conformation (Storey and Storey, 2004). (Storey, 1997)



Other important tools inhibiting ice growth are antifreeze-proteins (AFPs), which do not function in a colligative manner, but rather work via absorption on the ice surface. Though all AFPs work with the same principle, their chemistry and structure vary. However, this effect is limited and when temperatures drop low enough, rapid freezing takes place. The caused displacement between freezing and thawing is called *thermal hysteresis* (Kristiansen and Zachariassen, 2005). Antifreeze proteins have been found in a wide range of overwintering plants, where they not just inhibit ice growth but are important in inhibiting the recrystallization of ice. With their multiple hydrophilic ice binding sites, these proteins are quite unusual compared to most known AFPs (mostly from insects and fish), which are dominated by hydrophobic ice binding sites. In plants they do not impact the lethal temperature strongly, suggesting that their role is more focused on the recrystallization inhibition. Interestingly, most AFPs from plants seem to be modified pathogen related proteins, rendering them excellent models for evolutionary studies. (Griffith and Yaish, 2004)

Most freeze-tolerant organisms contain ice nucleating agents. These agents promote freezing in the extracellular spaces at rather mild temperatures, to avoid excessive supercooling and ensure a slow freezing process. These agents can be specifically evolved for this purpose, but can also other agents present inside the organisms or on its surface or in its surrounding environment. While species specialized on freeze avoidance have several mechanisms to exclude the influence of such agents, freeze tolerant species exploit them. An example for the exploitation of a foreign substance is the tree *Lobelia telekii*, growing on the Mt. Kenya. The tree has a huge reservoir filled with liquid that freezes when temperatures drop below 0°C because it contains highly potent bacterial INPs (Zachariassen and Kristiansen, 2000). The tree uses the heat released during freezing for protection of its more vulnerable parts, indicating that plant and

bacteria live in symbiosis (Zachariassen and Kristiansen, 2000). (Storey and Storey, 2004)

To reduce damage, many organisms use membrane protectants. Membrane protectants protect the structural integrity of the membrane via stabilizing the bilayer structure as the osmotic pressure rises causing compression stress. To prevent the cell volume from falling to a critical minimum, low molecular weight cryoprotectants are used, to increase the osmolality of the cell. The concentration of these cryoprotectants in freeze tolerant organisms is lower than in freeze avoiding organisms, but due to the water loss during ice formation, will rise to 1 M or more (if the frozen fraction exceeds 65% of total water). (Storey and Storey, 2004)

A schematic depiction of protected and unprotected freezing in the extracellular spaces is given in Figure 12.

If freezing occurs in plants, it can have lethal consequences as in most other organisms (Mazur, 1969; Burke *et al.*, 1976; Pearce, 2001). Therefore plants, as all other organisms, had to develop coping mechanisms if they want to thrive under cold climatic conditions. The use of ice nucleating agents is a well-known strategy for plants (Burke *et al.*, 1976; Pearce, 2001). As all other organisms, plants using this strategy will try to minimize damage and use mild freezing temperatures to prevent rapid ice formation or intercellular freezing caused by deep super cooling. However, multiple freeze-thaw cycles can seriously harm a plant by bubble formation leading to cavitation (Sperry and Sullivan, 1992). This cavitation leads to small conduits consisting of water vapour or air, reducing the ability of water transport in the Xylem and, if severe enough, limit growth (Schultz and Matthews, 1988). Therefore, many plants freeze at moderate temperatures, high enough to hinder intercellular ice formation, but low enough to not produce a high number of freeze-thaw cycles due to e.g. night frost.

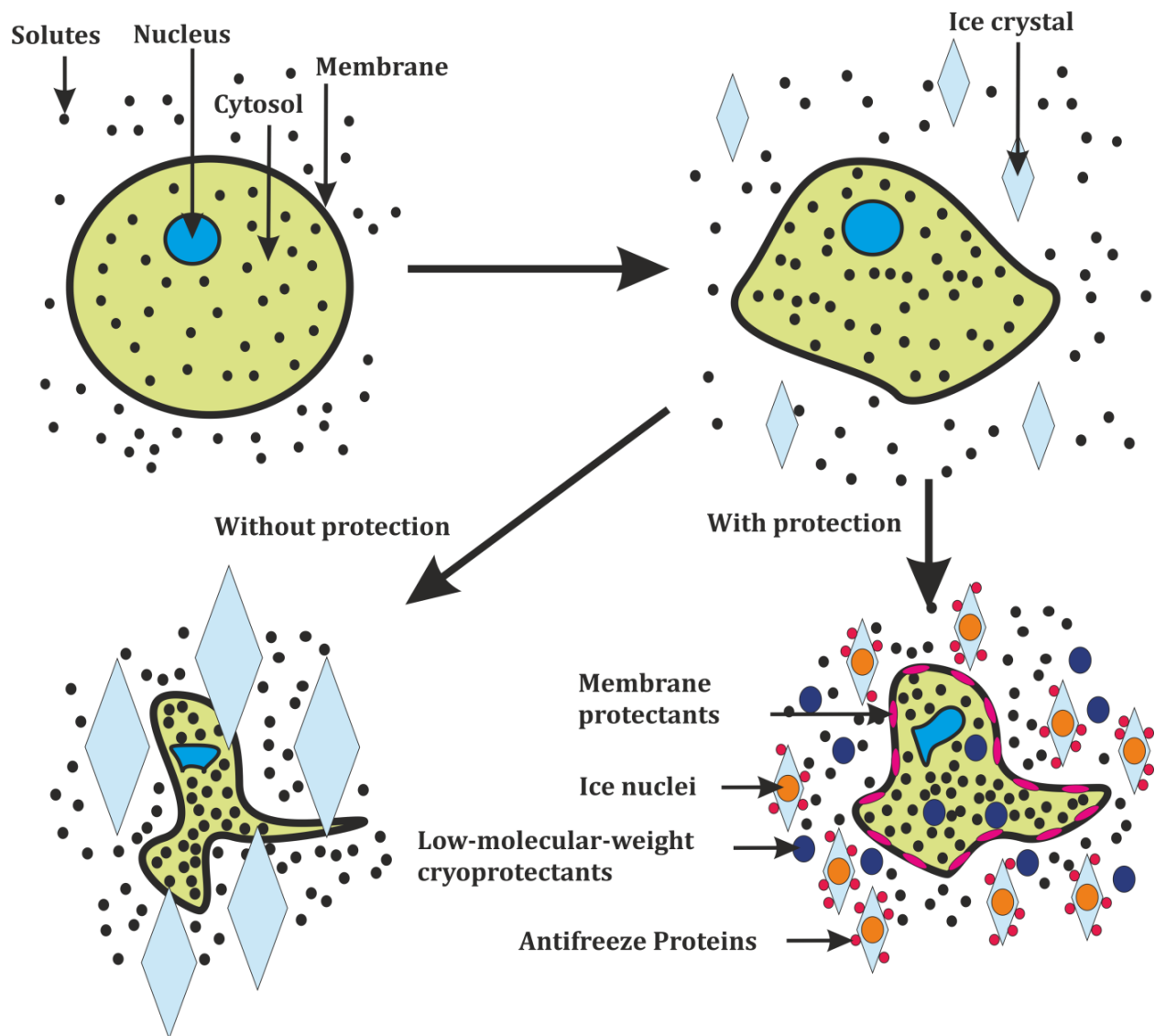


**Figure 12: Schematic depiction of freezing in the extracellular spaces. Top left: depiction of a cell, no ice present; top right: first ice crystals form; bottom left: if the organism has no protective mechanisms, ice crystals grow and eventually rupture the membrane; bottom right: cell of an organism with protective mechanisms (see e.g. Storey & Storey, 2004).**

## 1.5. Biological Ice Nuclei

Ice-nucleating substances have been found in most kingdoms of life, as e.g. several species of bacteria, which are among the most potent INP catalysing freezing temperatures in some cases as high as  $-1$  to  $-2^{\circ}\text{C}$  (Maki *et al.*, 1974; Lindow *et al.*, 1989; Lindow, Arny and Upper, 2013), and fungi (Stephan Pouleur *et al.*, 1992), as well as several lichen (Kieft, 1988). The most prominent and best described biological ice nucleus is derived from *Pseudomonas syringae*, a bacterium and plant pathogen, which produces an ice nucleation active protein. These proteins form aggregates on the membrane of the bacterium, where it is anchored (Govindarajan and Lindow, 1988; Lindow *et al.*, 1989). The proteins differ only slightly in their chemistry but mainly in their self-organisation and aggregation features (Schmid *et al.*, 1997). Membrane environment and aggregation seems to play a major part in the ice nucleation activity and therefore trigger the freezing temperature of this INP (Schmid *et al.*, 1997). The proteins have  $\beta$ -sheet rich areas which resemble the crystal pattern of ice (see Figure 13) and are believed to act as a template for ice formation (Kajava and Lindow, 1993). This behaviour has been found similarly for the ice nucleation active protein of *Pseudomonas borealis* (Garnham *et al.*, 2011).

Parts of several plants are already known to be capable of acting as INPs. Examples are the wood of *Prunus* trees (Gross, Proebsting and Maccrindle-zimmerman, 1988), *Citrus* fruits (Constantinidou and Menkissoglu, 1992), and rye leaves (*Secale cereale*; Brush *et al.*, 1994). Further, pollen of many different plant species have been shown to exhibit ice nucleation activity (Diehl *et al.*, 2001; Pummer *et al.*, 2012). While Diehl *et al.* (2001) focused on entire pollen grains, Pummer *et al.* (2012, 2015) showed that these pollen contain ice nucleation active macromolecules (INMs), which are only loosely attached to the pollen grain and can be easily washed off from the surface of the pollen. Oils from wood of several

species and other naturally emitted terpenes can show INA (Rosinski and Parungo, 1966). Decayed plant leaf litter contains ice nucleation active materials and the concentrations of these materials vary with different environmental conditions, however, the authors suggest that this ability is linked to bacteria (Schnell and Vali, 1976). The INA of sea buckthorn berries was found to depend on their region of origin with freezing temperatures ranging from  $-15.1$  to  $-6.1^{\circ}\text{C}$ , which strongly depend on the ripeness of the berries (Jann *et al.*, 1997; Lundheim and Wahlberg, 1998). Studies suggest that the ice nuclei can not only be extracted from the berries but also from the leaf tissue (Jann *et al.*, 1997). In the case of blueberry, stem, flower bud, fruits, and leaves of Japanese grown examples of *Vaccinium corymbosum* and *Vaccinium ashei* contain INPs (Kishimoto *et al.*, 2014). Highest concentration of INPs were found in bark material (Kishimoto *et al.*, 2014). Corresponding freezing temperatures of these plant materials are shown in Table 2.

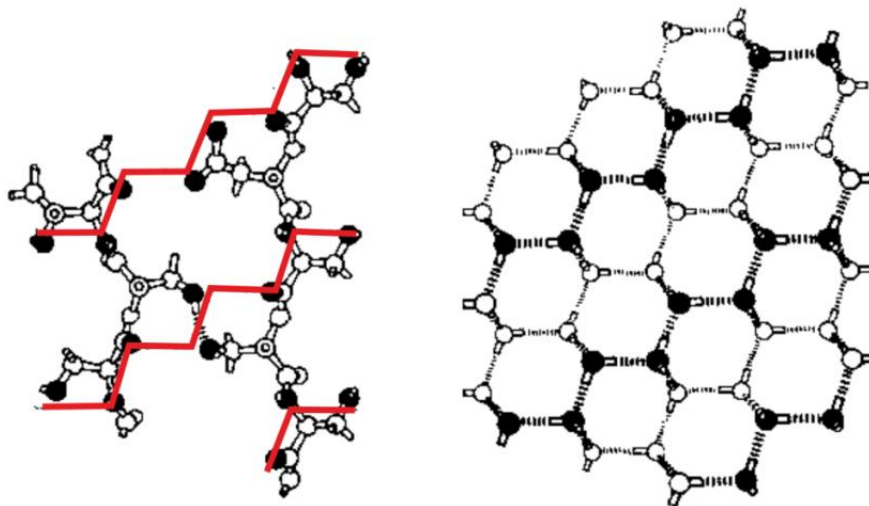


**Figure 13: Left: Model of two antiparallel  $\beta$ -sheets interacting via SER and ASP sidechains with peptide groups oriented along the viewing plane. Right: Fragment of an ice crystal structure. Black dots in both represent donors- acceptors for hydrogen bonds. The ice structure is indicated as red zigzag line. Adapted from Kajava & Lindow, 1993.**

**Table 2: The freezing temperature of selected plant materials which are known to exhibit INA. The table shows from left to right: the examined plant material, sample mass, freezing temperature, droplet volume/size for immersion freezing experiments, and the corresponding citation. Droplet is used as term for a single freezing unit (discrete water volume units).**

**The definition of freezing temperatures varies and is indicated at the bottom of the table. Differences in methods and droplet sizes render comparisons between temperatures between studies difficult:**

<b>Plant/ material</b>	<b>Sample mass</b>	<b>T [°C]</b>	<b>V</b>	<b>Citation</b>
<i>Prunus</i> _tree wood	5 cm sections	-2 <sup>A</sup>	24 ml	Gross <i>et al.</i> , 1988
<i>Citrus</i> fruits	A whole fruit per droplet	-2.5 <sup>A</sup>	150 ml	Constantinidou & Menkissoglu, 1992
Winter rye leaves ( <i>Secale cereale</i> )	0.1 g leaf tissue per droplet	-12 - -5 <sup>B</sup>	4 ml	Brush <i>et al.</i> , 1994
Birch pollen I	*	-12 <sup>C</sup>	*	Diehl <i>et al.</i> , 2001
Birch pollen II	50 mg/ml	-19 <sup>D</sup>	0.5 – 4200 pl	Pummer <i>et al.</i> , 2012
Birch pollen washing water	Aqueous extract of approx. 50 mg/ml pollen, product shows approx. 2.4 wt% residue	-18 <sup>D</sup>	0.5 – 4200 pl	Pummer <i>et al.</i> , 2012
Birch oil	*	-10 <sup>E</sup>	*	Rosinski & Parungo, 1966
Pine pollen I	*	-12 <sup>C</sup>	*	Diehl <i>et al.</i> , 2001
Pine pollen II	50 mg/ml	-20 <sup>D</sup>	0.5 – 4200 pl	Pummer <i>et al.</i> , 2012
Pine pollen washing	Aqueous extract of approx. 50 mg/ml	-21 <sup>D</sup>	0.5 –	Pummer <i>et al.</i> ,

water	pollen, product shows approx. 2.4 wt% residue		4200 pl	2012
Pine oil	*	-12- -9 <sup>E</sup>	*	Rosinski & Parungo, 1966
Decayed leaf litter	5-100 mg per test dispersed in air	-24- -4 <sup>F</sup>	N/A	Schnell & Vali, 1976
Ripe sea buckthorn berry juice	Tested pure	-7.9 - -7.3 <sup>D</sup>	10 µl	Jann <i>et al.</i> , 1997
Centrifuged sea buckthorn juice from ripe berries of different origins	Pure centrifuged filtered juice	-15.1 - -6.1 <sup>A</sup>	20 µl	Lundheim & Wahlberg, 1998
Blueberry stem	7.5 mm long increments per droplet	-2.3 <sup>D</sup>	0.5 ml	Kishimoto <i>et al.</i> , 2014
Blueberry fruits	A whole organ or half cut organ (to fit the tube) per droplet	-7.2 <sup>D</sup>	0.5 ml	Kishimoto <i>et al.</i> , 2014

**\* Used for measurements were methods working with condensation/deposition freezing, where water condenses/freezes directly on the IN. Droplet volume and sample concentration are not available.**

**<sup>A</sup> Mean temperature at which ice nucleation occurred**

**<sup>B</sup> Whole freezing range**

**<sup>C</sup> Temperature at which a mean freezing efficiency of 50% is reached**

**<sup>D</sup>  $T_{50}$  Temperature at which 50% of the droplets are frozen (median freezing temperature)**

**<sup>E</sup> Temperature of ice nucleation, not further defined**

**<sup>F</sup> Extracted data from available freezing nucleus spectra**

The chemical nature of most ice nuclei from plant materials remains widely unknown. In case of sea buckthorn, Jann *et al.* (1997) suspected that the INP is an aggregate comprising of a protein and a lipid part with the protein being in the size range of 25 to 27 kDa. Proteins also play a role in the ice nuclei in winter rye, which are believed to consist of complexes of proteins, carbohydrates and phospholipids (Brush, Griffith

and Mlynarz, 1994). In case of birch pollen the aqueous extract itself is known to contain saccharides, proteins, and lipids (Pummer *et al.*, 2013). Both Pummer *et al.* (2012) and Dreischmeier *et al.* (2017) suggested the INP to constitute of polysaccharides. Tong *et al.* (2015) on the other hand claim at least the most potent contained nucleus in the pollen washing water to be proteinaceous.

Field data shows that the biosphere acts as an important source for primary aerosol particles (see Jaenicke, 2005 and references therein). However, the content of biological particles in total aerosol varies. Analysing carbon sources of PM<sub>2.5</sub> particles (particulate matter with an aerodynamic diameter of 2.5 µm or smaller) collected at an urban and a rural site in Texas, Jia, Bhat & Fraser (2010) were able to attribute 5-13 % of the particle mass to primary biological sources and further 4-9 % to secondary organic aerosols depending on the sampling site. As all other aerosols, biological particles can agglomerate and age. Further, some biomolecules are easily adsorbed on dust particles (O'Sullivan *et al.*, 2016). The role of biological substances in cloud glaciation remains widely unknown (Möhler *et al.*, 2007; Murray *et al.*, 2012). However, even small amounts of biological matter can increase nucleation temperatures greatly (Conen *et al.*, 2011), and there is quite some data suggesting the importance of biological ice nuclei in the atmosphere. Schnell and Vali (1973) showed that bacterial INPs are available in all climatic zones, which was confirmed by several following studies (Schnell and Vali, 1976; Yankofsky *et al.*, 1981; Hazra *et al.*, 2004). Saxena showed (1983) that biogenic material is involved in the formation of Antarctic coastal clouds. Christner and colleagues analysed snow and rain samples from the U.S. (Montana and Louisiana), the Alps and the Pyrenees, Antarctica (Ross Island) and Canada (Yukon). In these samples, they found high concentrations of biological INPs (Christner *et al.*, 2008). Pratt *et al.* collected crystals from ice clouds over Wyoming, US at approx. 8 km



altitude and examined them via aerosol mass spectrometry. They found a third of this material to be of biological origin and further they found 60% of the highly abundant mineral dusts to be internally mixed with biological or humic substances (Pratt *et al.*, 2009). Kamphus *et al.* (2010) analysed ice crystal residues from mixed phase clouds at the Jungfernjoch station in the Swiss Alps and found that even at such a high altitude station (3500m) 2-3% of the material could be classified as biological. The data of Conen *et al.* (2016) indicates that leaf litter, which naturally hosts a vast variety of microorganisms, enrich Arctic air ice nucleating particles. Huffman *et al.* (2013) collected aerosols above woodlands in Colorado. Doing so, they observed a burst in number of biological INPs in the atmosphere linked to rain events. Since biological INPs seem to be capable of influencing cloud glaciation and precipitation (Sands *et al.*, 1982; Morris *et al.*, 2014), these rain induced bursts might be important contributors to atmospheric and hydrological processes.

## 2. Instrumental and Samples

### 2.1. VODCA

Data presented in this work is based on measurements done with the Vienna Optical Droplet Crystallization Analyser (VODCA). This setup allows observation of the freezing of droplets in the micrometre size range. The droplets are present in an emulsion. The emulsions consist of an aqueous phase and an inert oil phase. The aqueous phase consists of water (pure water for blank measurements, or samples in an aqueous phase). The inert oil phase consists of paraffin oil and lanolin, where lanolin acts as emulsifier. Paraffin oil and lanolin are mixed with 90 wt% paraffin oil and 10 wt% lanolin. When creating the emulsion, the oil phase is added in small excess (approx. 1:1.2 aqueous phase:oil phase). Emulsions are prepared in two ways. For larger quantities, aqueous and oil phase are mixed in a small vial and shaken well manually. The second strategy is for single measurement slides. Therefore, the phases are mixed directly on a clean thin glass slide with a pipette tip. Both mixing processes are done until the mixture turns opaque, indicating that Mie scattering occurs and therefore droplet sizes in the micrometre range are present. This process leads to aqueous droplets in an inert phase that can be used for freezing measurements (Hauptmann *et al.*, 2016).

The samples are cooled with the help of a cryo-cell. The cryo-cell is a hollow polymer cylinder that can be closed airtight. The compartment is equipped with a gas in- and outlet. To hinder humidity from interfering with measurements, one can flush the cell with dry nitrogen between measurements, or when changing samples. The main component of the cryo-setup is a Peltier element (Quick-cool QC-31-1.4-3.7M), which is mounted on a copper cooling block on ice water sewage, to remove heat generated by the Peltier element. The sewage is driven with a small water

pump. On top of the Peltier element, a thermocouple (type K) is fixed using thermal conductive glue, so the temperature of the element and therefore the temperature of the sample can constantly be monitored. The sample is applied as a thin film of emulsion on a clean glass slide and is placed on top of the element, right next to the link between Peltier element and thermocouple. A schematic depiction as well as a top view picture are given in Figure 14.

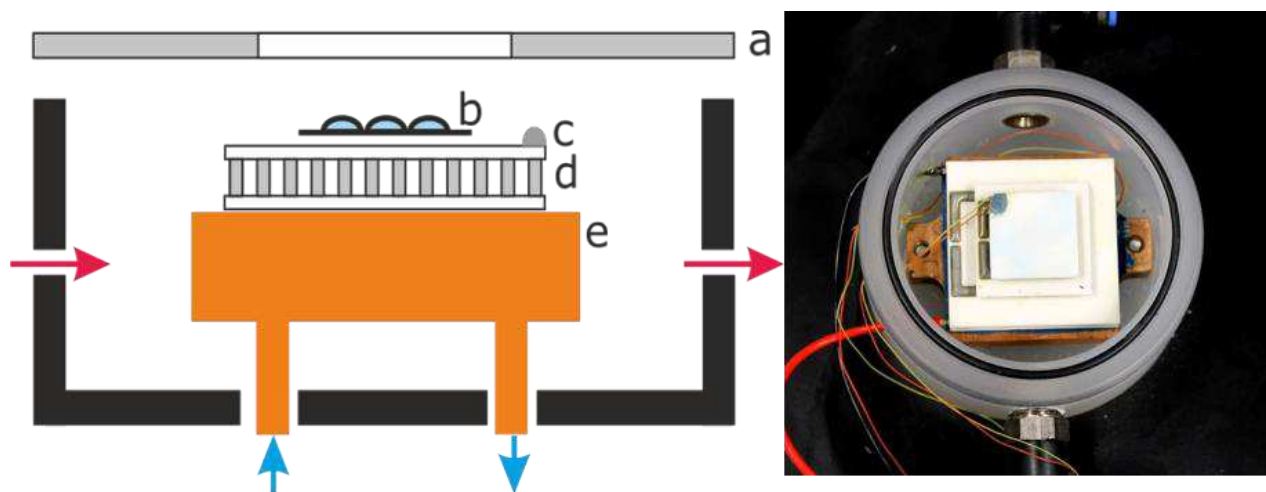


**Figure 14:** Left: schematic depiction of the cryo-cell. (a) cover with a glass window for observation. (b) sample on a thin glass slide. (c) a thermocouple (type K) is mounted on one corner of the Peltier element with a heat conductive adhesive. (d) Peltier element. (e) copper cooling block. Red arrows mark the direction of the nitrogen flow, blue arrows mark the ice water flow for cooling of the copper block.

**Right:** Top view on the cryo-cell. Peltier element (d) with the link to the thermocouple (c) can be seen clearly. Nitrogen in- and outlet are on top and bottom of the picture.

Peltier elements are named after the Peltier effect describing the generation of a temperature gradient via electric current flow. The element itself consists of an array of alternating coupled p- and n-doped semiconductors. Each pair represents a thermocouple. The semiconductors differ in the energy level of their conduction bands. Therefore, energy in the form of heat is absorbed on the junctions if the electrons are transferred from the n- to the p-doped semiconductor and released when electrons are transferred from the p- to the n-doped

semiconductor. A schematic depiction of a Peltier element is given in Figure 15.

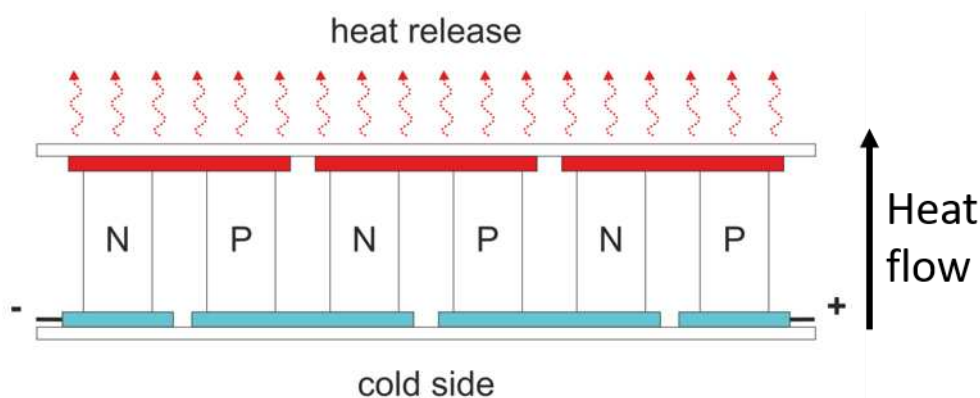


**Figure 15: Schematic depiction of a Peltier element, with the different p- and n-doped semiconductors joined with junctions. The thermocouples are covered with ceramic plates on top and bottom.**

Once the glass slide carrying a thin film of sample emulsion, it is placed on the peltier element, the cell is closed and measurements can be started. Two different cooling rates were used for the results presented in this work. For determining the INAs presented in chapter 3, the power supply was operated manually and cooled down rather quickly ( $>10$  °C/min) to 2-3°C above the temperature of interest. From thereon slow cooling rate of approx. 1°C/min was applied. The measurements for chapter 4 and 5 experiments were done with a fixed cooling rate of 1°C/min with the help of a LabVIEW based software. During the cooling process an airstream on the cover glass is applied to prevent fogging of the glass.

To observe the freezing events, the setup is equipped with an incident light microscope (Olympus BX51M) with an attached camera (Hengtech MDC320) linked to a computer. Since liquid droplets show a different light scattering behaviour compared to ice crystals, the process of freezing can be observed. With the setup, pictures and videos of the droplets as they are cooled down can be recorded. The freezing process is captured via photo-camera, with one photo of the unfrozen sample as a blank and

several photos during freezing with respective temperatures  $T_{photo}$ . Cooling continues until the whole sample is frozen. Figure 16 shows a series of photos taken during one experiment, the whole setup with all components is shown in Figure 17.

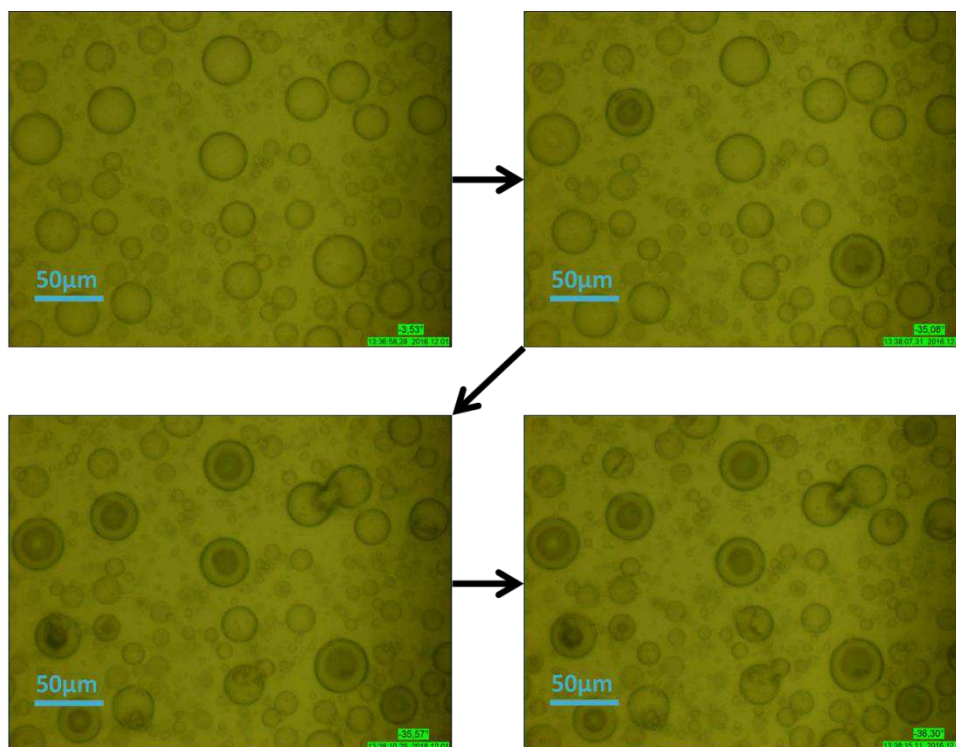


**Figure 16: Droplets freezing under the microscope. Top left: all droplets are liquid at  $-3.5$  °C. Top right: several droplets are frozen at  $-35.1$  °C, detectable by the darker colour and other changes in the appearance. Bottom left: further droplets are frozen at  $-35.6$  °C. Bottom right: All droplets are frozen at  $-36.3$  °C.**

For data evaluation, only droplets in the size range between 15 and 40  $\mu\text{m}$  in diameter (droplet volume: 1.8 – 34  $\mu\text{L}$ ) were included. This is done to minimize data variation due to different droplet sizes. Droplets of different sizes containing the same concentration of the same INP will freeze at different temperatures as the total number of INPs differs. The freezing temperature is dependent on the number of INPs contained in a droplet (Iannone *et al.*, 2011). Larger droplets contain a higher amount of INPs and correspondingly freeze at higher temperatures. The number of droplets frozen for each temperature was counted, allowing the

assignment of frozen droplet fractions to each observed temperature. This leads to freezing curves, as shown in Figure 18. The black curve depicted is a result of measuring ultrapure water (all ultrapure water was generated with Millipore© systems/  $M\Omega\cdot\text{cm}$  at 25 °C) and shows only homogeneous freezing. The pink curve shows a steep slope and freezes purely heterogeneously, which means that every observed droplet contained at least one INP. The green curve shows homogeneous and heterogeneous parts. Therefore, only a part of the droplets contained INPs and more than 40% did not. One can also see that the heterogeneous part of the curve does not follow a steep progression like the pink curve. This is due to the decreasing number of active sites, which can influence the nucleation temperature (see Section 1.2). It can also indicate the presence of various INPs active at different temperatures. For high enough concentrations, the most potent INP will be present in every droplet. Therefore, the whole sample will freeze at the temperature triggered by the most potent INP. The number of droplets not containing the most potent INP increases when the concentration decreases. Therefore, dilutions can be necessary to observe less potent INP.

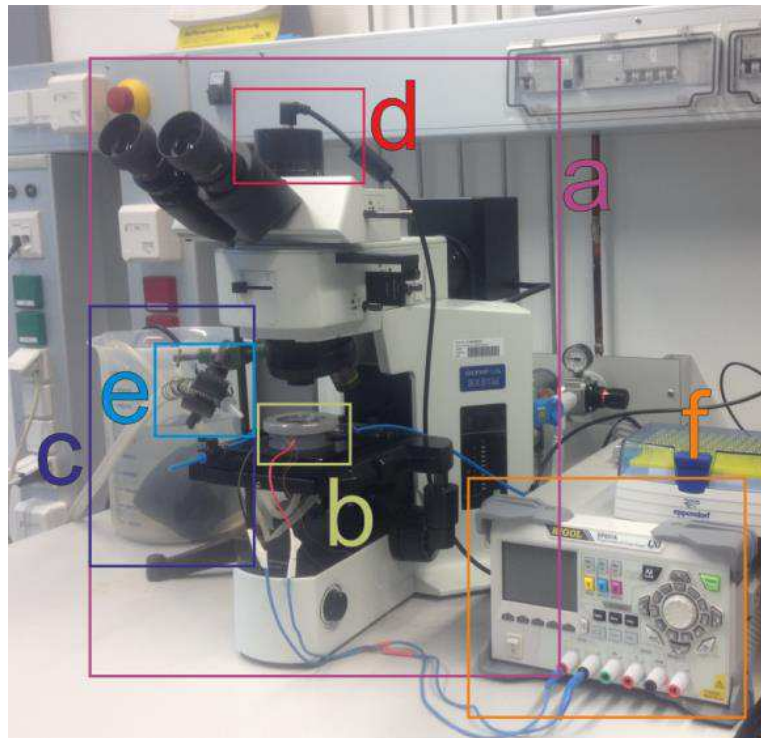


**Figure 17:** Picture of our setup: the microscope (a), cryo cell with nitrogen in- and outlet (blue tubes) and cooling water in- and outlet (white tubes at the bottom of the cell) (b), cooling water reservoir with pump (c), camera (d), dry air supply to prevent condensation on the cell window (e), power supply (f).

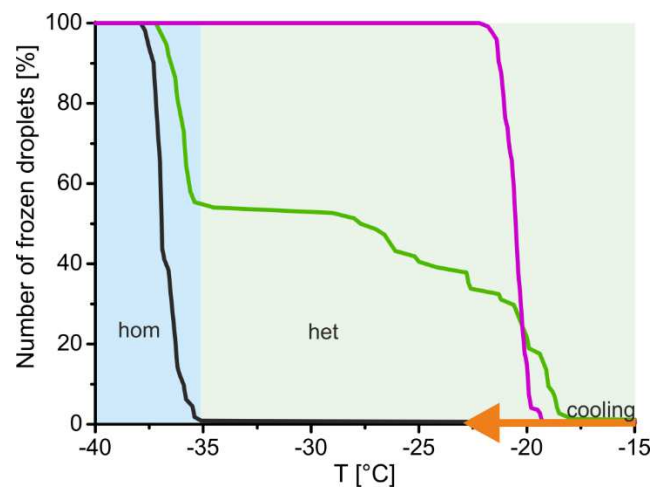


**Figure 18:** Three freezing curves, black represents pure homogeneous freezing, pink pure heterogeneous freezing and green is freezing partially homogeneous and heterogeneous. The homogeneous part of the plot is marked in blue, the heterogeneous part is marked in green.

### 2.1.1. Data Treatment

To make data more comparable, the results are given as mean freezing temperature (MFT) or as cumulative nucleus concentration at  $-34^{\circ}\text{C}$  ( $K(-34^{\circ}\text{C})$ ) see equation 17).

For the mean freezing temperature all observed droplets are taken into account taking the mean value as mean freezing temperature and the variation of freezing temperatures between the different droplets, to calculate the standard deviation.

$$MFT = \frac{\sum T_i * n_i}{n_{total}} \quad (\text{Equation 18})$$

with  $T_i$  being a recorded temperature,  $n_i$  being the number of droplets freezing at this temperature, and  $n_{total}$  being the total number of droplets observed during the experiment. For all birch samples, this only includes droplets freezing at temperatures above  $-35^{\circ}\text{C}$ . This threshold was introduced to only account for heterogeneous freezing. In case of the berries (Section 2.4) no threshold was applied. This was done as the berry samples contained high amounts of substances lowering the freezing temperatures. These substances shift both, homogenous and heterogeneous freezing temperatures. As it was possible to assign homogeneous freezing temperatures to each sample, no threshold was used.

Further, the initial freezing temperature is used as an indicator for INA. The initial freezing temperature is defined by the temperature at which the first droplet in a sample freezes. It is an indicator for the strongest INP contained in a sample. As the freezing curve gets steeper with higher concentrations, and the highest active INPs gain importance, the MFT is shifted towards the initial freezing temperature with decreasing concentration.



The cumulative nucleus concentration ( $K(T)$ ) gives the concentration of INPs active at or above a certain temperature. It is calculated via equation 17. As a comparison value,  $K(-34^{\circ}\text{C})$  was used. This value includes all INPs active at  $-34^{\circ}\text{C}$  or higher temperatures.  $-34^{\circ}\text{C}$  was used as threshold value to ensure that homogeneous nucleation events are not counted, since they were never observed at  $-34^{\circ}\text{C}$  or above using the described method. Calculation of  $K(T)$  includes the droplet volume. Droplets of 15 and 40  $\mu\text{m}$  in diameter were taken into account in our evaluations. For the calculation, the volume of all droplets was approximated using a 25  $\mu\text{m}$  diameter. The value is slightly smaller than the mean of 15 and 40. This was done to account for small droplets being present in excess in our measurements.

In literature, the  $n_s(T)$  value is often used to describe concentrations of active sites (e.g. Murray *et al.*, 2012).  $n_s(T)$  describes the cumulative active site density on a particle for sites that are active at temperature  $T$  or above. As the results given in this work focus on molecular INPs and not on coarse particles,  $n_s(T)$  is not used.

## 2.2. FT-IR-Spectroscopy

Fourier-Transformation-Infrared spectroscopy (FT-IR-spectroscopy) describes a method used to gather structural and chemical information of substances based on their interaction with infrared radiation. In comparison to dispersive IR spectroscopy, the FT-IR spectroscopy collects spectral information over a wide range of wave numbers simultaneously.

In FT-IR spectroscopy, the incident beam contains a broad spectrum of wavelengths. To analyse the absorption of a single wavelength, the spectrometer is equipped with an interferometer. The beam splitter ideally splits the light by half and reflects 50% to the fixed mirror, and 50% to the moving mirrors. Due to interferences, the resulting radiation differs depending on the difference in optical path length between the two arms. This difference is also known as retardation. Recording the signal at different retardations leads to an interferogram, with a maximum at zero retardation due to positive interferences. The presence of a sample affects the interferogram due to the absorption of different wavelength.

An interferogram is measured from zero to maximum retardation, whereby the maximum retardation can be adjusted and depending on the required resolution. Fourier transformation is used to create a spectrum out of the interferograms.

We used ATR unit as sample compartments. ATR stands for attenuated total reflection, describing a measuring method that uses the property of total internal reflection. This unit consists of a chamber focussing the beam on a crystal in an angle allowing it to reflect at least once from the surface of the crystal covered by the sample. The premise to this method is the formation of an evanescent wave, which will extend into the sample (typically 0.5 – 2  $\mu\text{m}$ ) when the beam is reflected. This evanescent wave

can only form if the crystal has a higher refractive index than the sample covering it.

To gather the data presented in this work, two different instruments were used. Measurements shown in chapter 3 are generated with a Vector 22 from Bruker, equipped with a DTGS (deuteriated triglycine sulphate) detector. Further, an ATR chamber from Harrick (Split Peak™ ATR microsampler), which was constantly flushed with dry air was used. The chamber contained three mirrors and a germanium crystal as total reflection window. The control software Opus 5.5 was used to operate the instrument. 512 scans of 1 s with a resolution of  $4\text{ cm}^{-1}$  were accumulated for each measurement.

The measurements shown in chapter 4 were conducted with a Vertex 80v from Bruker containing an MCT (mercury cadmium telluride) detector cooled with liquid nitrogen. The optical bank is evacuated (2.6 hPa) and holds a micro-ATR unit (Pike, GladiATR™ single reflection ATR accessory). The ATR chamber contains three mirrors and a diamond crystal as total reflection window. The software OPUS 6.5 was used as a control program. For each measurement 128 scans were accumulated with a resolution of  $0.5\text{ cm}^{-1}$ . The crystal surface was flushed with nitrogen to prevent humidity from interfering with our measurements.

For both instruments, each sample was applied by adding a thin liquid layer of the extract. Contained water was evaporated with a blow dryer. The temperature on the surface of the crystal during evaporation was approx.  $35^{\circ}\text{C}$ . This process was repeated until the dried residues of approx.  $20\text{ }\mu\text{L}$  sample were applied.

## 2.3. Samples, Sampling and Treatment

### 2.3.1. Birch Pollen Washing Water

All washing waters produced for the presented investigations are aqueous extracts of approx. 50 mg Pollen per mL of ultrapure water. That mixture was left to rest for 6-8 h, (with being shaken two to three times during that times span). Afterwards all solid content was removed via decantation and centrifuging (3500 rpm/1123xg for 5 min, Sartorius 2-16P, Sartorius), leaving a clear yellow liquid. Therefore, the washing waters did not contain any coarse material but only molecular components extractable from pollen. Approx. 30-40% of the pollen mass is extracted, leading to a concentration of approx. 20 mg/mL of the washing water.

All investigations on birch pollen presented in this work were done with pure, not- defatted *Betula pendula* pollen from AllergonAB (Thermo Fisher).

### 2.3.2. Tyrolian and Viennese Birches

Materials were collected from nine birches in Tyrol and one birch located in an urban park in Vienna. The Tyrolian birches are named TB for Tyrolian Birch and numbered A to I. The Viennese birch is named VB throughout this work. Larger branches were taken and divided in several parts: leaves, primary wood (green, active photosynthesis), and secondary wood (brown, no photosynthetic activity) (see Figure 19). The wood samples were cut into small segments (1-2 cm) and collected of two branches for each tree. All primary wood segments as well as all secondary wood segments for a branch were combined. For leaves, only whole leaves with no visible injuries were collected (approx. 3 leaves per branch).

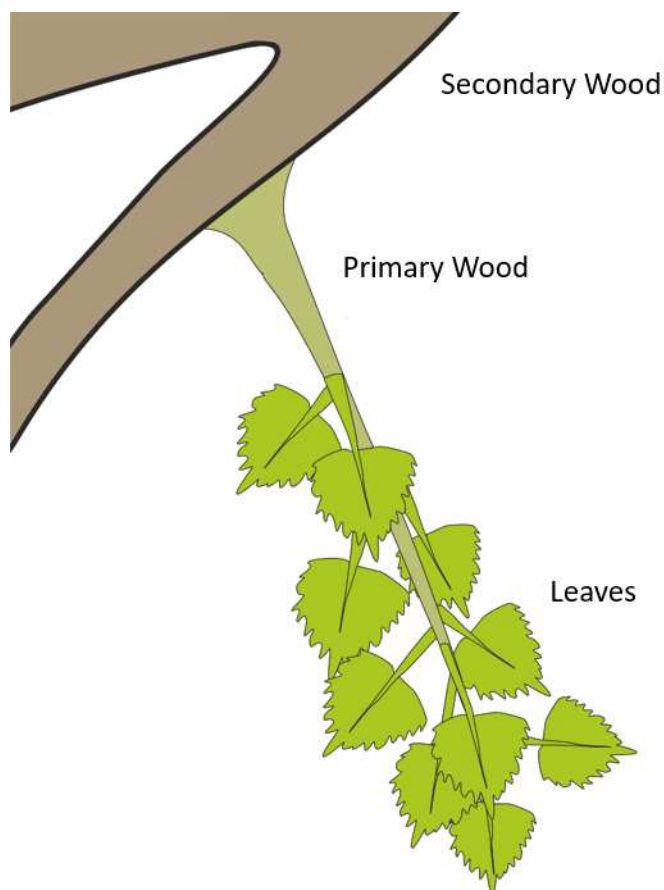


**Figure 19: Schematic of the distributions of the collected samples on a birch branch. The older browner secondary wood, the young green primary wood and the leaves.**

Collected branch samples for the birch TBD are shown in Figure 20.

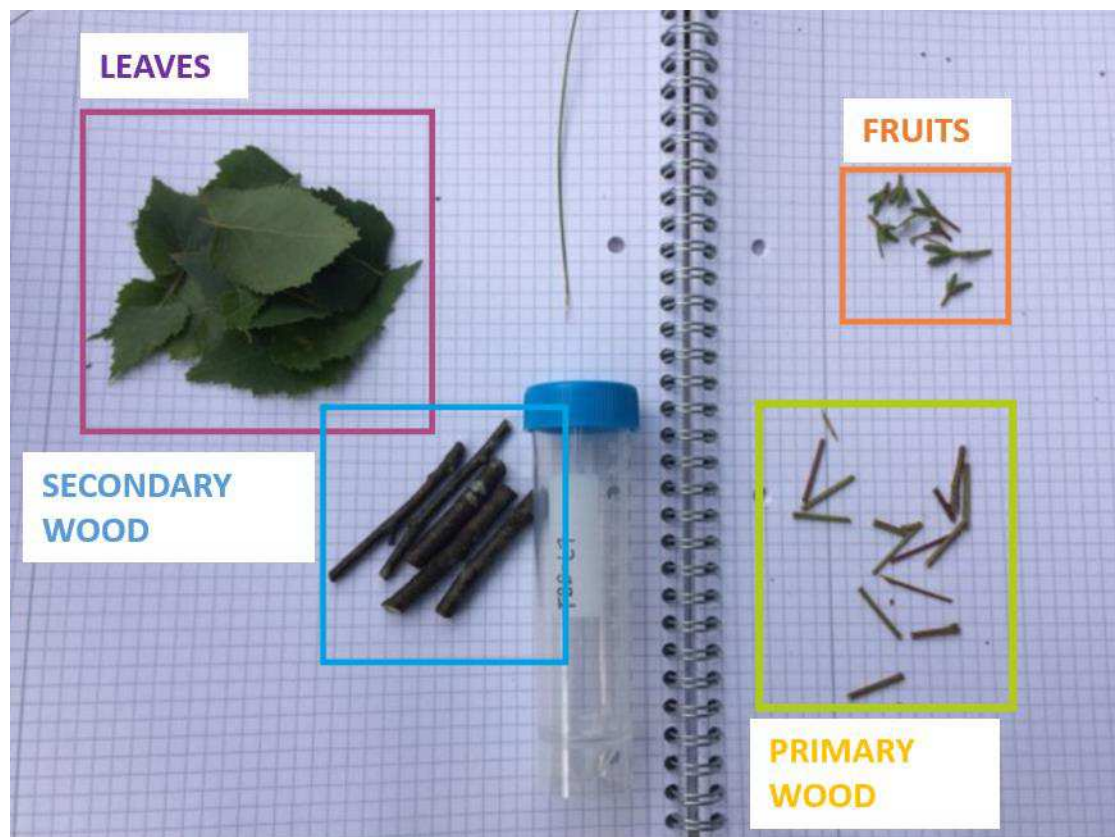


**Figure 20: Samples collected from a single branch of the birch TBD. Data gathered from fruits are not included in this work.**

Trunks were also sampled. Therefore, three cores of each trunk were drilled (at 0.5, 1, and 1.5 m height) with a pole testing drill (Haglölf, 5 mm diameter). Further, bark samples were collected (only from the Tyrolean trees). A drill core is shown in Figure 21, the sampling of bark was done via peeling off bits of the bark from the trunk using tweezers. This is shown in Figure Figure 22.



**Figure 21: Picture of a drill core. The left end marks die outside of the tree.**



**Figure 22: Collection of the bark from the tree TBD.**

All used tools were sterilized with ethanol. The samples were frozen as soon as possible. All samples were collected in spring and summer 2016. The Tyrolean samples were collected along an altitudinal gradient. Detailed descriptions of the different birches and information on their growing sites can be found in Table 3. Further, the sampling sites of the Tyrolean birches are also shown in Figure 23.



**Figure 23: Sampling sites in Tyrol along a valley with an altitudinal gradient. (adapted from Google Maps, 18.09.2017, taken from (Felgitsch et al., 2018))**

**Table 3: Information on the sampled birches, with sample name (ID), circumference, GPS waypoints, altitude of the growing site and a further description thereof:**

<b>ID</b>	<b>GPS waypoints</b>	<b>GPS altitude</b>	<b>Circumference of the tree at 1 m height</b>	<b>Location description</b>
TBA	47.214241, 10.798765	799 m	113 cm	Roadside birch in the valley
TBB	47.221615, 10.829835	799 m	54 cm	Roadside birch in the valley
TBC	47.186231, 10.908341	851 m	75 cm	River side birch in the valley
TBD	47.185387, 10.909587	851 m	35 cm	River side birch in the valley
TBE	46.973163, 11.010921	1343 m	96 cm	River side birch in Sölden next to a road with little traffic
TBF	46.974588,	1343 m	61 cm	River side birch in Sölden next to a



	11.011463			road with little traffic
TBG	46.878959, 11.024441	1925 m	67 cm	Timberline birch, the last birch and one of the last trees in general we encountered on our way up
TBH	46.873275, 11.026616	1883 m	36 cm	Riverside birch in Obergurgl close to the timberline
TBI	46.873279, 11.026736	1883 m	59 cm	Riverside birch in Obergurgl close to the timberline
VB	48.197796, 16.352189	195 m	86 cm	Located in the centre of a small park in Vienna, which is surrounded by heavy traffic

Two different types of extraction were used. For the milled samples, leaves, primary, and secondary wood were milled with a swing mill (Retsch MM400) operated with a frequency of  $25\text{ s}^{-1}$  and equipped with a stainless-steel ball. Each sample was cooled with liquid nitrogen between two milling steps. This was achieved by immersing the milling container and the ball (stainless steel) containing the sample in liquid nitrogen. After equilibrium was reached, the container was remounted on the mill and the next milling step was conducted. Each sample was milled four times for 30 s. After the milling process the products were dried in vacuum over silica gel until the weigh was constant. The dried samples were immersed in ultrapure water (1 ml per 50 mg of powder). It was shaken two to four times over a time of 6 h. Afterwards it was centrifuged (Sartorius 2-16P equipped with a Sigma 12148-H rotor, 3500 rpm/ 1123 g for 5 min) and

the supernatant was pressed through a 0.2  $\mu\text{m}$  syringe filter (VWR, cellulose acetate membrane, sterile).

Further, total surface extractions of leaves, primary, secondary wood, and bark, as well as of bark, bast, and the outer wood sections of selected drill cores were conducted. In the case of total surface extraction, the INPs are extracted over the intact surface of the sample. The exact sample size and weight as well as the used volume varied. In order to estimate the surface areas, approximations were used. Hereby core, secondary wood and primary wood samples were estimated as cylinders. For the core samples, we used the whole surface area. For the secondary and primary wood samples we used the curved surface area without the base (as the top and bottom base were covered with paraffin wax to hinder material from the cutting edges from leaking into to extracts). Leaves were approximated with two triangles to best capture the kite-like shape. A scheme of the approximation is given in Figure 24. In the surface estimation the up- and downside of the leaves was accounted for, but not the thickness as it is neglectable. For the bark samples two punches with a diameter of 5 mm were used. Therefore, the surface of each punch was approximated as the circular area multiplied with two to capture the top and bottom of the punch. Surface roughness was neglected in all cases. The estimated surface sites per mL water used for extraction are given in Table 4.

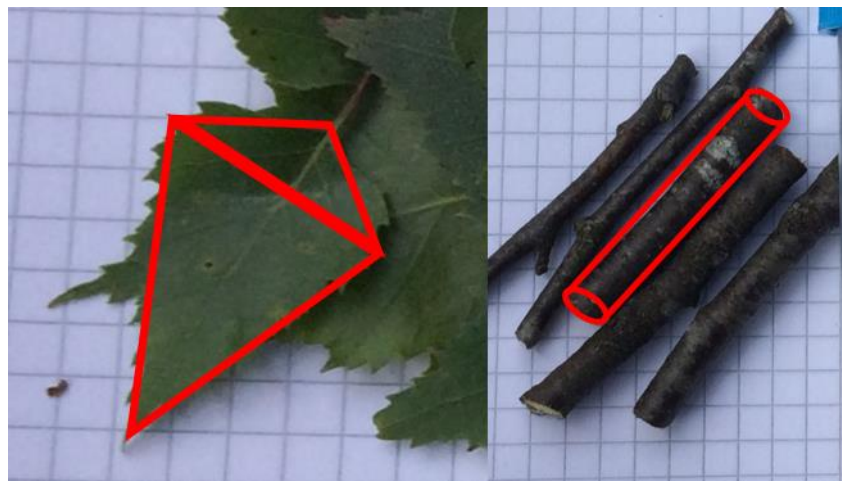


**Figure 24:** Depiction of the approximations of the surface area. On the left side a leaf approximated with two triangles. On the right side a piece of secondary wood approximated with a cylinder.

Again, we extracted over the time of 6 h in ultrapure water. The amount of water depends on the sample. For wood and core samples a volume was used so that the sample was covered well but not too much excess water was above the sample. For leaves the volume covered the whole leaf, but not the petiole. Afterwards it was centrifuged (Sartorius 2-16P equipped with a Sigma 12148-H rotor 3500 rpm/ 1123 g for 10 min) and the supernatant was pressed through a 0.2  $\mu\text{m}$  syringe filter (VWR, cellulose acetate membrane, sterile).

**Table 4:** Estimated surface area per mL water used for extraction of leaves, primary wood, secondary wood, and bark. The value depends on the estimated surface and the used water volume:

Birch	Leaves	Primary Wood	Secondary Wood	Bark
	[ $\text{cm}^2 \cdot \text{mL}^{-1}$ ]	[ $\text{cm}^2 \cdot \text{mL}^{-1}$ ]	[ $\text{cm}^2 \cdot \text{mL}^{-1}$ ]	[ $\text{cm}^2 \cdot \text{mL}^{-1}$ ]
TBA	1,6	0,5	2,0	1.2
TBB	2,0	0,4	1,6	1.2
TBC	4,1	0,6	0,8	1.2

TBD	1,2	0,3	0,5	1.2
TBE	1,2	0,5	0,4	1.2
TBF	0,9	0,4	0,9	1.2
TBG	2,8	0,9	1,8	1.2
TBH	2,2	0,3	1,2	1.2
TBI	2,2	0,5	1,6	1.2

**Table 5: Estimated surface area per mL water used for extraction of the core samples. The value depends on the estimated surface and the used water volume:**

Birch	Bark	Bast	C3	C4	C5
	[cm <sup>2</sup> *mL <sup>-1</sup> ]	[cm <sup>2</sup> *mL <sup>-1</sup> ]	[cm <sup>2</sup> *mL <sup>-1</sup> ]	[cm <sup>2</sup> *mL <sup>-1</sup> ]	[cm <sup>2</sup> *mL <sup>-1</sup> ]
TBC	0,8	0,9	0,9	0,9	1,1
TBI	0,4	0,8	1,2	1,2	1,0

### 2.3.3. Microscopic Analysis of the Leaves

The pictures shown in this chapter were obtained using equipment from the Institute of Chemical, Environmental and Bioscience Engineering, with supervision of Prof. Dr. Leopold Puchinger.

To gain more knowledge on the sampled trees, leaves of all trees were analysed via light microscopy (Zeiss Stemi 508 equipped with an Axio Cam ERc 5s, which was linked to a computer). Pictures were generated using the software Zen. 1x objective lens, 1.25x zoom and a 0.5x camera adapter were used.

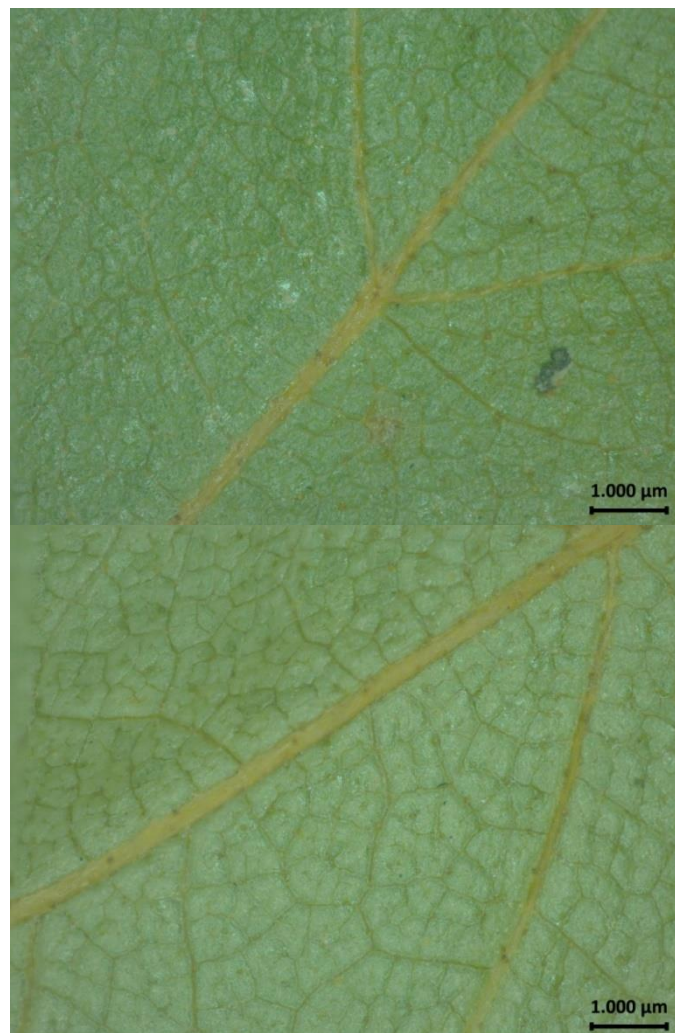


**Figure 25: Microscope picture of surface (top) and downside (bottom) of a leaf stemm from TBA. The black bars indicate 1000  $\mu\text{m}$ .**

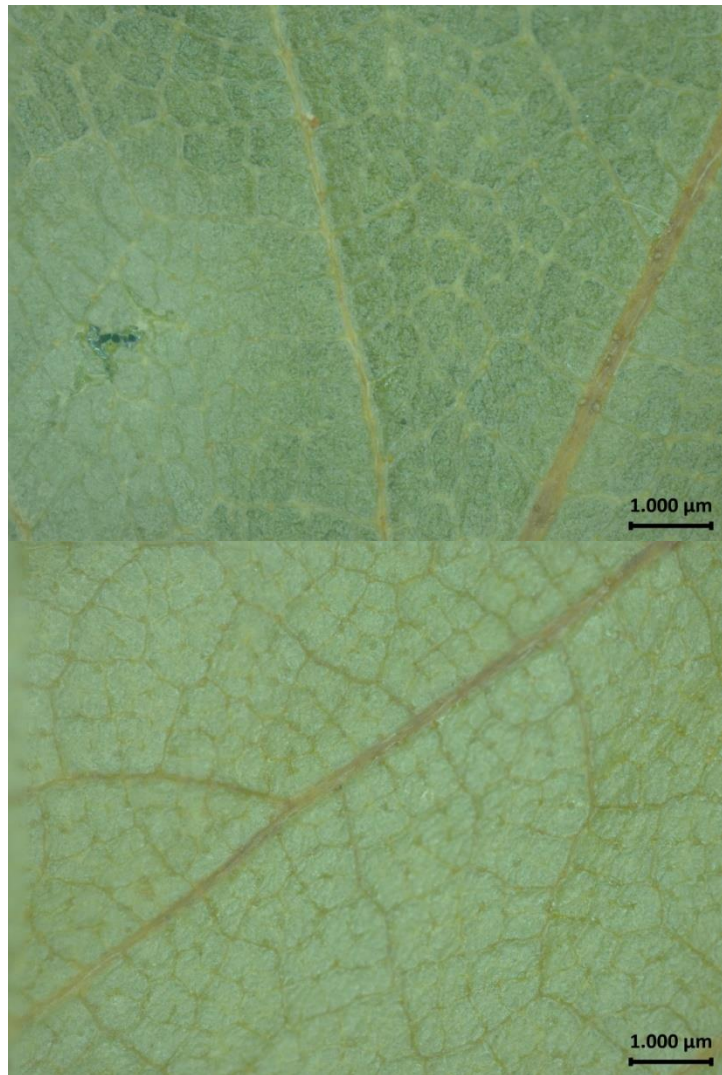


**Figure 26: Microscope picture of surface (top) and downside (bottom) of a leaf stemming from TBI. The black bars indicate 1000  $\mu\text{m}$ .**

The main birch species found in Europe are *Betula pendula* and *Betula pubescens* (Beck *et al.*, 2016). They cannot be differentiated with 100 % certainty via appearance (Hibschi-Jetter, 2008). However, several of their features can give a good hint. Leaves are typically less pointy for *Betula pubescens* and covered in fine hair (thus the common name downy birch) (Hibschi-Jetter, 2008; Beck *et al.*, 2016). Figure 25 and Figure 26 are given as examples for the leaves. All other analysed leaves looked similar. No hair was found on any of the regarded samples. Further, the stem of most sampled birches was strongly fissured and appeared dark towards

the ground, which is typical for *Betula pendula* (Hynynen *et al.*, 2010). Therefore, it can be assumed that analysed birches are *Betula pendula*.

#### 2.3.4. Berries and Leaves from Different Plants

In order to expand the number of analysed plants native to the Boreal regions, eighteen different samples from ten different perennial plants were analysed. Plants from the boreal regions were chosen as there is a known link between INA and cold hardiness (Storey and Storey, 2004). The focus was material from plants which are quite common in nature. A high occurrence equals a huge overall surface, which could act as a source for INPs in nature.

The samples used were commercially available juices, frozen berry samples, which were centrifuged and filtered to gain a liquid sample, dried berry extracts, and extracts from leaves. Table 6 gives an overview of the samples including sample IDs. All samples were stored at -18 °C.

The commercially available juices were of organic, so called "Muttersaft" quality. They have been pasteurized at temperatures around 85°C. Heating times were held as short possible. This is necessary to prevent microbial spoilage.

We worked with filtered and unfiltered juices. Filtered juice were first centrifuged at 3500 rpm (1123 g) (Sartorius 2-16P equipped with a Sigma 12148-H rotor used for all berry samples) for 20 min. This process resulted in clear liquids. In most cases no sediment was visible. Sea buckthorn juice did not just exhibit visible sediment. Approx. half of the particulate content floated on top after centrifugation. The clear liquid was retrieved with a syringe and then passed through a 0.2 µm syringe filter (VWR cellulose acetate membrane, sterile).

Frozen berries were examined via centrifuging the defrosted berries for 20 min at 3500 rpm (1123 g). The resulting liquid supernatant was passed through a 0.2  $\mu\text{m}$  syringe filters.

Dried berry extracts were produced by immersing dried berries in ultrapure water with 500 mg berries per ml of water. The berries were immersed in water for six hours at room temperature. The vial was shaken occasionally. After six hours a part of the supernatant was stored as pure extract sample. The rest was centrifuged and filtered like the juices to obtain the filtered samples.

For the leaf samples, a leave was immersed in water in a vial. We did not use a fixed volume of water for all samples but rather added water until the whole leave was submersed but the petiole was still above the water line. This was done in order to only extract INPs through the intact leave surface. In case of blueberry we used 2 mL of water, for juniper, raspberry and sea buckthorn we used 6 mL of water. The treatment after immersion was done similarly to the dried berry extracts.

**Table 6: An overview of all twelve examined samples. Listed are the common name, the sample ID, the type, brand, genus, volume/mass of the bought unit as well as a lot number if possible. We used seven commercially available juices (J1-J7). All of which were untreated and naturally cloudy. Further, we worked with two frozen berry samples. They were centrifuged prior to measuring and only the filtered supernatant was used. Additionally, we tested aqueous extractions of dried juniper-, rowan- and sea buckthorn berries:**

Common name	Sample ID	Type	Brand	Genus	Volume/ Mass	Lot number
Black currant	J1a	Juice	dmBio	<i>Ribes</i>	0.33 l	61493
Black	J1b	Juice	Alnavit	<i>Ribes</i>	0.33 l	n/a



currant						
Blueberry	J2	Juice	Alnavit	<i>Vaccinium</i>	0.33 l	BL 57408
Chokeberry	J3	Juice	Alnavit	<i>Aronia</i>	0.33 l	n/a
Cranberry	J4	Juice	Alnavit	<i>Vaccinium</i>	0.33 l	n/a
Lingonberry	J5	Juice	Alnavit	<i>Vaccinium</i>	0.33 l	HL 56893
Sambucus	J6	Juice	Alnavit	<i>Sambucus</i>	0.33 l	n/a
Sea buckthorn	J7a	Juice	dmBio	<i>Hippophae</i>	0.33 l	60857
Sea buckthorn	J7b	Juice	Alnavit	<i>Hippophae</i>	0.33 l	n/a
Raspberry	B1	Frozen berries	Spar Natur*pur	<i>Rubus</i>	200g	L5017
Rowanberry	B2	Frozen berries	Obst Oswald	<i>Sorbus</i>	n/a	n/a
Juniper berry	E1	Extract of dried berries	Sonnentor	<i>Juniperus</i>	35 g	ALB14013003F10
Rowanberry	E2	Extract of dried berries	Paulaner Apotheke	<i>Sorbus</i>	100 g	n/a
Sea buckthorn	E3	Extract of dried berries	n/a	<i>Hippophae</i>	n/a	n/a
Blueberry	L1	Extracts of leaves	Collected in Upper Austria	<i>Vaccinum</i>	n/a	n/a
Juniper	L2	Extracts of leaves	Collected in Upper Austria	<i>Juniperus</i>	n/a	n/a
Raspberry	L3	Extracts of leaves	Collected in Upper Austria	<i>Rubus</i>	n/a	n/a
Sea buckthorn	L4	Extracts of leaves	Collected in Upper Austria	<i>Hippophae</i>	n/a	n/a

### 3. Investigations on the Birch Pollen INMs

The chemical nature of birch pollen INMs (ice nucleation active macromolecules, see Section 1.5) is still under discussion. While studies showed that polysaccharides are an important component (Pummer *et al.*, 2012; Dreischmeier *et al.*, 2017), also proteins could play a vital role (Tong *et al.*, 2015). Understanding the chemical characteristics of birch pollen INMs is vital to understand the ice nucleating mechanism and to reliably detect birch pollen INMs in natural samples. As the birch pollen washing water contains a vast mixture of different substances from different classes, the main challenge lies in separating the components in order to analyse them individually.

#### 3.1. Solid Phase Extraction

Solid phase extraction (SPE) is a sample preparation technique that works with prepacked cartridges containing different stationary phases. Its aim is to separate analytes in aqueous solution or suspension based on their physical or chemical properties. The analyte in solution (mobile phase) is passed through a solid phase (stationary phase). Presented experiments were performed using C18 cartridges (HyperSep™).

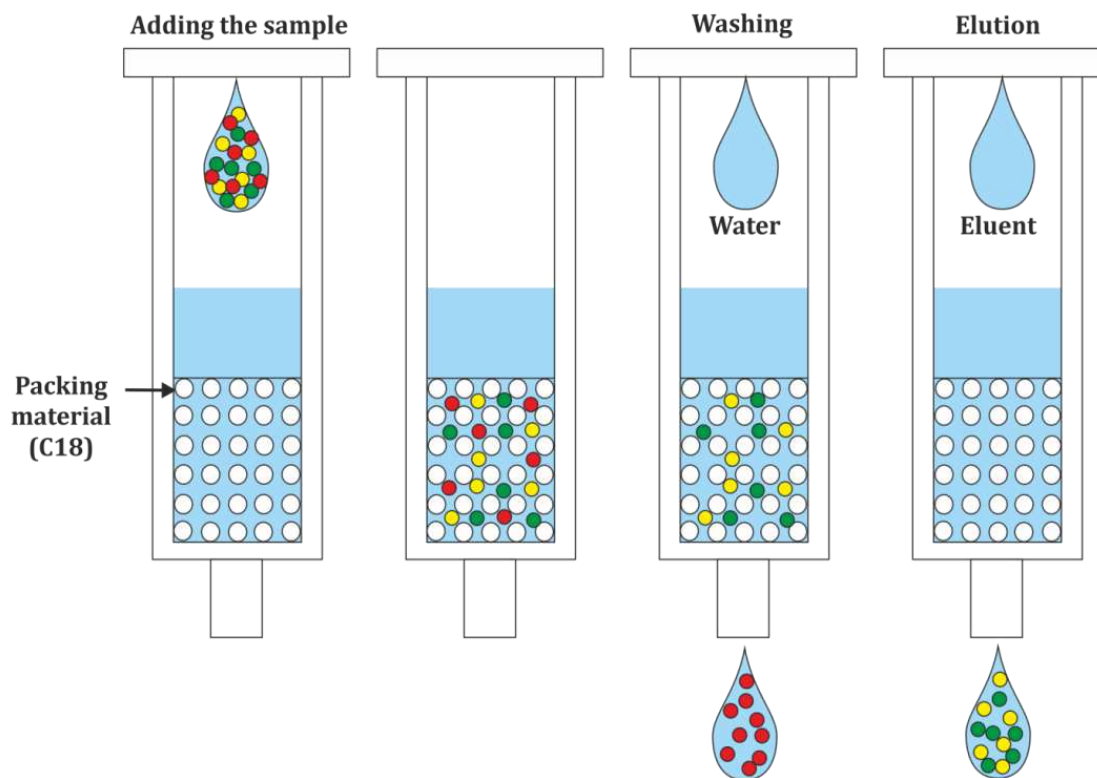


**Figure 27: Working principle of a SPE cartridge. Left and middle left: adding of the sample and loading of the cartridge; middle right: washing of the cartridge, removing analytes that do not interact with the stationary phase; right: elution of the analytes interacting with the stationary phase.**

C18 is a highly nonpolar material consisting of long C-H-chains, which are fixated on the stationary phase particles via Si-O- groups (see Figure 28). C18 separates materials based on their polarity. Nonpolar materials interact with the stationary phase and get held back, while more polar materials will elute very easily. The schematic of this process is depicted in Figure 27.

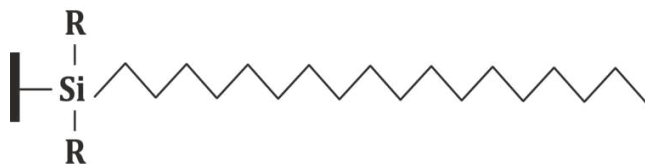


**Figure 28: Structure of a single C18 building block**

The columns were washed with water and conditioned with methanol prior to sample application. Samples were not modified prior application.

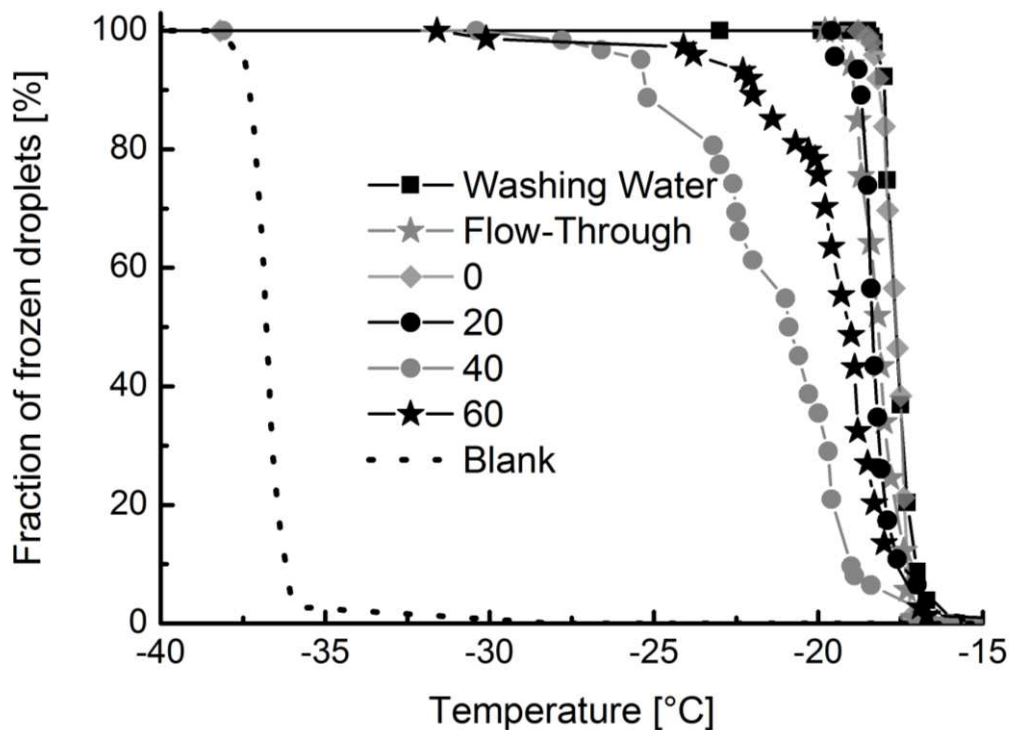


**Figure 29: Freezing curves of the C18 SPE fractions. The flow-through fraction is the first fraction. It is not eluted using eluents but is the rest of the washing water after passing the cartridge. The eluted fractions are marked with 0, 20, 40, and 60, which corresponds to the percentage of methanol in the eluent (in all cases, a mixture of methanol and ultrapure water). Further depicted is pure birch pollen washing water (washing water) and ultrapure water (blank). The freezing curves of elutes with higher methanol fractions tend to freeze at lower temperatures.**

As eluent water/methanol (Sigma-Aldrich 34860, HPLC grade  $\geq 99.9\%$ ) mixtures with increasing methanol contents (0, 20, 40, and 60) were used. Preliminary experiments revealed the fraction eluted with 80% and 100% methanol to be barely ice nucleation active, therefore focus lay on the fractions with methanol content up to 60%. Further, the fraction flowing directly through the cartridges was collected if possible. All

obtained fractions were dried to remove the methanol. Freezing curves of different SPE fractions are depicted in Figure 29. A cartridge with a capacity was functionalized with 2x5 mL of methanol and then washed with 3x5 mL of ultrapure water. 2x5 mL and 1x2.5 mL (in total 12.5 mL) of birch pollen washing water were added. The solvents were evaporated using a rotary evaporator. Further information on the fractions is given in Table 7.

The freezing curves (Figure 29) clearly show that all analysed fraction exhibit ice nucleation activity in a similar range as birch pollen washing water (also plotted in Figure 29). However, the nucleation efficiencies of the fractions eluted with 40 % methanol and with 60 % methanol are clearly lower compared to the efficiency of birch pollen washing water and the other fractions indicating a decrease in efficiency for higher non-polarities. Since C18 is highly nonpolar, the INMs must have nonpolar properties to be able to interact with the stationary phase. However, to be well soluble in water and in order to be able to be eluted with polar solvents, they need to exhibit polar properties as well. This indicates that the INMs from birch pollen are an amphiphilic substance with both, polar and nonpolar structural regions.

**Table 7: The different SPE fractions given with their name, the used solvent and its volume, the colour of the resulting fraction and the settings for the rotary evaporator. For the Fraction 40 and 60, we did the evaporation stepwise, removing the methanol with 250 mbar and the remaining water with 150 mbar:**

<b>Fraction</b>	<b>Solvent Volume</b>	<b>Colour</b>	<b>Rotary Evaporation Settings</b>
Flow-through	3x 5 mL water	Slight pink	73°C/ 150 mbar
0	3x 5 mL water	Slight pink	73°C/ 150 mbar

20	3x 5 mL methanol/water (20:80)	Slight yellow	70°C/ 150 mbar
40	3x 5 mL methanol/water (40:60)	Strong yellow	70°C/ 250 mbar/150 mbar
60	3x 5 mL methanol/water (60:40)	Slight yellow	70°C/ 250 mbar/150 mbar

Due to the differing in colour of the different fractions, UV/VIS spectra were recorded. As the different colours absorb different wavelengths, the separation performance can be visualized by UV/Vis spectroscopy. Spectra of the different fractions are shown in Figure 30. The spectra show clear differences concerning the region around 350 nm. While this band is only present as a slight shoulder in the flow-through and 20 % methanol fraction, and not visible for the 0 % methanol fraction, we found distinctive bands in this region for the 40 and 60 % methanol fraction.

Assigning UV/VIS bands to different chemical substances is not possible if one operates with a mixture of many different substances of which not all are known and described. Further, it must be mentioned that only substances are visible in these spectra, which interact with the corresponding wavelength.

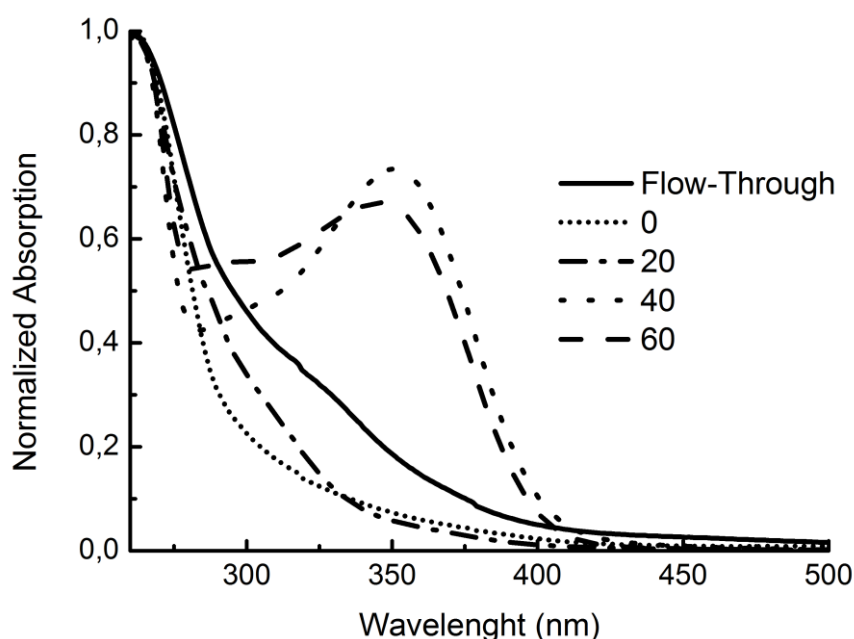


**Figure 30: UV/VIS spectra of the different C18 fractions (the numbers correspond to the %methanol used for elution).**

### 3.1.1. Ammonium Sulphate Precipitation

To further separate the washing water and get a better understanding of its components, ammonium sulphate precipitation was used. Ammonium sulphate (Merck, 1.01217) is highly soluble in water ( $\sim 750$  g/L at  $20^{\circ}\text{C}$ ). Added to a solution of different components, it will lead to precipitation of components with less solubility. It is typically used for protein purification.

For precipitation approx. 300 mg/mL washing water were added, which led to two different precipitates: a flaky precipitate which swims on top of the solution and a fine greyish precipitate which sits on the bottom. The precipitate of 7 mL birch pollen washing water was used. The precipitate was filtered using regular laboratory grade filter paper and washed with concentrated ammonium sulphate solution. The precipitate was then re-suspended in 2 mL water. The solid phase extraction procedure was

slightly changed for this experiment. A C18 cartridge was functionalized with 2x5 mL methanol, and then washed with water. Another washing step was added using 5 mL of hydrochloric acid (pH2). The sample was also adjusted to pH 2 using hydrochloric acid.

After 8 mL of the suspended precipitate were applied, it was washed with 30 mL of water to get rid of most of the ammonium sulphate, which should not interact with the stationary phase due to its polarity. As the sample contained high quantity of salt, it was not possible to evaluate the flow-through or fraction 0.

To remove the solvents, fractions were placed as thin liquid layers in a glass petri dish and put on a heating plate at 50°C. Residues were dissolved in 3 mL of ultrapure water. Results of ice nucleation measurements of the different fractions are shown in Figure 31. While all measured fractions were still clearly ice nucleation active, the number of INMs contained declined. Only 10 to 20 % of the analysed droplets of the ammonium sulphate – SPE fractions still contained INMs.



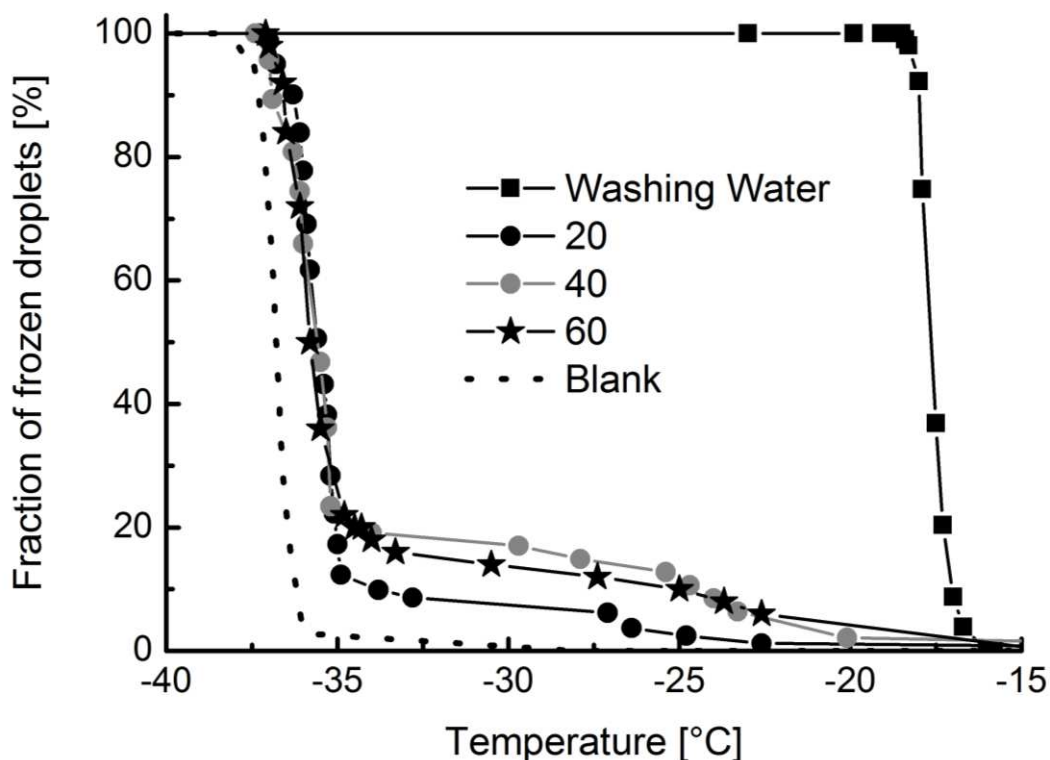


**Figure 31:** Freezing curves of the C18 SPE fractions (eluted with 20, 40, and 60 % methanol – marked as 20, 40, and 60) from the ammonium sulphate precipitate. Further depicted are pure birch pollen washing water (washing water – not processed) and ultrapure water (blank). All fractions were ice nucleation active, however, only 10 to 20 % of the droplets contained INPs.

The different fractions were again analyzed using UV/VIS spectroscopy. Resulting spectra are given in Figure 32. Around 350 nm all three spectra behave very differently. Other than before the ammonium sulphate precipitation, this time also the 40 and 60 % methanol fraction can be clearly differentiated, with the 40 % fraction forming a band with a maximum at 350 nm and a broad shoulder towards smaller wavelengths and the 60 % methanol fraction showing two maxima at 325 and 300 nm.

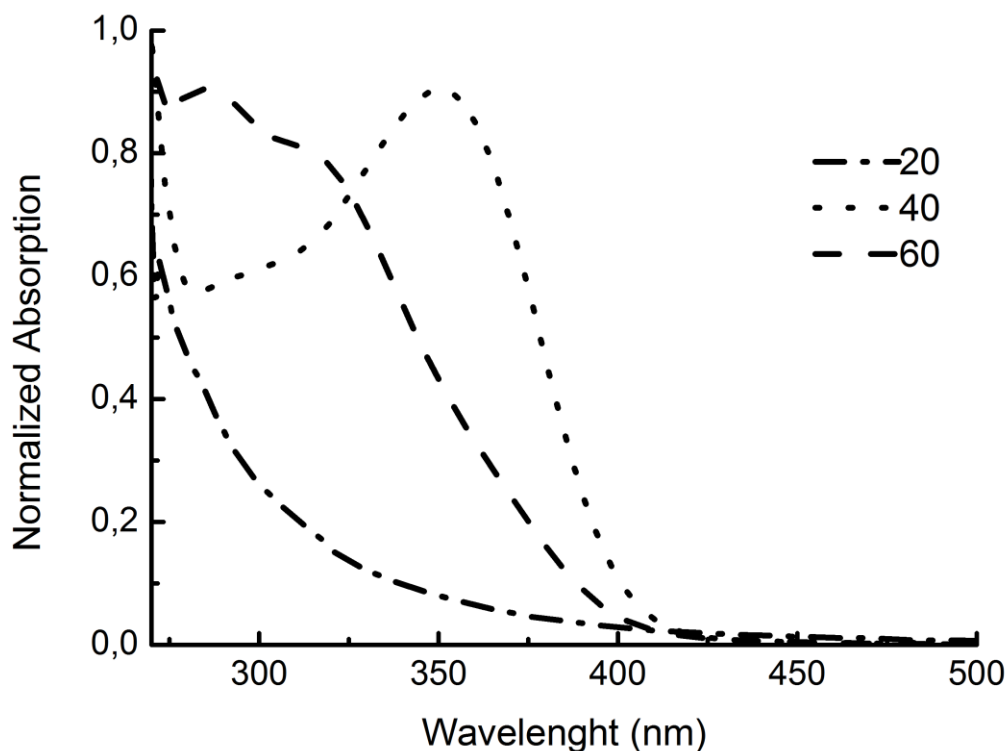


**Figure 32: UV/VIS spectra of the different C18 fractions of the ammonium sulphate precipitate (the numbers correspond to the %methanol used for elution).**

To gain information on their chemical characteristics, the three collected fractions were analyzed via FT-IR spectroscopy. The resulting spectra are shown in Figure 33. The typical area for O-H-stretching and N-H-stretching, as well as the area for aliphatic C-H-stretching are marked in grey. Possible band assignments for the bands at wavenumbers of  $1700\text{ cm}^{-1}$  and below are given in Table 8. Three bands from the 20 % methanol fraction are marked in green. These bands match the spectrum of ammonium sulphate, which exhibits bands at approx.  $1100\text{ cm}^{-1}$  and  $1400\text{ cm}^{-1}$ , as well as a broad band with two maxima between  $2500$  and  $3600\text{ cm}^{-1}$  (NIST, retrieved November 5, 2017). The ammonium sulphate bands are marked in green in Figure 33. These bands are not prominent in the 40 and 60 % methanol fractions, which are both less polar fractions.

We therefore conclude that these bands derive from ammonium sulphate and are not related to the birch pollen washing water fraction.

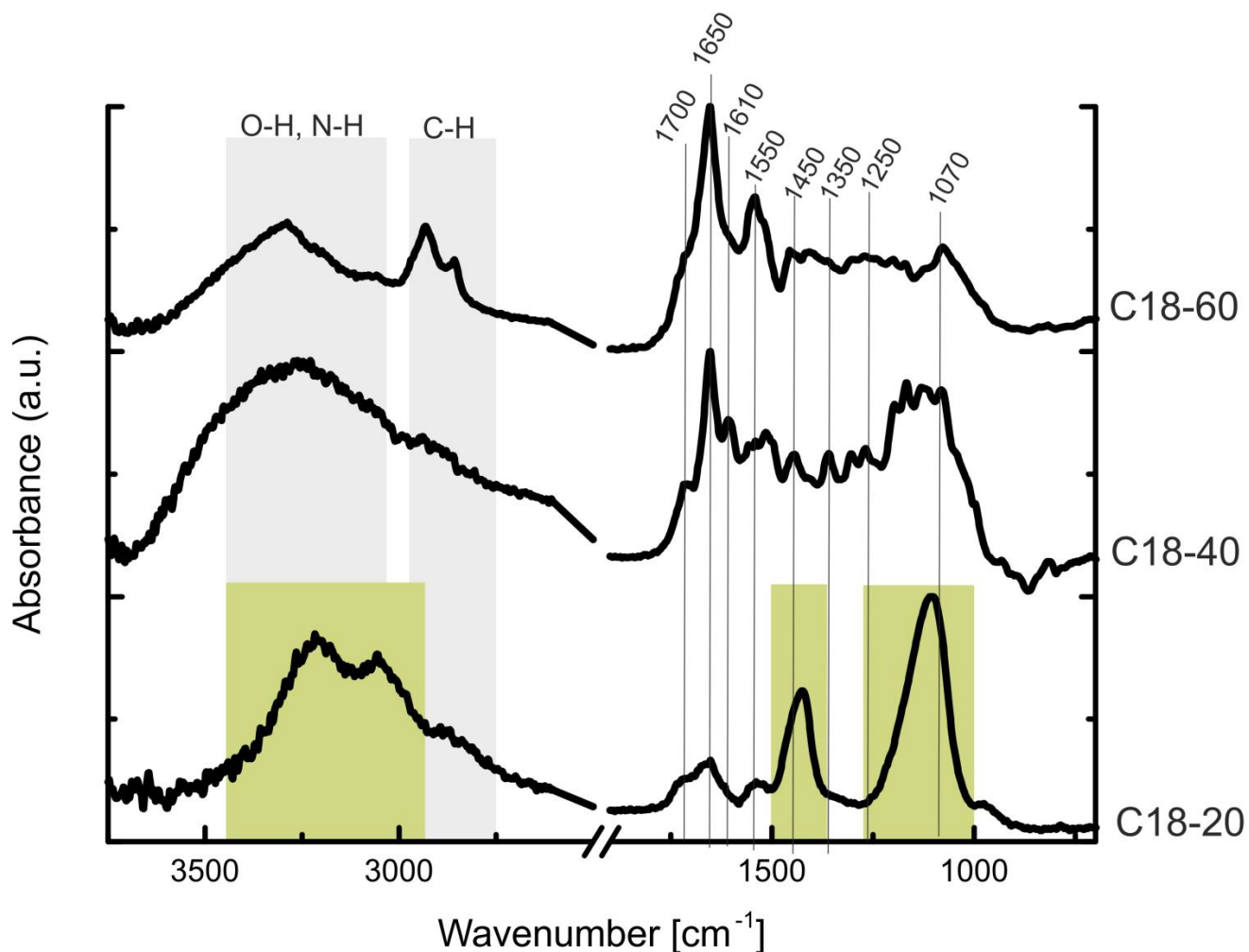


**Figure 33: FT-IR spectra of the 20 %, 40 %, and 60 % methanol C18 fractions from the ammonium sulphate precipitation experiment. Possible peak assignments in the area typical for O-H and N-H stretching, as well as aliphatic C-H stretching are marked in grey. Bands that are likely to stem from ammonium sulphate (NIST, retrieved November 5, 2017) are marked in green.**

The spectra exhibit bands in all three amid regions, which is typical for the presence of proteins. Further, several bands in regions which can be assigned to sporopollenin and carotenoids are present. Both are typical components of pollen.

**Table 8: Possible band assignments for the FT-IR spectra of the ammonium sulphate precipitation experiment given in Figure 33 (Miyazawa, Shimanouchi and Mizushima, 1956; Kačuráková et al., 2000; Schulz and Baranska, 2007; Pummer et al., 2013):**

<b>Band wavenumber [cm<sup>-1</sup>]</b>	<b>Assignment of IR spectra</b>
1700	C=O, xylan
1650	C=O stretch, C=C, Amid I
1610	C=O stretch, C=C, Amid I,
1550	C=O stretch, Amid II,
1450	CH <sub>2</sub> deformation
1350	C-H deformation (ring)
1250	C-O, C-N, C-N-C, C-C-O of phenolic compounds, Amid III, sporopollenin and carotenoids
1070	C-H stretch, C-C stretch, sporopollenin and carotenoids

### 3.2. Size Exclusion Chromatography

Size exclusion chromatography is a separation technique based on the hydrodynamic volume (which corresponds to the size) of the analyte. The stationary phase consists of a porous material. Smaller analytes are presented with a higher volume available for diffusion. Larger analytes cannot permeate into the pores of the stationary phase and pass right through. Therefore, larger analytes have a shorter elution time span than smaller analytes. Two different materials were used for the analysis: Sephadex® G-25 and G-50

Columns for the separation were prepared with approx. 1000 mg G-25 and 500 mg G-50. Both were swelled in 10 mL ultrapure water. Glass wool was put in 10 ml disposable pipettes to keep the material in the column. Afterwards the columns were packed with the swelled G-25 and G-50. Each column was loaded with 100 µl of birch pollen washing water. Ultrapure water was used as mobile phase. Table 9 (G-25) and Table 10 (G-50) show the INA of the different collected fractions.

***Table 9: Results of the G25 measurements, including retention time and volume of the sample and the INA indicated as + for ice nucleation active, / for little activity and - for ice nucleation inactive:***

<b>Time [min]</b>	<b>Volume [ml]</b>	<b>INA</b>
Blank	Blank	-
0:20	1,25	-
1:00	4,5	+
1:40	7,75	+
2:20	11	/
3:00	14,25	/
3:40	17,5	/
4:20	20,75	-
5:00	24	-
5:40	27,25	-

6:20	30,5	-
7:00	33,75	-
7:40	37	-
8:40	42	-

**Table 10: Results of the G50 measurements, including retention time and volume of the sample and the INA indicated as + for ice nucleation active, / for little activity and - for ice nucleation inactive:**

<b>Time [min]</b>	<b>Volume [ml]</b>	<b>INA</b>
Blank	Blank	-
0:20	1,25	-
1:00	4,5	+
1:40	7,75	+
2:20	11	/
3:00	14,25	-
3:40	17,5	-
4:20	20,75	-
5:00	24	-
5:40	27,25	-
6:20	30,5	-
7:00	33,75	-
7:40	37	-
8:40	42	-

In both cases, the retention time of the ice nucleation active analyte was quite long. In case of G-25, we retrieved ice nucleation active fractions for 3 min equalling a volume of 16.25 mL. For G-50 we retrieved ice nucleation active fractions for 120 s equalling a volume of 9.75 mL. This indicates that the birch pollen washing water is not suitable for size exclusion chromatography since it is likely that the analyte interacts with the inert column material.

### 3.3. Urea and Enzyme Treatment

Proteins describe linear polymers consisting of amino acids, whereby amino acids conjoined via peptide bonds are called peptides (smaller sections), or polypeptides (usually 100 amino acids or more). Proteins are determined by their structure, which can be classified in primary, secondary, tertiary and quaternary structure. The primary structure describes the sequence of the contained amino acids. Hereby the free amino group is called N-terminus and the free carboxylic group is called C-terminus. The secondary structure is the arrangement of the contained polypeptides. The most common secondary structures are  $\alpha$ -helices and  $\beta$ -sheets (depicted in Figure 34).  $\alpha$ -Helices describe a spiral conformation, while  $\beta$ -sheets consist of connected so called  $\beta$ -strands. Tertiary structure and quaternary structure relate to the folding of a protein and the organization of polypeptides via weaker bonds. (Ringo, 2004, pp. 18-21). The role of proteins in ice nucleation is described in Section 1.5.

Several agents are known to disturb the secondary structure of proteins. A commonly used reagent is guanidiniumhydrochloride, which is often used to unfold proteins and has already shown to not affect the INPs from birch pollen (Pummer *et al.*, 2012). Urea works differently compared to guanidiniumhydrochloride. It destabilizes the protein structure starting with the  $\beta$ -sheets, while guanidiniumhydrochloride destabilizes  $\alpha$ -helices first (Camilloni *et al.*, 2008).

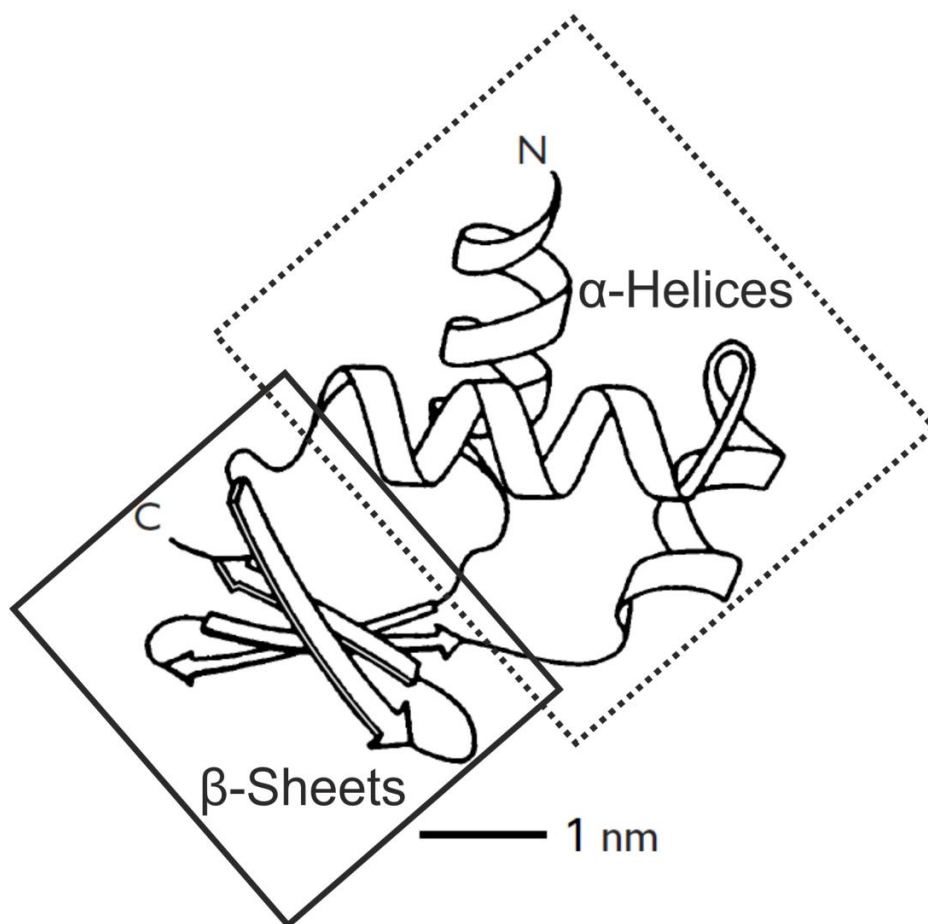


**Figure 34** Secondary structures of a protein with  $\alpha$ -helices on top (indicated with a dashed line) and  $\beta$ -sheets on bottom (indicated with a solid line). Adapted from Ringo, 2004, p. 20.

Two protease containing reagents were already used on birch pollen washing water (papain and pronase) and shown to have no major effect (Pummer *et al.*, 2012). However, there are proteins too stable or not suitable for these enzymes. The urea helps to examine this possibility, since it disturbs or even completely destroys the secondary structure of proteins, inhibiting stabilizing steric factors. Urea is prone to both, polar and nonpolar groups (though polar groups are preferred), which eases the penetration of proteinaceous structures (Rossky, 2008). In general, urea works directly and indirectly. Indirect via influencing the solvent (water) leading it to dissolving more nonpolar structures than usual and directly



by interacting with the protein – especially with polar residues and peptide backbones (Bennion and Daggett, 2003). Urea preferentially destroys beta sheet structures (Rocco *et al.*, 2008). The importance of beta sheets in biological ice nucleation is explained in Section 1.5.

Subtilisin was chosen as enzyme due to its resistance towards urea. Even though urea decreases its activity, it is not completely lost and exhibits still more than 10% of its activity compared to aqueous buffer without urea, with the used urea concentration of approx. 6.7 M (Guo and Clark, 2001). Subtilisin A from *Bacillus licheniformis* (Sigma Aldrich P5380) was dissolved with a concentration of 2 mg/mL in tris buffer (100 mM tris(hydroxymethyl)aminomethane (Sigma Aldrich 252859) in ultrapure water and adjusted to a pH of 8 (with 2 M hydrochloric acid). Subtilisin, urea, and the tris buffer themselves showed no ice nucleation activity; however, they showed strong freezing point depression. Three birch sample fractions were measured. For this 500 µL of birch pollen washing water were dried two times in the desiccator over silica gel. The first residue was suspended in 1.1 mL urea (8 M) and the second residue in 1.1 mL ultrapure water. The measured sample fractions were:

I: 500 µL residue in ultrapure water + 100 µL tris buffer

II: 500 µL residue in urea + 100 µL tris buffer

III: 500 µL residue in urea +100 µL subtilisin solution (2 mg/mL in tris buffer)

The resulting concentration of urea was approx. 6.7 M. The solutions were incubated in an oven at 60°C. Aliquots were taken after 0, 1, 6 and 24 h and measured concerning their ice nucleation behaviour. For the ice nucleation measurements, 10-fold dilutions were used (2 µL sample + 18 µL water) to avoid strong freezing point depression caused by the high urea concentrations. The tris puffer in sample I and II was added to

account for the tris buffer contained in the subtilisin solution. The resulting freezing curves after 0, 1, 6, and 24 h are depicted in Figure 35 (sample I, washing water with tris buffer), Figure 36 (sample II, washing water with tris buffer and urea), and Figure 37 (sample III, washing water with urea and subtilisin tris buffer).

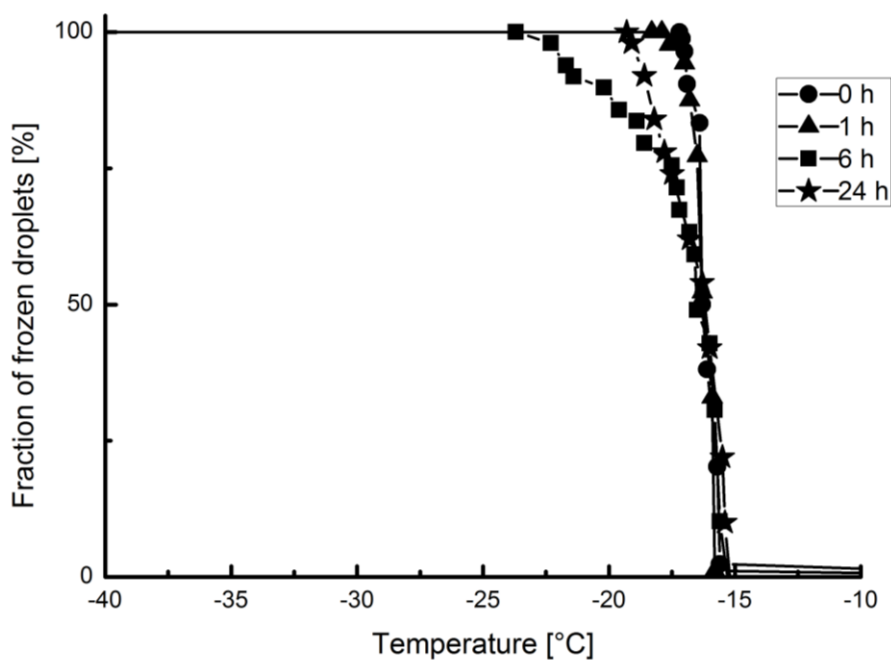


**Figure 35: Freezing curves of birch pollen washing water with 100 µL of tris buffer (sample I) after 0, 1, 6, and 24 h at 60 °C. A slight decrease in INA over time is visible.**

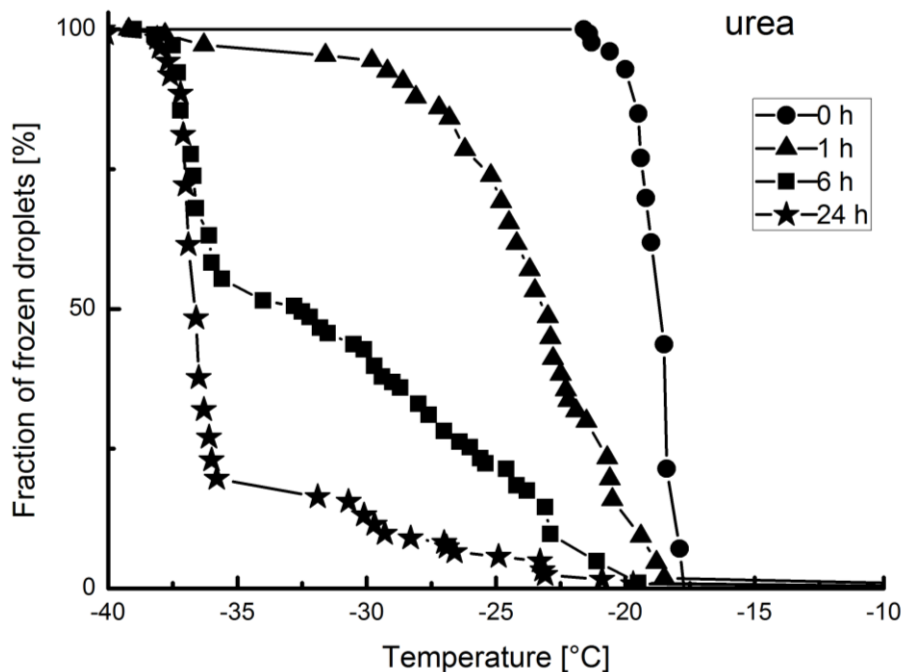


**Figure 36:** Freezing curves of birch pollen washing water with urea (sample II) after 0, 1, 6, and 24 h at 60 °C. The curves show a strong decrease of INA over time.

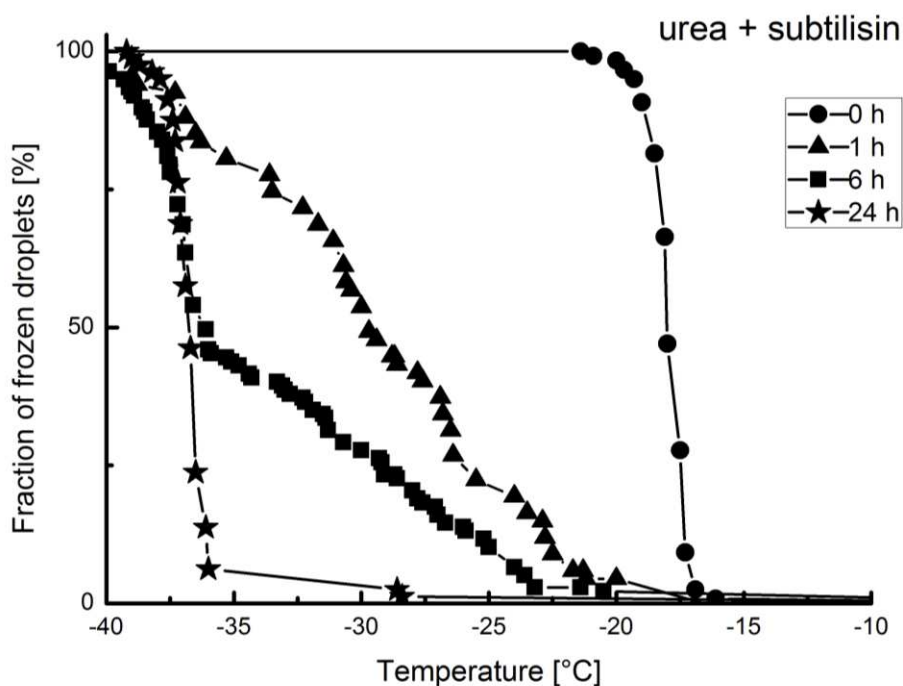


**Figure 37:** Freezing curves of birch pollen washing water with urea and subtilisin (sample III) after 0, 1, 6, and 24 h at 60 °C. The curves show an even more dramatic decrease of INA over time than with urea alone.

Sample I, which did not contain urea or subtilisin, showed only a very slight decrease assumingly originating solely from the temperature (60°C) (Figure 35). Other than that, both, urea and urea with subtilisin led to a strong decrease in INA. In case of urea (sample II, Figure 36) only 20 % of droplets of the 24 h fraction froze at temperatures above -35 °C. In the urea and subtilisin sample (sample III, Figure 37), the INA decreased even further with the 24 h sample only being left with INPs in 3 % of the droplets. This result indicates a strong influence of urea and subtilisin on the INA of birch pollen washing water.

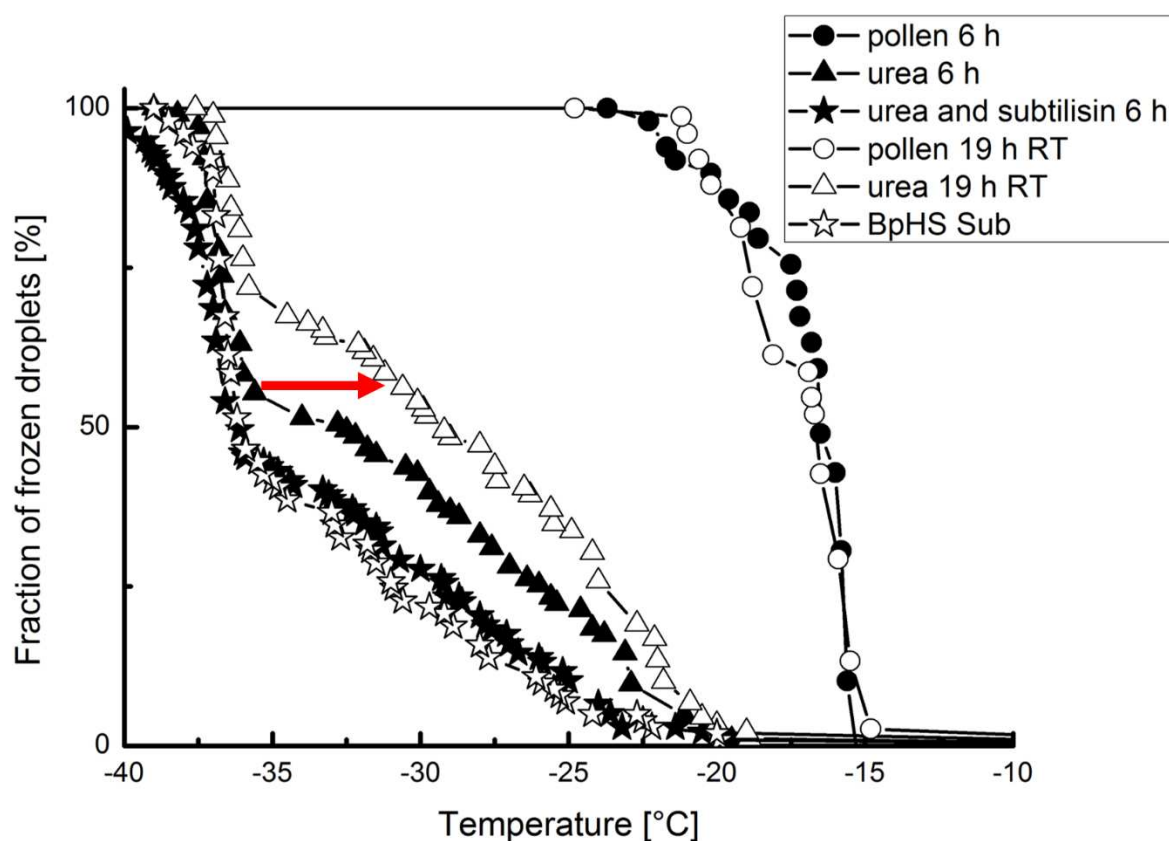


**Figure 38: Freezing curves of all three 6 h samples: sample I (resuspended pollen washing water and tris buffer) marked with circles, sample II (resuspended washing water in urea with tris buffer) marked with triangles, and sample III (resuspended pollen washing water in urea with subtilisin in tris buffer) marked with stars. The samples were stored at room temperature (RT) for 19 h. Results before storage correspond to filled symbols, results after storage correspond to hollow symbols. Sample**

***II showed a shift towards warmer temperatures induced by the storage (marked with an arrow).***

To further analyse the influences of urea and subtilisin, a renaturation experiment was done. Since urea does not destroy bindings within the proteins but only disturbs structural features, proteins should be able to recover at least partially from this. The fractions taken after 6 h were diluted 10-fold with ultrapure water for the ice nucleation measurements (as described above, this is done to decrease the freezing point depressing properties of urea, which hinders ice nucleation measurements). At these small concentrations, urea loses its denaturation-effect. A part of the dilution was incubated at room temperature for 19 h to see if renaturation processes influence the INA. Results of the freezing measurements of the fractions before and after 19 h at room temperature are given in Figure 38. The pollen washing water without urea and subtilisin did not change during the 19 h at room temperature. The same is true for the sample with urea and subtilisin. The sample containing only urea increased in its INA over the course of the 19 h (from ~50 % to ~60 % heterogeneously frozen droplets). Since the INA of the urea sample without subtilisin increased, but the INA of the urea sample with subtilisin did not, it is very likely that subtilisin had an irreversible effect on the contained INMs. This is a strong indicator that proteins play a vital role in the ice nucleating properties of birch pollen washing water.

### 3.4. Ozone Treatment

Samples were exposed to ozone to examine their oxidative stability to this atmospheric component. Therefore, an ozone generator (Fischer Ozon Generator 500) and a washing flask were connected with a flexible tube. The throughput of the ozone generator was approx. 1-10 mL/s (with ~10 % ozone content). The washing flask, containing the sample in liquid form, was mounted on a magnetic stirrer and the sample was stirred throughout the whole process. A schematic depiction of the setup is given in Figure 39.

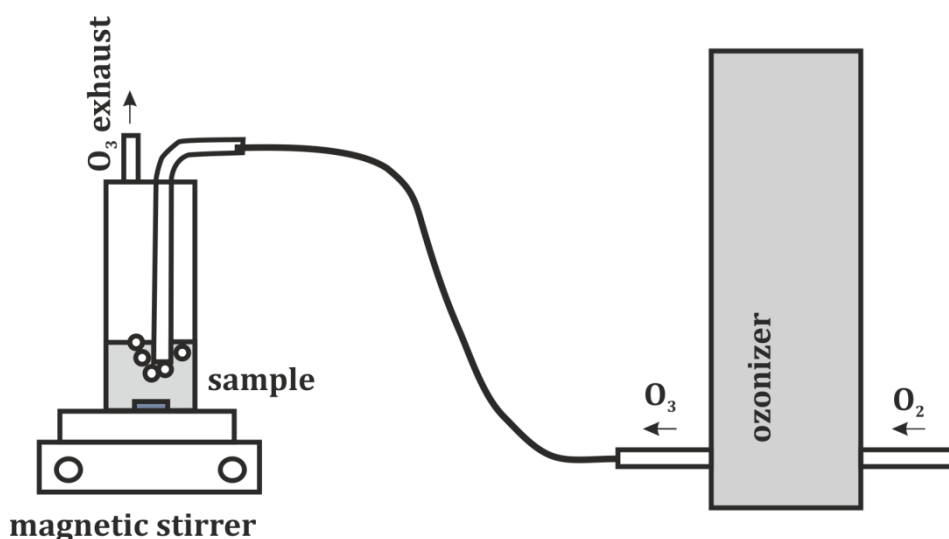


**Figure 39: Schematic depiction of the ozone treatment setup on the righthand-side is the ozone generator connected to an oxygen source on the inlet side and to a flexible tube connecting it to the sample on the outlet side. Left in the picture is the washing flask containing the sample mounted on a magnetic stirrer. Adapted from Felgitsch et al., 2019.**

To check the ozone generation, a potassium iodide solution was used (containing approx. 100 ml of water and approx. 25 g potassium iodide). The potassium iodide solution is colourless. Ozone leads to the release of iodine and therefore a brown colouration of the sample solution. The

sample solution turned completely brown after a few seconds, indicating the presence of high amounts of ozone.

For the analysis of the birch pollen washing water 50 mL of a 10-fold dilution of birch pollen washing water was used. The flow of ozone was set to 1-10 mL/s. Fractions of the washing water were collected after 0, 5, 8, 10, and 12 h and analysed with VODCA. Freezing curves of the different fractions are shown in Figure 40. Further, an overview of the MFT values of the different fractions as a function of ozone treatment time is given in Figure 41.

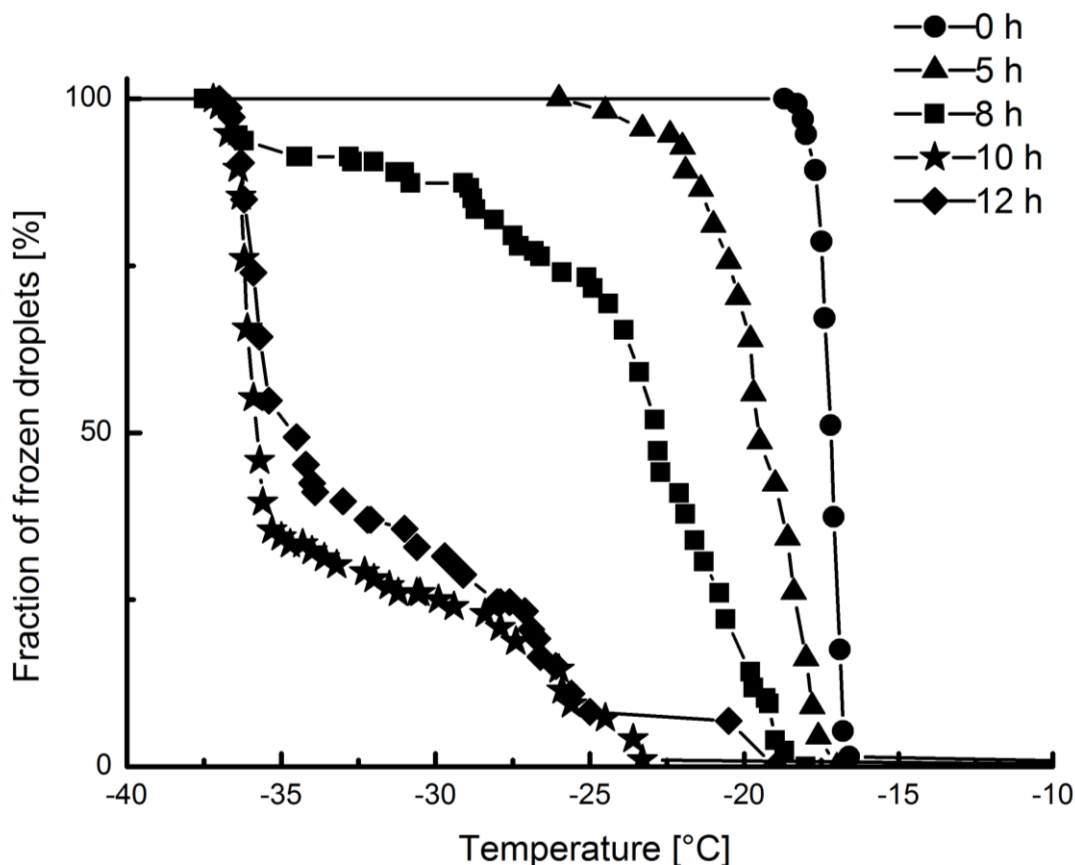


**Figure 40: Freezing curves of the different birch pollen washing water fractions treated with ozone (collected after 0, 5, 8, 10, and 12 h).**

Birch pollen washing water loses INA during the process of ozone treatment. However, even after 10 to 12 h of treatment more than a third of the droplets still froze heterogeneously. Hence, 12 h of ozone with a flow as high as 1-10 mL/s was not enough to completely diminish the INA of birch pollen washing water. This indicates a high resilience of its activity against oxidation via ozone.

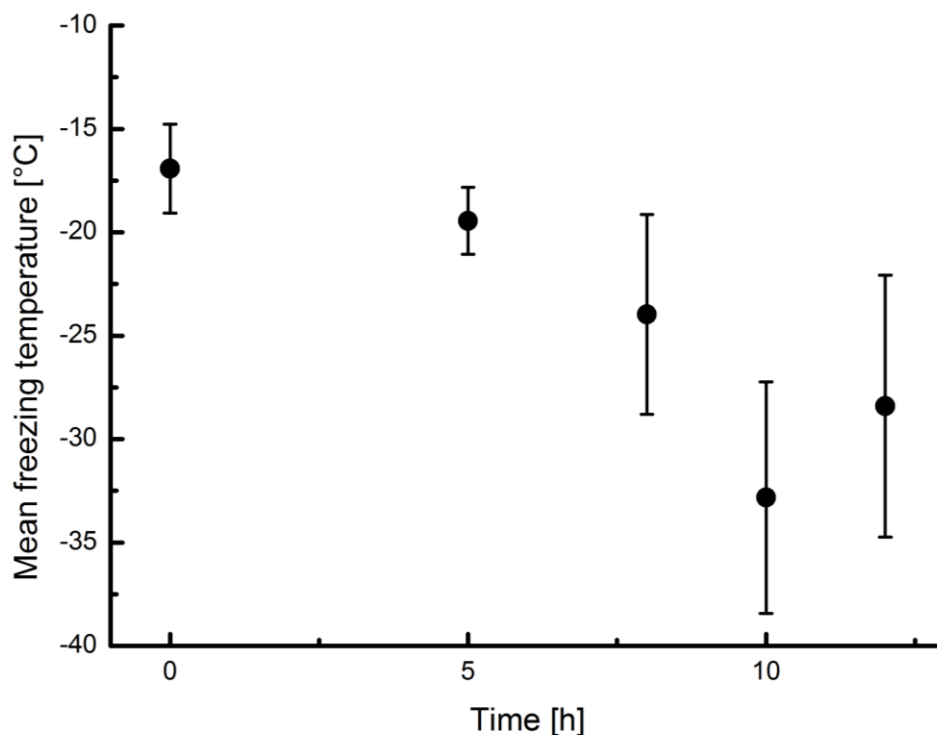


**Figure 41:** MFT values of the five collected fractions plotted with the corresponding standard deviation against the ozone treatment time.



### 3.5. Discussion – Analysis of Birch Pollen INPs

In all our experiments, pure and untreated birch pollen washing water exhibited mean freezing temperatures of approx.  $-17\text{ }^{\circ}\text{C}$ . This is well in line with the reported values in literature for aqueous birch pollen extracts. They range between  $-15\text{ }^{\circ}\text{C}$  and  $-23\text{ }^{\circ}\text{C}$  depending on the methodology (droplet size, freezing mode, and freezing rates) (Diehl *et al.*, 2001; Pummer *et al.*, 2012; Augustin *et al.*, 2013; O’Sullivan *et al.*, 2015)

Most biological INPs, as e.g. certain bacteria, trigger freezing at temperatures higher than  $-10\text{ }^{\circ}\text{C}$  (Murray *et al.*, 2012). In contrast to this, birch pollen trigger freezing below  $-10\text{ }^{\circ}\text{C}$ . In the group of substances freezing below  $-10\text{ }^{\circ}\text{C}$ , birch pollen are among the most active substances with initial freezing temperatures above most of the active mineral dusts, ash, and soot samples (Murray *et al.*, 2012). INPs triggering freezing at temperatures above  $-10\text{ }^{\circ}\text{C}$  are rare. Most atmospheric INPs trigger freezing below  $-10\text{ }^{\circ}\text{C}$  (DeMott *et al.*, 2010; Petters and Wright, 2015). Most aerosols are a crude mixture where it is difficult to distinguish between biological and non-biological material. Pummer *et al.* (2012) showed that INPs from birch pollen are rather heat resistant. Detection of biological INPs due to heat induced activity decrease is therefore not advised. To be able to distinguish INPs from birch pollen from other INPs and to be able to detect their presence in atmospheric samples, a better understanding of the chemical nature of these INPs is necessary.

Some research has already been done on this topic, however, results varied. Optical spectroscopy finds evidence that proteins, saccharides, and lipids are easily extracted aqueously from birch pollen (Pummer *et al.*, 2013). On the one hand, Pummer *et al.* (2012) and Dreischmeier *et al.* (2017) attribute the INA to carbohydrates. On the other hand Tong *et al.* (2015), suggest that proteins are the major source for INA. Further, it has

been shown that cellulose, which is a carbohydrate ubiquitously present in plants, has ice nucleating abilities in the temperature range of interest (Hiranuma *et al.*, 2015). Proteins are typically easily destroyed with high temperatures, therefore, the temperature resistance of the INPs from birch pollen does not point towards proteins. However, the subtilisin experiment showed that proteins have to play a role in the INA of birch pollen. These controversies and the contradictory literature on the topic lead to the assumption, that the INPs are not single components but are probably a multi-component system with aggregate character.

Based on our results, we make two assumptions:

- The birch pollen washing water strongly interacts with nonpolar surfaces, which can be seen in our SEC experiments and in our SPE experiments. As the INPs are also easily extractable in water, we assume the responsible material to be amphiphile.
- The subtilisin and urea experiments strongly suggests that proteins play an important role in the INA of birch pollen.
- Ozone experiments suggest that the INPs in birch pollen washing water are rather stable towards reactive oxygen species.

As there are indicators for both an impact of proteins and an impact of carbohydrates, it is easily possible that the responsible material is not a single molecule but rather the combination of several substances. Brush *et al.* (1994) already showed more than 20 years ago that the ice nucleation active component in winter rye is composed of a complex composition of proteins, carbohydrates and phospholipids. It seems likely that the chemistry of the INPs of birch pollen is similarly complex.

## 4. Ice Nucleation Activity of Plant Materials

### 4.1. Ice Nucleation Activity of Birch Trees

As already established, birch pollen are well known to contain INPs, which are in the macromolecular size range and are easily detached from the pollen grain. However, little is known about the INA of the rest of the tree.

To examine the ice nucleation activity of birch trees, we analysed samples from ten trees, nine of which samples in Tyrol along an altitudinal gradient and one sampled in a small urban park in Vienna (see Table 3). We examined extracts of milled samples to gain the maximum of extractable INPs (presented in Section 4.1.1, published in the article Felgitsch *et al.*, 2018), as well as surface extracts to investigate the available amount of INPs for the environment (presented in Section 4.1.2).

#### 4.1.1. INA of Milled Samples

##### 4.1.1.1. Freezing temperature and ice nuclei concentration

All of the analysed 30 extracts of birch trees were ice nucleation active (Figure 42, the corresponding gained values are given in Table 11. The highest variation in mean freezing temperature (MFT) was found for the extracts from the leaves, which showed the highest (TBC-L  $-15.6$  °C) and lowest (TBI-L  $-31.3$  °C) MFT amongst all analysed samples (Figure 42). Of the ten birch trees, the leaves of only five trees (TBC-L, TBD-L, TBF-L, TBG-L, VB-L) showed freezing temperatures close to the birch pollen line ( $-17.1$  °C see solid line in Figure 42). Those samples froze between  $-15.6$  °C (TBC-L) and  $-19.3$  °C (TBD-L and VB-L). The residue of the analysed leaf extracts froze at temperatures of  $-25.4$  °C and below.

All of the primary wood extracts were ice nucleation active, with most MFT values between  $-17.5$  °C (TBE-P) and  $-22.6$  °C (TBI-P). Further, two samples froze at  $-25.4$  °C (TBH-P, TBD-P). For most secondary wood

extracts, we found slightly higher MFTs than for the primary wood samples. The values ranged from  $-17.2\text{ }^{\circ}\text{C}$  (TBB-S) to  $-22.8\text{ }^{\circ}\text{C}$  (TBH-S). The MFTs of the majority of the wood samples were close to the birch pollen line ( $-17.1\text{ }^{\circ}\text{C}$ , see Figure 42).

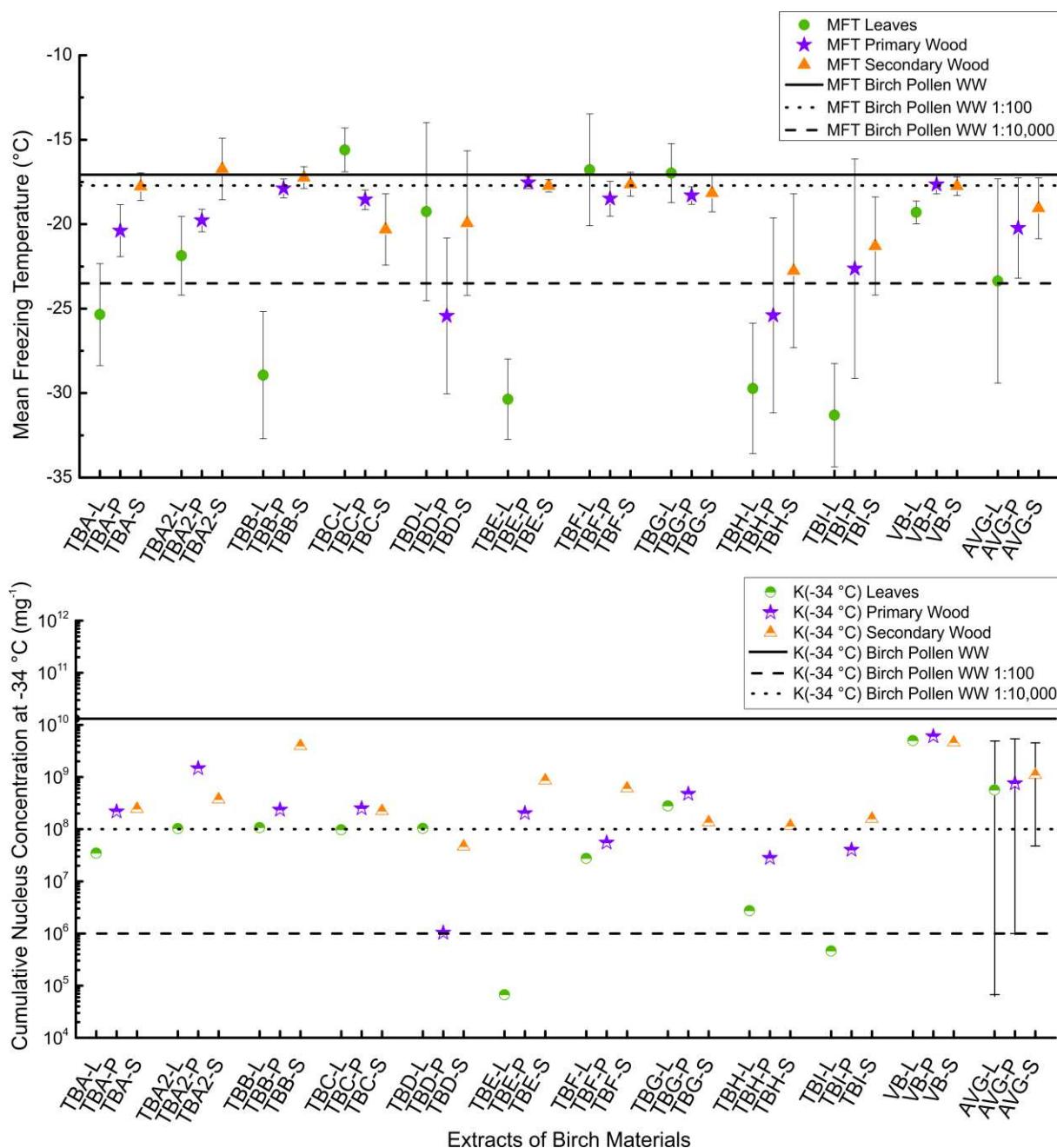


**Figure 42: (a) Mean freezing temperature (MFT) of the different birch samples. Leaf extracts (L) are marked with green circles, primary wood extracts (P) with violet stars, and secondary wood extracts (S) with orange triangles. The solid line is the MFT of birch pollen washing water ( $-17.1\text{ }^{\circ}\text{C}$  with a standard deviation of  $-0.5\text{ }^{\circ}\text{C}$  (not plotted)). The**

*dotted line represents the MFT of a dilution equivalent to  $10^8$  INPs  $\text{mg}^{-1}$  ( $-17.7$  °C with a standard deviation of  $-1.1$  °C (not plotted)) and the dashed line refers to the MFT of a dilution equivalent to  $10^6$  INPs  $\text{mg}^{-1}$  ( $-23.5$ °C with a standard deviation of  $-3.6$  °C (not plotted)). The three values on the far-right side of (a) represent the average of all mean freezing temperatures for leaves (AVG-L), primary wood (AVG-P), and secondary wood (AVG-S) with the corresponding standard deviation. (b) Cumulative nucleus concentration at  $-34$  °C ( $K(-34$  °C)) of the different birch samples  $\text{mg}^{-1}$  extracted sample. Assignment of the symbols is similar to the top plot. The solid line refers to the  $K(-34$  °C) of birch pollen washing water  $\text{mg}^{-1}$  extracted pollen ( $1.3 \cdot 10^{10}$   $\text{mg}^{-1}$ ); the dotted and dashed line refer to the dilutions from birch pollen washing water introduced in (a). The three values on the far right side represent the average of all  $K(-34$  °C) values. Error bars point to the area of trust, ranging from the highest to the lowest measured values. Taken from Felgitsch et al., 2018.*

Mean freezing temperature values depend on the nature and on the contained concentration of INPs. A higher concentration in INPs leads to a higher freezing temperature. If a mixture of different INPs is present, the strongest INP will trigger the freezing event. With lower concentrations, less droplets will contain this INP, leading to freezing being triggered by less potent INPs, shifting the MFT to colder temperatures. Therefore, not just MFT but also the cumulative nucleus concentration needs to be regarded.

The cumulative nucleus concentration  $K(T)$  showed a trend similar to the MFT (as depicted for  $-34$  °C in Figure 42, and for all temperatures above  $-35$  °C in Figure 43 for leaves, Figure 44 for primary wood, and Figure 45 for secondary wood). Leaf extracts mostly exhibited cumulative nucleus concentration at  $-34$  °C between  $2.8 \cdot 10^6$   $\text{mg}^{-1}$  (TBH-L) and  $5.0 \cdot 10^9$   $\text{mg}^{-1}$  (VB-L), with two outliers exhibiting  $4.6 \cdot 10^5$   $\text{mg}^{-1}$  (TBI-L) and  $6.7 \cdot 10^4$   $\text{mg}^{-1}$  (TBE-L). However, these two outliers with the low INM concentrations were the two leaf samples exhibiting the lowest MFT values (TBE-L  $-30.4$  °C, TBI  $-31.3$  °C). This indicates that the unusually low MFTs are a result of low concentrations of INMs in the samples. Leaf extracts, which exhibited the highest variation in MFT also exhibited the highest variation in INM concentration (see Figure 42, Figure 43, and Figure 46).

For primary wood extracts, most values for  $K(-34\text{ °C})$  ranged between  $1.0 \cdot 10^6\text{ mg}^{-1}$  (TBD-P) and  $6.1 \cdot 10^9\text{ mg}^{-1}$  (VB-P). Secondary wood extracts again exhibited the least variation, which can be seen best in Figure 42, Figure 45, and Figure 46. Their cumulative nucleus concentrations at  $-34\text{ °C}$  ranged from  $4.6 \cdot 10^7$  (TBD-S) to  $4.6 \cdot 10^9\text{ mg}^{-1}$  (VB-S, TBB-S). Figure 45 shows that this decreased variation compared to the other samples is not just true for the cumulative nucleus concentration at  $-34\text{ °C}$ , but over the whole temperature regime.

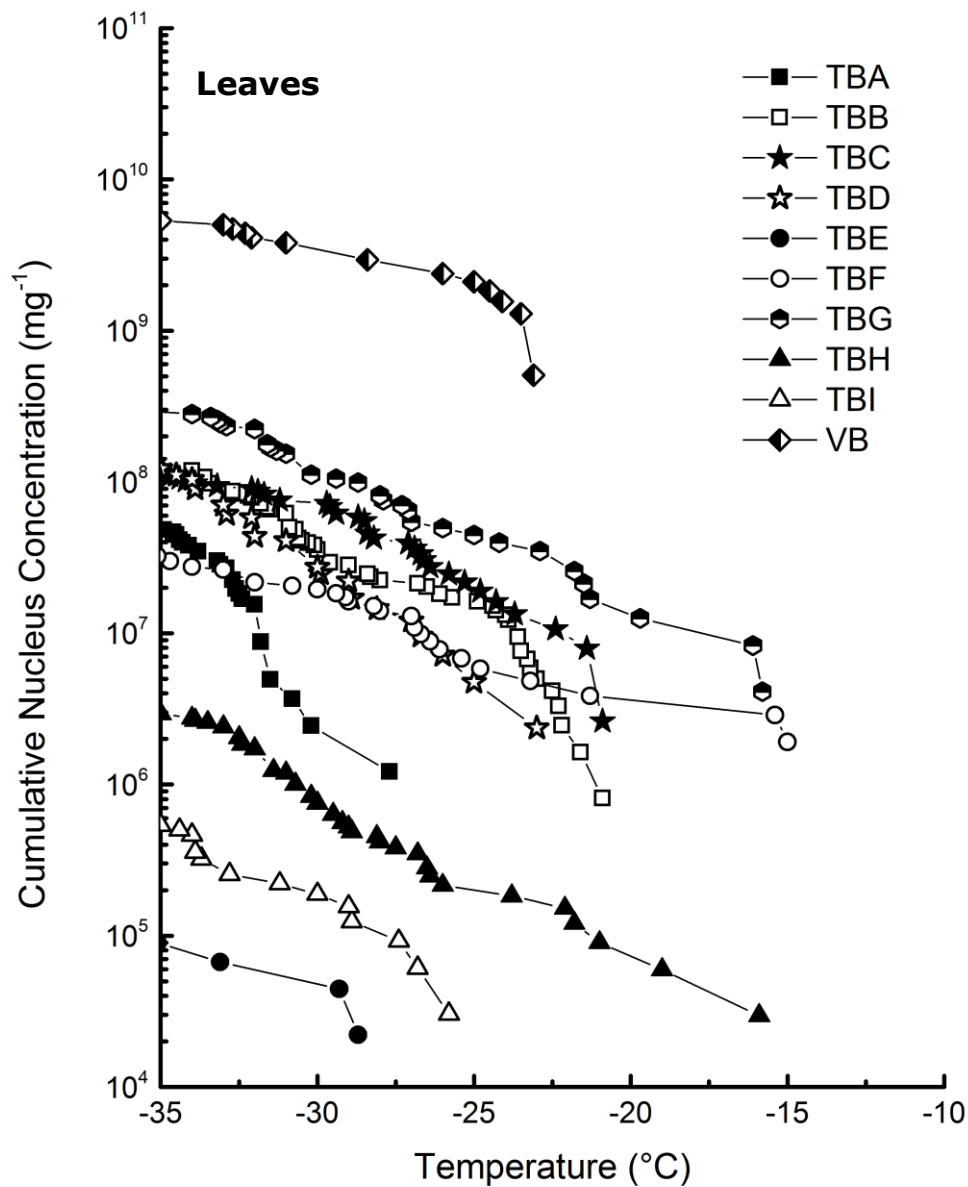


**Figure 43:** Cumulative nucleus concentration as a function of temperature for leaf extracts. The diagram is cut off at  $-35\text{ }^{\circ}\text{C}$ , since we cannot contribute freezing events below this temperature to heterogeneous nucleation. The symbols used for the different data points are grouped. Birches growing in close proximity under similar conditions are marked with the same symbol (different fillings). Adapted from Felgitsch et al., 2018.

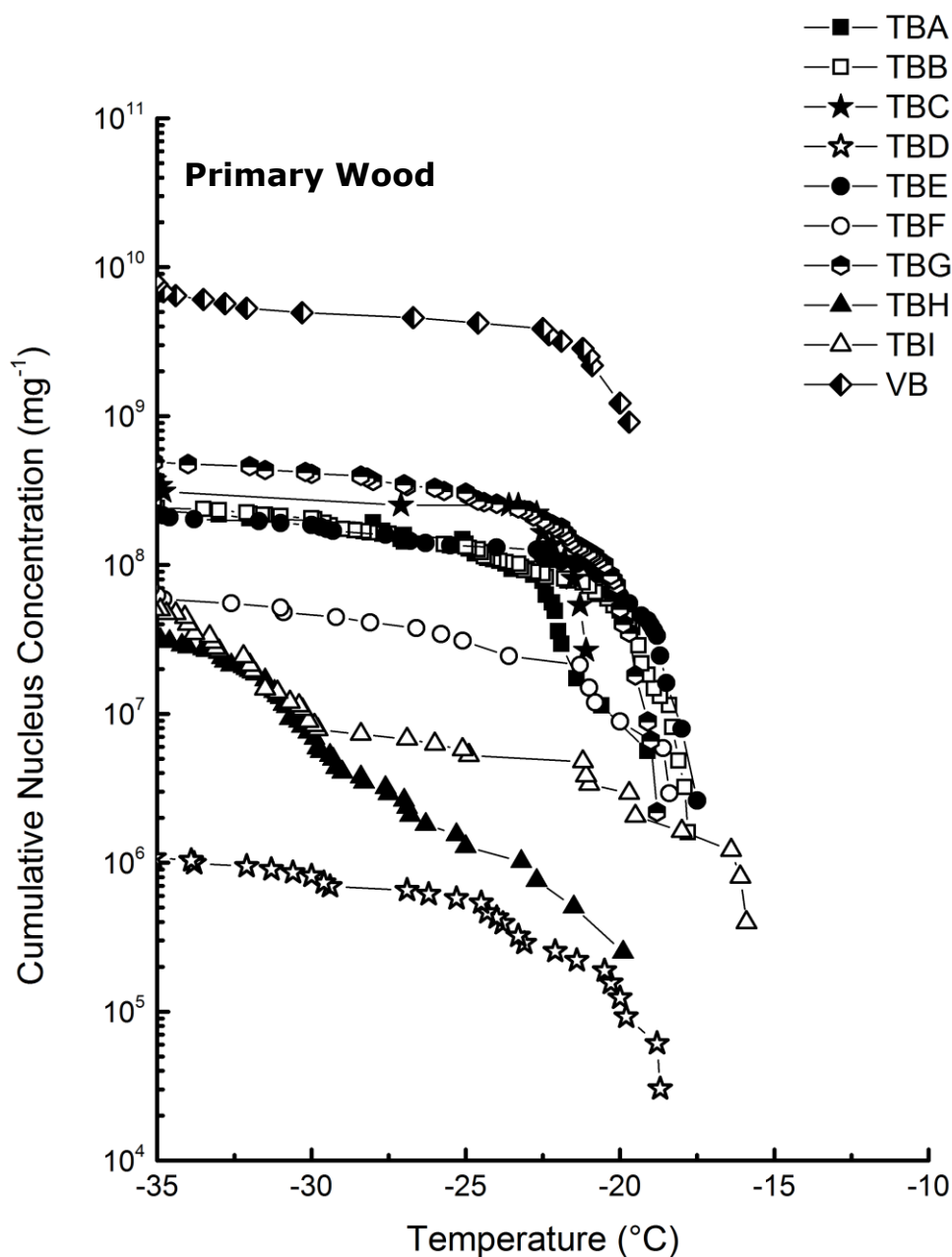


**Figure 44:** Cumulative nucleus concentration as a function of temperature for primary wood extracts. The diagram is cut off at  $-35\text{ }^{\circ}\text{C}$ , since we cannot contribute freezing events below this temperature to heterogeneous nucleation. The symbols used for the different data points are grouped. Birches growing in close proximity under similar conditions are marked with the same symbol (different fillings). Adapted from Felgitsch et al., 2018.



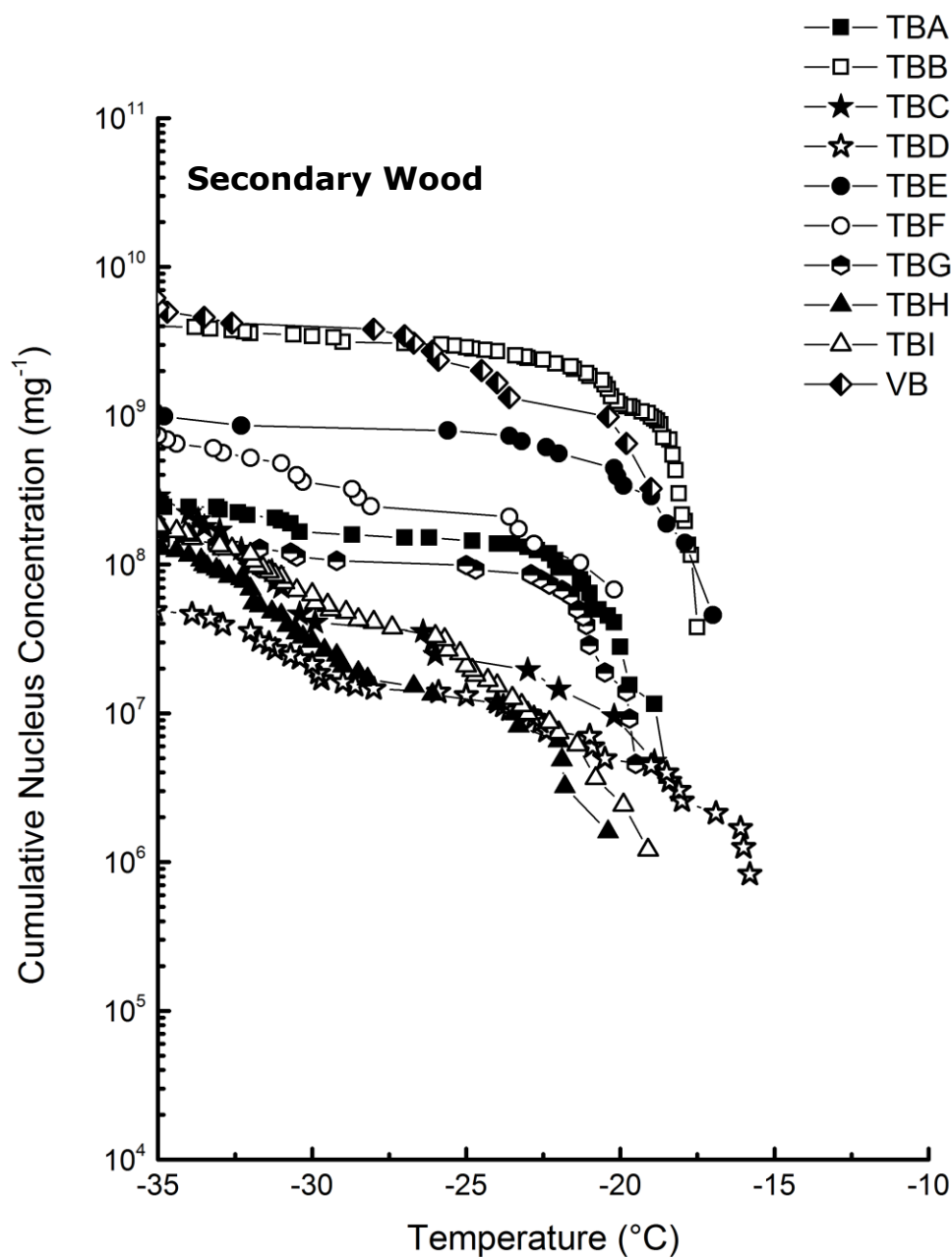


**Figure 45:** Cumulative nucleus concentration as a function of temperature for and secondary wood extracts. The diagram is cut off at  $-35^{\circ}\text{C}$ , since we cannot contribute freezing events below this temperature to heterogeneous nucleation. The symbols used for the different data points are grouped. Birches growing in close proximity under similar conditions are marked with the same symbol (different fillings). Adapted from Felgitsch et al., 2018.

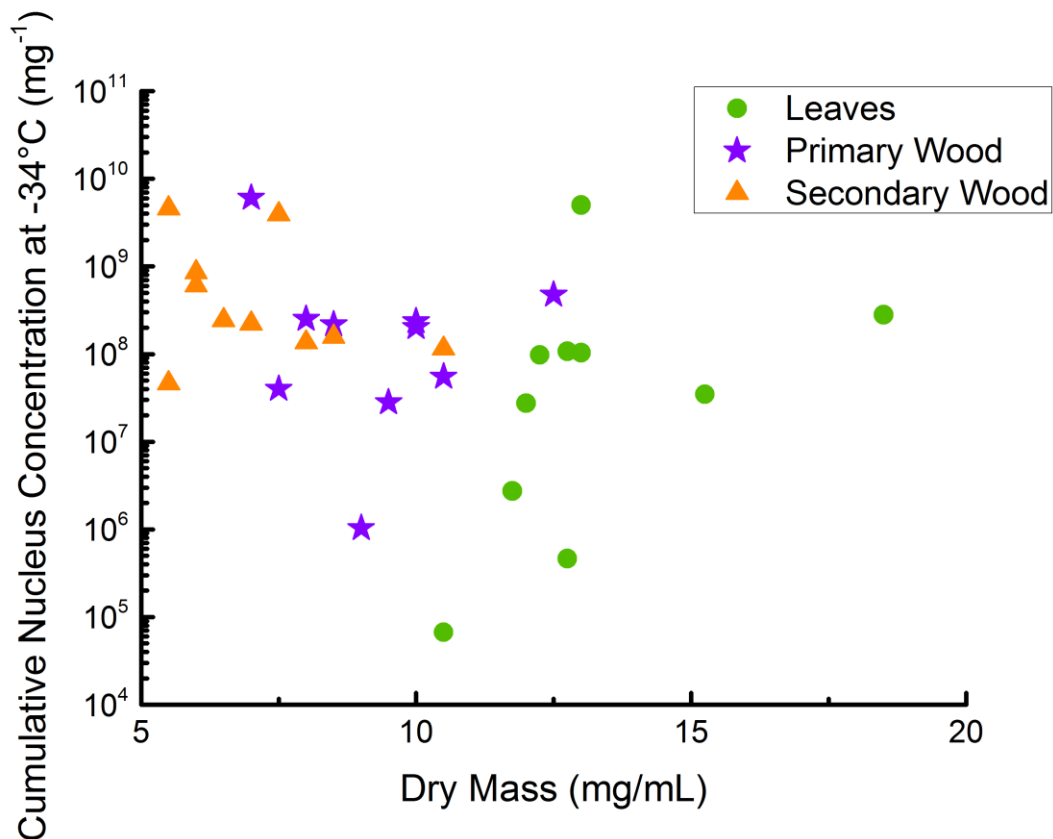


**Figure 46: Scatterplot of dry mass (dry residues of the different filtered extracts) and cumulative nucleus concentration at -34°C per sample mass. The dry mass is the mass extracted with the 50 mg/mL suspensions. The data show that secondary wood, which contained mostly the highest INM concentrations and lowest variations between different samples, also contained the lowest extractable mass. Therefore, INM ratios in the extractable content of the different samples were highest in secondary wood samples. Taken from Felgitsch et al., 2018.**

To determine branch to branch variations, a second branch of TBA was analysed (marked as TBA-2 in Figure 42 and in Table 11). No major differences can be found regarding freezing temperature of the wood samples if the two different branches are compared. This indicates that freezing temperature of wood is a tree specific trait. However, the primary wood of the second branch showed a nearly 10fold increased INP concentration. Leaves on the other hand varied in both, freezing temperature and INP concentration.

Further, the relationship of the extractable INM concentration and the extractable total mass was analysed. The total extractable mass (given as dry mass in Figure 46) describes the weight of the dry residue of a filtered extract in mg/mL. It was highest for leaf extracts and lowest for the secondary wood extracts. As in the other attributes, leaf extracts exhibited the highest variations with dry masses ranging from 11 (TBE-L) to 19 mg/mL (TBG-L), followed by primary wood extracts ranging from 7 (VB-S) to 13 mg/mL (TBG-P). Dry masses of the secondary wood extracts ranged from 6 (TBD-S, TBE-S, TBF-S, VB-S) to 11 mg/mL (TBH-S). The secondary wood samples tended to exhibit highest concentrations of INMs per mg sample mass, they also had the highest ratio of INMs compared to dry mass (see Figure 46). The lowest ratio was found for the leaf extracts. In general, Figure 46 clearly shows that dry mass and INA do not correlate. Therefore, the INA of the analysed extracts is not a result of the dry mass content.

While the results show that all analysed birch trees were ice nucleation active, it was also found that the trees themselves vary in their activity if compared to each other. Lowest concentrations of INMs (if all samples are regarded) were found for TBD, TBH, and TBI (see Figure 42, Figure 43, Figure 44, and Figure 45), all of which were growing along a riverbank with no traffic next to the trees. Only one tree with these growing conditions was found to exhibit high INM concentrations (TBC). Highest concentrations were found in the samples of the Viennese birch, located in a small park in Vienna, surrounded by heavy traffic. Trees, which were growing in close proximity to each other (see Figure 42) often exhibited comparable INA. This is especially true for TBA and TBB, as well as TBH and TBI. TBE and TBF match each other well except for the INA of the analysed leaves. TBC and TBD however acted significantly different if compared to each other, with TBD showing decreased INM concentrations.

**Table 11: The gained MFT values with corresponding standard deviation and the  $K(-34\text{ °C})$  values of the milled leaf, primary wood, and secondary wood samples:**

	Leaves			Primary Wood			Secondary Wood		
	MFT (°C)	$\sigma$	$K(-34\text{ °C})$ ( $\text{mg}^{-1}$ )	MFT (°C)	$\sigma$	$K(-34\text{ °C})$ ( $\text{mg}^{-1}$ )	MFT (°C)	$\sigma$	$K(-34\text{ °C})$ ( $\text{mg}^{-1}$ )
TBA	-25.4	3.0	$3.5 \cdot 10^7$	-20.4	1.5	$2.2 \cdot 10^8$	-17.8	0.8	$2.4 \cdot 10^8$
TBA2	-21.9	2.3	$1.0 \cdot 10^8$	-19.8	0.7	$1.5 \cdot 10^9$	-16.7	1.8	$3.7 \cdot 10^8$
TBB	-28.9	3.8	$1.1 \cdot 10^8$	-17.9	0.6	$2.4 \cdot 10^8$	-17.2	0.6	$3.9 \cdot 10^9$
TBC	-15.6	1.3	$9.8 \cdot 10^7$	-18.6	0.6	$2.5 \cdot 10^8$	-20.3	2.1	$2.2 \cdot 10^8$
TBD	-19.3	5.3	$1.0 \cdot 10^8$	-25.4	4.6	$1.0 \cdot 10^6$	-19.9	4.3	$4.6 \cdot 10^7$
TBE	-30.4	2.4	$6.7 \cdot 10^4$	-17.5	0.3	$2.0 \cdot 10^8$	-17.7	0.4	$8.6 \cdot 10^8$
TBF	-16.8	3.3	$2.8 \cdot 10^7$	-18.5	1.0	$5.5 \cdot 10^7$	-17.6	0.7	$6.0 \cdot 10^8$
TBG	-17.0	1.7	$2.8 \cdot 10^8$	-18.3	0.5	$4.8 \cdot 10^8$	-18.2	1.1	$1.4 \cdot 10^8$
TBH	-29.7	3.8	$2.7 \cdot 10^6$	-25.4	5.8	$2.8 \cdot 10^7$	-22.8	4.6	$1.1 \cdot 10^8$
TBI	-31.3	3.0	$4.6 \cdot 10^5$	-22.6	6.5	$4.0 \cdot 10^7$	-21.3	2.9	$1.6 \cdot 10^8$
VB	-19.3	0.7	$5.0 \cdot 10^9$	-17.7	0.6	$6.1 \cdot 10^9$	-17.7	0.5	$4.6 \cdot 10^9$
AVG	-23.4	6.0	$5.7 \cdot 10^8$	-20.2	3.0	$7.6 \cdot 10^8$	-19.1	1.8	$1.1 \cdot 10^9$

#### 4.1.1.2. Heat Treatment

Pummer et al. (2012) showed that INPs derived from birch pollen are resistant against heat (100 °C and higher). As we assume that the INPs present in birch trees and in pollen thereof are similar, heat resistance should be a uniform trait. Therefore, the extracts of birch TBA were tested in regards of reaction to heat. All three extracts of the birch were treated following the protocol introduced by Pummer et al. (2012). 100  $\mu\text{L}$  of each sample were pipetted onto a clean glass slide. The glass slides were put in

an oven, which was set to 100 °C. After one hour, the glass slides were removed, and the dry residues were resuspended in 100 µL of ultrapure water. INA was tested of all treated samples. The results are shown in Figure 47. The corresponding values are given in Table 12.

We observed no major changes in INP concentration and the MFT values stayed well within the standard deviations of each other. Therefore, we conclude that heat treatment does not affect INPs derived from birch wood and leaves.

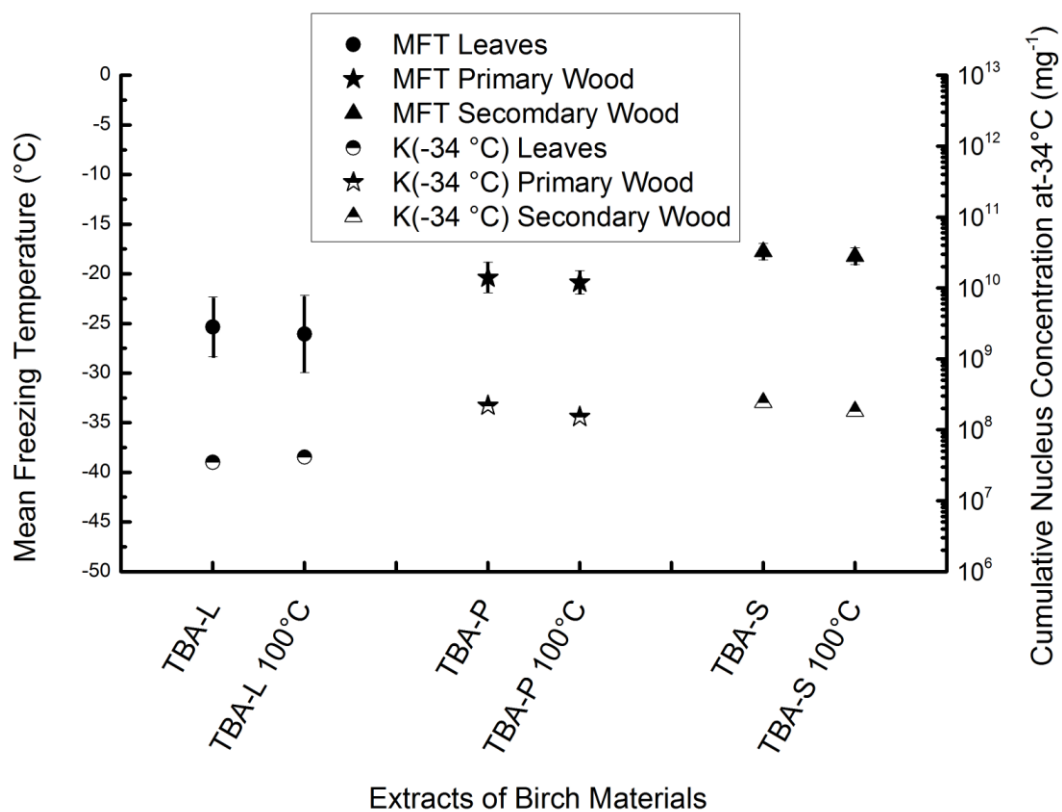


**Figure 47: Results of the heat treatment of TBA. MFT values are symbolized using filled symbols, which correspond to the left y-axis; cumulative nucleus concentration at -34 °C is symbolized by half-filled symbols, which correspond to the right y-axis. Leaves are marked with circles, primary wood extracts with stars and secondary wood extracts with triangles. Left samples are untreated extracts, right samples are treated extracts (marked with a 100 °C in the sample name). Adapted from Felgitsch et al., 2018.**

It should be mentioned that this method is not ideal. Heating the thin liquid layer leads to a rapid evaporation of water. Therefore, the heating process is mostly done to dried residues. A possibility to handle this problem would be working with an autoclave.

**Table 12: Mean freezing temperature (MFT) and corresponding standard deviation  $\sigma$ , as well as cumulative nucleus concentration at  $-34\text{ }^{\circ}\text{C}$  ( $K(-34\text{ }^{\circ}\text{C})$ ) for the extracts of TBA branches (leaves, primary wood, and secondary wood). Treated refers to a heat treatment at  $100\text{ }^{\circ}\text{C}$ :**

	$K(-34\text{ }^{\circ}\text{C})$ ( $\text{mg}^{-1}$ )	MFT ( $^{\circ}\text{C}$ )	$\sigma$ ( $^{\circ}\text{C}$ )
Leaves untreated	$3.5 \cdot 10^7$	-25.4	3.5
Leaves treated	$4.1 \cdot 10^7$	-26.1	4.1
Primary wood untreated	$2.2 \cdot 10^8$	-20.4	2.2
Primary wood treated	$1.5 \cdot 10^8$	-20.9	1.5
Secondary wood untreated	$2.4 \cdot 10^8$	-17.8	2.4
Secondary wood treated	$1.8 \cdot 10^8$	-18.2	1.8

#### 4.1.1.3. Similarities between the INPs

Based on our results, we assume that all measured samples contain similar INPs compared birch pollen. To test this hypothesis, the Wilcoxon-Mann-Whitney test was used. This test is a non-parametric test, which is used to analyse if median values of two distributions can be differentiated (DePuy, Berger and Zhou, 2005). In this case the distributions are the

droplet assays with all droplets frozen in the heterogeneous temperature regime and their corresponding freezing temperature.

The biggest problem in comparing two INP samples from birches is the concentration dependency (see Figure 48). As dilution highly influences the temperature, one cannot just introduce pure birch pollen washing water but also needs additional dilutions thereof. Dilutions used were: 1:100 (similar in concentration to wood samples exhibiting  $\sim 10^8$  INPs per mg) and 1:10,000 (similar in concentration to wood samples exhibiting  $\sim 10^6$  INPs per mg).

The n-values used for the calculation were the number of droplets frozen heterogeneously during the analysis of each sample/standard. They ranged between 28 and 118 for the samples and between 92 and 125 for the comparison standards. The n-values and test results are given in Table 13. The shown p-values are indicators for the significance of the result based on the significance level (in our case 0.1 %). Calculated p-values which lie above the significance level indicate that the null hypothesis can be rejected. In this case the test stated that no significant difference can be found between the distribution of two samples within the set level of significance.

The test showed similarities for pure birch pollen washing water with TBB-S and TBD-L. Both were among the samples with the highest activity.

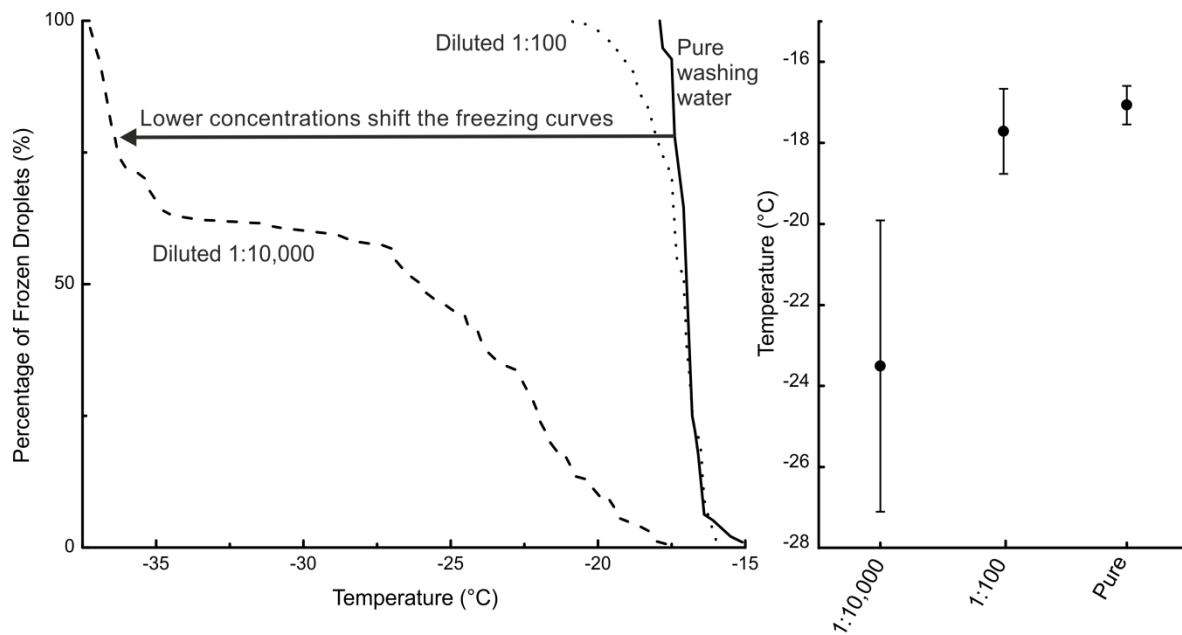


**Figure 48: Concentration dependency of the freezing temperature of birch pollen washing water. Left: freezing events over the whole temperature regime for pure washing water, a 1:100 dilution and a 1:10,000 dilution. Right: corresponding mean freezing temperatures with standard deviation. Taken from Felgitsch et al., 2018.**

Further, similarities were found between the 1:100 dilution and both, TBA-S, and TBA2-S. The 1:10,000 dilution of birch pollen washing water was found to be similar to TBD-P, TBH-P, TBH-S, and TBI-P. The latter are amongst the samples tested exhibited the lowest activity.

**Table 13: The results for the Wilcoxon–Mann–Whitney test. All given samples were shown to match birch pollen washing water or a dilution thereof. Pure birch pollen washing water is marked with pure, the 1:100 dilution equivalent to  $10^8$  INPs per mg is marked with 1:100, the 1:10,000 dilution equivalent to  $10^6$  INPs per mg is marked with 1:10,000.  $n$  represents the number of data points used for comparison for each sample<sup>a</sup>. The used significance level  $\alpha^b$  was 0.1 % (taken from Felgitsch et al., 2018):**



Sample	n	Birch pollen washing water concentration	p-value <sup>c</sup>
TBB-S	50	Pure	$6.6 \cdot 10^{-3}$
TBD-L	70	Pure	$2.8 \cdot 10^{-1}$
TBA-S	48	1:100	$1.3 \cdot 10^{-3}$
TBA-S2	118	1:100	$2.7 \cdot 10^{-1}$
TBD-P	28	1:10,000	$8.3 \cdot 10^{-2}$
TBH-P	117	1:10,000	$1.9 \cdot 10^{-3}$
TBH-S	102	1:10,000	$1.3 \cdot 10^{-1}$
TBI-P	43	1:10,000	$6.6 \cdot 10^{-2}$

<sup>a</sup>*n is equivalent to the number of droplets frozen homogeneously. n-values of the used standards were: (pure washing water)=96, n(1:100)=135, n(1:10,000)=92.*

<sup>b</sup>*The significance level marks the probability of falsely assuming two populations to differ in their distribution.*

<sup>c</sup>*The p-value indicates the significance of the result. If the p-value is higher than the used significance level, the statistics indicate no difference between two distributions.*

If birch pollen washing water is diluted, the mean freezing temperature decreases and the freezing curve is shifted towards lower temperatures (see Figure 48). In order to correlate all our samples with birch pollen washing water, it would be necessary to analyse more dilutions thereof. However, highly active samples were correlated with pure washing water and weak samples with strong dilutions thereof. This is a strong indicator that the temperature ranges match and that the freezing behaviour of the contained INPs is similar.

#### 4.1.1.4. FT-IR-Spectroscopy

FT-IR-spectroscopy was used to examine similarities in chemical composition between the extracts of TBA (leaves, primary and secondary wood) and aqueous birch pollen extract. The normalized FT-IR-spectra are shown in Figure 49. Table 14 contains assignments for the band positions. On the left side of the spectrum, there is a broad band with a maximum at approx.  $3300\text{ cm}^{-1}$  typical for N-H and O-H stretching vibrations, and further, a bisected band with maxima at  $2940\text{ cm}^{-1}$  and  $2890\text{ cm}^{-1}$ , which can be assigned to aliphatic C-H stretching vibrations. All four spectra show a weak shoulder at approximately  $2700\text{ cm}^{-1}$  which is linked to O-H stretching vibrations.  $2700\text{ cm}^{-1}$  can also be linked to aldehydes (maximum typically at  $2720\text{ cm}^{-1}$ ). However, due to the presence of bands at  $920\text{ cm}^{-1}$  and in the range between  $1420 - 1330\text{ cm}^{-1}$ , which can be linked to O-H, we assume the band  $2700\text{ cm}^{-1}$  to be linked to O-H as well. On the low-frequency side ( $1800$  to  $750\text{ cm}^{-1}$ ) a broad array of bands was found. 19 maxima were assigned. Several of these bands are typical for saccharides as well as for xylan, pointing to the importance of polysaccharides in the extracts. Also, bands in all three typical amid regions are present. All three regions can be assigned to other biomolecules (e.g. polyketides) as well; therefore, the presence of peptides is not entirely clear. The spectra of the different extracts of TBA (Figure 49) show a strong resemblance to each other, but three main differences were found. (a) The intensity at  $1510\text{ cm}^{-1}$ : while the band is intense in the spectrum of secondary wood extracts, it is much less pronounced in the spectra of primary wood and leaf extracts. (b) The band at  $1070\text{ cm}^{-1}$  is very intensive for the leaf extract, where it nearly overlaps with its neighbour at  $1110\text{ cm}^{-1}$ , while it is only present as a slight shoulder in the wood extracts. (c) The region of  $920\text{ cm}^{-1}$  and below increases in intensity from leaf extract over primary wood extract to

secondary wood extract. These differences indicate slight differences in the chemical components of the extracts, or in their concentration ratio.

Comparing the birch pollen washing water to the TBA extracts, we see an enhancement of the low-frequency site of the spectrum. All maxima present in the pollen washing water spectrum are also in the other extracts: However, some bands, which are clearly pronounced in the pollen spectrum, are only very weak shoulders in the TBA extracts (1350, 1300, 1270, 1200, 1140, 810, and 770  $\text{cm}^{-1}$ ). Furthermore, maxima of the two most pronounced bands (3300 and 1050  $\text{cm}^{-1}$  given for the TBA extracts) is shifted slightly by approx. 25  $\text{cm}^{-1}$ .

The IR spectra of all primary wood, secondary wood and leaf extract sample are given in Figure 50, Figure 51, and Figure 52.

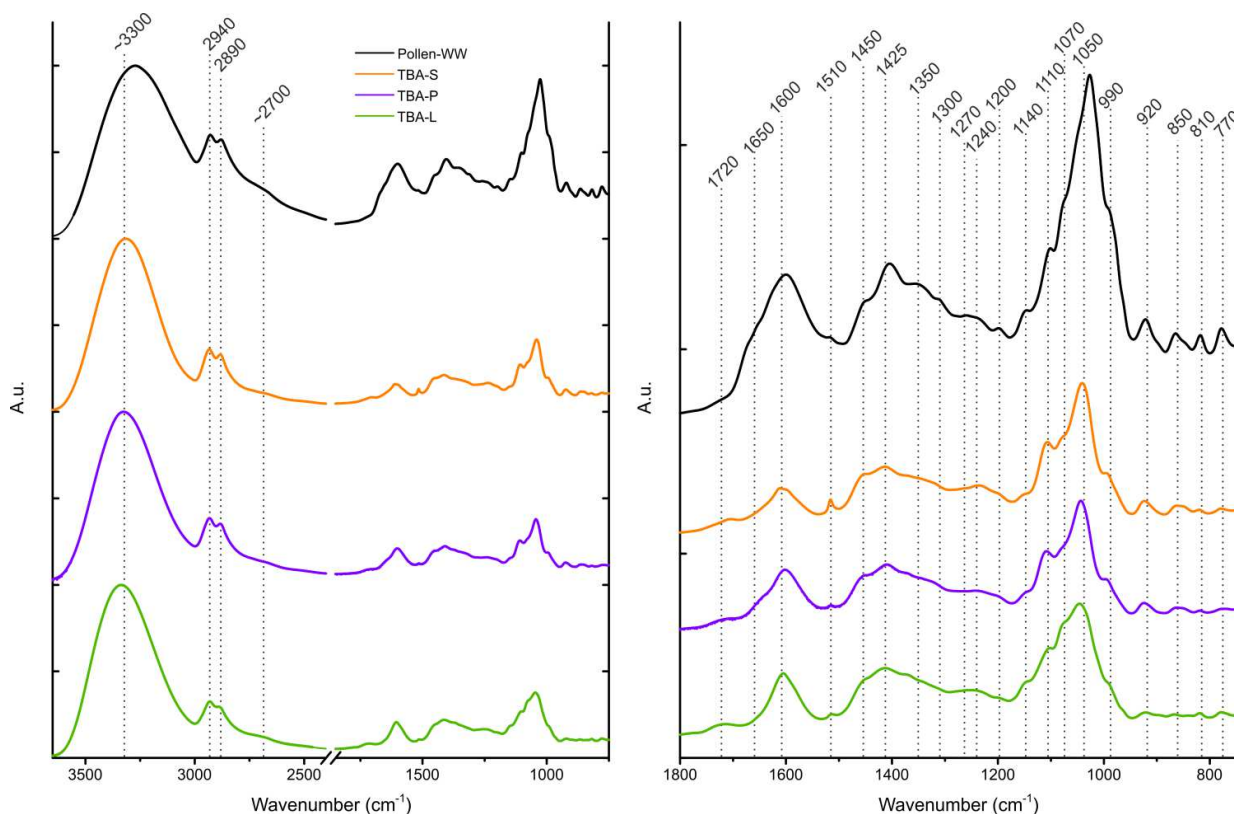


**Figure 49: IR spectra of the TBA extracts (leaves in green, primary wood in violet and secondary wood in orange) and birch pollen washing water (black). Left: the whole spectrum between 3650  $\text{cm}^{-1}$  and 750  $\text{cm}^{-1}$ . Right: enlarged right side of the spectrum**

between  $1800\text{ cm}^{-1}$  and  $750\text{ cm}^{-1}$ . Possible band assignments are given in Table 14. Taken from Felgitsch et al., 2018.

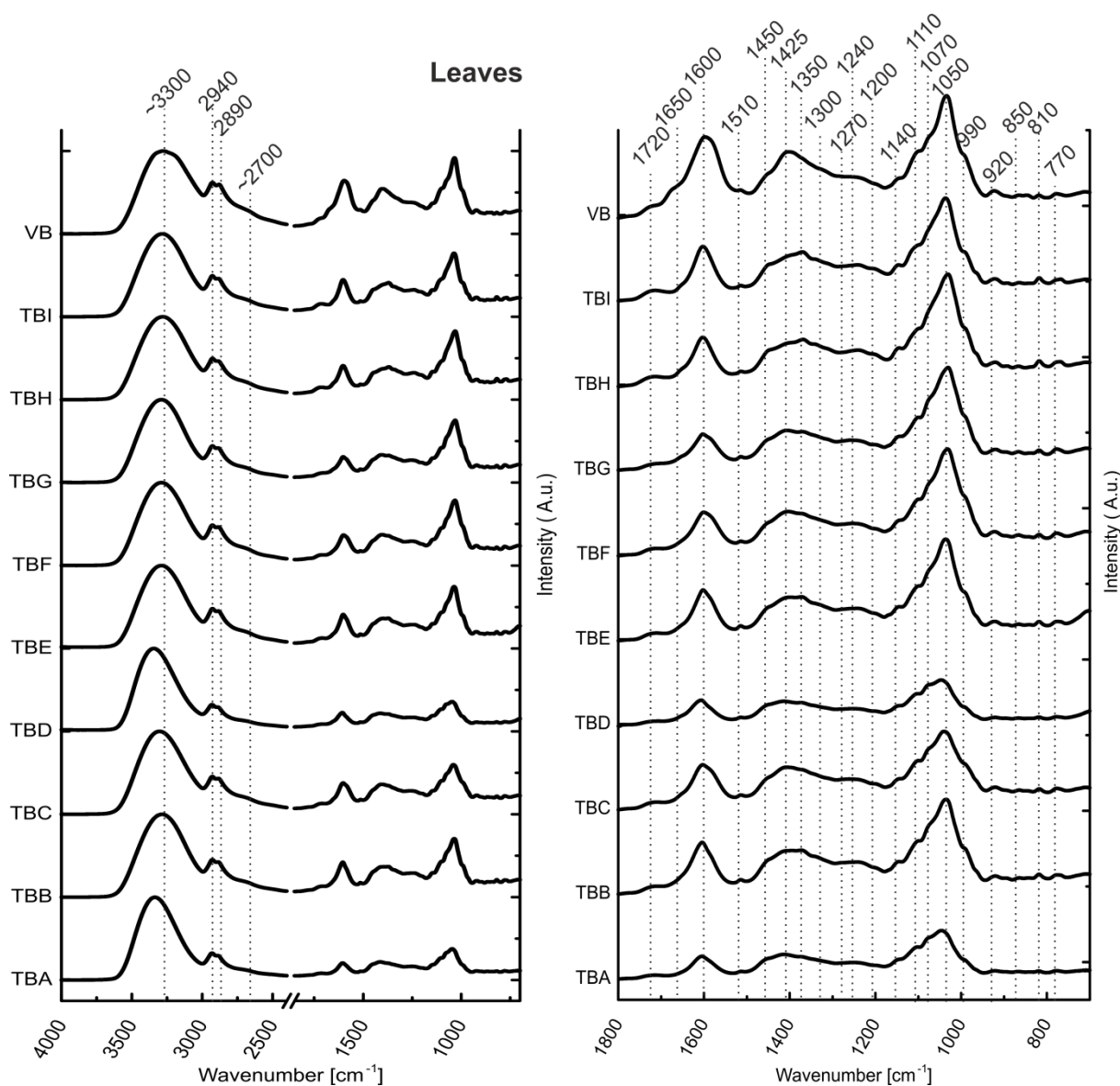


**Figure 50:** IR spectra of the leaf extracts of all analysed birches. Left: the whole spectrum between  $3650\text{ cm}^{-1}$  and  $750\text{ cm}^{-1}$ . Right: enlarged right side of the spectrum between  $1800\text{ cm}^{-1}$  and  $750\text{ cm}^{-1}$ . Possible band assignments are given in Table 14. Taken from Felgitsch et al., 2018.

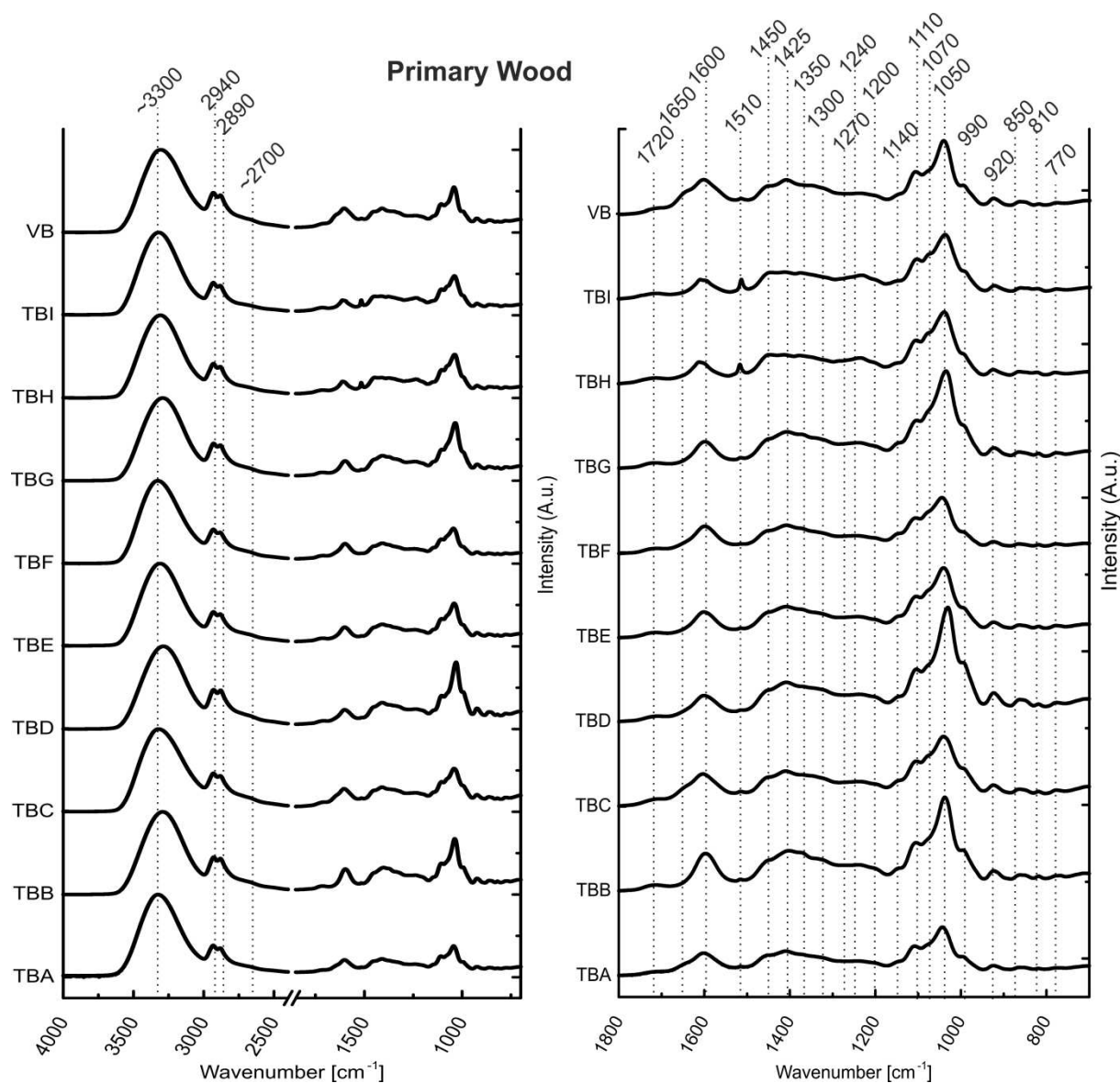


**Figure 51:** IR spectra of the primary wood extracts of all analysed birches. Left: the whole spectrum between  $3650\text{ cm}^{-1}$  and  $750\text{ cm}^{-1}$ . Right: enlarged right side of the spectrum between  $1800\text{ cm}^{-1}$  and  $750\text{ cm}^{-1}$ . Possible band assignments are given in Table 14. Taken from Felgitsch et al., 2018.

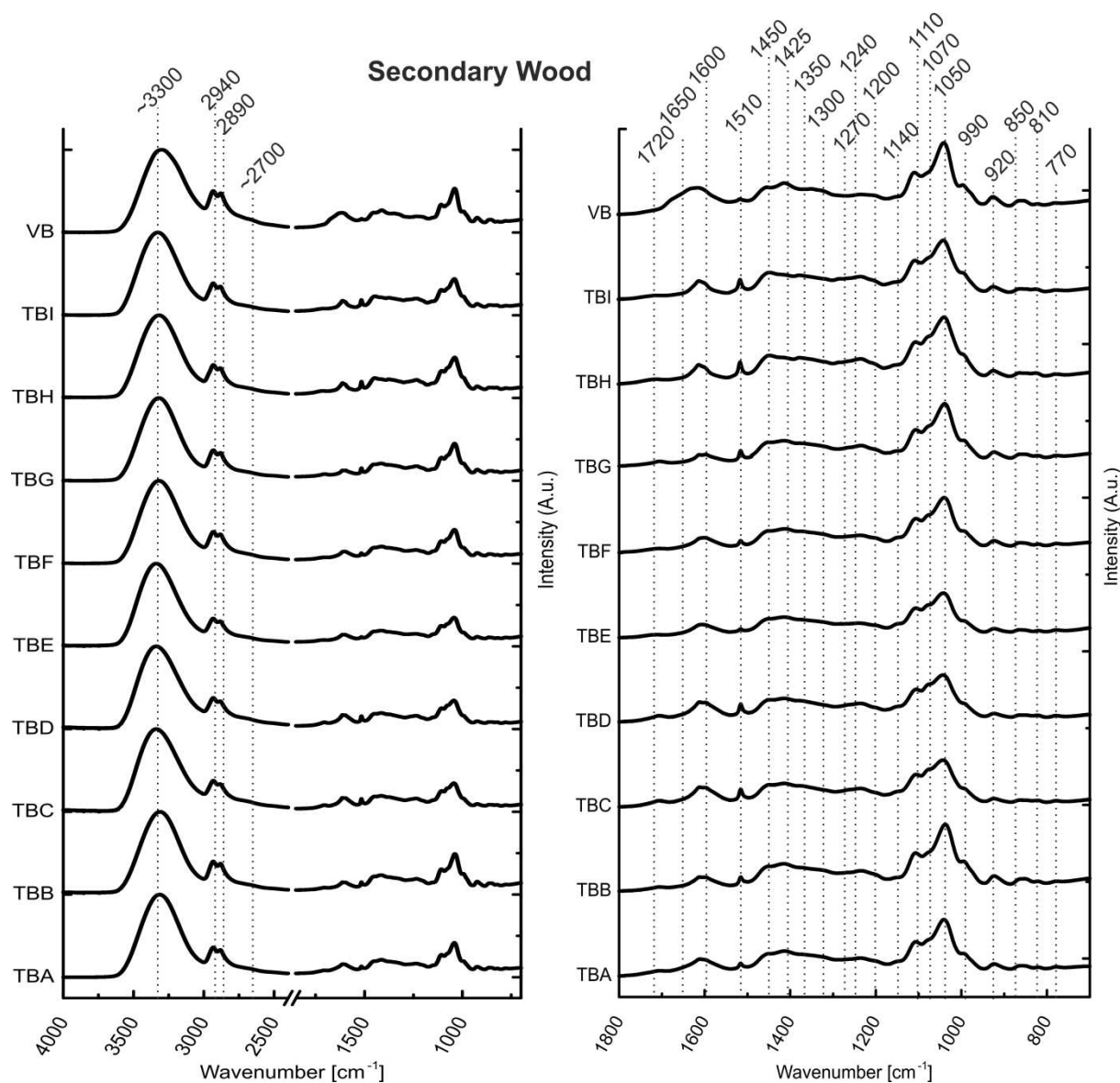


**Figure 52: IR spectra of the secondary wood extracts of all analysed birches. Left: the whole spectrum between  $3650 \text{ cm}^{-1}$  and  $750 \text{ cm}^{-1}$ . Right: enlarged right side of the spectrum between  $1800 \text{ cm}^{-1}$  and  $750 \text{ cm}^{-1}$ . Possible band assignments are given in Table 14. Taken from Felgitsch et al., 2018.**

**Table 14: Band assignment of the IR spectra of TBA extracts (leaves, primary wood, and secondary wood) and birch pollen washing water (Miyazawa, Shimanouchi and Mizushima, 1956; Kačuráková et al., 2000; Schulz and Baranska, 2007; Chen, Hazra and Levin, 2008; Pummer et al., 2013) (taken from Felgitsch et al., 2018):**

Band wavenumber [cm <sup>-1</sup> ]	Assignment of IR spectra
3300	O-H stretch/ N-H stretch
2940	C-H stretch
2890	C-H stretch
2700	O-H stretch, aldehydes (C=O)
1720	C=O, xylan
1650	C=O stretch, C=C, Amid I
1600	C=O stretch (lignin), C=C, Amid I,
1510	C=O stretch (lignin), Amid II,
1450	CH <sub>2</sub> deformation (lignin and xylan)
1425	Aromatic skeletal combined with C-H
1350	C-H deformation (ring), O-H deformation
1300	N-H C-H deformation, Amid III
1270	C=O stretch (lignin), Amid III
1240	C-O, C-N, C-N-C, C-C-O of phenolic compounds, Amid III
1200	Phosphate, C-C-O of phenolic compounds
1140	C-O-C stretching (pyronase rings), C=O stretching (aliphatic groups), Guanine, Tyrosine, Tryptophane
1110	Sugar skeletal vibration
1070	C-H stretch, C-C stretch
1050	C-H stretch, C-C stretch, Guaiacyl units (Lignin)
990	OCH <sub>3</sub> (polysaccharides)
920	C=C, cellulose P-chains, polysaccharides - β-linkage, phenolic compounds O-H (carbonic acid dimers)
850	C-O-C skeletal mode (polysaccharides - α-linkage, COPOC RNA, phenolic compounds)
810	C=O deformation (polysaccharides), phenolic compounds
770	Phosphate stretch

#### 4.1.1.5. Discussion – INPs from Different Parts of Birch Trees

##### INPs Retrieved from milled birch samples

INPs were found in all analysed samples. During the experiment, most of these samples froze in the temperature range between -15 °C and -23 °C, which marks the freezing temperature range of birch pollen washing water in literature (Diehl *et al.*, 2001; Pummer *et al.*, 2012; Augustin *et al.*, 2013; O’Sullivan *et al.*, 2015). This is true for half of all leaf samples (TBC-L, TBD-L, TBF-L, TBG-L, and VB-L). Further, this freezing range was found for 8 of the ten primary wood samples (TBA-P, TBB-P, TBC-P, TBE-P, TBF-P, TBG-P, TBI-P, and VB-P) and for all secondary wood samples. If dilutions of birch pollen washing water are included in the observation, freezing events can be observed over the whole temperature range down to homogeneous freezing (see Figure 48). Nearly all heterogeneous freezing events observed for the extracts of milled samples froze in the window between -15 and -35 °C. The only exception being leaves, which occasionally showed freezing events at higher temperatures. We were able to further strengthen this observation using the Wilcoxon-Mann-Whitney test which correlated more than a quarter of our samples to birch pollen washing water using pure washing water and only two dilutions thereof. Calculations matched both, some of the most and some of the least active samples, with birch pollen washing water and dilutions thereof. The correlation between concentration of INMs and freezing temperature is well known and has been shown previously. Due to our results, we assume a general correlation between the INMs of birch pollen and the INMs found in the rest of the tree, as temperature differences seem to be mostly based on concentration differences.

Another indicator for a strong similarity between the INPs in birch pollen, in wood and in leaves is their heat resistance. The experiment was repeated with extracts of the birch TBA. Results showed that the activity of our samples survives treatment temperatures up to 100 °C.



On the basis of our data we find that the average freezing temperatures of leaves, primary wood, and secondary wood differ slightly. These differences follow the same pattern as the INM concentration which suggests that this is a concentration effect. We hypothesize, based on our results, that the INPs are rather similar throughout the tree, including leaves, primary wood, secondary wood, and pollen as source.

### **Growing Conditions**

Looking at the variability regarding a sample group, we find the highest variabilities for leaves. We even see differences when analysing the leaves of two branches of the same tree. These high variabilities might derive from external influences on the tree. Leaves are easily influenced by growing conditions. Leaves e.g. exhibit reduced dry masses and nitrogen contents if growing in the shades (Eichelmann *et al.*, 2005). Further, their hydrological conductivity is influenced by radiation (Sellin *et al.*, 2011). Not just the availability of radiation has an impact. Trees growing next to a river exhibit enhanced water availability. This can cause increased leaf conductivity and transpiration rate in the lower crown (Sellin and Kupper, 2007).

Birches are native throughout most of Europe. They can be found even up to central Siberia and throughout boreal regions. In general, birches are capable of growing at high altitudes (Beck *et al.*, 2016). Due to the changing conditions caused by climate change paired with their resistance to cold and high altitudes, some species even populate regions above the tree line (Truong, Palmé and Felber, 2007). This area of distribution is vast and varies greatly, which is already true if only Europe is regarded. These environmental conditions could affect the production and release of INMs from birch trees. There are several factors that impact physiology and growth of plants as e.g. humidity (Sellin *et al.*, 2013), atmospheric ozone concentration (Maurer and Matyssek, 1997; Harmens *et al.*, 2017),

CO<sub>2</sub> (Rey and Jarvis, 1998; Kuokkanen *et al.*, 2001), NO<sub>x</sub> and SO<sub>2</sub> (Freer-Smith, 1985; Martin, Bytnerowicz and Thorstenson, 1988), or exposure to light and its radiation depending on wavelength and intensity (Eichelmann *et al.*, 2005; Sellin *et al.*, 2011). Each factor could possibly interfere in the production of INMs, both positively or negatively.

We can group our birches into roadside birches (medium to high traffic) and riverside birches (birches growing beside a river). For TBE and TBF both is true, TBG grew at the timberline with no river or road next to it. We found that wood samples of the birches TBD, TBH, and TBI, all of which grew next to a river, froze at lower temperatures than other birches. However, this is not true for TBC, TBE, and TBF (all of which grew next to a river, the latter two also next to a road). We found in our experiments that birches, which grew next to roads (TBA, TBB, TBE, TBF, and VB), exhibited increased INA. If the production of INMs is based on a stress or defence mechanism, regular exposure to traffic exhaust as e.g. NO<sub>x</sub> (Franco *et al.*, 2013) could influence the INA of birch trees. NO<sub>x</sub> can have differing effects on plants. On the one hand, it is a potential harm to plants, while on the other hand, some plants use it as a nitrogen source (Allen, 1990). Next to river and roadsides, we covered a broad variety of altitudes with our samples, however, we found no correlation between altitude and freezing abilities. Our results suggest that further investigations on the influence of growing conditions on the INA of birch trees are necessary.

### **IR Spectroscopy**

The measured birch pollen extracts (see Figure 49, Figure 50, Figure 51, and Figure 52) indicate a chemical similarity between the different extracts. This is true for both, if the extracts of woods and leaves of a tree are compared (see Figure 49), as well as if the primary wood, secondary wood, or leaf samples of the different trees are compared to each other

(see Figure 50, Figure 51, and Figure 52). Further, the spectra of tree samples and birch pollen show strong similarities.

Most of the bands found in our samples match carbohydrate bands. This met expectations, as plants do contain a variety of polysaccharides and several water soluble carbohydrates (Magel, Einig and Hampp, 2000). Chen et al. (2010) measured birch wood pressed in KBr pellets. Their resulting spectra match our wood spectra very well. The range between  $1150\text{ cm}^{-1}$  and  $1300\text{ cm}^{-1}$  was strongly enhanced compared to our spectra, especially in regard of the band at  $1270\text{ cm}^{-1}$ . Further, the band at  $1510\text{ cm}^{-1}$  had a stronger intensity in the pure wood spectra compared to our extract spectra. Both bands are typical for lignin. Lignin is a major component in wood, and it is only weakly soluble in water, therefore it was not expected to find pronounced lignin bands in our aqueous extract spectra. As the remaining weak bands can be assigned to other substances, we assume no lignin to be present in our extracts. Except for the typical lignin features, our spectra matched the birch wood spectra well. We assume these similarities to be an indicator that we can retrieve the majority of components with our extraction method.

Birch pollen washing water has been measured and published previously. Our gained spectrum (see Figure 49) is in good agreement with these literature data (Pummer *et al.*, 2013; Dreischmeier *et al.*, 2017).

### 4.1.2. Surface Extracts

In Section 4.1.1 we established that birch trees contain INPs. To retrieve these INPs, the samples were milled. The obtained concentration does not reflect the amount of INP, available for the surrounding environment of the tree. In order to estimate, how much ice nucleation active material is easily released from the trees, surface extracts were done, in which the INP were extracted from the intact surface of the plant materials.

#### 4.1.2.1. Branch Samples

As an indicator for the INA of the branch samples we used cumulative nucleus concentration indicating the number of INMs extractable per cm<sup>2</sup> surface of the used sample. The estimated surface areas of the samples are given in Table 4. Since the amount of sample per extract varied, we did not include mean freezing temperatures for the branch samples. Nearly all analysed samples released INMs active at temperatures of -34 °C or above, which are indicated by their cumulative nucleus concentration at this temperature  $K(-34\text{ °C})$  marked with filled symbols in Figure 53. The obtained  $K(-34\text{ °C})$  can be found in Table 15. The cumulative nucleus concentration is also given for -20 °C  $K(-20\text{ °C})$  in Figure 53 and marked with hollow symbols.

Figure 53 shows that all leave samples contained INMs active at -34 °C or higher, with rather low concentration values compared to the other branch samples. The  $K(-34\text{ °C})$  values of the leaves ranged between  $9.9 \cdot 10^5\text{ cm}^{-2}$  (TBH-L) and  $1.3 \cdot 10^8$  (TBA-L).

Two of the primary wood extracts did not contain any INMs active at temperatures of -34 °C or above (TBF-P and TBH-P). This could mean an absence of INMs in these samples or be an effect of the small surface of the rather thin primary wood samples, leading to an INM concentration too low to capture with our method. The rest of the samples ranged

between  $8.3 \cdot 10^6 \text{ cm}^{-2}$  (TBD-P) and  $1.7 \cdot 10^9 \text{ cm}^{-2}$  (TBC-P). Other than the primary woods, all secondary woods were ice nucleation active, exhibiting  $K(-34 \text{ }^\circ\text{C})$  values between  $1.7 \cdot 10^7 \text{ cm}^{-2}$  (TBD-S) and  $9.8 \cdot 10^8 \text{ cm}^{-2}$  (TBB-S). The secondary wood extracts often exhibited the highest  $K(-34 \text{ }^\circ\text{C})$  values (for TBB, TBE, TBF, TBH, TBI, and VB) of all branch sample classes. Further, we find the least variation between the INM content of the different trees for the secondary woods.

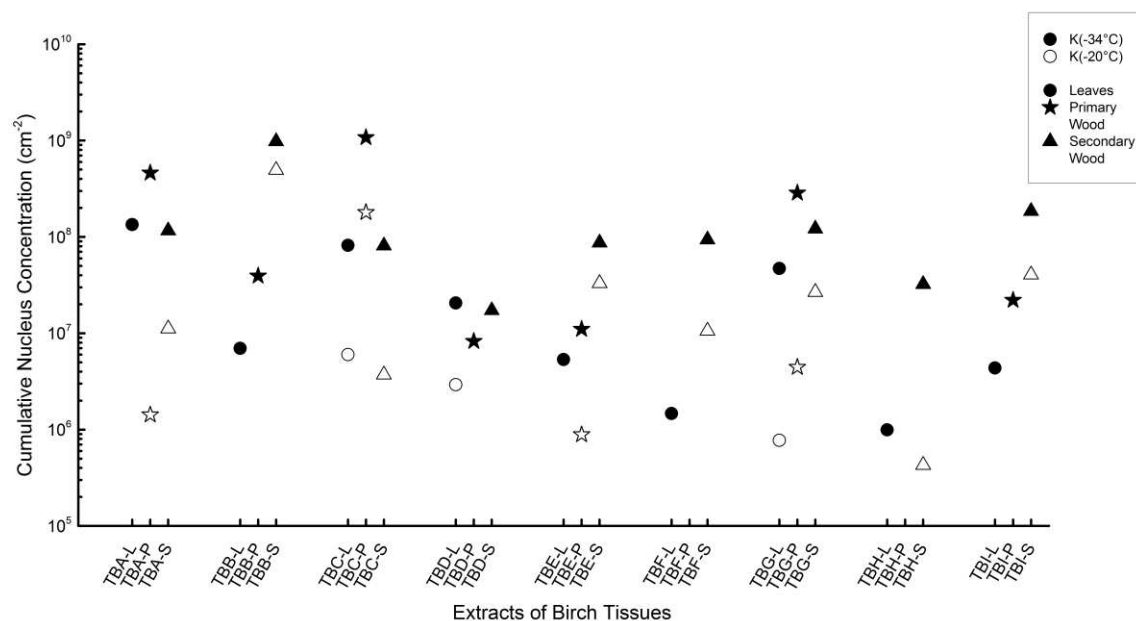


**Figure 53: Cumulative nucleus concentration of the different surface extracts of the branch samples at  $-34^\circ\text{C}$  (hollow symbols) and at  $-20^\circ\text{C}$  (filled symbols). Leaf extracts (L) are marked with a circle, primary wood extracts (P), with a star, and secondary wood extracts (S) with a triangle. Secondary wood extracts of TBF and TBH did not exhibit INMs active at  $-34 \text{ }^\circ\text{C}$  or higher.**

The secondary woods tended to exhibit the highest initial freezing temperatures. Nine out of ten secondary wood samples contained INMs active at  $-20 \text{ }^\circ\text{C}$  or above, indicated by the  $K(-20 \text{ }^\circ\text{C})$  (marked with hollow symbols in Figure 53). The only sample not containing INMs active at such high temperatures was TBD-S, corresponding with the lowest  $K(-34 \text{ }^\circ\text{C})$

value found for the secondary woods. Only three of the leaf samples (TBC-L, TBD-L, and TBG-L), and four of the primary wood samples (TBA-P, TBC-P, TBD-P, and TBG-P) exhibited INMs active at  $-20\text{ }^{\circ}\text{C}$  or higher.

To examine a possible influence of the different sample surfaces per extract, we plotted the estimated surface site concentration against  $K(-34\text{ }^{\circ}\text{C})$  (see Figure 54). Primary wood and secondary wood show no trend, with coefficients of determination  $R^2$  of 0.068 for primary and  $2.8 \cdot 10^{-5}$  for secondary wood. Leaves, which exhibited the highest surface site concentrations, showed a slight positive trend, however, with a very low  $R^2$  value of 0.21. We therefore assume that the used variations in surface site for the different samples did not alter the results.

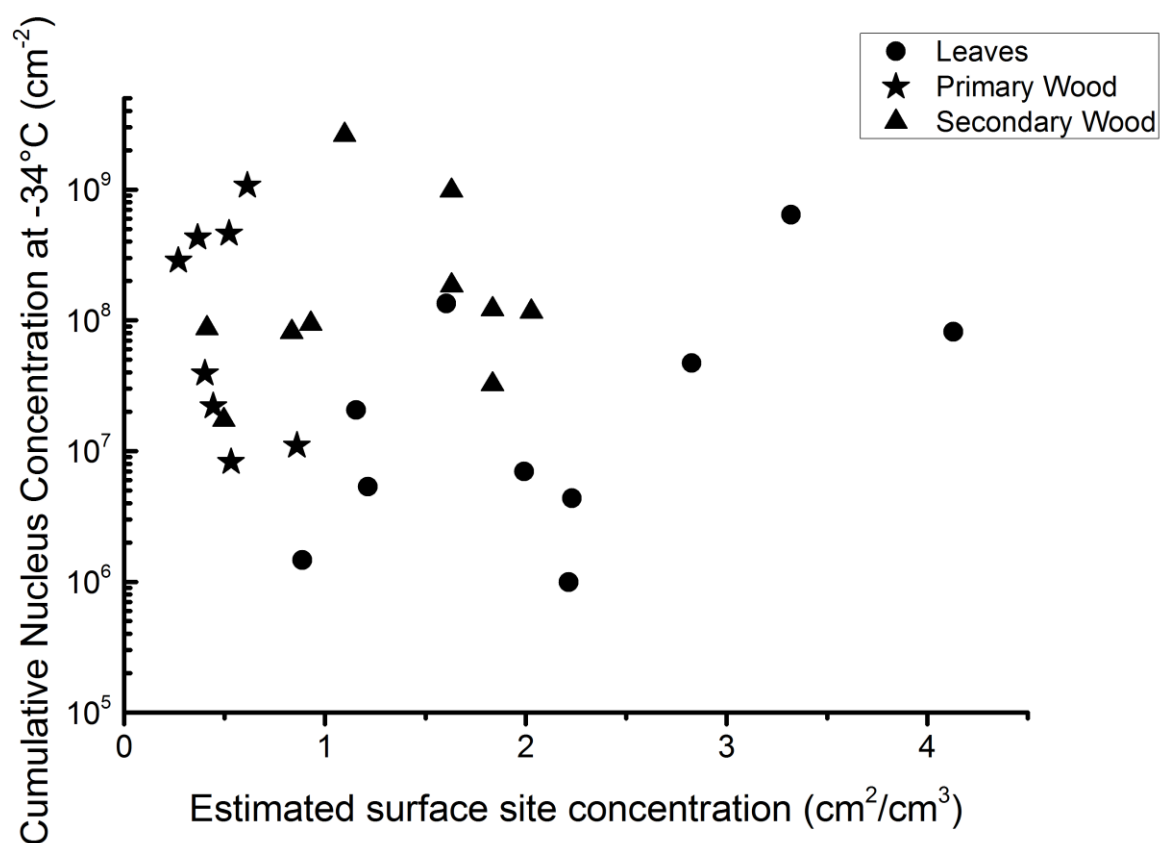
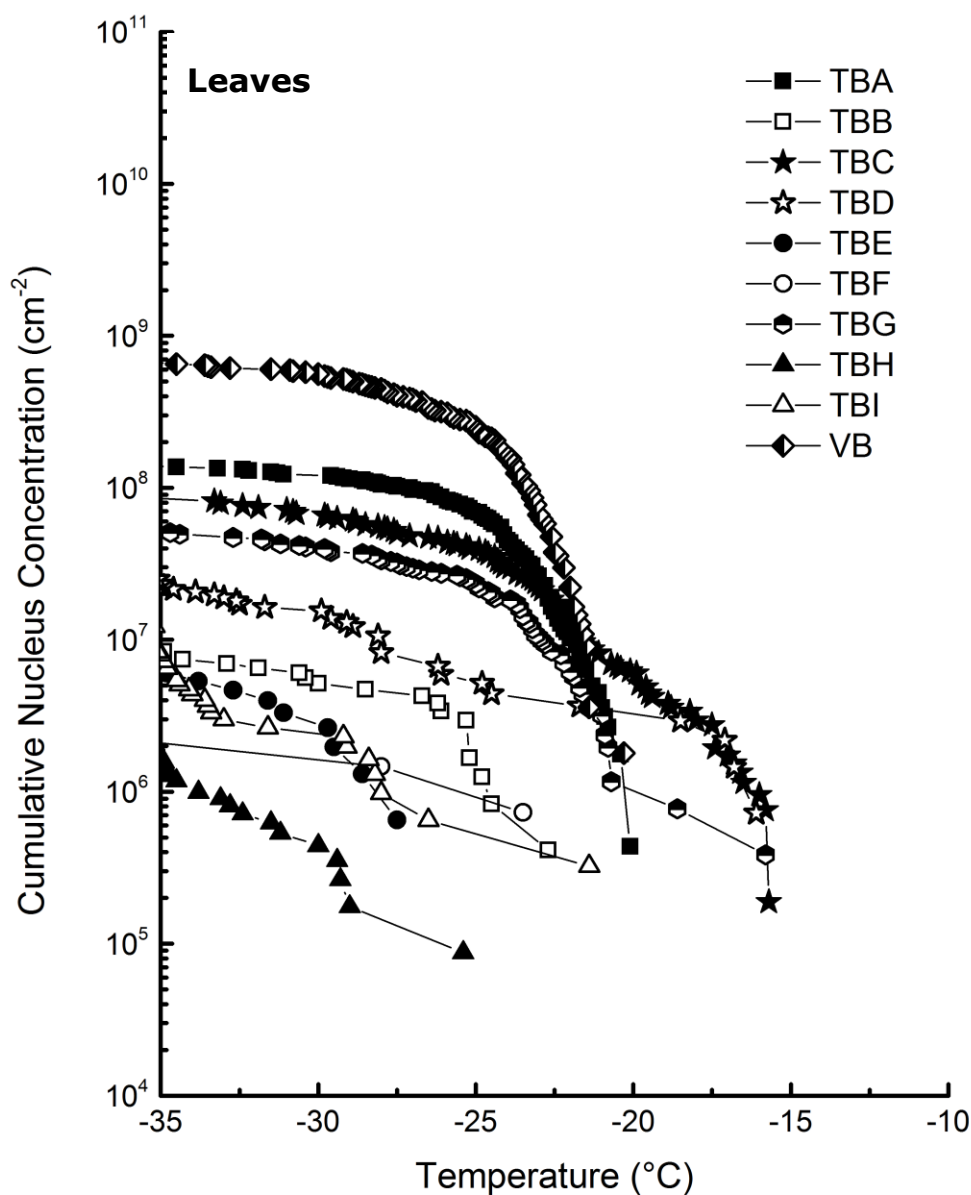


**Figure 54:** Relationship between the cumulative nucleus concentration at  $-34\text{ }^{\circ}\text{C}$  and the estimated surface site concentration to examine, if the non-uniformity of the measured sample surface areas influenced the results. Leaf extracts are marked with a circle, primary wood extracts with a star and secondary wood extracts with a triangle.

Cumulative nucleus concentrations over all temperatures above  $-35\text{ }^{\circ}\text{C}$  are plotted in Figure 55 (leaves), Figure 56 (primary wood), and Figure 57 (secondary wood).

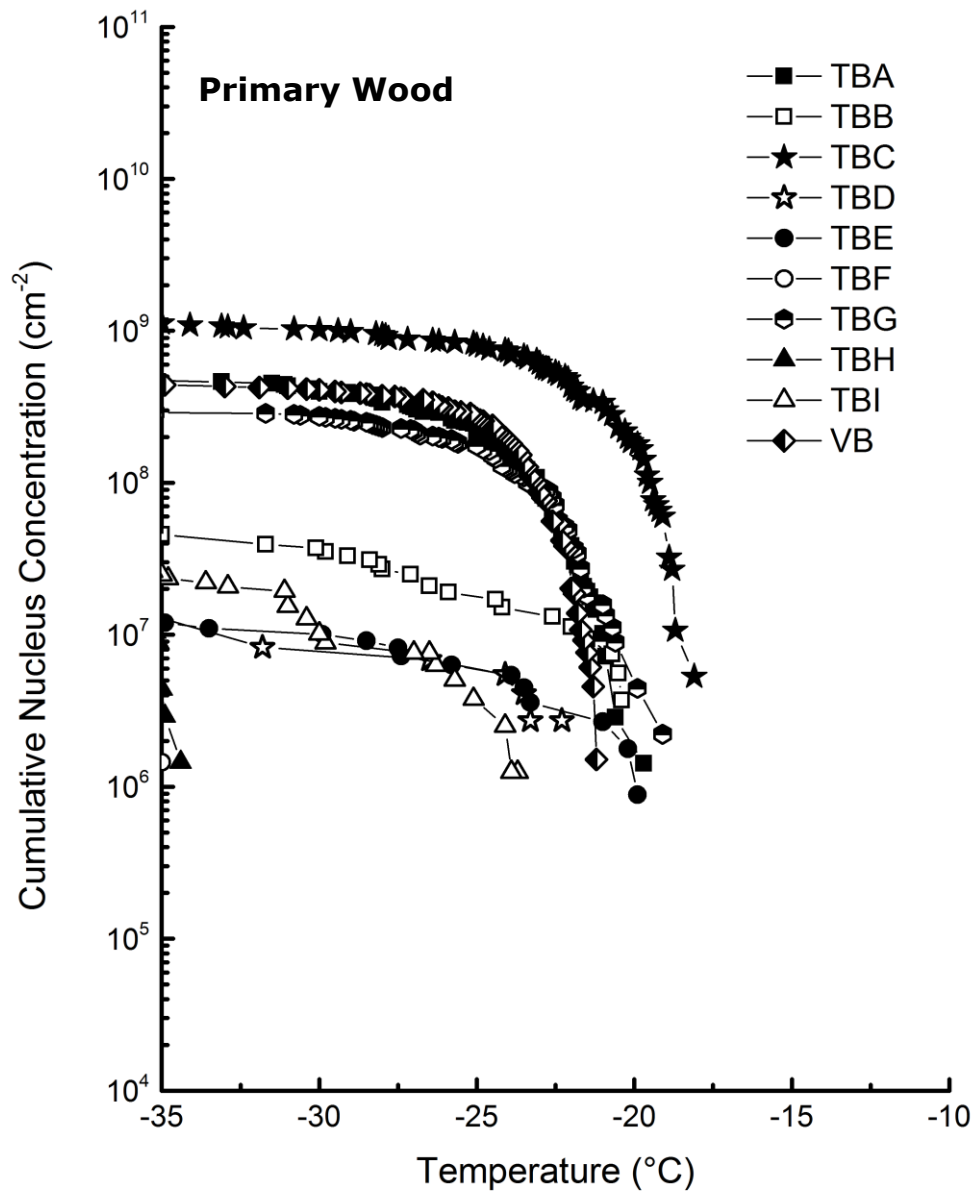
Figure 57 shows that surface extracts from secondary wood samples again exhibited freezing events at higher temperatures than primary wood or leaf extracts (Figure 55, Figure 56). This effect cannot be attributed to concentration alone, as secondary wood extracts did not exhibit significantly higher concentrations of INPs active at or above  $-34^{\circ}\text{C}$  (which we use as a proxy for total number of contained INPs) in all cases (see Figure 53).

Figure 55 shows that leaf extracts again exhibited the highest variations. However, the difference between the samples is less pronounced than for the milled samples.



**Figure 55:** Cumulative nucleus concentration as a function of temperature for leaf surface extracts. The diagram is cut off at  $-35^{\circ}\text{C}$ , since we cannot contribute freezing events below this temperature to heterogeneous nucleation. The symbols used for the different data points are grouped. Birches growing in close proximity under similar conditions are marked with the same symbol (different fillings).





**Figure 56:** Cumulative nucleus concentration as a function of temperature for primary wood surface extracts. The diagram is cut off at  $-35^{\circ}\text{C}$ , since we cannot contribute freezing events below this temperature to heterogeneous nucleation. The symbols used for the different data points are grouped. Birches growing in close proximity under similar conditions are marked with the same symbol (different fillings).

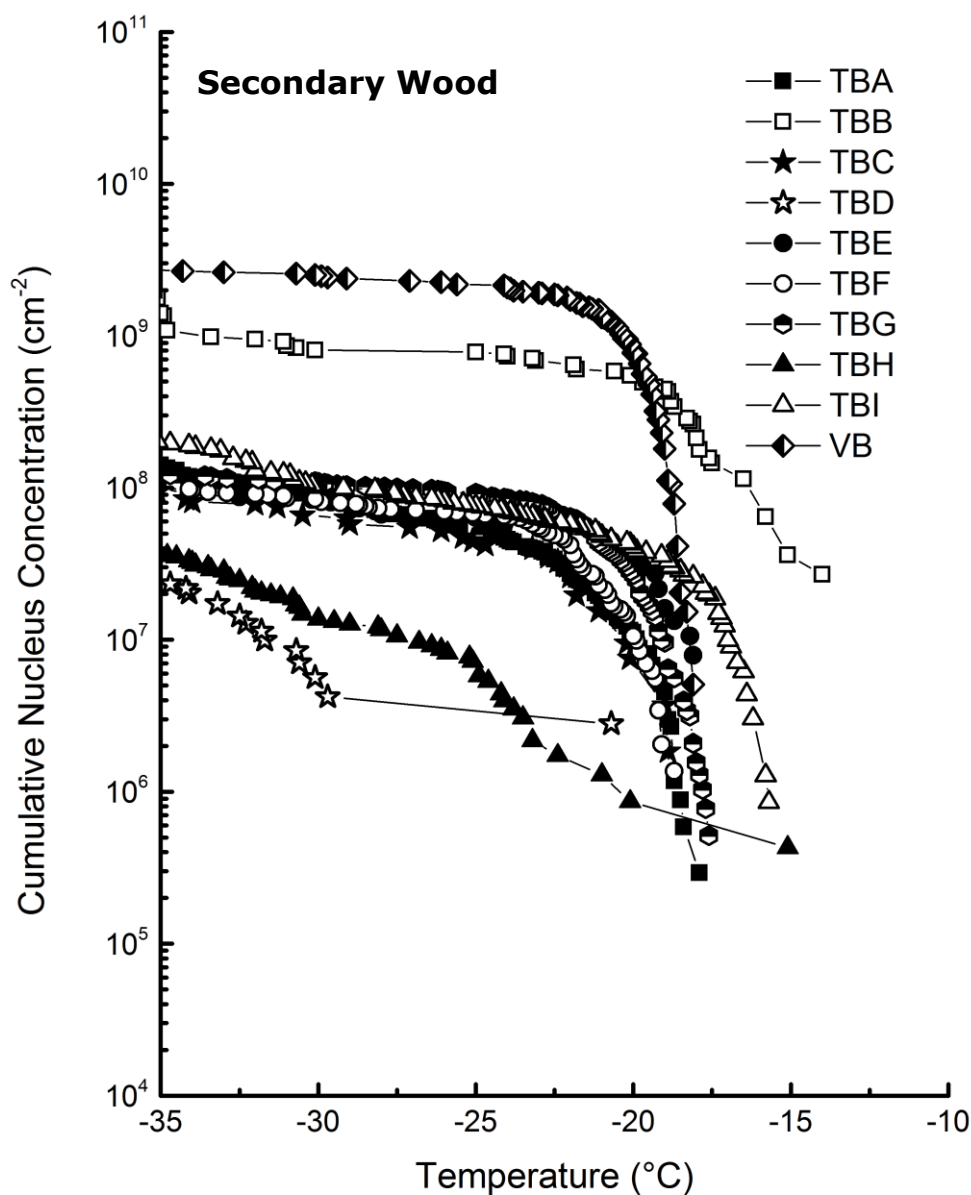


**Figure 57:** Cumulative nucleus concentration as a function of temperature for and secondary wood surface extracts. The diagram is cut off at -35 °C, since we cannot contribute freezing events below this temperature to heterogeneous nucleation. The symbols used for the different data points are grouped. Birches growing in close proximity under similar conditions are marked with the same symbol (different fillings).

**Table 15: The  $K(-34\text{ °C})$  values per  $\text{cm}^2$  of surface for leaves, primary wood and secondary wood of the nine Tyrolean birches:**

	Leaves	Primary Wood	Secondary Wood
	$K(-34\text{ °C})$ ( $\text{cm}^{-2}$ )	$K(-34\text{ °C})$ ( $\text{cm}^{-2}$ )	$K(-34\text{ °C})$ ( $\text{cm}^{-2}$ )
TBA	$1.3 \cdot 10^8$	$4.6 \cdot 10^8$	$1.2 \cdot 10^8$
TBB	$7.0 \cdot 10^6$	$3.9 \cdot 10^7$	$9.8 \cdot 10^8$
TBC	$8.1 \cdot 10^7$	$1.1 \cdot 10^9$	$8.1 \cdot 10^7$
TBD	$2.1 \cdot 10^7$	$8.3 \cdot 10^6$	$1.7 \cdot 10^7$
TBE	$5.3 \cdot 10^6$	$1.1 \cdot 10^7$	$8.7 \cdot 10^7$
TBF	$1.5 \cdot 10^6$	n/a	$9.4 \cdot 10^7$
TBG	$4.7 \cdot 10^7$	$2.9 \cdot 10^8$	$1.2 \cdot 10^8$
TBH	$9.9 \cdot 10^5$	n/a	$3.2 \cdot 10^7$
TBI	$4.4 \cdot 10^6$	$2.2 \cdot 10^7$	$1.8 \cdot 10^8$

#### 4.1.2.2. Bark Samples

The results of the analysis of the different bark samples of the birches are shown in Figure 58, which includes the  $K(-34\text{ °C})$  and  $K(-20\text{ °C})$  value as an indicator for INM content and the mean freezing temperature (MFT) as well as the initial freezing temperature (the freezing temperature of the first recorded freezing event). MFT values and their corresponding standard deviation, as well as the  $K(-34\text{ °C})$  values can be found in Table 16. The cumulative nucleus concentration over a broader temperature range is given in Figure 59. Freezing temperatures were included since the sample surface used per extract was uniform (in all cases approx.  $0.8\text{ cm}^2\text{mL}^{-1}$ ), rendering the temperature values comparable. The initial freezing temperature is the temperature at which we recorded the first freezing event of all measurements of a single sample. Further, Figure 58 includes two reference values: the mean freezing temperatures of birch pollen washing water ( $-17.1\text{ °C}$ ) and ultrapure water ( $-36.2\text{ °C}$ , as a sum of regular measurements done during the sample measurement period). The  $K(-34\text{ °C})$  values ranged from  $6.5 \cdot 10^6\text{ cm}^{-2}$  (TBH-B) to  $1.8 \cdot 10^9\text{ cm}^{-2}$  (TBF-B). TBH-B showing the lowest  $K(-34\text{ °C})$  value was the only sample not exhibiting INMs active at  $-20\text{ °C}$  or higher. The highest  $K(-20\text{ °C})$  value of  $5.4 \cdot 10^8\text{ cm}^{-2}$  (TBF-B) corresponds to the sample with the highest  $K(-34\text{ °C})$  value.

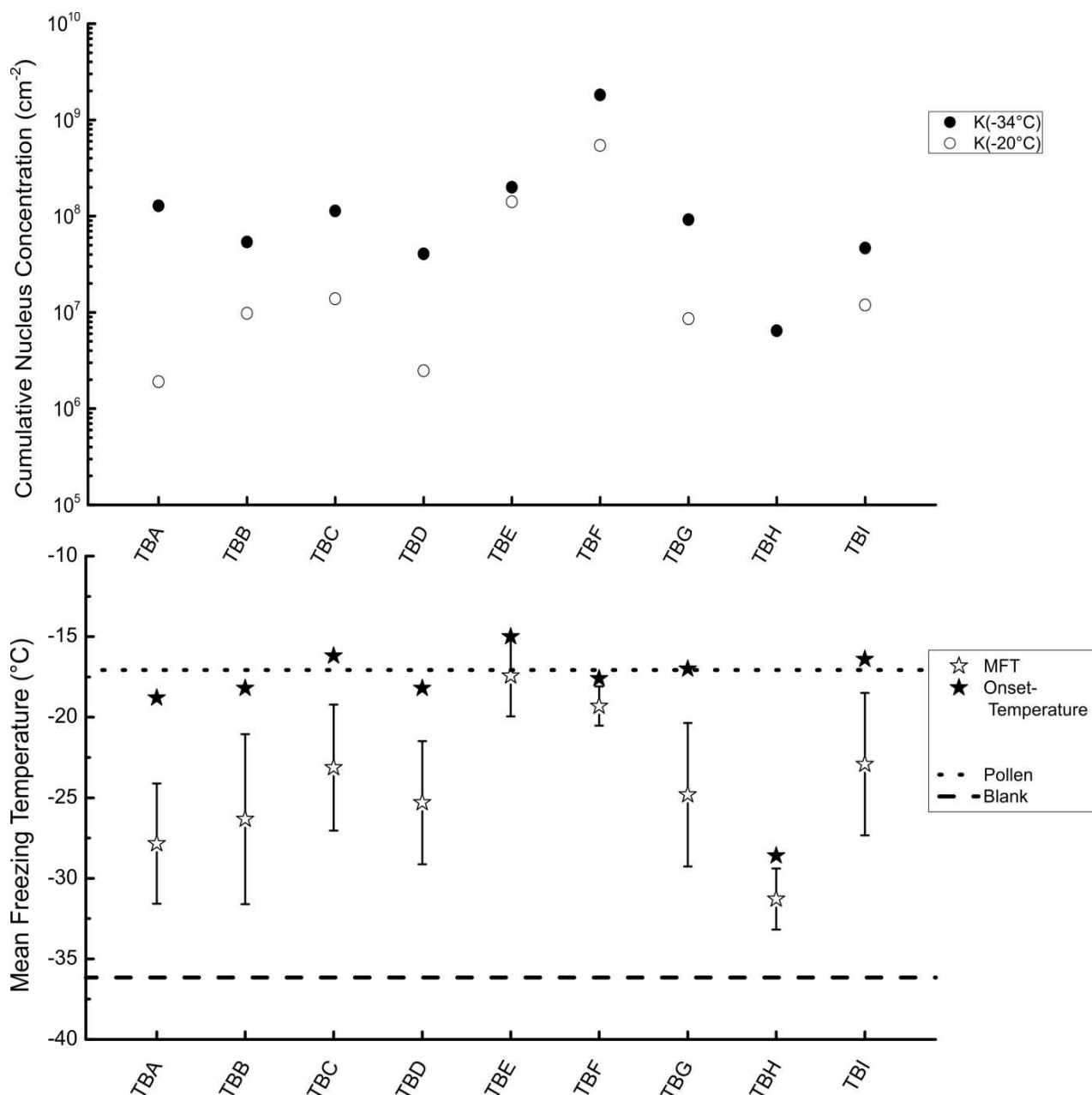


**Figure 58: Top: Cumulative nucleus concentration of the bark samples at -34 °C (hollow circles) and at -20 °C (filled circles). Bottom: Mean freezing temperature of the samples (hollow stars) with the corresponding standard deviation and initial freezing (onset) temperature (filled stars). Further, this figure includes the mean freezing temperature of birch pollen washing water (-17.1 °C dotted line) and of an ultrapure water sample, as a sum of standard measurements during our measurement period (-36.2 °C dashed line).**

The mean freezing temperatures reflect all freezing events above  $-35\text{ }^{\circ}\text{C}$ . Droplets freezing below this temperature were excluded to prevent homogeneous nucleation events from altering the results. The mean freezing temperatures ranged from  $-17.4\text{ }^{\circ}\text{C}$  (TBE-B) to  $-31.3\text{ }^{\circ}\text{C}$  (TBH-B). The latter is again the sample which already exhibited the lowest  $K(-34\text{ }^{\circ}\text{C})$  value. In general, the freezing temperature data followed the same trend as the cumulative nucleus concentration data (see Figure 58 and Figure 59), showing the relationship between INM concentrations and freezing temperatures. The mean freezing temperatures exhibited quite high standard deviations (from  $1.2\text{ }^{\circ}\text{C}$  (TBF-B) to  $5.3\text{ }^{\circ}\text{C}$  (TBB-B)), reflecting freezing events over a broad temperature regime. Due to this broad freezing regime we also depicted the initial freezing temperature, to reflect the highest freezing capacity of each sample. These initial freezing temperatures ranged mostly between  $-15^{\circ}\text{C}$  (TBE-B) and  $-18.8\text{ }^{\circ}\text{C}$  (TBA-B), with one outlier exhibiting a drastically lower initial freezing temperature: TBH-B ( $-28.6\text{ }^{\circ}\text{C}$ ). Except for TBH-B, all initial freezing temperatures range around the freezing temperature of birch pollen washing water ( $-17.1\text{ }^{\circ}\text{C}$ , see Figure 58).

**Table 16: MFT values with the corresponding standard deviation and  $K(-34\text{ }^{\circ}\text{C})$  values per  $\text{cm}^2$  surface for the extracts of bark from the nine Tyrolean birches:**

	MFT ( $^{\circ}\text{C}$ )	$\sigma$	$K(-34\text{ }^{\circ}\text{C})$ ( $\text{cm}^{-2}$ )
TBA	-27.8	$\pm 3.7$	$1.3 \cdot 10^8$
TBB	-26.3	$\pm 5.3$	$5.4 \cdot 10^7$
TBC	-23.1	$\pm 3.9$	$1.1 \cdot 10^8$
TBD	-25.3	$\pm 3.8$	$4.0 \cdot 10^7$
TBE	-17.4	$\pm 2.5$	$2.0 \cdot 10^8$
TBF	-19.3	$\pm 1.2$	$1.8 \cdot 10^9$

TBG	-24.8	$\pm 4.5$	$9.2 \cdot 10^7$
TBH	-31.3	$\pm 1.9$	$6.5 \cdot 10^6$
TBI	-22.9	$\pm 4.4$	$4.7 \cdot 10^7$

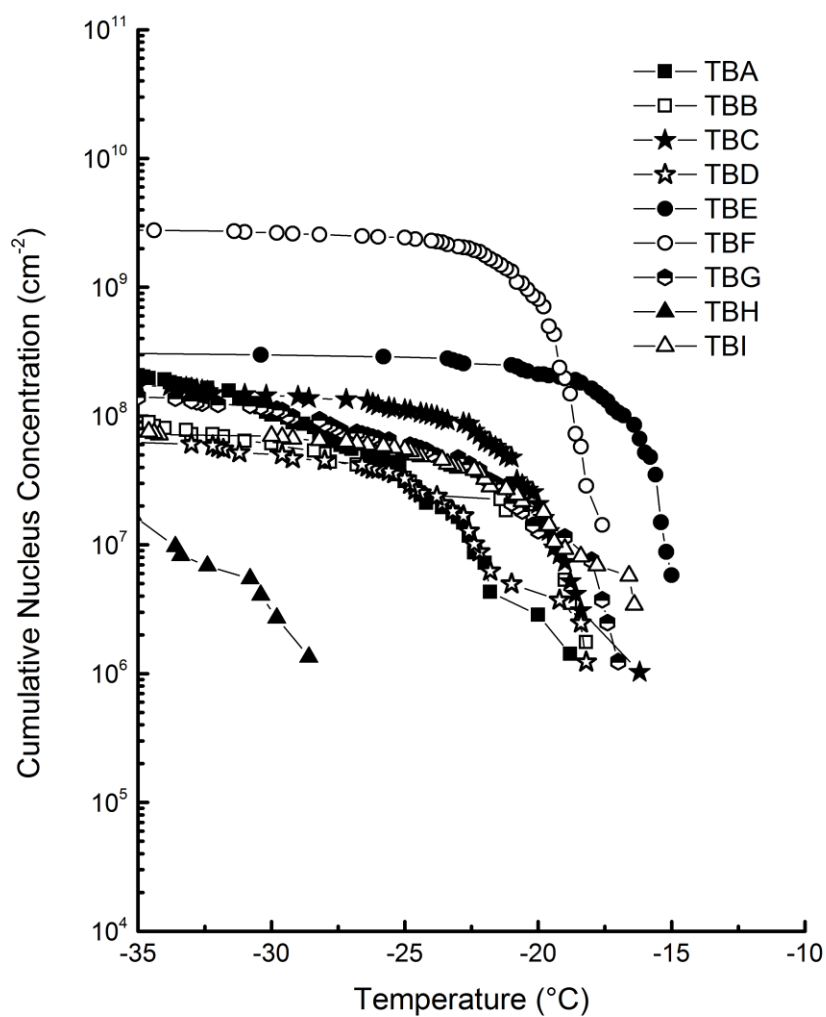


**Figure 59:** Cumulative nucleus concentration as a function of temperature for bark surface extracts. The diagram is cut off at  $-35\text{ }^{\circ}\text{C}$ , since we cannot contribute freezing events below this temperature to heterogeneous nucleation. The symbols used for the

***different data points are grouped. Birches growing in close proximity under similar conditions are marked with the same symbol (different fillings).***

In summary, bark material contains easily extractable and potent INMs, which resemble the freezing behaviour of birch pollen washing water. Further, the bark material showed less variation in concentration from sample to sample as the other analysed materials.

#### **4.1.2.3. Core Samples**

In order to assess if the INM concentration is constant throughout the trunk or if it changes with the depth profile, drill cores of the trunk were analysed. The drill cores were taken at 1 m height for the birch trees TBC and TBI. The surface site per mL water used to extract the INMs is given in Table 4. The cumulative nucleus concentration at  $-34\text{ }^{\circ}\text{C}$  is plotted against the sample depth in Figure 60. The corresponding values are given in Table 17. Hereby the outermost analysed fraction is the bark, followed by the bast and three core sections of the inner wood, each approx. 0.5 cm in length. To estimate the depth of the analysed core segments we used the centre of each segment. A microscopic picture of the bark, bast and inner wood segment of TBC is shown in Figure 61.

Figure 60 shows that the  $K(-34\text{ }^{\circ}\text{C})$  values are highest at the outermost segments, meaning the bark and the bast. The bark and bast values of the core from TBC were  $9.8 \cdot 10^7\text{ cm}^{-2}$  (TBC-bark) and  $4.2 \cdot 10^8\text{ cm}^{-2}$  (TBC-bast). TBI bast and bark sample from the core exhibited the values of  $1.1 \cdot 10^8\text{ cm}^{-2}$  (TBI-bark) and  $2.7 \cdot 10^7\text{ cm}^{-2}$  (TBI-bast). The inner wood segments of both cores exhibited significantly lower INM concentrations, which all ranged around the same value between  $2.3 \cdot 10^6\text{ cm}^{-2}$  (TBC-C3) and  $7.6 \cdot 10^6\text{ cm}^{-2}$  (TBI-C1).



The bark sample from the drill cores are well comparable to the samples punched directly from the bark with the values  $9.8 \cdot 10^7 \text{ cm}^{-2}$  (drill core) and  $1.1 \cdot 10^8 \text{ cm}^{-2}$  (bark punches) for TBC and  $1.1 \cdot 10^8 \text{ cm}^{-2}$  (drill core) and  $4.7 \cdot 10^7 \text{ cm}^{-2}$  (bark punches) for TBI.

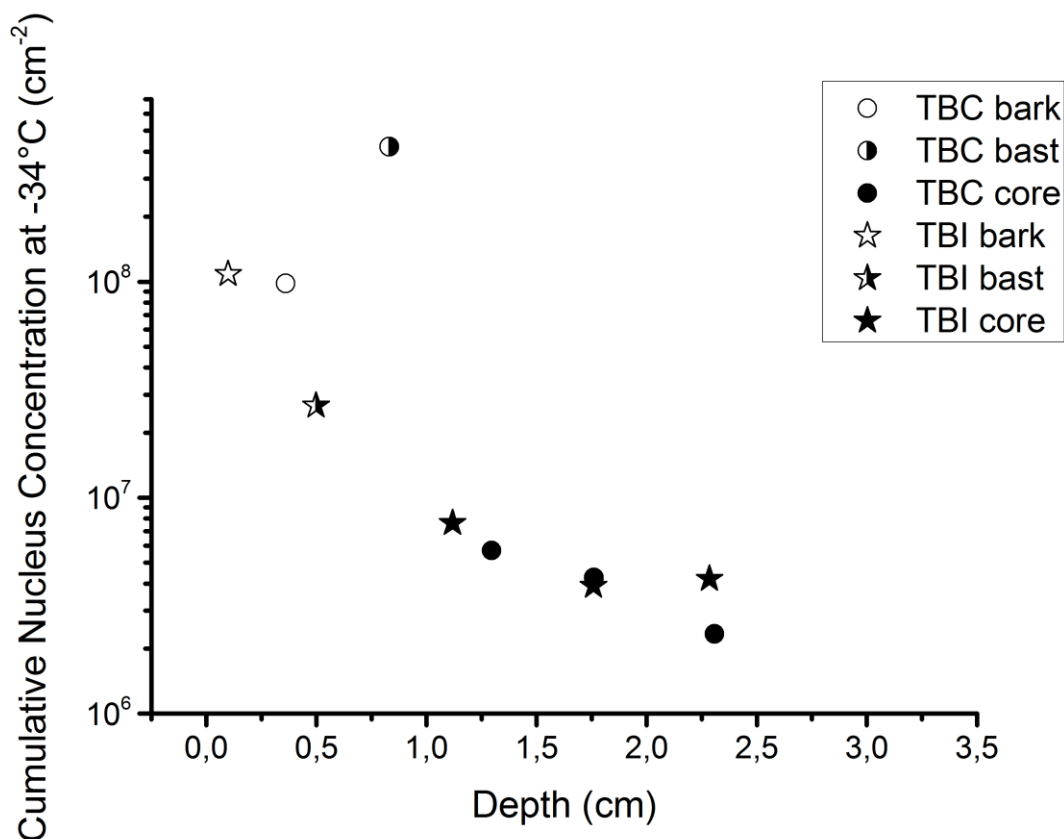


**Figure 60:** Cumulative nucleus concentration at -34 °C for the analysed core samples of TBC (marked with a circle), and TBI (marked with a star). Bark samples are marked with a hollow symbol, bast samples are marked with a half-filled symbols. Filled symbols correspond to inner wood samples. To assign the depth of the different core segments, the centre of the segments was used.

**Table 17:  $K(-34\text{ °C})$  values per  $\text{cm}^2$  surface for small segments of drill cores from the birches TBI and TBC with their corresponding sample depth:**

TBC	TBC	TBI	TBI
Depth (cm)	$K(-34\text{ °C})$ ( $\text{cm}^{-2}$ )	Depth (cm)	$K(-34\text{ °C})$ ( $\text{cm}^{-2}$ )
0.4	$9.8 \cdot 10^7$	0.1	$1.1 \cdot 10^8$
0.8	$4.2 \cdot 10^8$	0.5	$2.7 \cdot 10^7$
1.3	$5.7 \cdot 10^6$	1.1	$7.6 \cdot 10^6$
1.8	$4.3 \cdot 10^6$	1.8	$3.9 \cdot 10^6$
2.3	$2.3 \cdot 10^6$	2.3	$4.2 \cdot 10^6$

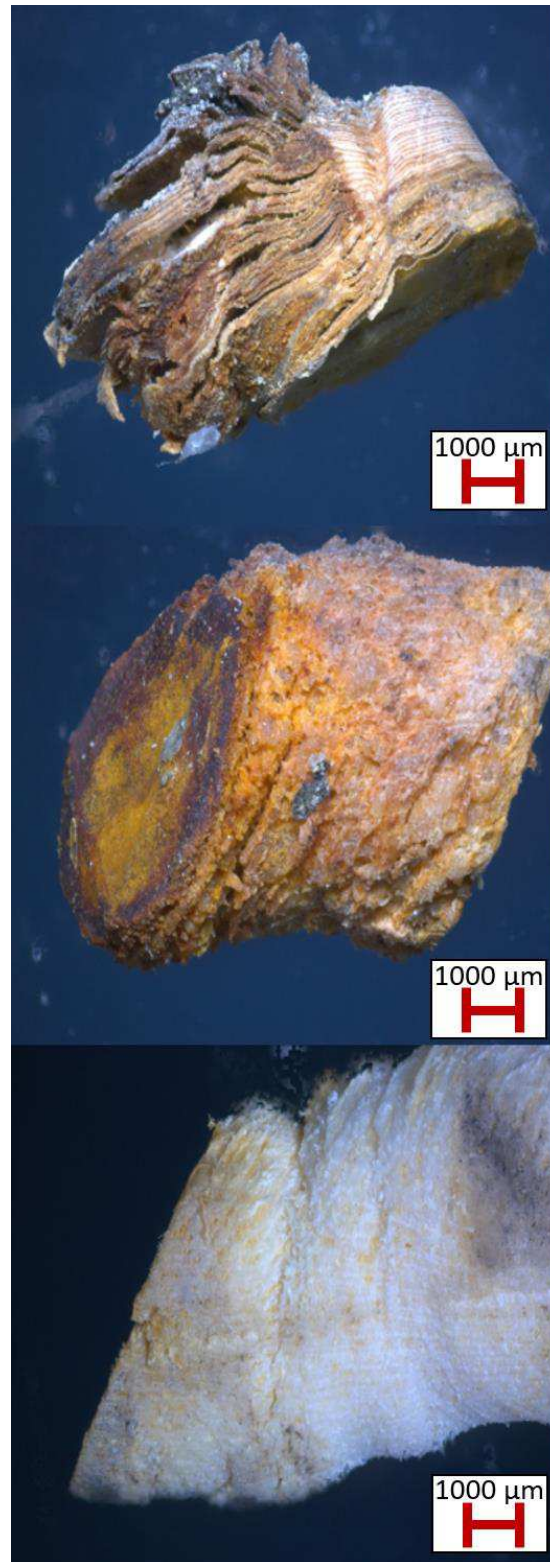


**Figure 61: Microscope picture of the TBC core samples. Top: Bark, Middle: Bast, Bottom, the inner wood. The red scale bars indicate 1000 µm. The pictures were obtained using equipment from the Institute of Chemical, Environmental and Bioscience Engineering, with supervision of Prof. Dr. Leopold Puchinger.**

#### 4.1.2.4. Discussion – Surface Availability of INPs from Birch Trees

INM concentrations extractable from birch surface materials ranged between  $1.5 \cdot 10^6$  (TBF-L) and  $1.8 \cdot 10^9$  (TBF-B) INMs per  $\text{cm}^2$  active at  $-34^\circ\text{C}$  or higher, excluding two samples from which we were not able to extract INMs (TBF-P and TBH-P). All branch samples used originate from the lower crown. We cannot exclude the possibility that material collected from the upper crown behaves differently, since light and water availability differ throughout the crown (Sellin and Kupper, 2006; Sellin, Eensalu and Niglas, 2010; Sellin *et al.*, 2011). However, INM concentration throughout the different materials and the different trees range mostly in a similar order of magnitude, suggesting this to be a property found in similar scale throughout the tree.

The birches we sampled are likely to be of the phenotype *Betula pendula* (see Section 2.3.3). Under the assumption that *Betula pendula* and *Betula pubescens*, which are the main birch species found in Europe (Beck *et al.*, 2016), behave similarly concerning INA and that the INA throughout the crown of the tree stays comparable, we can try to estimate the role of birch trees in environmental INM concentrations in Europe. The leaf area index LAI describes the leaf area to ground area ratio in a forest and varies depending on the analysed forest and the method of determination. The LAI of selected studies for Northern birch forests and birch tree stands lays between 0.66 and  $4,09 \text{ m}^2\text{m}^{-2}$  (Johansson, 1999; Dahlberg *et al.*, 2004; Karlsson, Weih and Borg, 2005; Heiskanen, 2006; Uri *et al.*, 2007). Assuming that the birch trees in Northern birch forests behave similarly to our measured trees and that leaves in the upper canopy are comparable to those in the lower canopy, the aqueously extractable INM fraction is  $6.6 \cdot 10^9$  to  $5.5 \cdot 10^{12}$  INMs per  $\text{m}^2$  forest for the leaves alone. However, estimating the general leaf area of a tree is extremely inaccurate since

density of a crown is highly dependent on the stand density (Hynynen *et al.*, 2010).

To estimate the surface of the stem, we took the data from investigations of *Betula pendula* stands containing trees between 7 and 60 years of age and field data from a boreal forest. The data showed a height between 3.2 and 28 m, and diameters between 3.2 and 64.0 cm (Johansson, 1999; Hynynen *et al.*, 2010; Ene, Næsset and Gobakken, 2012). Taking these values as average and approximating the stem of the tree as cone, we can estimate the surface area of the stem leading to a surface area between 0.2 and 28.2 m<sup>2</sup>. This adds another  $1.0 \cdot 10^{10}$  to  $5.1 \cdot 10^{14}$  INMs for the bark on the stem per birch tree. Taking the data from two multiple birch stand investigations the density varied between 0.04 and 10 trees per m<sup>2</sup> (Johansson, 1999; Hynynen *et al.*, 2010; Uri *et al.*, 2012). Leading to  $3.9 \cdot 10^8$  to  $5.1 \cdot 10^{15}$  INMs per m<sup>2</sup> of the birch stands. This calculation contains an overestimation of the maximum tree surface per m<sup>2</sup> since the densest stands are typically young stands with rather thin stems.

Similar to the crowns, the surface of twigs in birch trees is difficult to determine since their density, diameter, length and over all appearance depends on many factors (Kostina *et al.*, 2015; Wang *et al.*, 2016, 2017). In contrary to the leaves, standard measurements of area indices were not done for branches. Due to the lack of data we did not include the branches in our estimation. From our data we assume the number of INMs active at -34°C or higher extractable per m<sup>2</sup> of a birch stand to range between the orders of magnitude of  $10^9$  to  $10^{15}$  excluding the surface of the branch wood.

## 4.2. Ice Nucleation Activity of Different Berries

Due to our promising results gained from birch trees, the effort was started to test a wider variety of plants native to the boreal regions. The chosen plants for testing were fruit bearing bushes, for which samples were easily available. Juices of berries and surface extracts of leaves were measured. As the analysed plants are highly robust in nature and widely used in agriculture, they exhibit a vast number in nature and therefore a huge total surface to release INP into the environment. The results presented in this chapter have been published in Felgitsch *et al.*, 2019.

### 4.2.1. INA of Filtered and Unfiltered Samples

This chapter contains the results of our investigation of different berries as juices, dried berries, and frozen berries, as well as various leaves, which all stem from plants native to the boreal regions (a more detailed description of samples is given in Section 2.3.4). To compare the freezing behaviour of the different plant materials the mean freezing temperature (MFT) and the cumulative nucleus concentration ( $K(T)$ ) of the pure plant materials were determined. The results are plotted in Figure 62 (MFT and  $K(-34\text{ °C})$ ), Figure 64 ( $K(T)$  of the juices), Figure 65 ( $K(T)$  of frozen berries and extracts), and Figure 66 ( $K(T)$  of the leaves). Further, all results are given in Table 18.

In order to assess the freezing abilities of the different plant materials, next to the mean freezing temperature (MFT), the initial freezing temperature was determined. The initial freezing temperature is defined by the temperature at which we observed the first freezing event of a sample. Further, the  $K(-34\text{ °C})$  value was calculated in order to assess contains INP concentrations. All three values are given in Figure 62. Further, aqueous birch pollen washing water ( $-17.1\text{ °C}$ ) and juniper pollen

washing water (-21.4 °C) were included as reference standards. Birch pollen washing water is a well-established plant based INP. Juniper pollen washing water was chosen as two juniper samples (leaf L2 and fruit E1) are presented here as well. The MFT value of ultrapure water (-36.8 °C as mean value during the course of measuring the plant materials presented in this Section) is also plotted. The cumulative nucleus concentration over a broader temperature range is discussed in Section 4.2.2.

We found INPs active at -34 °C and higher in all analysed samples. As we did not observe homogeneous freezing events at such high temperatures with our setup, we conclude that all analysed samples were ice nucleation active.

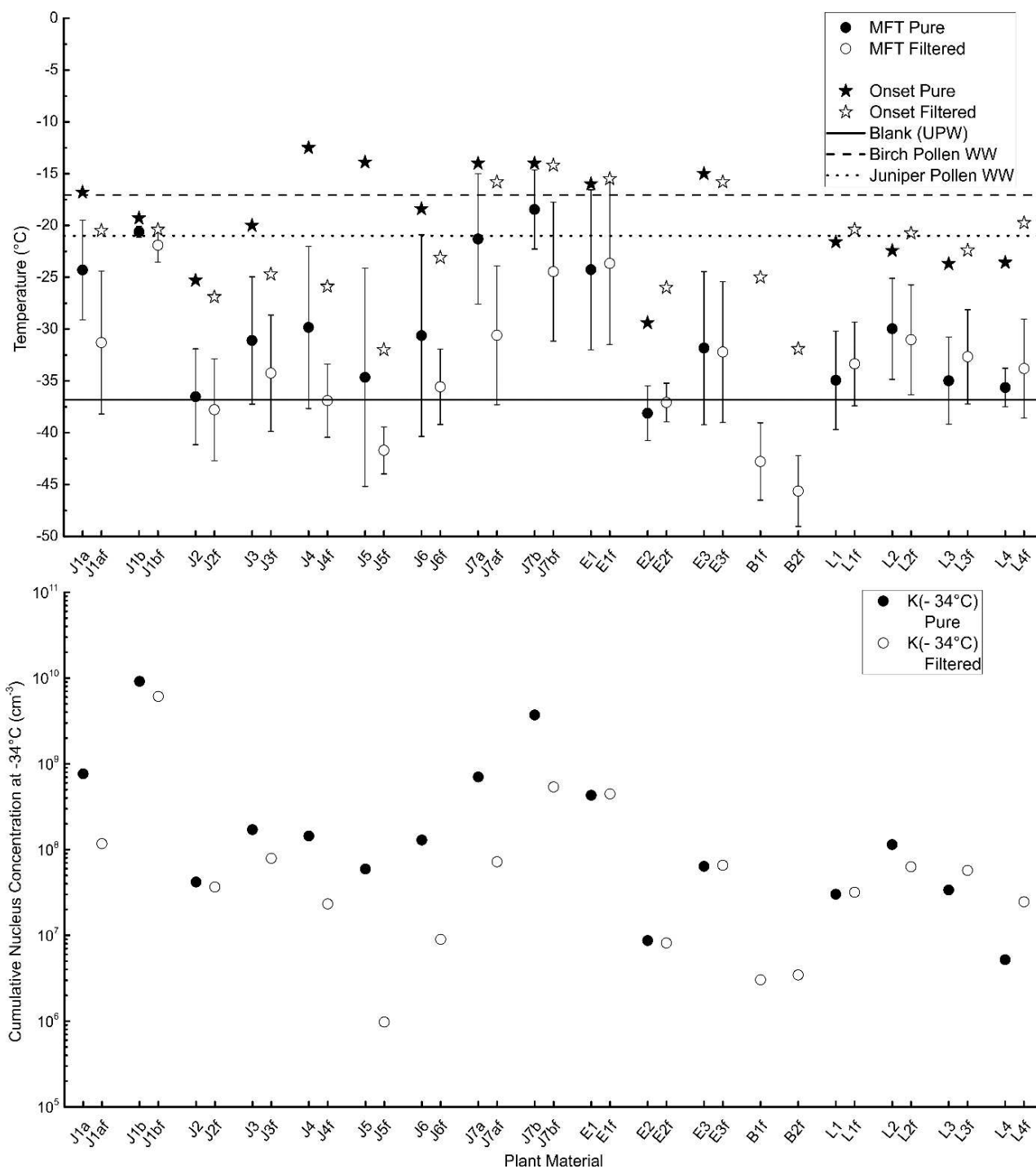


**Figure 62: top: MFT (circles) and initial freezing (onset) temperature (stars) of the analysed juices (black currant (J1), blueberry (J2), chokeberry (J3), cranberry (J4), lingonberry (J5), sambucus (J6), sea buckthorn (J7)), dried berry extracts (juniper berries (E1), rowanberries (E2), sea buckthorn (E3)), frozen berries (blueberry (B1) and Raspberry (B2)) and leaf extracts ((L1) blueberry, (L2) juniper, (L3) raspberry, (L4) sea buckthorn). Samples marked with an f are filtered (particles < 0.2  $\mu\text{m}$  in diameter) and are displayed as hollow symbols; filled symbols correspond to unfiltered samples. MFTs**



*are given with the respective standard deviation as error bar. The graph contains three lines: the dashed line refers to the mean freezing temperature of birch pollen washing water (-17.1 °C), the dotted line to juniper pollen washing water (-21.4 °C, extracted from Pummer et al., 2012), and the solid line refers to the MFT of ultrapure water (UPW) measured with our setup during the measurement series (-36.8 °C). (b): The cumulative nucleus concentration at -34 °C ( $K(-34 \text{ °C})$ ). Again, filtered samples are marked with an *f* and hollow symbols, while unfiltered samples are represented by filled symbols. Adapted from Felgitsch et al., 2019.*

### **Unfiltered Samples:**

The MFT values of the unfiltered juices ranged from -18.5 °C (sea buckthorn J7b) to -36.5 °C (blueberry J2). The MFT values of unfiltered extracts ranged from -24.3 °C (juniper berries E1) to -38.1 °C (rowanberries E2). The MFT values of unfiltered leaf extracts ranged between -30 °C (L2, juniper) and -35.6 °C (L4, sea buckthorn).

Initial freezing temperatures of most unfiltered samples were above -25 °C. The only exception were J2 (blueberry,  $T_{\text{onset}}$  -25.2 °C) and E2 (rowanberry  $T_{\text{onset}}$  -29.4 °C). The determined MFT values of the regarded samples are mainly below the MFTs of the comparison standards juniper pollen washing water and birch pollen washing water. However, the initial freezing temperatures show a different picture. Most initial freezing temperatures were above or between the two lines (see Figure 62). Only exceptions were the leaf samples, which all lay slightly below the two lines.

Some samples exhibited exceptionally low MFT values. Blueberry Juice (J2) exhibited a MFT close to homogeneous freezing and the MFT of rowanberry extract (E2) was even below the homogeneous freezing line (see Figure 62). This behaviour is due to two factors: (a) these samples exhibited a low INP concentration, which can be seen by the corresponding rather low  $K(-34 \text{ °C})$  values; and (b) ions and small sugars,

which can be expected to be present in juices and extracts originating from berries, lead to a freezing point depression. With samples with low INP concentrations, we typically see not just heterogeneous, but also homogeneous freezing events. This is due to droplets containing no INP as the concentration is too low. Freezing point depression decreases the freezing temperature of these droplets to temperatures below homogeneous freezing temperatures of water. Therefore, the resulting MFT, which includes all freezing events recorded per sample, can be in the range or even below the homogeneous freezing temperatures of water, even if heterogeneous freezing events are present. As we recorded heterogeneous freezing events for all samples (see  $K(-34\text{ °C})$  - Figure 62), we know that INPs are present, even in these samples. This shows well that the MFT reflects INP concentrations.

The dry mass of the unfiltered fruit juices varied in the range between  $\sim 100$  and  $\sim 200$  mg/mL. As this is a broad range, we wanted to see if the dry mass content influences the INP concentration. Therefore the concentrations of INPs active at or above  $-34\text{ °C}$  ( $K(-34\text{ °C})$ ) were plotted against the corresponding dry mass contents (see Figure 63) of the unfiltered fruit juices. A linear fit yields an  $R^2$  value of 0.0124. This shows that the INP concentration is not a function of dry mass and that the varying dry mass cannot explain the variation of INPs, i.e. different plants contain different amounts of INPs.

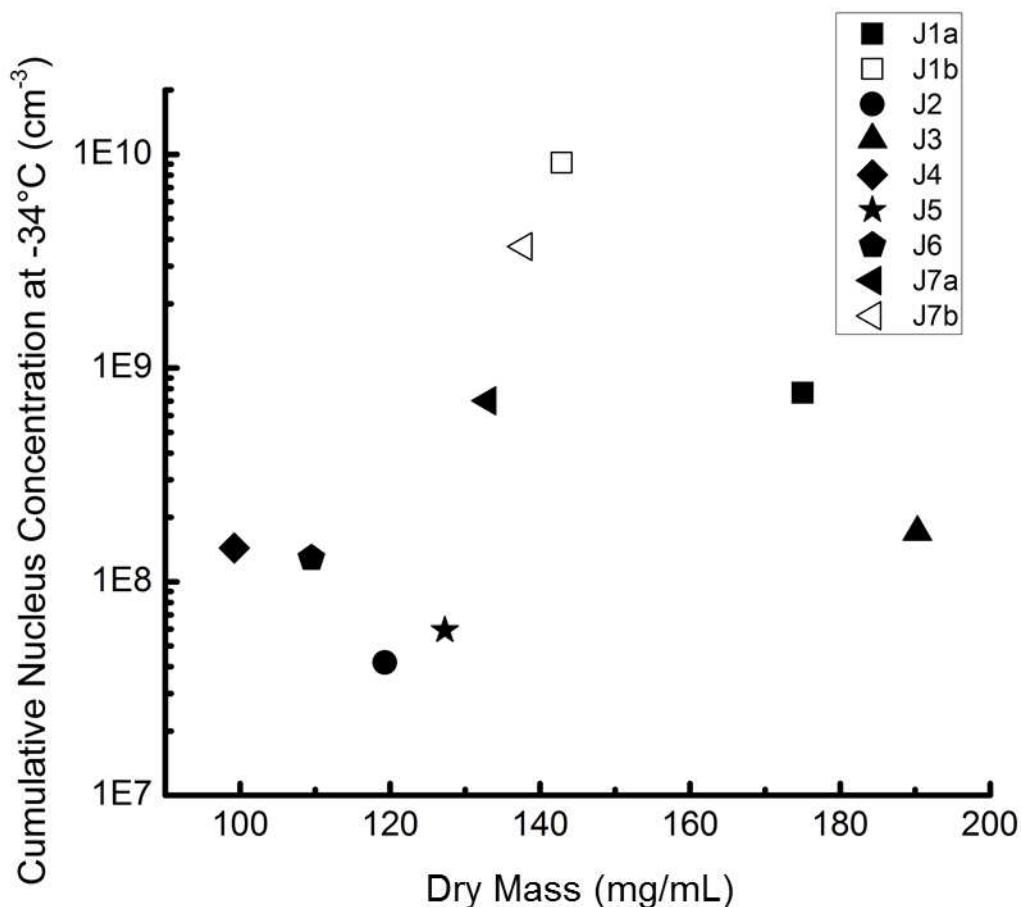


**Figure 63: Relationship between the INP concentration of the juice samples and their dry mass. Included juices were black currant (J1a, J1b), blueberry (J2), chokeberry (J3), cranberry (J4), lingonberry (J5), sambucus (J6), and sea buckthorn (J7a, J7b). Linear regression (not shown) yields an R2 value of 0.0124. Taken from Felgitsch et al., 2019.**

### **Filtered Samples:**

In order to assess whether INPs are a property of the coarse particle fraction, or part of the solution, the freezing abilities of filtered samples were determined. To obtain filtered samples, the samples were pressed through 0.2  $\mu\text{m}$  syringe filters. The resulting liquids did not contain any particles with a diameter of 0.2  $\mu\text{m}$  or larger and therefore only contained solutes and particles in the nanometre size-range.

A decrease in freezing temperature was observed for all filtered fruit juices compared to the unfiltered samples (see Figure 62). However, even after filtration, INPs were still present in all samples (see Figure 62). The highest loss of INPs (represented by  $K(-34\text{ °C})$  values) due to filtration was found for lingonberry juice (J5, approx. 98%). The smallest loss of INPs in the juice sample group was found for blueberry juice (J2, approx. 13%). Pure black currant juice (J1b) was the sample with the highest INP content of the analysed samples. It lost about a third of its INPs due to filtration. The extracts showed a different behaviour than the juices. Their INP concentrations did not drop due to filtration, which clearly shows that our analysed extracts did not contain INPs larger than  $0.2\text{ }\mu\text{m}$ . The freezing temperature of the extracts, if filtered and unfiltered samples are compared, stayed within the standard deviation of each other. Only for L4 the freezing behaviour was slightly impacted. However, an increase instead of a decrease in freezing temperature was observed, which is more likely due to variation than due to filtration.

Further, juices which were produced in the lab from frozen berries were examined. As the production of these samples included centrifugation, liquid samples containing the whole range of particles present were not available. Therefore, these samples were only measured as filtered samples and were not represented in the unfiltered sample group. These samples were derived from frozen raspberries (B1f) and frozen rowanberries (B2f) and they exhibited the lowest MFT values of all analysed samples and rather low cumulative nucleus concentrations. Only filtered lingonberry juice (J5f) exhibited lower  $K(-34\text{ °C})$  values.

INPs were present in all filtered samples. The concentrations varied. We assume these INPs to be INMs, as they are in submicron size-range. Six of the analysed unfiltered samples exhibited freezing temperatures at or below the homogeneous freezing line. These samples were blueberry juice

(J2f), lingonberry juice (J5f), sambucus juice (J6f), rowanberry extract (E2f), frozen raspberries (B1f), and frozen rowanberries (B2f). The MFT values of all other samples varied between  $-21.9\text{ }^{\circ}\text{C}$  (J1bf, black currant) and  $-35.6\text{ }^{\circ}\text{C}$  (J6f, sambucus). Initial freezing temperatures were in the range between  $-14.2\text{ }^{\circ}\text{C}$  (J7bf) and  $-31.9\text{ }^{\circ}\text{C}$  (B2f).

As the freezing temperature correlates to the INPs (or in this case INMs) concentration, we found a similar trend for the  $K(-34\text{ }^{\circ}\text{C})$  values. The values for all presented samples are given in Table 18.

**Table 18: Results of the measurements for the different samples (filtered and unfiltered), with the mean freezing temperature and corresponding standard deviation and the cumulative nucleus concentration at  $-34^{\circ}\text{C}$ . Some samples exhibit rather low freezing temperatures, which can be attributed to freezing point depression and low INP concentrations. However, we found INPs in every sample:**

Common name	Sample ID	Type	MFT [ $^{\circ}\text{C}$ ]	$\sigma$ [ $^{\circ}\text{C}$ ]	$K(-34^{\circ}\text{C})$ [ $\text{cm}^{-3}$ ]
Black currant	J1a	Juice	-24.3	4.8	$7.7 \cdot 10^8$
Black currant	J1af	Filtered juice	-31.3	6.9	$1.2 \cdot 10^8$
Black currant	J1b	Juice	-20.6	0.5	$9.2 \cdot 10^9$
Black currant	J1bf	Filtered juice	-21.9	1.7	$6.1 \cdot 10^9$
Blueberry	J2	Juice	-36.5	4.6	$4.2 \cdot 10^7$
Blueberry	J2f	Filtered juice	-37.8	4.9	$3.7 \cdot 10^7$
Chokeberry	J3	Juice	-31.1	6.1	$1.7 \cdot 10^8$
Chokeberry	J3f	Filtered juice	-34.3	5.6	$7.9 \cdot 10^7$
Cranberry	J4	Juice	-29.8	7.8	$1.4 \cdot 10^8$

Cranberry	J4f	Filtered juice	-36.9	3.5	$2.3 \cdot 10^7$
Lingonberry	J5	Juice	-34.7	10.5	$5.9 \cdot 10^7$
Lingonberry	J5f	Filtered juice	-41.7	2.3	$9.7 \cdot 10^5$
Sambucus	J6	Juice	-30.6	9.7	$1.3 \cdot 10^8$
Sambucus	J6f	Filtered juice	-35.6	3.6	$9.0 \cdot 10^6$
Sea buckthorn	J7a	Juice	-21.3	6.3	$7.0 \cdot 10^8$
Sea buckthorn	J7af	Filtered juice	-30.6	6.7	$7.2 \cdot 10^7$
Sea buckthorn	J7b	Juice	-18.5	3.8	$3.7 \cdot 10^9$
Sea buckthorn	J7bf	Filtered juice	-24.5	6.7	$5.4 \cdot 10^8$
Raspberry	B1f	Filtered frozen berries	-42.8	3.7	$3.0 \cdot 10^6$
Rowanberry	B2f	Filtered frozen berries	-45.6	3.4	$3.4 \cdot 10^6$
Juniper berry	E1	Extract of dried berries	-24.3	7.7	$4.3 \cdot 10^8$
Juniper berry	E1f	Filtered extract of dried berries	-23.7	7.8	$4.5 \cdot 10^8$
Rowanberry	E2	Extract of dried berries	-38.1	2.6	$8.7 \cdot 10^6$
Rowanberry	E2f	Filtered extract of dried berries	-37.1	1.9	$8.2 \cdot 10^6$
Sea buckthorn	E3	Extract of dried berries	-31.8	7.4	$6.4 \cdot 10^7$
Sea buckthorn	E3f	Filtered extract of dried berries	-32.2	6.8	$6.6 \cdot 10^7$
Blueberry	L1	Extract of leaves	-34.9	4.8	$3.0 \cdot 10^7$

Blueberry	L1f	Filtered extract of leaves	-33.4	4.0	$3.2 \cdot 10^7$
Juniper	L2	Extract of leaves	-30.0	4.9	$1.1 \cdot 10^8$
Juniper	L2f	Filtered extract of leaves	-31.0	5.3	$6.3 \cdot 10^7$
Raspberry	L3	Extract of leaves	-34.9	4.2	$3.4 \cdot 10^7$
Raspberry	L3f	Filtered extract of leaves	-33.4	4.6	$5.7 \cdot 10^7$
Sea buckthorn	L4	Extract of leaves	-35.6	1.8	$5.2 \cdot 10^7$
Sea buckthorn	L4f	Filtered extract of leaves	-33.8	4.8	$2.5 \cdot 10^7$

#### 4.2.2. Comparison of Samples

Several samples originated from similar plants. Two different black currant juices (J1a and J1b), and two different sea buckthorn juices (J7a and J7b) were analysed. In case of black currant, comparison shows that INP concentrations were reduced in the juices marked with an a and therefore also reduced initial freezing temperature and MFT values. In the case of sea buckthorn both juices behaved similarly. While variations were found for the two sea buckthorn and two black currant juices, their cumulative nucleus concentrations over the whole heterogeneous temperature range matched well but was shifted regarding their INP concentration (see Figure 64). We assume this to be an indicator that similar INPs are present in samples originating from similar plants, however, the concentration varied between the different samples. Filtration impacted the black currant juices and the sea buckthorn juices similarly. In both cases, we see stronger losses for the juices marked with a.

Rowanberries were analysed as extracts of dried berries (E2) and as frozen berries (B2). Both samples exhibited rather low freezing temperature and INP concentrations.

In the case of juniper, extracts of leaves (L2) and of dried berries (E1) were tested. The cumulative nucleus concentration over the heterogeneous temperature range of the two samples show similar curve progressions for temperatures below -20 °C (see Figure 65, and Figure 66). Again, a lack in INPs above -20 °C for the leaves was observed indicating that they have no potent INPs (which are present in the berries). MFT values of both extracts are below the juniper pollen line, however, initial freezing temperature of the frozen berry extract are above the juniper pollen line and initial freezing temperature of the leaves are at the juniper pollen line, indicating that the down shift in MFT is a result of reduced INP concentrations.

Two different raspberry samples were analysed: Frozen berries (B1) and leaf extracts (L3). The curve progressions of the cumulative nucleus concentrations are similar, with leaves shifted towards higher concentrations (see Figure 65, and Figure 66).

For blueberry, results for leave extracts (L1) and for a juice (J2) were available. Other than in previous cases, a higher freezing temperature for the leaves was observed, even though INP concentrations are in a comparable range (see Figure 62, Figure 64, and Figure 65).

In the case of sea buckthorn, extracts of dried sea buckthorn berries (E3) and sea buckthorn leaves (L4), as well as juices were analysed. Extracts of dried berries behaved similarly to the juices but are shifted in concentration. The leaves, however, not just exhibit a shift in concentration but also a lack in freezing events above -20 °C, indicating the absence of potent INPs (which are present in the berries) (see Figure 64, Figure 65, and Figure 66).



Results for rowanberry plants as frozen berries (B2) and as aqueous extract of dried berries (E2) were compared. The INP concentrations of the two samples and curve progression of the cumulative nucleus concentration matched well (see Figure 65). However, the frozen berries exhibited a significantly lower MFT value (see Figure 62)

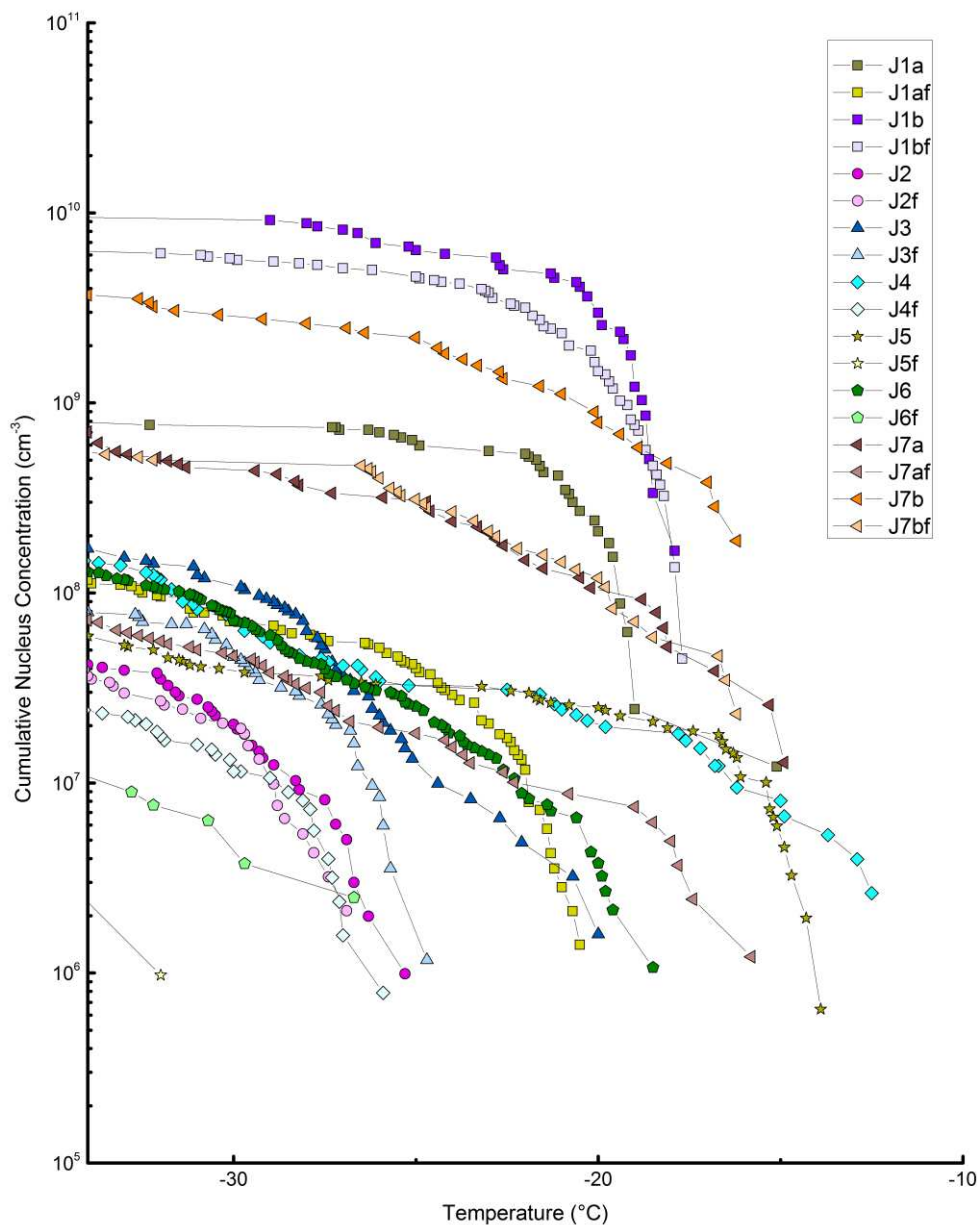


**Figure 64:**  $K(T)$  of the analysed juices (black currant (J1a, J1b), blueberry (J2), chokeberry (J3), cranberry (J4), lingonberry (J5), sambucus (J6) sea buckthorn (J7a, J7b)). Samples marked with an *f* are filtered and do not contain particles bigger 0.2  $\mu\text{m}$ . We cut off the data points at temperatures below  $-35^\circ\text{C}$ , since we cannot exclude homogeneous nucleation events at lower temperatures and therefore cannot attribute those data points to INMs with full certainty. Adapted from Felgitsch et al., 2019.

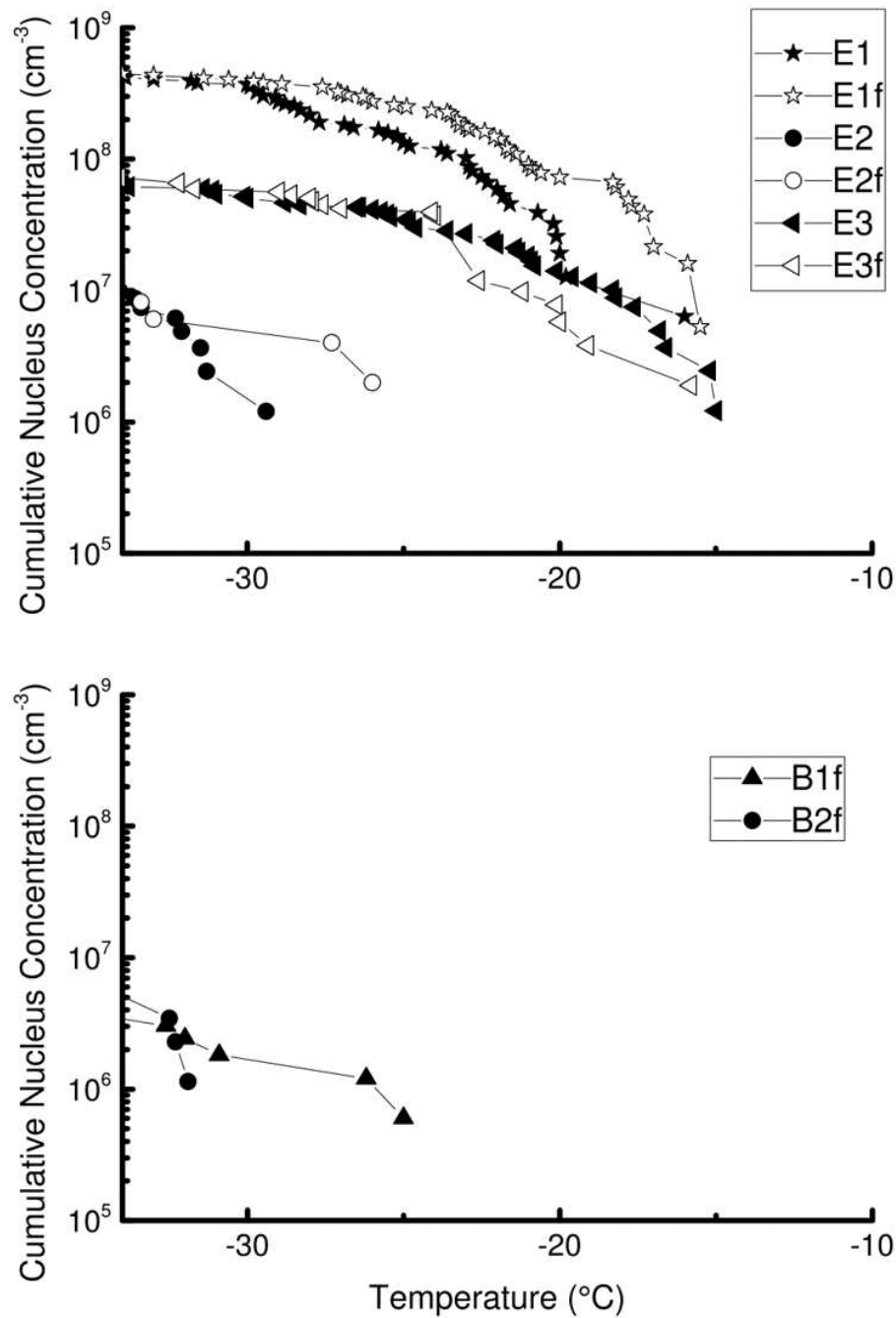


**Figure 65:**  $K(T)$  of the analysed extracts on the top (juniper berries (E1), rowanberries (E2), sea buckthorn (E3)) and frozen berries on the bottom right (blueberry (B1) and raspberry (B2)). Samples marked with an *f* are filtered and do not contain particles bigger 0.2  $\mu\text{m}$ . We cut off the data points at temperatures below  $-35^\circ\text{C}$ , since we cannot exclude homogeneous nucleation events at lower temperatures and therefore cannot attribute those data points to INMs with full certainty. Adapted from Felgitsch et al., 2019.

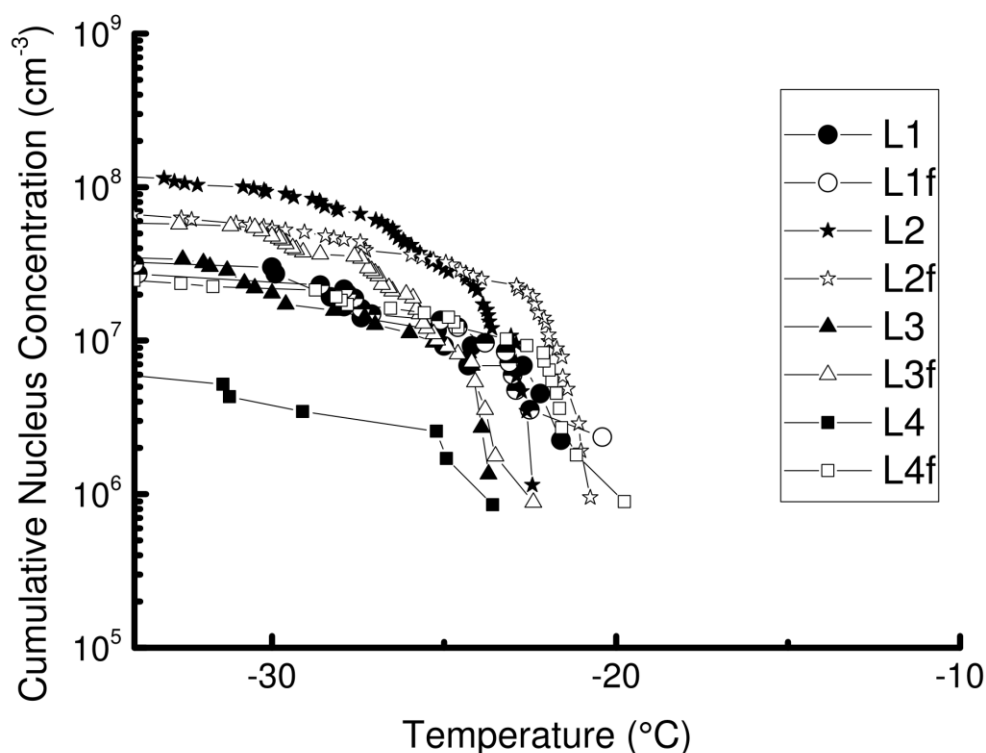


**Figure 66:**  $K(T)$  of the analysed extracts of leaves: blueberry (L1), juniper (L2) raspberry (L3), and sea buckthorn (L4). Samples marked with an f are filtered and do not contain particles bigger  $0.2 \mu\text{m}$ . We cut off the data points at temperatures below  $-35^\circ\text{C}$ , since we cannot exclude homogeneous nucleation events at lower temperatures and therefore cannot attribute those data points to INMs with full certainty. Adapted from Felgitsch et al., 2019.

When the curve progressions of the cumulative nucleus concentrations are compared (see Figure 64, Figure 65, and Figure 66) the different samples can be categorised into four groups in respect of initial freezing temperature:

- The group of samples containing the most potent INPs exhibit initial freezing temperatures around  $-15^\circ\text{C}$ . This group contains nearly all black currant juice samples (J1a, J1b, and J1bf), unfiltered cranberry juice (J4) unfiltered lingonberry juice (J5), sea buckthorn

juice (J7a, J7af, J7b, and J7bf), extracts of dried juniper berries (E1 and E1f) and extracts of dried sea buckthorn berries (E3 and E3f).

- The second group contains samples with initial freezing temperatures ranging around -20 °C. Those samples are unfiltered chokeberry juice (J3), unfiltered sambucus juice (J6), filtered black currant juice a (J1a) and all leaf extracts (blueberry - L1, juniper - L2, raspberry - L3 and sea buckthorn - L4).
- The third group exhibits initial freezing temperatures around -25 °C. This group contains filtered chokeberry juice (J3f), filtered cranberry juice (J4f), filtered sambucus juice (J6f), blueberry juice (J2 and J2f), and frozen raspberries (B1f)
- The fourth group shows the lowest initial freezing temperatures, which range around -30 °C. This group contains filtered lingonberry juice (J5f), frozen rowanberries (B2f), and extracts from dried rowanberries (E2 and E2f).

Interestingly, unfiltered cranberry, lingonberry and sambucus juice (J3, J4, and J6) exhibited a stepwise curve progression at which the second step of the curve occurs at the same temperature as the corresponding initial freezing temperature of the filtered samples. This could indicate that filtering the sample led to the loss of the INPs with the highest potency.

### 4.2.3. Ozone Treatment of Black Currant Juice

Black currant juice (J1b) was analysed regarding its stability towards ozone following the procedure introduced in Section 3.4. For this experiment 35 mL of black currant juice was used, all other parameters remained the same. Due to the ozone decolouration of the juice was observed, shown in Figure 67. The freezing curves of the different collected fractions are depicted in Figure 68.

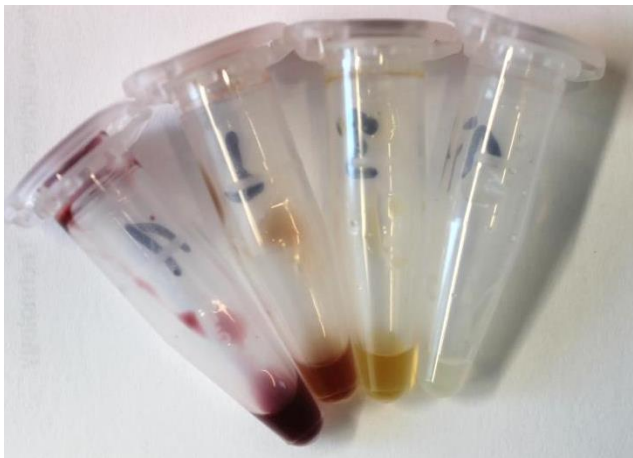


**Figure 67:** Different fractions of black currant juice showing the depletion of colour due to ozone over time.

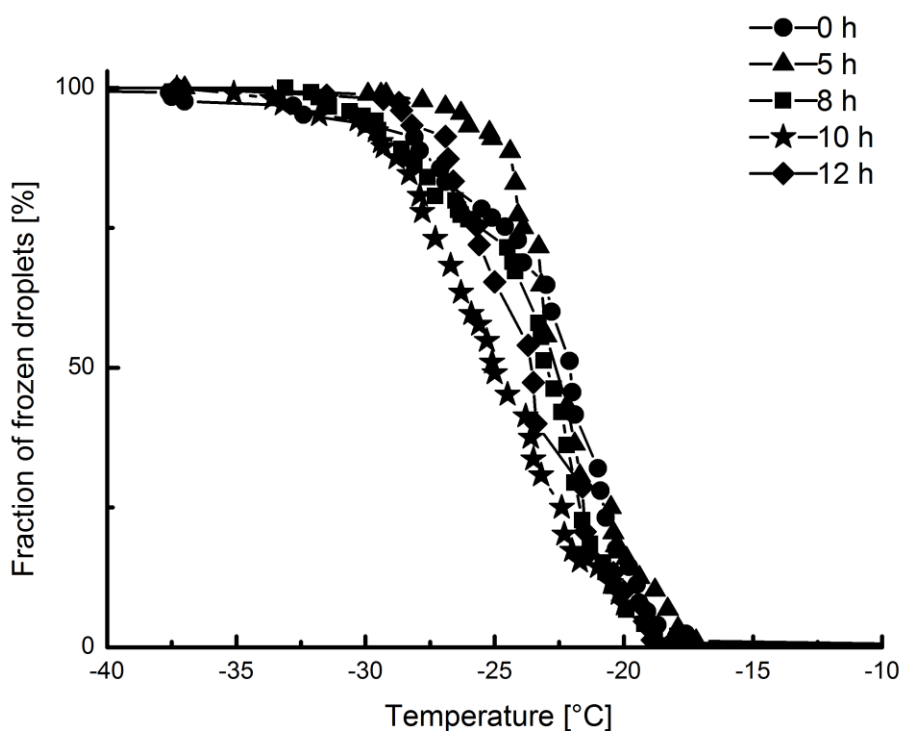


**Figure 68:** Freezing curves of the different black currant juice fractions treated with ozone (collected after 0, 5, 8, 10, and 12 h).

Further, an overview over the mean freezing temperature as a function of treatment time is given in Figure 69.

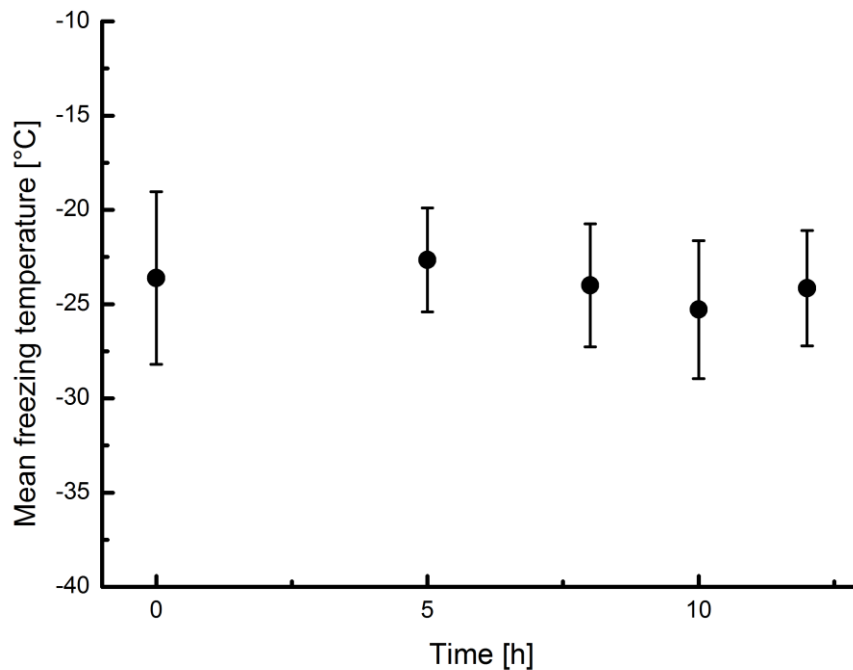


**Figure 69: MFT values of the five collected fractions plotted with the corresponding standard deviation against the ozone treatment time. Taken from Felgitsch et al., 2019.**

Other than for birch pollen washing water, which showed a decrease in INA (see chapter 3.4.); the INA of black currant juice was not affected by the ozone treatment. During the whole exposition time, the mean freezing temperature fluctuated around a value of approx.  $-24\text{ °C}$  (see Figure 69). This experiment shows that the INPs contained in black currant juice exhibit a high resistance towards oxidation by ozone.

#### 4.2.4. Discussion – INPs Distribution Throughout Various Plants Native to the Boreal Region

Our results clearly show that all analysed plant materials (see Table 6) from berries of plants native to the boreal regions contained INPs that were active at or above  $-34^{\circ}\text{C}$ . These results indicate that INA is a trait common in plants native to the boreal regions and it is important to conduct further studies on the nature and the release mechanisms of these small INPs from plants. Further, we found that the samples still contained INPs if centrifuged and filtered with a  $0.2\ \mu\text{m}$  size cut-off, with varying losses. We assume the remaining INPs to be INMs, indicating similarities in size to INMs found in birch pollen (Pummer *et al.*, 2012, 2015). INPs present in black currant are highly stable towards ozone oxidation. This is an indicator for stability towards reactive oxygen species, which would lead to a higher active atmospheric lifespan.

In the presented sample group, plant materials deriving from different plants of the same species (e.g. sea buckthorn-available as different juices and dried berries or rowanberries-available as frozen berries and dried berries) often exhibit strong similarities in their freezing behaviour (see Section 4.2.2). This indicates similarities between the contained INPs of the different samples. Interestingly, we found that leaves often tend to contain less potent INPs, with lower initial freezing temperatures. However, at lower temperatures, the curve progression of leaves and correlating other samples match in nearly all cases.

Differences in MFT can derive directly from the concentration of INPs in the analysed material and does not directly reflect the nature of the INPs. Differences in the curve progression of the  $K(T)$  however cannot be explained by this concentration effect alone. This either means that various INPs are present and their concentration ratio varies, or that the INPs present vary themselves. Differences of the INPs can be of chemical



nature or due to a variation in size of the responsible active sites. INPs could form aggregates, which could have different composition or structure from sample to sample. Ice nucleation active material from winter rye, for example, has a complex composition of proteins, carbohydrates and phospholipids (Brush, Griffith and Mlynarz, 1994). Small changes in one component could impact the freezing behaviour.

We found freezing point depression in several samples. This is to be expected, as it is a widely used cold hardiness mechanism of plants (Storey and Storey, 2004). In order to achieve lowered freezing temperatures, plants produce specific substances such as small sugars or special antifreeze proteins (Griffith *et al.*, 1992; Urrutia, Duman and Knight, 1992). The concentration of those molecules can be highly dependent on the analysed cell type as well as the season of harvesting (Kasuga, Arakawa and Fujikawa, 2007). This property affects the presented MFT values as present homogeneous freezing events are shifted towards lower concentrations.

Studies addressing the ice nucleation activity of the plant materials presented in this chapter are sparse. The INA of the sea buckthorn berries was investigated by Lundheim and Wahlberg (1998). They found freezing temperatures of different phenotypes to range between  $-15.1$  and  $-6.1^{\circ}\text{C}$  (see Table 2). Other than that, our sea buckthorn juice froze at  $-18.5^{\circ}\text{C}$ , which is slightly below this temperature range. However, Lundheim and Wahlberg (1998) used  $20\ \mu\text{l}$  ( $20\ \text{mm}^3$ ) droplets, which are five orders of magnitude larger than the ones we examine with our setup. Increasing the droplet size of our samples would lead to an increase in freezing temperature. In the case of blueberry, we found an MFT of only  $-36.5^{\circ}\text{C}$ . Kishimoto *et al.* (2014) state a freezing temperature of  $-7.2^{\circ}\text{C}$  (see Table 2) for blueberry. However, Kishimoto *et al.* (2014) worked with  $500\ \mu\text{l}$  droplets and half a fruit per droplet. Again, these huge differences in

methodology make results hard to compare. These two cases show how important the determination of INP concentrations is. Other than the freezing temperatures, it allows a comparison between different methods of immersion freezing experiments.

### 4.3. Discussion – INPs from Plants and their INA

With our investigations on the INA of plants we were able to show that a variety of plants native to the boreal regions contain INPs. In all cases we found that at least a portion of these INPs are in the submicron size range and we refer to these INPs as INMs. Due to their small size, INMs can exhibit a long atmospheric lifespan if they become airborne (up to several days depending on the altitude for particle in the size range of 0.2  $\mu\text{m}$  and smaller (Pruppacher and Klett, 1997), increasing their possible importance in atmospheric processes. Further, INMs can be absorbed on non-active or less active particles, adding a new active centre (e.g. dust particles (O’Sullivan *et al.*, 2016)). As the awareness of such small INPs is growing, more and more research is done on possible sources and the existence of INMs has been found in diverse biological materials (Schnell and Vali, 1973; Pummer *et al.*, 2012, 2015; Fröhlich-Nowoisky *et al.*, 2015; O’Sullivan *et al.*, 2015). While the exact influence of these INMs in atmospheric processes is still unclear, several studies point out the importance of biological components in the INA of soil and dust particles (Conen *et al.*, 2011; O’Sullivan *et al.*, 2014; Tobo *et al.*, 2014; Hill *et al.*, 2016), indicating the importance of biological INMs. Via the release of INMs as active particles themselves and as active centres on larger particles, ice nucleation active plants could influence their local environment.

Next to released INMs, plant debris itself could be an important factor. Plant debris contributes to ambient particulate matter (Matthias-Maser and Jaenicke, 1995; Andreae, 2007; Winiwarter *et al.*, 2009). As the underlying processes of the release of plant debris into the atmosphere are not fully understood, predictions of their atmospheric impact cannot be made with a sufficient level of certainty (Andreae, 2007; Winiwarter *et al.*, 2009). An important contributor to atmospheric aerosols from plants is cellulose, which is so common that it can be used as a proxy for plant

debris (Sánchez-Ochoa *et al.*, 2007). Leaves could be an important source for INPs as they are shed and reproduces annually. Decaying leaf litter has already been shown to be a potent source for INPs (Schnell and Vali, 1973). Further, it was found that air masses which pass over land can be enriched with INPs deriving from leaf litter (Conen, Stopelli and Zimmermann, 2016; Conen *et al.*, 2017).

Most of the plant materials analysed for this work were collected in nature. Therefore, we cannot rule out possible contaminations, which could influence the INA of our samples. Ice nucleation active bacteria are common on nature (e.g. *Pseudomonas syringae* (Leroy R. Maki *et al.*, 1974)). However, these bacteria are typically in a size range  $>1 \mu\text{m}$  (Monier and Lindow, 2003) and therefore should not play a role in our filtered samples. Further, lichen are known to be ice nucleation active (Kieft, 1988). Some microorganisms are capable of releasing their INPs in the aqueous phase, e.g. *Mortierella alpine*, which produces small extracellular ice nucleation active proteins, which are easily released (Fröhlich-Nowoisky *et al.*, 2015) or *Lysinibacillus*, a Gram-positive bacterium that secretes its non-proteinaceous INPs (Failor *et al.*, 2017). These INPs cannot not be removed using a filter. However, lichen, other microorganisms as well as INPs released from microorganisms typically freeze at significantly higher temperatures than our analysed samples ( $>-10 \text{ }^\circ\text{C}$  (Leroy R. Maki *et al.*, 1974; Kieft, 1988; S. Pouleur *et al.*, 1992; Murray *et al.*, 2012; Fröhlich-Nowoisky *et al.*, 2015), with very little known exceptions (Iannone *et al.*, 2011). As our initial freezing temperatures observed were all well below  $-10 \text{ }^\circ\text{C}$  and often close to the initial freezing temperature of birch pollen washing water (approx.  $-15 \text{ }^\circ\text{C}$ ), we assume that biological contaminations of microorganisms do not play a role in our samples. We further cannot rule out that soot and other anthropogenic emissions influence our results (DeMott, 1990; Murray *et*

*al.*, 2012), however, these substances are in most cases only weakly soluble in water, therefore a large impact is not likely.

Our results suggest that plants native to boreal regions can act as source for INPs and could contribute to the INA of mixed-phase particles. To deepen the understanding of their possible influence on the local climate, further analysis of the influence of species and growing conditions are necessary.

## 5. Summary and Conclusion

- Our analysis of INPs from birch pollen and their interaction with nonpolar material (SPE, SEC) showed that the INPs are likely to have amphiphilic character.
- We were able to destroy the INA of aqueous birch pollen extracts with subtilisin (a protease) and urea. Further, ammonium sulphate precipitation led to a precipitate, which was highly active. IR analysis of the precipitate showed spectra typical for proteins. It is therefore very likely that proteins play an important role in the INA of birch pollen. However, possible influences of other substance classes on the INA cannot be excluded.
- We analysed milled extracts of leaves, primary wood, and secondary wood of ten different birch trees. We found that all of the samples exhibited INA. We were able to correlate the freezing behaviour of more than a quarter of our samples to birch pollen washing water or dilutions thereof. This indicates that the INMs found in both birch pollen and birch trees are similar.
- Infrared analysis of the extracts of milled birch samples showed strong similarities between leaf, wood, and pollen extracts. Further, we found that our extracts match the FTIR-spectrum of pure wood well, except for an expected decrease in lignin signal. No major differences between the different trees was found. The spectra show that polysaccharides are a major component of our extracts. Further, we found all typical protein bands.
- We examined the surface availability of INMs from the nine Tyrolean birch trees. We were able to extract INMs from all trees and nearly all samples.
- Further analyses of bark and drill cores of the stem of the Tyrolean birch trees showed that INPs are concentrated in the outermost

parts. The concentrations of INPs drop drastically when moving towards the inner part of the stem.

- Results of the surface extracts led to estimates that birch stands release on average about  $10^9$  to  $10^{15}$  INMs per  $m^2$  without accounting for INMs from branch wood.
- We analysed various berries and leaves of plants native to the boreal region and found not just that every singly sample contained INPs but further that they all also contained INMs.
- Birch pollen washing water and black currant both were resistant against oxidation with ozone. In combination with the small size of the contained INPs, this resistance against oxidation is another indicator of a possible long atmospheric lifespan.

## References:

Allen, L. H. (1990) 'Plant Responses to Rising Carbon Dioxide and Potential Interactions with Air Pollutants', *Journal of Environment Quality*, 19(1), p. 15. doi: 10.2134/jeq1990.00472425001900010002x.

Alpert, P. A. and Knopf, D. A. (2016) 'Analysis of isothermal and cooling-rate-dependent immersion freezing by a unifying stochastic ice nucleation model', *Atmospheric Chemistry and Physics*, 16(4), pp. 2083–2107. doi: 10.5194/acp-16-2083-2016.

Andreae, M. O. (2007) 'Aerosols before pollution', *Science*, 315(5808), pp. 50–51. doi: 10.1126/science.1136529.

Augustin, S., Wex, H., Niedermeier, D., Pummer, B., Grothe, H., Hartmann, S., Tomsche, L., Clauss, T., Voigtländer, J., Ignatius, K., and Stratmann, F. (2013) 'Immersion freezing of birch pollen washing water', *Atmospheric Chemistry and Physics*, 13(21), pp. 10989–11003. doi: 10.5194/acp-13-10989-2013.

Beck, P., Caudullo, G., de Rigo, D., and Tinner, W. (2016) 'Betula pendula, Betula pubescens and other birches in Europe: distribution, habitat, usage and threats', in San-Miguel-Ayanz, J., de Rigo, D., Caudullo, G., Houston Durrant, T., Mauri, A. (eds) *European Atlas of Forest Tree Species*. Luxembourg: Publ. Off. EU, p. e010226+. doi: 10.2788/4251.

Bennion, B. J. and Daggett, V. (2003) 'The molecular basis for the chemical denaturation of proteins by urea', *Proceedings of the National Academy of Sciences of the United States of America*, 100(9), pp. 5142–5147. doi: 10.1073/pnas.0930122100.

Bigg, E. K. (1953) 'The Supercooling of Water', *Proceedings of the Physical Society. Section B*, 66(8), pp. 688–694. doi: 10.1088/0370-1301/66/8/309.

Bingemer, H., Klein, H., Ebert, M., Haunold, W., Budke, U., Herrmann, T., Kandler, K., Müller-Ebert, D., Weinbruch, S., Judt, A., Wéber, A., Nillius, B., Ardon-Dryer, K., Levin, Z., and Curtius, J. (2012) 'Atmospheric ice nuclei in the Eyjafjallajökull volcanic ash plume', *Atmospheric Chemistry and Physics*, 12(2), pp. 857–867. doi: 10.5194/acp-12-857-2012.

Brooks, S. D., Suter, K., and Olivarez, L. (2014) 'Effects of chemical aging on the ice nucleation activity of soot and polycyclic aromatic hydrocarbon aerosols', *Journal of*



*Physical Chemistry A*, 118(43), pp. 10036–10047. doi: 10.1021/jp508809y.

Brovchenko, I. and Oleinikova, A. (2008) 'Multiple phases of liquid water', *ChemPhysChem*, 9(18), pp. 2660–2675. doi: 10.1002/cphc.200800639.

Brush, R. A., Griffith, M., and Mlynarz, A. (1994) 'Characterization and Quantification of Intrinsic Ice Nucleators in Winter Rye (*Secale-Cereale*) Leaves', *Plant Physiology*, 104(2), pp. 725–735. doi: 10.1104/pp.104.2.725.

Burke, M. J. *et al.* (1976) 'Freezing and Injury in Plants', *Annual Review of Plant Physiology*, 27, pp. 507–528. doi: 10.1146/annurev.pp.27.060176.002451.

Caballero, R. (2014) *Physics of the Atmosphere*. Bristol: IOP Publishing. ISBN: 978-0-7503-1053-6.

Camilloni, C., Guerini Rocco, A., Eberini, I., Gianazza, E., Broglia, R.A., and Tiana, G. (2008) 'Urea and Guanidinium Chloride Denature Protein L in Different Ways in Molecular Dynamics Simulations', *Biophysical Journal*, 94(12), pp. 4654–4661. doi: 10.1529/biophysj.107.125799.

Chen, H., Ferrari, C., Angiuli, M., Yao, J., Raspi, C., and Bramanti, E. (2010) 'Qualitative and quantitative analysis of wood samples by Fourier transform infrared spectroscopy and multivariate analysis', *Carbohydrate Polymers*. Elsevier Ltd., 82(3), pp. 772–778. doi: 10.1016/j.carbpol.2010.05.052.

Chen, J. P., Hazra, A. and Levin, Z. (2008) 'Parameterizing ice nucleation rates using contact angle and activation energy derived from laboratory data', *Atmospheric Chemistry and Physics*, 8(24), pp. 7431–7449. doi: 10.5194/acp-8-7431-2008.

Christner, B. C., Morris, C. E., Foreman, C. M., Skidmore, M. L., Cai, R., and Sands, D. E. (2008) 'Ubiquity of biological ice nucleators in snowfall.', *Science (New York, N.Y.)*, 319(5867), p. 1214. doi: 10.1126/science.1149757.

Conen, F., Morris, C. E., Leitfeld, J., Yakutin, M. V., and Alewell, C. (2011) 'Biological residues define the ice nucleation properties of soil dust', *Atmospheric Chemistry and Physics*, 11(18), pp. 9643–9648. doi: 10.5194/acp-11-9643-2011.

Conen, F., Yakutin, M. V., Yttri, K. E., and Hueglin, C. (2017) 'Ice nucleating particle concentrations increase when leaves fall in autumn', *Atmosphere*, 8(10), pp. 1–9. doi: 10.3390/atmos8100202.

Conen, F., Stopelli, E., and Zimmermann, L. (2016) 'Clues that decaying leaves enrich Arctic air with ice nucleating particles', *Atmospheric Environment*, 129, pp. 91–94. doi: 10.1016/j.atmosenv.2016.01.027.

Connolly, P. J., Möhler, O., Field, P. R., Saathoff, H., Burgess, R., Choularton, T., and Gallagher, M. (2009) 'Studies of heterogeneous freezing by three different desert dust samples', *Atmospheric Chemistry and Physics*, 9(8), pp. 2805–2824. doi: 10.5194/acp-9-2805-2009.

Constantinidou, H. A. and Menkissoglu, O. (1992) 'Characteristics and importance of heterogeneous ice nuclei associated with citrus fruits', *Journal of Experimental Botany*, 43(249), pp. 585–591. doi: 10.1093/jxb/43.4.585.

Crawford, I., Bower, K. N., Choularton, T. W., Dearden, C., Crosier, J., Westbrook, C., Capes, G., Coe, H., Connolly, P. J., Dorsey, J. R., Gallagher, M. W., Williams, P., Trembath, J., Cui, Z., and Blyth, A. (2012) 'Ice formation and development in aged, wintertime cumulus over the UK: Observations and modelling', *Atmospheric Chemistry and Physics*, 12(11), pp. 4963–4985. doi: 10.5194/acp-12-4963-2012.

Dahlberg, U., Berge, T. W., Petersson, H., and Vencatasawmy, P. (2004) 'Modelling Biomass and Leaf Area Index in a Sub-arctic Scandinavian Mountain Area', *Scandinavian Journal of Forest Research*, 19(1), pp. 60–71. doi: 10.1080/02827580310019266.

DeMott, P. J. (1990) 'An Exploratory Study of Ice Nucleation by Soot Aerosols', *Journal of Applied Meteorology*, 29(10), pp. 1072–1079. doi: 10.1175/1520-0450(1990)029<1072:AESOIN>2.0.CO;2.

DeMott, P. J., Prenni, J., Liu, X., Kreidenweis, S. M., Petters, M. D., Twohy, C. H., Richardson, M. S., Eidhammer, T., and Rogers, D. C. (2010) 'Predicting global atmospheric ice nuclei distributions and their impacts on climate', *Proceedings of the National Academy of Sciences*, 107(25), pp. 11217–11222. doi: 10.1073/pnas.0910818107.

DePuy, V., Berger, V. W. and Zhou, Y. (2005) 'Wilcoxon – Mann – Whitney Test', *Encyclopedia of Statistics in Behavioral Science*, 4, pp. 2118–2121. doi: 10.1002/0470013192.bsa712.

Diehl, K., Quick, C., Matthias-Maser, S., Mitra, S.K., and Jaenicke, R. (2001) 'The ice nucleating ability of pollen Part I: Laboratory studies in deposition and condensation freezing modes', *Atmospheric Research*, 58(2), pp. 75–87. doi: 10.1016/S0169-

8095(01)00091-6.

Dorsch, R. G. and Hacker, P. T. (1950) 'Technical Note 2142: Photomicrographic Investigation of Spontaneous Freezing Temperatures of Supercooled Water Droplets', *National Advisory Committee for Aeronautics*.

Dreischmeier, K., Budke, C., Wiehemeier, L., Kottke, T., and Koop, T. (2017) 'Boreal pollen contain ice-nucleating as well as ice-binding "antifreeze" polysaccharides', *Scientific Reports*, 7(41890). doi: 10.1038/srep41890.

Durant, A. J., Shaw, R. A., Rose, W. I., Mi, Y., Ernst, G. G. J. (2008) 'Ice nucleation and overseeding of ice in volcanic clouds', *Journal of Geophysical Research Atmospheres*, 113(9), pp. 1–13. doi: 10.1029/2007JD009064.

Dymarska, M., Murray, B. J., Sun, L., Eastwood, M. L., Knopf, D. A., and Bertram, A. K. (2006) 'Deposition ice nucleation on soot at temperatures relevant for the lower troposphere', *Journal of Geophysical Research Atmospheres*, 111(D4), pp. 1–9. doi: 10.1029/2005JD006627.

Eastwood, M. L., Cremel, S., Gehrke, C., Girard, E., and Bertram, A. K. (2008) 'Ice nucleation on mineral dust particles: Onset conditions, nucleation rates and contact angles', *Journal of Geophysical Research Atmospheres*, 113(D22), pp. 1–9. doi: 10.1029/2008JD010639.

Eichelmann, H., Oja, V., Rasulov, B., Padu, E., Bichele, I., Pettai, H., Mänd, P., Kull, O., and Laisk, A. (2005) 'Adjustment of leaf photosynthesis to shade in a natural canopy: reallocation of nitrogen', *Plant, Cell and Environment*, 28, pp. 389–401. doi: 10.1111/j.1365-3040.2004.01275.x, 2005.

Ene, L., Næsset, E. and Gobakken, T. (2012) 'Single tree detection in heterogeneous boreal forests using airborne laser scanning and area-based stem number estimates', *International Journal of Remote Sensing*, 33(16), pp. 5171–5193. doi: 10.1080/01431161.2012.657363.

Ervens, B. and Feingold, G. (2012) 'On the representation of immersion and condensation freezing in cloud models using different nucleation schemes', *Atmospheric Chemistry and Physics*, 12(13), pp. 5807–5826. doi: 10.5194/acp-12-5807-2012.

Failor, K. C., Schale, D. G. III, Vinatzer, B. A., and Monteil C. L. (2017) 'Ice nucleation active bacteria in precipitation are genetically diverse and nucleate ice by employing different mechanisms'. *Nature Publishing Group*, 11(12), pp. 2740–2753. doi:

10.1038/ismej.2017.124.

Felgitsch, L., Baloh, P., Burhart, J., Mayr, M., Momken, M. E., Seifried, T. M., Winkler, P., Schmale, D. G. III, and Grothe, H. (2018) 'Birch leaves and branches as a source of ice-nucleating macromolecules', *Atmospheric Chemistry and Physics*, 18, pp. 16063–16079. doi: 10.5194/acp-18-16063-2018.

Felgitsch, L., Bichler, M., Burkart, J., Fiala, B., Häusler, T., Hitzemberger, R., and Grothe, H. (2019) 'Heterogeneous Freezing of Liquid Suspensions Including Juices and Extracts from Berries and Leaves from Perennial Plants', *Atmosphere*, 10(1), 37. doi: 10.3390/atmos10010037.

Findeisen, W. (1938) 'Die kolloidmeteorologischen Vorgänge bei der Niederschlagsbildung', *Meteorologische Zeitschrift*, 55, pp. 121–133.

Forster, P., Ramaswamy, V., Artaxo, P., Berntsen, T., Betts, R., Fahey, D. W., Haywood, J. Lean, J., Lowe, D. C., Myhre, G., Nganga, J., Prinn, R., Raga, G., Schulz M., and Van Dorland R. (2007) Changes in Atmospheric Constituents and in Radiative Forcing. In: *Climate Change 2007: The Physical Science Basis. Contribution of Working Group I to the Fourth Assessment Report of the Intergovernmental Panel on Climate Change* [Solomon, S., Qin, D., Manning, M., Chen, Z., Marquis, M., Averyt, K. B., Tignor, M., and Miller, H. L. (eds.)]. Cambridge University Press, Cambridge, United Kingdom and New York, NY, USA

Franco, V., Kousoulidou, M., Muntean, M., Ntziachristos, L., Hausberger, S., and Dilara, P. (2013) 'Road vehicle emission factors development: A review', *Atmospheric Environment*, 70, pp. 84–97. doi: 10.1016/j.atmosenv.2013.01.006.

Freer-Smith, P. H. (1985) 'The influence of SO<sub>2</sub> and NO<sub>2</sub> on the growth, development and gas exchange of *Betula pendula* roth', *New Phytologist*, 99(3), pp. 417 – 430. doi: 10.1111/j.1469-8137.1985.tb03669.x.

Friedman, B., Kulkarni, G., Beránek, J., Zelenyuk, A., Thornton, J. A., and Cziczo, D. J. (2011) 'Ice nucleation and droplet formation by bare and coated soot particles', *Journal of Geophysical Research Atmospheres*, 116(D17), pp. 1–11. doi: 10.1029/2011JD015999.

Fröhlich-Nowoisky, J., Hill, T. C. J., Pummer, B. G., Yordanova, P., Franc G. D., and Pöschl, U. (2015) 'Ice nucleation activity in the widespread soil fungus *Mortierella alpina*', *Biogeosciences*, 12(4), pp. 1057–1071. doi: 10.5194/bg-12-1057-2015.

Garnham, C. P., Campbell, R. L., Walker, V. K., and Davies, P. L. (2011) 'Novel dimeric  $\beta$ -helical model of an ice nucleation protein with bridged active sites', *BMC Structural Biology*. BioMed Central Ltd, 11:36. doi: 10.1186/1472-6807-11-36.

Geru, I. I. (2014) 'Water Structure, Quantum Nature of Hydrogen Bonds and Diffusion of Water Molecules in Chloride Aqueous Solutions', in *Management of Water Quality in Moldova*, pp. 21–35. doi: 10.1007/978-3-319-02708-1\_2.

Gorbunov, B., Baklanov, A., Nakutkina, N., Windsor, H. L., and Toumi, R. (2001) 'Ice nucleation on soot particles', *Journal of Aerosol Science*, 32(2), pp. 199–215. doi: 10.1016/S0021-8502(00)00077-X.

Govindarajan, A. G. and Lindow, S. E. (1988) 'Size of bacterial ice-nucleation sites measured in situ by radiation inactivation analysis.', *Proceedings of the National Academy of Sciences of the United States of America*, 85(5), pp. 1334–1338. doi: 10.1073/pnas.85.5.1334.

Griffith, M., Ala, P., Yang, D. S., Hon, W. C., and Moffatt, B. A. (1992) 'Antifreeze Protein Produced Endogenously in Winter Rye Leaves', *Plant Physiology*, 100(2), pp. 593–596. doi: 10.1104/pp.100.2.593.

Griffith, M. and Yaish, M. W. F. (2004) 'Antifreeze proteins in overwintering plants: A tale of two activities', *Trends in Plant Science*, 9(8), pp. 399–405. doi: 10.1016/j.tplants.2004.06.007.

Gross, D. C., Proebsting, E. L., and Maccrindle-zimmerman, H. (1988) 'Development, Distribution, and Characteristics of Intrinsic, Nonbacterial Ice Nuclei in Prunus Wood', *Plant Physiology*, 88, pp. 915–922. doi: 10.1104/pp.88.3.915.

Guo, Y. and Clark, D. S. (2001) 'Activation of enzymes for nonaqueous biocatalysis by denaturing concentrations of urea', *Biochimica et Biophysica Acta - Protein Structure and Molecular Enzymology*, 1546(2), pp. 406–411. doi: 10.1016/S0167-4838(01)00163-7.

Hallett, J. and Mossop, S. C. (1974) 'Production of secondary ice particles during the riming process', *Nature*, 249, pp. 26–28. doi: 10.1038/249026a0.

Harmens, H., Hayes, F., Sharps, K., Mills, G., and Calatayud, V. (2017) 'Leaf traits and photosynthetic responses of *Betula pendula* saplings to a range of ground-level ozone concentrations at a range of nitrogen loads', *Journal of Plant Physiology*. Elsevier GmbH., 211, pp. 42–52. doi: 10.1016/j.jplph.2017.01.002.

Hartmann, S., Wex, H., Clauss, T., and Augustin-Bauditz, S. (2016) 'Immersion Freezing of Kaolinite: Scaling with Particle Surface Area', *Journal of the Atmospheric Sciences*, 73(1), pp. 263–278. doi: 10.1175/JAS-D-15-0057.1.

Hauptmann, A., Handle, K. F., Baloh, P., Grothe, H., and Loerting, T. (2016) 'Does the emulsification procedure influence freezing and thawing of aqueous droplets?', *Journal of Chemical Physics*, 145(211923). doi: 10.1063/1.4965434.

Häusler, T., Gebhardt, P., Iglesias, D., Rameshan, C., Marchesan, S., Eder, D., and Grothe, H. (2018) 'Ice Nucleation Activity of Graphene and Graphene Oxides', *The Journal of Physical Chemistry C*, 122, pp. 8182–8190. doi: 10.1021/acs.jpcc.7b10675.

Hazra, A., Saha, M., De, U. K., Mukherjee, J., and Goswami, K. (2004) 'Study of ice nucleating characteristics of *Pseudomonas aeruginosa*', *Journal of Aerosol Science*, 35(11), pp. 1405–1414. doi: 10.1016/j.jaerosci.2004.06.075.

Heiskanen, J. (2006) 'Estimating aboveground tree biomass and leaf area index in a mountain birch forest using ASTER satellite data', *International Journal of Remote Sensing*, 27(6), pp. 1135–1158. doi: 10.1080/01431160500353858.

Hibsch-Jetter, C. (2008) *Birken in den Alpen. Taxonomisch-ökologische Untersuchungen an Betula pubescens EHRH. und Betula pendula ROTH.* Edited by E. Führer and P. Schütt. Feddes Repertorium. doi: 10.1002/fedr.19951060325.

Hill, T. C. J., DeMott, P. J., Tobo, Y., Fröhlich-Nowoisky, J., Moffett, B. F., Franc, G. D., and Kreidenweis, S. M. (2016) 'Sources of organic ice nucleating particles in soils', *Atmospheric Chemistry and Physics*, 16, pp. 7195–7211. doi: 10.5194/acp-16-7195-2016.

Hiranuma, N., Möhler, O., Yamashita, K., Tajiri, T., Saito, A., Kiselev, A., Hoffmann, N., Hoose, C., Jantsch, E., Koop, T., and Murakami, M. (2015) 'Ice nucleation by cellulose and its potential contribution to ice formation in clouds', *Nature Geoscience*, 8(4), pp. 273–277. doi: 10.1038/ngeo2374.

Hirsh, A. G., Williams, R. J., and Merymen, H. T. (1985) 'A Novel Method of Natural Cryoprotection: Intracellular Glass Formation in Deeply Frozen Populus', *Plant Physiology*, 79, pp. 41–56. doi: 10.1104/pp.79.1.41.

Hoffer, T. E. (1961) 'A Laboratory Investigation of Droplet Freezing', *JOURNAL OF METEOROLOGY*, 18, pp. 766–778. doi: 10.1175/1520-0469(1961)018<0766:ALIODF>2.0.CO;2.

Hoyle, C. R., Pinti, V., Welti, A., Zobrist, B., Marcolli, C., Luo, B., Höskuldsson, Á, Mattsson, H. B., Stetzer, O., Thorsteinsson, T., Larsen, G., and Peter, T. (2011) 'Ice nucleation properties of volcanic ash from Eyjafjallajökull', *Atmospheric Chemistry and Physics*, 11(18), pp. 9911–9926. doi: 10.5194/acp-11-9911-2011.

Huang, J. and Bartell, L. S. (1995) 'Kinetics of homogeneous nucleation in the freezing of large water clusters', *Journal of Physical Chemistry*, 99(12), pp. 3924–3931. doi: 10.1021/j100012a010.

Huffman, J. A., Prenni, A. J., DeMott, P. J., Pöhlker, C., Mason, R. H., Roninson, N. H., Fröhlich-Nowoisky, J., Tobo, Y., Deprés, V. R., Garcia, E., Gochis, D. J., Harris, E., Müller-Germann, I., Ruzene, C., Schmer, B., Sinha, B., Day, D. A., Andreae, M. O., Jimenez, J. L., Gallagher, M., Kreidenweis, S. M., Bertram, A. K., and Pöschl, U. (2013) 'High concentrations of biological aerosol particles and ice nuclei during and after rain', *Atmospheric Chemistry and Physics*, 13(13), pp. 6151–6164. doi: 10.5194/acp-13-6151-2013.

Hynynen, J., Niemistö, P., Viherä-Aarnio, A., Brunner, A., Hein, S., and Velling, P. (2010) 'Silviculture of birch (*Betula pendula* Roth and *Betula pubescens* Ehrh.) in Northern Europe', *Forestry*, 83(1), pp. 103–119. doi: 10.1093/forestry/cpp035.

Iannone, R., Chernoff, D. I., Pringle, A., Martin, S. T., and Bertram, A. K. (2011) 'The ice nucleation ability of one of the most abundant types of fungal spores found in the atmosphere', *Atmospheric Chemistry and Physics*, 11(3), pp. 1191–1201. doi: 10.5194/acp-11-1191-2011.

Ickes, L., Welti, A., Hoose, C., and Lohmann, U. (2015) 'Classical nucleation theory of homogeneous freezing of water: thermodynamic and kinetic parameters', *Phys. Chem. Chem. Phys.*, 17(8), pp. 5514–5537. doi: 10.1039/C4CP04184D.

Jaenicke, R. (2005) 'Abundance of cellular material and proteins in the atmosphere', *Science*, 308(5718), p. 73. doi: 10.1126/science.1106335.

Jann, A., Lundheim, R., Niederberger, P., and Richard, M. (1997) 'Increasing freezing point of food with sea buckthorn ice nucleating agent'. United States Patent (08/673261).

Jia, Y., Bhat, S., and Fraser, M. P. (2010) 'Characterization of saccharides and other organic compounds in fine particles and the use of saccharides to track primary biologically derived carbon sources', *Atmospheric Environment*, 44(5), pp. 724–732. doi: 10.1016/j.atmosenv.2009.10.034.

Johansson, T. (1999) 'Biomass equations for determining fractions of common and grey alders growing on abandoned farmland and some practical implications', *Biomass and Bioenergy*, 16, pp. 223–238. doi: [https://doi.org/10.1016/S0961-9534\(98\)00075-0](https://doi.org/10.1016/S0961-9534(98)00075-0).

Kačuráková, M., Capek, P., Sasinková, V., Wellner, N., and Ebringerová, A. (2000) 'FT-IR study of plant cell wall model compounds: pectic polysaccharides and hemicelluloses', 43(2), *Carbohydrate Polymers*, 43(2), pp. 195–203. doi: 10.1016/S0144-8617(00)00151-X.

Kajava, A. V. and Lindow, S. E. (1993) 'A Model of the Three-dimensional Structure of Ice Nucleation Proteins', *Journal of Molecular Biology*, pp. 709–717. doi: 10.1006/jmbi.1993.1424.

Kamphus, M., Ettner-Mahl, M., Klimach, T., Drewnick, F., Keller, L., Cziczo, D. J., Mertes, S., Borrmann, S., and Curtius, J. (2010) 'Chemical composition of ambient aerosol, ice residues and cloud droplet residues in mixed-phase clouds: Single particle analysis during the cloud and aerosol characterization experiment (CLACE 6)', *Atmospheric Chemistry and Physics*, 10(16), pp. 8077–8095. doi: 10.5194/acp-10-8077-2010.

Karlsson, P. S., Weih, M., and Borg, C. (2005) 'Mountain Birch Growth in Relation to Climate and Herbivores', in Karlsson, P. S., Neuvonen, S., and Thannheiser, D. (eds) *Plant Ecology, Herbivory, and Human Impact in Nordic Mountain Birch Forests*, pp. 71–86.

Kasuga, J., Arakawa, K., and Fujikawa, S. (2007) 'High accumulation of soluble sugars in deep supercooling Japanese white birch xylem parenchyma cells', *New Phytologist*, 174(3), pp. 569–579. doi: 10.1111/j.1469-8137.2007.02025.x.

Khvorostyanov, V. I. and Curry, J. A. (2014) 'Thermodynamics, Kinetics and Microphysics of Clouds', 1<sup>st</sup> Edition, New York Cambridge University Press.

Kieft, T. L. (1988) 'Ice nucleation activity in lichens.', *Applied and environmental microbiology*, 54(7), pp. 1678–1681.

Kiehl, J. T. and Trenberth, K. E. (1997) 'Earth ' s Annual Global Mean Energy Budget Satellite radiometer data', *Bulletin of the American Meterological Society*, 78(2), pp. 197–208. doi: 10.1175/1520-0477(1997)078<0197>

Kiselev, A., Bachmann, F., Pedevilla, P., Cox, S. J., Mechaelides, A., Gerthsen, D., and Leisner, T. (2017) 'Active sites in heterogeneous ice nucleation—the example of K-rich feldspars', *Science*, 355(6323), p. 367 LP-371. doi: 10.1126/science.aai8034.



Kishimoto, T., Yamazaki, H., Saruwatari, A., Murakawa, H., Sekozawa, Y., Kuchitsu, K., Prise, W. S., and Ishikawa, M. (2014) 'High ice nucleation activity located in blueberry stem bark is linked to primary freeze initiation and adaptive freezing behaviour of the bark', *AoB PLANTS*, 6, plu044, pp. 1–17. doi: 10.1093/aobpla/plu044.

Kostina, M. V., Barabanshikova, N. S., Bityugova, G. v., Yasinskaya, O. I., and Dubach, A. M. (2015) 'Structural modifications of birch (*Betula pendula* Roth.) crown in relation to environmental conditions', *Contemporary Problems of Ecology*, 8(5), pp. 584–597. doi: 10.1134/S1995425515050091.

Krämer, B., Hübner, O., Vortisch, H., Wöste, L., and Leisner, T. (1999) 'Homogeneous nucleation rates of supercooled water measured in single levitated microdroplets', *The Journal of Chemical Physics*, 111(14), pp. 6521–6527. doi: 10.1063/1.479946.

Kristiansen, E. and Zachariassen, K. E. (2005) 'The mechanism by which fish antifreeze proteins cause thermal hysteresis', *Cryobiology*, 51(3), pp. 262–280. doi: 10.1016/j.cryobiol.2005.07.007.

Kulkarni, G. and Dobbie, S. (2010) 'Ice nucleation properties of mineral dust particles: Determination of onset RH<sub>i</sub>, in active fraction, nucleation time-lag, and the effect of active sites on contact angles', *Atmospheric Chemistry and Physics*, 10(1), pp. 95–105. doi: 10.5194/acp-10-95-2010.

Kuokkanen, K., Julkunen-Tiitto, R., Keinänen, M., Niemelä, P., and Tahvanainen, J. (2001) 'The effect of elevated CO<sub>2</sub> and temperature on the secondary chemistry of *Betula pendula* seedlings', *Trees - Structure and Function*, 15(6), pp. 378–384. doi: 10.1007/s004680100108.

Langham, E. J. and Mason, B. J. (1958) 'The heterogeneous and homogeneous nucleation of supercooled water', *Proceedings of the Royal Society of London. Series A, Mathematical and Physical Sciences*, 247(1251). doi: 10.1098/rspa.1958.0207.

Levine (1950) 'Technical Note 2234: Statistical Explanation of Spontaneous Freezing of Water Droplets', *National Advisory Committee for Aeronautics*.

Lindow, S. E., Lahue, E., Govindarajan, A. G., Panopoulos, J., and Gies, D. L. (1989) 'Localization of Ice Nucleation Activity and the iceC Gene Product in *Pseudomonas syringae* and *Escherichia coli*', *Molecular Plant-Microbe Interactions*, 2(5), pp. 262–272. doi: 10.1094/MPMI-2-262.

Lindow, S. E., Arny, D. C., and Upper, C. D. (2013) 'Erwinia herbicola: a bacterial ice

nucleus active in increasing frost injury to corn', *Phytopathology*, 68(3), pp. 523–527. doi: 10.1094/Phyto-68-523.

Linstrom, P. J. and Mallard, W. G. (eds) *NIST Chemistry WebBook, NIST Standard Reference Database Number 69*. Gaithersburg MD, 20899: National Institute of Standards and Technology. doi: 10.18434/T4D303. Spectrum: <https://webbook.nist.gov/cgi/cbook.cgi?ID=C7783202&Type=IR-SPEC&Index=1>  
07.07.2019

Lundheim, R. and Wahlberg, K. (1998) 'Ice nucleation in fruit juice from different varieties of sea buckthorn *Hippophaë rhamnoides* L.', *Euphytica*, 102(1), pp. 117–124. doi: 10.1023/A:1018336413479.

Magel, E., Einig, W., and Hampp, R. (2000) 'Carbohydrates in trees', *Developments in Crop Science*, 26(C), pp. 317–336. doi: 10.1016/S0378-519X(00)80016-1.

Maki, L. R., Galayan, E. L., Chang-Chien, M., and Caldwell, R. (1974) 'Ice nucleation induced by *Pseudomonas syringae*', *Applied Microbiology*, 28(3), pp. 456–459. doi: 10.1111/1462-2920.12668.

Malkin, T. L., Murray, B. J., Brukhno, A. V., Anwar, J., and Salzmann, C. G. (2012) 'Structure of ice crystallized from supercooled water', *Proceedings of the National Academy of Sciences*, 109(4), pp. 1041–1045. doi: 10.1073/pnas.1113059109.

Martin, B., Bytnerowicz, A., and Thorstenson, Y. R. (1988) 'Effects of Air Pollutants on the Composition of Stable Carbon Isotopes,  $\delta^{13}C$ , of Leaves and Wood, and on Leaf Injury.', *Plant Physiology*, 88(1), pp. 218–23. doi: 10.1104/pp.88.1.218.

Matthias-Maser, S. and Jaenicke, R. (1995) 'The size distribution of primary biological aerosol particles with radii  $> 0.2 \mu m$  in an urban/rural influenced region', *Atmospheric Research*, 39(4), pp. 279–286. doi: 10.1016/0169-8095(95)00017-8.

Maurer, S. and Matyssek, R. (1997) 'Nutrition and the ozone sensitivity of birch (*Betula pendula*)', *Trees*, 12(1), p. 11. doi: 10.1007/s004680050116.

Mazur, P. (1969) 'Freezing Injury in Plants', *Annual Review of Plant Physiology*, 20, pp. 419–448. doi: 10.1146/annurev.pp.20.060169.002223.

Mishchenko, M. I., Rossow, W. B., Macke, A., and Lacis, A. A. (1996) 'Sensitivity of cirrus cloud albedo, bidirectional reflectance and optical thickness retrieval accuracy to ice particle shape', *Journal of Geophysical Research*, 101(D12), p. 16,973-16,985. doi:

10.1029/96JD01155.

Miyazawa, T., Shimanouchi, T., and Mizushima, S. I. (1956) 'Characteristic infrared bands of monosubstituted amides', *The Journal of Chemical Physics*, 24(2), pp. 408–418. doi: 10.1063/1.1742489.

Möhler, O., Field, P. R., Connolly, P., Benz, S., Saathoff, M., Wagner, R., Cotton, R., Krämer, M., Mangold, A., and Heymsfield, A. J. (2006) 'Efficiency of the deposition mode ice nucleation on mineral dust particles', *Atmospheric Chemistry and Physics*, 6(10), pp. 3007–3021. doi: 10.5194/acp-6-3007-2006.

Möhler, O., DeMott, P. J., Vali, G., and Levin, Z. (2007) 'Microbiology and atmospheric processes: The role of biological particles in cloud physics', *Biogeosciences*, 4(6), pp. 1059–1071. doi: 10.5194/bg-4-1059-2007.

Monier, J.-M. and Lindow, S. E. (2003) 'Pseudomonas syringae Responds to the Environment on Leaves by Cell Size Reduction', *Phytopathology*, 93(10), pp. 1209–1216. doi: 10.1094/PHYTO.2003.93.10.1209.

Morris, C. E., Conen, F., Huffman, A., Phillips, V., Pöschl, U., and Sands, D. C. (2014) 'Bioprecipitation: A feedback cycle linking Earth history, ecosystem dynamics and land use through biological ice nucleators in the atmosphere', *Global Change Biology*, 20(2), pp. 341–351. doi: 10.1111/gcb.12447.

Mortimer, C. E. and Müller, U. (2003) *Chemie: Das Basiswissen der Chemie*. 8. edition. Stuttgart: Georg Thieme Verlag.

Murray, B. J., Broadley, S. L., Wilson, T. W., Bull, S. J., Wills, R. H., Christenson, H. K., and Murray, E. J. (2010) 'Kinetics of the homogeneous freezing of water', *Physical Chemistry Chemical Physics*, 12(35), pp. 10380–10387. doi: 10.1039/c003297b.

Murray, B. J., Broadley, S. L., Wilson, T. W., Atkinson, J. D., and R. H. Wills (2011) 'Heterogeneous freezing of water droplets containing kaolinite particles', *Atmospheric Chemistry and Physics*, 11(9), pp. 4191–4207. doi: 10.5194/acp-11-4191-2011.

Murray, B. J., O'Sullivan, D., Atkinson, J. D., and Webb, M. E. (2012) 'Ice nucleation by particles immersed in supercooled cloud droplets', *Chemical Society Reviews*, 41(19), pp. 6519–6554. doi: 10.1039/c2cs35200a.

Murray, B. J. and Bertram, A. K. (2006) 'Formation and stability of cubic ice in water droplets', *Physical Chemistry Chemical Physics*, 8(1), pp. 186–192. doi:

10.1039/b513480c.

Murray, B. J. and Bertram, A. K. (2008) 'Inhibition of solute crystallisation in aqueous H(+)-NH(4)(+)-SO4(2-)-H2O droplets.', *Physical Chemistry Chemical Physics*, 10(22), pp. 3287–3301. doi: 10.1039/b802216j.

Murray, B. J., Knopf, D. A., and Bertram, A. K. (2005) 'The formation of cubic ice under conditions relevant to Earth's atmosphere', *Nat.*, 434(7030), pp. 202–205. doi: 10.1038/nature03403.

Niedermeier, D., Shaw, R. A., Hartmann, S., Wex, H., Clauss, T., Voigtländer, J., and Stratmann, F. (2011) 'Heterogeneous ice nucleation: Exploring the transition from stochastic to singular freezing behavior', *Atmospheric Chemistry and Physics*, 11(16), pp. 8767–8775. doi: 10.5194/acp-11-8767-2011.

O'Sullivan, D., Murray, B. J., Malkin, T. L., Whale, T. F., Umo, N. S., Atkinson, J. D., Price, H. C., Baustian, K. J., Browse, J., and Webb, M. E. (2014) 'Ice nucleation by fertile soil dusts: Relative importance of mineral and biogenic components', *Atmospheric Chemistry and Physics*, 14(4), pp. 1853–1867. doi: 10.5194/acp-14-1853-2014.

O'Sullivan, D., Murray, B. J., Ross, J. F., Whale, T. F., Price, H. C., Atkinson, J. D., Umo, N. S., and Webb, M. E. (2015) 'The relevance of nanoscale biological fragments for ice nucleation in clouds', *Scientific Reports*, 5, pp. 1–7. doi: 10.1038/srep08082.

O'Sullivan, D., Murray, B. J., Ross, J. F., and Webb, M. E. (2016) 'The adsorption of fungal ice-nucleating proteins on mineral dusts: A terrestrial reservoir of atmospheric ice-nucleating particles', *Atmospheric Chemistry and Physics*, 16, pp. 7879–7887. doi: 10.5194/acp-16-7879-2016.

Pearce, R. (2001) 'Plant Freezing and Damage', *Annals of Botany*, 87(4), pp. 417–424. doi: 10.1006/anbo.2000.1352.

Petters, M. D. and Wright, T. P. (2015) 'Revisiting ice nucleation from precipitation samples', *Geophysical Research Letters*, 42(20), pp. 8758–8766. doi: 10.1002/2015GL065733.

Popovicheva, O., Kireeva, E., Persiantseva, N., Khokhlova, T., Shonija, N., Tishkova, V., and Demirdjan, B. (2008) 'Effect of soot on immersion freezing of water and possible atmospheric implications', *Atmospheric Research*. Elsevier B.V., 90(2–4), pp. 326–337. doi: 10.1016/j.atmosres.2008.08.004.

Pouleur, S., Richard, C., Martin, J.-G., and Antoun, H. (1992) 'Ice nucleation activity in *Fusarium acuminatum* and *Fusarium avenaceum*', *Applied and Environmental Microbiology*, 58(9), pp. 2960–2964.

Pratt, K. A., DeMott, P. J., French, J. R., Wang, Z., Westphal, D. L., Heymsfield, A. J., Twohy, C. H., Prenni, A. J., and Prather, K. A. (2009) 'In situ detection of biological particles in cloud ice-crystals', *Nature Geoscience*. Nature Publishing Group, 2(6), pp. 398–401. doi: 10.1038/ngeo521.

Price, W. S., Ide, H., and Arata, Y. (1999) 'Self-Diffusion of Supercooled Water to 238 K Using PGSE NMR Diffusion Measurements', *Journal of Physical Chemistry A*, 103(4), pp. 448–450. doi: 10.1021/jp9839044.

Pruppacher, H. R. and Klett, J. D. (1997) *Microphysics of Clouds and Precipitation*. 2. edition. Dordrecht: Kluwer Academic Publishers.

Pummer, B. G., Bauer, H., Bernardi, J., Bleicher, S., and Grothe, H. (2012) 'Suspendable macromolecules are responsible for ice nucleation activity of birch and conifer pollen', *Atmospheric Chemistry and Physics*, 12(5), pp. 2541–2550. doi: 10.5194/acp-12-2541-2012.

Pummer, B. G., Bauer, H., Bernardi, J., Chazallon, B., Facq, S., Lendl, B., Whitmore, K., and Grothe, H. (2013) 'Chemistry and morphology of dried-up pollen suspension residues', *Journal of Raman Spectroscopy*, 44(12), pp. 1654–1658. doi: 10.1002/jrs.4395.

Pummer, B. G., Budke, C., Augustin-Bauditz, S., Niedermeier, D., Felgitsch, L., Kampf, C. J., Huber, R. G., Liedl, K. R., Loerting, T., Moschen, T., Schauerl, M., Tollinger, M., Morris, C. E., Wex, H., Grothe, H., Pöschl, U., Koop, T., and Fröhlich-Nowoisky, J. (2015) 'Ice nucleation by water-soluble macromolecules', *Atmospheric Chemistry and Physics*, 15, pp. 4077–4091. doi: 10.5194/acp-15-4077-2015.

Rey, A. and Jarvis, P. G. (1998) 'Long-term photosynthetic acclimation to elevated atmospheric CO<sub>2</sub> in birch (*Betula pendula* Roth.)', *Impacts of Global Change on Tree Physiology and Forest Ecosystems*, 52(October), pp. 87–91. doi: 10.1007/978-94-015-8949-9\_12

Ringo, J. (2004) *Fundamental Genetics*. New York: Cambridge University Press. doi: 10.1017/CBO9780511807022.

Rocco, A. G., Mollica, L., Ricchiuto, P., Baptista, A. M., Gianazza, E., and Eberini, I.

(2008) 'Characterization of the Protein Unfolding Processes Induced by Urea and Temperature', *Biophysical Journal*, 94(6), pp. 2241 – 2251. doi: 10.1529/biophysj.107.115535.

Rogers, D. C., DeMott, P. J., Kreidenweis, S. M., and Chen, Y. (1998) 'Measurements of ice nucleating aerosols during SUCCESS', *Geophysical Research Letters*, 25(9), pp. 1383–1386. doi: 10.1029/97GL03478.

Rosinski, J. and Parungo, F. (1966) 'Terpene-Iodine Compounds as Ice Nuclei', *Journal of Applied Meteorology*, 5(1), pp. 119–123. doi: 10.1175/1520-0450(1966)005<0119:TICAIN>2.0.CO;2.

Rosky, P. J. (2008) 'Protein denaturation by urea: Slash and bond', 105(44), pp. 16825–16826. doi: 10.1073/pnas.0809224105.

Saha, K. (2008) *The Earth's Atmosphere: Its Physics and Dynamics*, Berlin Heidelberg: Springer. ISBN: 978-3-540-78426-5.

Salby, M. L. (2012) *Physics of the Atmosphere and Climate*. New York: Cambridge University Press. doi: 10.1088/978-0-7503-1052-9.

Sánchez-Ochoa, A., Kasper-Giebl, A., Puxbaum, H., Gelencser, A., Legrand, M., and Pio, C. (2007) 'Concentration of atmospheric cellulose: A proxy for plant debris across a west-east transect over Europe', *Journal of Geophysical Research Atmospheres*, 112(23), pp. 1–8. doi: 10.1029/2006JD008180.

Sands, D. C., Langhans, V. E., Scharen, A. L., and De Smet, G. (1982) 'The association between bacteria and rain and possible resultant meteorological implications', *Időjárás*, 86(2–4), pp. 148–152.

Saxena, V. K. (1983) 'Evidence of the Biogenic Nuclei Involvement in Antarctic Coastal Clouds', *The Journal of Physical Chemistry*, 87(21), pp. 4130–4134. doi: 10.1021/j100244a029.

Schmid, D., Pridmore, D., Capitani, G., Battistutta, R., Neeser, J. R., and Jann, A. (1997) 'Molecular organisation of the ice nucleation protein InaV from *Pseudomonas syringae*', *FEBS Letters*. Federation of European Biochemical Societies, 414(3), pp. 590–594. doi: 10.1016/S0014-5793(97)01079-X.

Schnell, R. C. and Vali, G. (1973) 'World-wide Source of Leaf-derived Freezing Nuclei', *Nature*, 246, pp. 212–213. doi: 10.1038/246212a0.

Schnell, R. C. and Vali, G. (1976) 'Biogenic Ice Nuclei: Part I. Terrestrial and Marine Sources', *Journal of the Atmospheric Sciences*, 33(8), pp. 1554–1564. doi: 10.1175/1520-0469(1976)033<1554:BINPIT>2.0.CO;2.

Schultz, H. R. and Matthews, M. A. (1988) 'Resistance to water transport in shoots of *Vitis vinifera* L.', *Plant Physiology*, 88, pp. 718–724. doi: 10.1104/pp.88.3.718.

Schulz, H. and Baranska, M. (2007) 'Identification and quantification of valuable plant substances by IR and Raman spectroscopy', *Vibrational Spectroscopy*, 43(1), pp. 13–25. doi: 10.1016/j.vibspec.2006.06.001.

Schumann, U. (1994) 'On the Effect of Emissions from Aircraft Engines on the State of the Atmosphere', *Annales Geophysicae*, 12, pp. 365–384. doi: 10.1007/s00585-994-0365-0.

Seinfeld, J. H. and Pandis, S. N. (1998) *Atmospheric Chemistry and Physics: From Air Pollution to Climate Change*. New York: John Wiley & Sons, Inc. ISBN: 0471178160.

Sellin, A., Sack, L., Öunapuu, E., and Karusion, A. (2011) 'Impact of light quality on leaf and shoot hydraulic properties: A case study in silver birch (*Betula pendula*)', *Plant, Cell and Environment*, 34(7), pp. 1079–1087. doi: 10.1111/j.1365-3040.2011.02306.x.

Sellin, A., Tullus, A., Niglas, A., Öunapuu, E., Karusion, A., and Lõhmus, K. (2013) 'Humidity-driven changes in growth rate, photosynthetic capacity, hydraulic properties and other functional traits in silver birch (*Betula pendula*)', *Ecological Research*, 28(3), pp. 523–535. doi: 10.1007/s11284-013-1041-1.

Sellin, A., Eensalu, E., and Niglas, A. (2010) 'Is distribution of hydraulic constraints within tree crowns reflected in photosynthetic water-use efficiency? An example of *Betula pendula*', *Ecological Research*, 25(1), pp. 173–183. doi: 10.1007/s11284-009-0641-2.

Sellin, A. and Kupper, P. (2006) 'Spatial variation in sapwood area to leaf area ratio and specific leaf area within a crown of silver birch', *Trees - Structure and Function*, 20(3), pp. 311–319. doi: 10.1007/s00468-005-0042-2.

Sellin, A. and Kupper, P. (2007) 'Effects of enhanced hydraulic supply for foliage on stomatal responses in little-leaf linden (*Tilia cordata* Mill.)', *European Journal of Forest Research*, 126(2), pp. 241–251. doi: 10.1007/s10342-006-0140-8.

Sperry, J. S. and Sullivan, J. E. M. (1992) 'Xylem Embolism in Response to Freeze-Thaw Cycles and Water Stress in Ring-Porous, Diffuse-Porous, and Conifer Species', *Plant*

*Physiology*, 100(2), pp. 605–613. doi: 10.1104/pp.100.2.605.

Spracklen, D. V., Carslaw, K. S., Merikanto, J., Mann, G. W., Reddington, C. L., Pickering, S., Ogren, J. A., Andrews, E., Baltensperger, U., Weingartner, E., Boy, M., Kulmala, M., Laakso, L., Lihavainen, H., Kivekäs, N., Komppula, M., Mihalopoulos, N., Kouvarakis, G., Jennings, S. G., O'Dowd, C., Birmili, W., Wiedensohler, A., Weller, R., Gras, J., Laj, P., Sellegri, K., Bonn, B., Krejci, R., Laaksonen, A., Hamed, A., Minikin, A., Harrison, R. M., Talbot, R., and Sun, J. (2010) 'Explaining global surface aerosol number concentrations in terms of primary emissions and particle formation', *Atmospheric Chemistry and Physics*, 10(10), pp. 4775–4793. doi: 10.5194/acp-10-4775-2010.

Steinke, I., Möhler, O., Kiselev, A., Niemand, M., Saathoff, H., Schnaiter, M., Skrotzki, J., Hoose, C., and Leisner, T. (2011) 'Ice nucleation properties of fine ash particles from the Eyjafjallajökull eruption in April 2010', *Atmospheric Chemistry and Physics*, 11(24), pp. 12945–12958. doi: 10.5194/acp-11-12945-2011.

Storey, J. M. and Storey, K. B. (2004) 'Cold Hardiness and Freeze Tolerance', in Storey, K. B. (ed.) *Functional Metabolism: Regulation and Adaptation*. Hoboken: John Wiley & Sons, Inc, pp. 470–503. doi: 10.1002/047167558X.ch17.

Storey, K. B. (1997) 'Organic solutes in freezing tolerance', *Comparative Biochemistry and Physiology Part A: Physiology*, 117(3), pp. 319–326. doi: 10.1016/S0300-9629(96)00270-8.

Tobo, Y., DeMott, P. J., Hill, T. C. J., Prenni, A. J., Swoboda-Colberg, N. G., Franc, G. D., Kreidenweis, S. M. (2014) 'Organic matter matters for ice nuclei of agricultural soil origin', *Atmospheric Chemistry and Physics*, 14, pp. 8521–8531. doi: 10.5194/acp-14-8521-2014.

Tong, H. J., Ouyang, B., Nikolovski, N., Lienhard, D. M., Pope, F. D., and Kalberer, M. (2015) 'A new electrodynamic balance (EDB) design for low-temperature studies: Application to immersion freezing of pollen extract bioaerosols', *Atmospheric Measurement Techniques*, 8(3), pp. 1183–1195. doi: 10.5194/amt-8-1183-2015.

Le Treut, H. and Sommerville, R., Cubash, U., Ding, Y., Mauritzen, C., Mokssit, A., Peterson, T., and Prather, M. (2007) 'Historical Overview of Climate Change Science', in Solomon, S., Qin, D., Manning, M., Chen, Z., Marquis, M., Averyt, K. B., Tignor, M., and Miller, H. L. (eds) *Climate Change 2007: The Physical Science Basis. Contribution of Working Group I to the Fourth Assessment Report of the Intergovernmental Panel on Climate Change*. New York: Cambridge University Press, pp. 93–127.



- Truong, C., Palmé, A. E., and Felber, F. (2007) 'Recent invasion of the mountain birch *Betula pubescens* ssp. *tortuosa* above the treeline due to climate change: Genetic and ecological study in northern Sweden', *Journal of Evolutionary Biology*, 20(1), pp. 369–380. doi: 10.1111/j.1420-9101.2006.01190.x.
- Uri, V., Lõhmus, K., Ostonen, I., Tullus, H., Lastik, R., and Vildo, M. (2007) 'Biomass production, foliar and root characteristics and nutrient accumulation in young silver birch (*Betula pendula* Roth.) stand growing on abandoned agricultural land', *European Journal of Forest Research*, 126(4), pp. 495–506. doi: 10.1007/s10342-007-0171-9.
- Uri, V., Varik, M., Aosaar, J., Kanal, A., Kukumägi, M., and Lõhmus, K. (2012) 'Biomass production and carbon sequestration in a fertile silver birch (*Betula pendula* Roth) forest chronosequence', *Forest Ecology and Management*. Elsevier B.V., 267, pp. 117–126. doi: 10.1016/j.foreco.2011.11.033.
- Urrutia, M. E., Duman, J. G., and Knight, C. A. (1992) 'Plant thermal hysteresis proteins', *Biochimica et Biophysica Acta (BBA)/Protein Structure and Molecular*, 1121(1–2), pp. 199–206. doi: 10.1016/0167-4838(92)90355-H.
- Vali, G. (1971) 'Quantitative Evaluation of Experimental Results on the Heterogeneous Freezing Nucleation of Supercooled Liquids', *Journal of the Atmospheric Sciences*, 28(3), pp. 402–409. doi: 10.1175/1520-0469(1971)028<0402:QEOERA>2.0.CO;2.
- Vali, G. (1994) 'Freezing Rate Due to Heterogeneous Nucleation', *Journal of the Atmospheric Sciences*, 51(13), pp. 1843–1856. doi: 10.1175/1520-0469(1994)051<1843:FRDTHN>2.0.CO;2.
- Vali, G. (2008) 'Repeatability and randomness in heterogeneous freezing nucleation', *Atmospheric Chemistry and Physics*, 8(16), pp. 5017–5031. doi: 10.5194/acp-8-5017-2008.
- Vali, G. (2014) 'Interpretation of freezing nucleation experiments: Singular and stochastic; Sites and surfaces', *Atmospheric Chemistry and Physics*, 14(11), pp. 5271–5294. doi: 10.5194/acp-14-5271-2014.
- Vali, G. (2019) 'Revisiting the differential freezing nucleus spectra derived from drop freezing experiments; methods of calculation, applications and confidence limits', *Atmospheric Measurement Techniques Discussions*, 12, pp. 1219–1231. doi: 10.5194/amt-12-1219-2019.
- Vali, G. and Stansbury, E. J. (1966) 'Time-Dependent Characteristics of the

Heterogeneous Nucleation of Ice', *Canadian Journal of Physics*, 44(3), pp. 477–502. doi: 10.1139/p66-044.

Vrbka, L. and Jungwirth, P. (2006) 'Homogeneous freezing of water starts in the subsurface', *Journal of Physical Chemistry B*, 110(37), pp. 18126–18129. doi: 10.1021/jp064021c.

Wang, B. and Knopf, D. A. (2011) 'Heterogeneous ice nucleation on particles composed of humic-like substances impacted by O<sub>3</sub>', *Journal of Geophysical Research Atmospheres*, 116(3), pp. 1–14. doi: 10.1029/2010JD014964.

Wang, C. S., Hein, S., Zhao, Z. G., Guo, J. J., and Zeng, J. (2016) 'Branch occlusion and discoloration of *Betula alnoides* under artificial and natural pruning', *Forest Ecology and Management*. Elsevier B.V., 375, pp. 200–210. doi: 10.1016/j.foreco.2016.05.027.

Wang, C. S., Zeng, J., Hein, S., Zhau, Z. G., Guo, J. J., and Zeng, J. (2017) 'Crown and branch attributes of mid-aged *Betula alnoides* plantations in response to planting density', *Scandinavian Journal of Forest Research*, 32(8), pp. 679–687. doi: 10.1080/02827581.2016.1261936.

Wang, P. K. (2013) *Physics and dynamics of clouds and precipitation*. Cambridge: Cambridge University Press. ISBN: 978-1-107-00556-3.

Welti, A., Lüönd, F., Kanji, Z. A., Stetzer, O., and Lohmann, U. (2012) 'Time dependence of immersion freezing: An experimental study on size selected kaolinite particles', *Atmospheric Chemistry and Physics*, 12(20), pp. 9893–9907. doi: 10.5194/acp-12-9893-2012.

Wharton, D. and Ferns, D. (1995) 'Survival of intracellular freezing by the Antarctic nematode *Panagrolaimus davidi*', *The Journal of experimental biology*, 198(Pt 6), pp. 1381–1387.

Wheeler, M. J. and Bertram, A. K. (2012) 'Deposition nucleation on mineral dust particles: A case against classical nucleation theory with the assumption of a single contact angle', *Atmospheric Chemistry and Physics*, 12(2), pp. 1189–1201. doi: 10.5194/acp-12-1189-2012.

Winiwarter, W., Bauer, H., Caserio, A., and Puxbaum, H. (2009) 'Quantifying emissions of primary biological aerosol particle mass in Europe', *Atmospheric Environment*. Elsevier Ltd, 43(7), pp. 1403–1409. doi: 10.1016/j.atmosenv.2008.01.037.

Ten Wolde, P. R. and Frenkel, D. (1999) 'Homogeneous nucleation and the Ostwald step rule', *Physical Chemistry Chemical Physics*, 1(9), pp. 2191–2196. doi: 10.1039/a809346f.

Wright, T. P. and Petters, M. D. (2013) 'The role of time in heterogeneous freezing nucleation', *Journal of Geophysical Research Atmospheres*, 118(9), pp. 3731–3743. doi: 10.1002/jgrd.503652013.

Yankofsky, S. A. et al. (1981) 'Some Basic Characteristics of Bacterial Freezing Nuclei', *Journal of Applied Meteorology*, 20, pp. 1013–1019. doi: 10.1175/1520-0450(1981)020<1013:SBCOBF>2.0.CO;2.

Zachariassen, K. E. and Kristiansen, E. (2000) 'Ice Nucleation and Antinucleation in Nature', *Cryobiology*, 41(4), pp. 257–279. doi: 10.1006/cryo.2000.2289.

Zimmermann, F., Weinbruch, S., Schütz, L., Hofmann, H., Ebert, M., Kandler, K., and Worringer, A. (2008) 'Ice nucleation properties of the most abundant mineral dust phases', *Journal of Geophysical Research Atmospheres*, 113(23). doi: 10.1029/2008JD010655.

Zolles, T, Burkart, J., Häusler, T., Pummer, B., Hitzemberger, R., and Grothe, H. (2015) 'Identification of ice nucleation active sites on feldspar dust particles', *Journal of Physical Chemistry A*, 119(11), pp. 2692–2700. doi: 10.1021/jp509839x.

## Personal Publication List

### Book Contributions:

Felgitsch, L. and Grothe, H. (2015) 'Up into the Sky' in *A voyage through scales*, Blöschl, G., Thybo, H., and Savenije, H. (eds), Vienna: Edition Lammerhuber, pp. 32-37. ISBN: 978-3-901753-84-8.

### Journal Articles:

Haller, T., Rentenberger, C., Meyer, J., Felgitsch, L., Grothe, H., and Hitzenberger, R. (2019) 'Structural changes of CAST soot during a thermal-optical measurement protocol', *Atmospheric Measurement Techniques*, 12, pp. 3503-3519. doi: 10.5194/amt-12-3503-2019.

Felgitsch, L., Bichler, M., Burkart, J., Fiala, B., Häusler, T., Hitzenberger, R., and Grothe, H. (2019) 'Heterogeneous Freezing of Liquid Suspensions Including Juices and Extracts from Berries and Leaves from Perennial Plants', *Atmosphere*, 10(1), 37, pp. 1-22. doi: 10.3390/atmos10010037.

Felgitsch, L., Baloh, P., Burkart, J., Mayr, M., Momken, E., Seifried, T. M., Winkler, P., Schmale III, D. G., and Grothe, H. (2018) 'Birch leaves and branches as a source of ice-nucleating macromolecules', *Atmospheric Chemistry and Physics*, 18, pp. 16063-16079. doi: 10.5194/acp-18-16063-2018.

DeMott, P., Möhler, O., Cziczo, D., Hiranuma, N., Petters, M., Petters, S., Belosi, F., Bingemer, H., Brooks, S., Budke, C., Burkert-Kohn, M., Collier, K., Danielczok, A., Eppers, O., Felgitsch, L., Garimella, S., Grothe, H., Herenz, P., Hill, T., Höhler, K., Kanji, Z., Kiselev, A., Koop, T., Kristensen, T., Krüger, K., Kulkarni, G., Levin, E., Murray, B., Nicosia, A., O´Sullivan, D., Peckaus, A., Polen, M., Price, H., Reicher, N., Rothenberg, D., Rudich, Y., Santachiara, G., Schiebel, T., Schrod, J., Seifried, T. M., Stratmann, F., Sullivan, R., Suski, K., Szakáll, M., Taylor, H., Ullrich, R., Vergara-Temprado, J., Wagner, R., Whale, T., Weber, D., Welti, A., Wilson, T., Wolf, M., and Zenker, J. (2018) 'The Fifth International Workshop on Ice Nucleation phase 2 (FIN-02): Laboratory intercomparison of ice nucleation measurements', *Atmospheric Measurement Techniques*, 11, pp. 6231-6257. doi: 10.5194/amt-2018-191.

Häusler, T., Witek, L., Felgitsch, L., Hitzenberger, R., and Grothe, H. (2018) 'Freezing on a Chip-A New Approach to Determine Heterogeneous Ice Nucleation of Micrometer-Sized Water Droplets', *Atmosphere*, 9(4), 140; pp. 1-14. doi:10.3390/atmos9040140.

Coluzza, I., Creamean, J., Rossi, J., Wex, H., Alpert, P., Bianco, V., Boose, Y., Dellago, C., Felgitsch, L., Fröhlich-Nowoisky, J., Herrmann, H., Jungblut, S., Kanji, Z., Menzl, G., Moffett, B., Moritz, C., Mutzel, A., Pöschl, U., Schauperl, M., Scheel, J., Stopelli, E., Stratmann, F., Grothe, H., and Schmale III, D. G. (2017) 'Perspectives on the Future of Ice Nucleation Research: Research Needs and Unanswered Questions Identified from Two International Workshops', *Atmosphere*, 13, 8; pp. 1-28. doi: 10.3390/atmos8080138.

Pummer, B. G., Budke, C., Augustin-Bauditz, S., Niedermeier, D., Felgitsch, L., Kampf, C., Huber, R., Liedl, K., Loerting, T., Moschen, T., Schauperl, M., Tollinger, M., Morris, C., Wex, H., Grothe, H., Pöschl, U., Koop, T., and Fröhlich-Nowoisky, J. 'Ice nucleation by water-soluble macromolecules', *Atmospheric Chemistry and Physics*, 15, pp. 4077-4091. doi: 10.5194/acp-15-4077-2015.

## Talks

Baloh, P., Hanlon, R., Pietsch, R., Dolan, E., Burkart, J., Felgitsch, L., Anderson, C., Schmale III, D. G., and Grothe, H. (2018) 'Time and spot dependency of ice nuclei from water sources in the mountains of Tyrol, Austria' Talk: EGU General Assembly 2018, Vienna, 08.04.2018-13.04.2018, in: *EGU General Assembly 2018*, Geophysical Research Abstracts, 20, EGU2018-1648.

Felgitsch, L., Bichler, M., Vogel, A., Häusler, T., and Grothe, H. (2016) 'Biological particles capable of triggering ice nucleation in the atmosphere', Talk: EGU General Assembly 2016, Vienna, 17.04.2016-22.04.2016, in: *EGU General Assembly 2016*, Geophysical Research Abstracts, EGU2016-8232.

Felgitsch, L., Bichler, M., and Grothe, H. (2016) 'Macromolecular Ice Nuclei of Biological Origin and their Possible Atmospheric Relevance' Talk: 2nd International Conference on Atmospheric Dust, Castellaneta Marina; 12.06.2016-17.06.2016; in: *Scientific Research Abstracts*, 5, p. 54. ISBN: 978-88-7522-091-4.

Häusler, T., Felgitsch, L., Khaybulkina, E., and Grothe H. (2015) 'Cellulose and Their Characteristic Ice Nucleation Activity', Talk: ICCPA International Conference on Carbonaceous Particles in the Atmosphere, Lawrence Berkeley National Laboratory, Berkeley, 10.08.2015-13.08.2015.

Häusler, T., Felgitsch, L., Khaybulkina, E., and Grothe, H. (2016) 'Cellulose and Their Characteristic Ice Nucleation Activity- Freezing on a Chip' Talk: DUST 2016- 2nd International Conference on Atmospheric Dust, Bari, 12.06.2016-17.06.2016; in: *Scientific Research Abstracts*, 5, p. 69. ISBN: 978-88-7522-091-4.

## Posters

Seifried, T. M., Bieber, P., Poon, F., Felgitsch, L., Baloh, P., Burkart, J., Mayr, M., Momken, E., Winkler, P., Crockett, H., Schmale III, D. G., and Grothe, H. (2019) 'Ice Nucleation Activity and Fluorescence Measurements of Ice Nucleating Particles from Birch Trees', Poster: EGU General Assembly 2018, Vienna, 07.04.2019-12.04.2019, in: *EGU General Assembly 2019*, Geophysical Research Abstracts, 21, EGU2019-14007.

Felgitsch, L., Seifried, T. M., Baloh, P., Burkart, J., Mayr, M., Momken, E., Winkler, P., Schmale III, D. G., and Grothe, H. (2018) 'Birch leaves and branches as a source of ice-nucleating macromolecules', Poster: EGU General Assembly 2018, Vienna, 08.04.2018-13.04.2018, in: *EGU General Assembly 2018*, Geophysical Research Abstracts, 20, EGU2018-1531.

Seifried, T. M., Weiss, V., Felgitsch, L., Allmaier, G., Marchetti-Deschmann, M., and Grothe, H. (2018) 'Analytical Characterization of Macromolecular Ice Nuclei from Birch Pollen Grains' Poster: EGU General Assembly 2018, Vienna, 08.04.2018-13.04.2018, in: *EGU General Assembly 2018*, Geophysical Research Abstracts, 20, EGU2018-14346.

Felgitsch, L., Seifried, T. M., Winkler, P., Schmale III, D. G., and Grothe, H. (2017) 'Ice Nuclei from Birch Trees' Poster: EGU General Assembly 2017, Vienna, 23.04.2017-28.04.2017, in: *EGU General Assembly 2017*, Geophysical Research Abstracts, 19, EGU2017-14053.

Fiala, B., Felgitsch, L., and Grothe, H. (2017) 'Comparison of ice nuclei from fruit juices and their properties' Poster: EGU General Assembly 2017, Vienna, 23.04.2017-28.04.2017, in: *EGU General Assembly 2017*, Geophysical Research Abstracts, 19, EGU2017-8143.

Häusler, T., Witek, L., Felgitsch, L., Hitzenberger, R., and H. Grothe (2017) 'The Ice Nucleation Activity of Surface Modified Soot' Poster: EGU General Assembly 2017, Vienna, 23.04.2017-28.04.2017, in: *EGU General Assembly 2017*, Geophysical Research Abstracts, 19, EGU2017-12834.

Häusler, T., Witek, L., Felgitsch, L., Hitzenberger, R., and Grothe, H. (2017) 'Heterogeneous freezing of super cooled water droplets in micrometre range- freezing on a chip', Poster: EGU General Assembly 2017, Vienna, 23.04.2017- 28.04.2017, in: *EGU General Assembly 2017*, Geophysical Research Abstracts, 19, EGU2017-7515.



Felgitsch, L., Pummer, B. G., Chazallon, G., Facq, S., and Grothe, H. (2015) 'Vibrational Spectroscopy and Microscopy of Tree Pollen', Poster: ICAVS 8, Vienna, 12.07.2015-17.07.2015, in: *Abstracts Poster*, (2015), pp. 176-177. ISBN: 978-3-200-04205-6.

Felgitsch, L., Bichler, M., Häusler, T., Weiss, V., Marchetti-Deschmann, M., Allmaier, G., and Grothe, H. 'Molecular Ice Nucleation Activity of Birch Polle' Poster: EGU General Assembly 2015, Vienna, 12.04.2015-17.04.2015; in: *EGU General Assembly 2017*, Geophysical Research Abstracts, EGU2015-1560.

Häusler, T., Felgitsch, L., Khaybulkina, E., and Grothe, H. (2015) 'Investigation of Microcrystalline Cellulose as Ice Nucleus in Immersion Freezing Processes', Poster: EGU General Assembly 2015, Vienna, 12.04.2015-17.04.2015, in: *EGU General Assembly 2015*, 17, EGU2015-1734.

Bichler, M., Felgitsch, L., Seidl-Seiboth, V., and Grothe, H. (2015) 'Ice Nucleation Triggered by Biological Substances' Poster: EGU General Assembly 2015, Vienna, 12.04.2015-17.04.2015 in: *EGU General Assembly 2015*, Geophysical Research Abstracts, 17, EGU2015-1805.

Felgitsch, L., Pummer, B. G., Weiss, V., Allmaier, G., and Grothe, H. (2014) 'Determination of suspendable ice nuclei from various pollen species', Poster: EGU General Assembly 2014, Vienna, 27.04.2014-

02.05.2014; in: *EGU General Assembly 2014*, Geophysical Research Abstracts, 16, EGU2014-5420.

Häusler, T., Felgitsch, L., and Grothe, H. (2014) 'Investigation of Microcrystalline Cellulose as Ice Nucleus in Immersion Freezing Processes' Poster: Workshop on Chemical Atmosphere-Snow-Sea Ice Interactions: taking the next big step in the field, lab & modelling, Cambridge, 13.10.2014-15.10.2014; in: *Workshop on Chemical Atmosphere-Snow-Sea Ice Interactions: taking the next big step in the field, lab & modelling*, (2014), P31.

### Thesis:

Felgitsch, L. (2013) 'Determination of Oxidative Properties of Ambient Particulate Matter based on Ascorbic Acid', Supervisor: Kasper-Giebl, A., Chemical Technologies and Analytics

## Curriculum Vitae

Name: Laura Felgitsch

Date of Birth: 06.10.1988

Citizenship: Austrian

### Education:

1998-2002 HS Staudinger, Leibnitz

2002-2006 BORG Monsberger, Graz

2006-2011 BSc in Chemistry at TU Graz (Graz University of Technology)

2011-2013 MSc in Technical Chemistry - Materials Technology and Materials Analytics – at TU Wien (Vienna University of Technology)

2013-2019 PhD studies at TU Wien (Vienna University of Technology)

### Experience:

2007-2011 Laboratory employee at Lactan, Graz (minor employment via Manpower)

2013-2017 University assistant at TU Wien (Vienna University of Technology)

Spring/Summer 2018 Project assistant at TU Wien (Vienna University of Technology)

Since december 2018 CAPA and Change Control Specialist at Takeda, Vienna